Morphology and Sedimentology of Eskers in the Lac de Gras Area, Northwest Territories, Canada

By

Neil D. Prowse

A thesis submitted to the Faculty of Graduate and Postdoctoral Affairs in partial fulfillment of the requirements for the degree of

Master of Science

Department of Earth Sciences

Carleton University

Ottawa, Ontario

ABSTRACT

An integrated dataset, including LiDAR, grain-size samples, GPR, and augered boreholes, was used to perform a morphological and sedimentological analysis of eskers in the Lac de Gras area, NWT. Esker segments were classified based on morphology and surficial grain size, and depositional environments were interpreted based on sedimentological data gathered from GPR and boreholes. Peaked ridges of cobbles and boulders (Type 1 components) are inferred to be deposited subglacially, and flat topped ridges of finer sediment (Type 2, 3, 4 components) are inferred to have been deposited deltaically. Deltaic deposits are either found overlying or at the down esker extents of Type 1 ridges. Evidence points to a time transgressive depositional model, with maximum length of depositionaly related esker segments not exceeding approximately 5 km in the study area. These results have potential implications for mineral exploration. Transport distance within eskers may not substantially exceed that of the subglacial till.

ACKNOWLEDGEMENTS

Working on this thesis was a fantastic opportunity to expand my knowledge of Quaternary geology and sedimentary processes. For this opportunity, and for all the support, assistance, and ideas along the way, I would like to give my deepest gratitude to Dr. Don Cummings. My field work was made possible by the organization and hard work of Barrett Elliott and the Northwest Territories Geological Survey, with funding provided by the Canadian Northern Economic Development Agency. I must also thank the research team, and all of my fellow students, at the field camp over the summer of 2015. Their expertise and enthusiasm created an atmosphere of academic collaboration and an excellent work environment. I extend a special thank you to Dr. Stephen Gruber, for an incredible LiDAR DEM and some quick programming wizardry that solved what could have been a major problem. Finally, I give my thanks to the faculty, staff and students of the Earth Sciences department at Carleton University, for all the support over my two degrees.

TABLE OF CONTENTS

LIST OF TABLES

LIST OF FIGURES

Chapter 1: Introduction

1.1 Introduction and research goals

Nearly all of the present Canadian landmass was glaciated during the Quaternary Period and, as such, sediment deposited directly from glacier ice (i.e., till *sensu* Dreimanis, 1989) and from glacial meltwater (e.g., eskers, glaciolacustrine mud) is ubiquitous (Fulton, 1995). In most areas, bedrock is partially to completely buried by this sediment, which can render mineral exploration difficult. Because of this, drift prospecting is often employed to quickly and cost-effectively survey an area for economic viability. Drift prospecting is a mineral exploration technique that involves the sampling and analysis of the surficial sediment cover (the "drift") in glaciated terrain to identify trails ("dispersal trains") of gravel, sand, and/or mud particles emanating downflow from ore bodies. Although till is the dominant drift-prospecting medium, eskers—ridges of glaciofluvial sand and gravel derived primarily from till and deposited, at least in part, in subglacial meltwater conduits (Hellakoski, 1931; Shilts, 1976; Brennand, 2000)—are also commonly sampled. Esker sampling has led to major mineral discoveries in Canada. For example, kimberlite indicator minerals (KIMs) discovered in the longest esker in Canada—the ~700 km long Exeter Lake esker—led to the discovery of the Lac de Gras kimberlite field, home to Canada's first diamond mine (Krajick, 2001). Long eskers like the Exeter Lake esker are commonly sampled when the target area is expansive and exploration is in a preliminary stage (i.e., no exploration targets exist), the idea being that the eskers can function as regional "dipsticks" for the surrounding bedrock lithologies (e.g., Atkinson, 1989; Craigie, 1993) in a similar way that large stream networks do in non-glacial settings (e.g. Sutherland, 1982). However,

the publicly available data put this exploration model into question: esker dispersal trains published to date are generally short and typically extend no more than several kilometers past the till-dispersal trains from which they were derived (Cummings et al., 2011). Does this reflect how eskers form?

A longstanding debate exists as to the length of the subglacial meltwater conduits believed to be associated with esker deposition (e.g., Brennand, 2000). One end-member school of thought argues that eskers form "synchronously", in long, subglacial conduits beneath stagnant ice, whereas the other argues that they form "time-transgressively" in short subglacial conduits as the ice front retreats (Figure 1.1). Some of the best-studied eskers have been interpreted both ways, with the two different groups presenting convincing arguments to back their case (e.g., the Katahdin Esker, Maine; Shreve, 1985a,b; Hooke and Fastook, 2007). Resolving the debate is not simply an academic exercise: Long subglacial conduits open the possibility for long-distance dispersal of gravel, sand and mud sized particles of ore along an esker distributary system, whereas short conduits preclude this. As such, determining whether eskers tend to form by the long- or short-conduit model (Figure 1.1) has the potential to improve the effectiveness of mineral exploration in glaciated terrain.

In this thesis, an integrated dataset (LiDAR, ground penetrating radar, augured boreholes, and surficial grain-size samples) was used to investigate a 13-km-long segment of the Exeter Lake esker and a 28-km-long segment of the adjoining Misery tributary esker (Figure 1.2). The principal objective is to obtain a better understanding of depositional processes and accumulation. The study area is located northeast of Lac de Gras, Northwest Territories, approximately 300 km northeast of Yellowknife, near the

geographic center of the Slave Craton of the Precambrian Canadian Shield (Fig 1.2). The area is located in the Barrenlands above the tree line and, as such, exposure of the esker and the adjacent landscape is excellent. Nearby exploration camps and diamond mines afforded accommodation and easy helicopter-supported access during fieldwork. The dataset collected and assembled is unique and substantial. Never before has as esker been studied over such a large area in such high resolution using such a multifaceted dataset. The chapters in this thesis present the methodology and results of the study, and discuss the implications of the results with respect to esker genesis and mineral exploration.

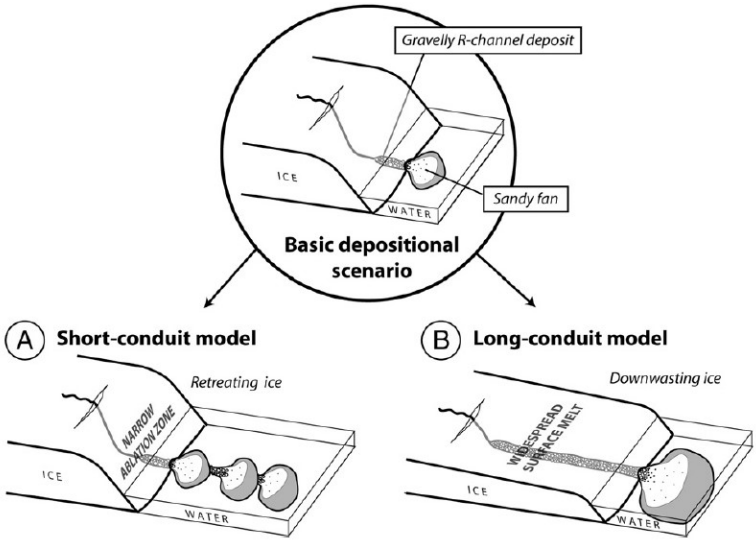

Figure 1.1: End-member scenarios for esker deposition (Cummings et al., 2011). (A) The "short conduit" model of esker deposition (e.g., DeGeer, 1912; Wilson, 1939; Banerjee and MacDonald, 1975; Shilts, 1984; Boulton, 2008) that invokes a relatively steep ice front, a narrow ablation zone, and time-transgressive esker deposition in short subglacial meltwater conduits as the ice front retreats. (B) The "long conduit" model of esker deposition (e.g., Sollas, 1896; Flint, 1930; Shreve, 1985b; Brennand, 1994) that invokes widespread downwasting of the glacier, a large ablation zone, and synchronous esker deposition in a long subglacial meltwater conduit.

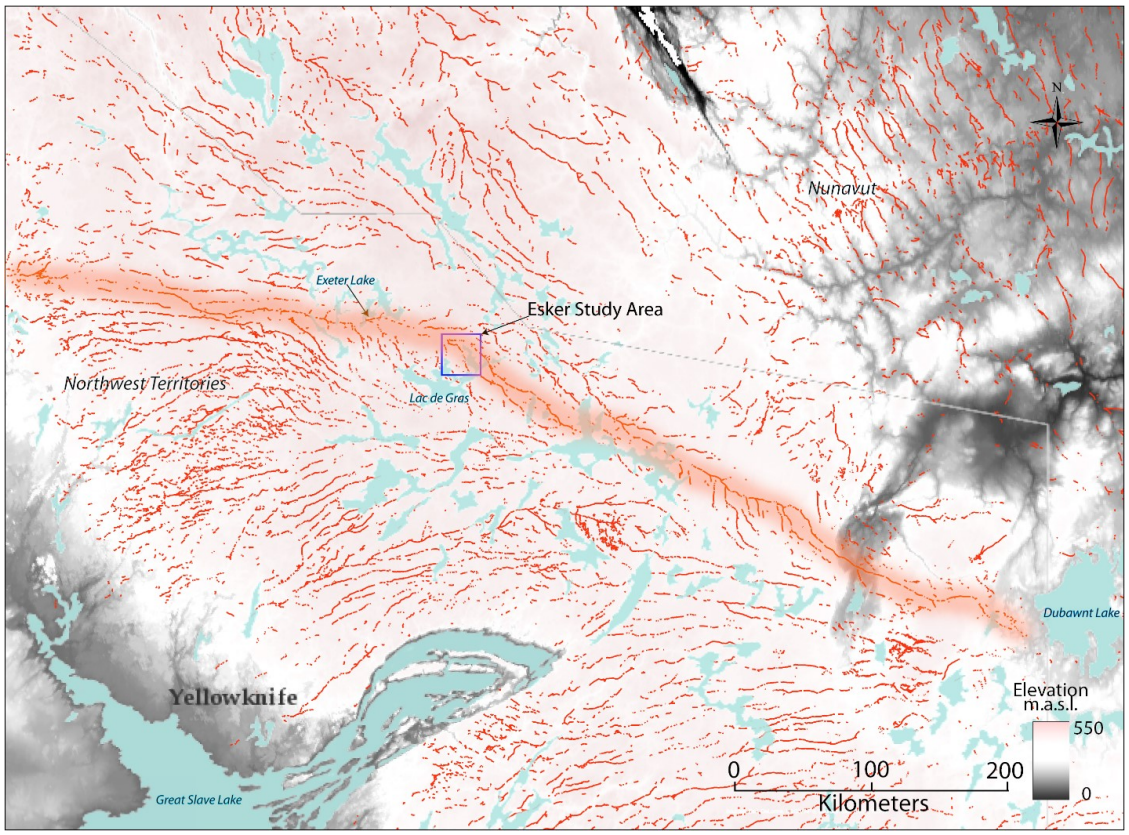

Figure 1.2: Esker locations defined from air-photo analysis within the Canadian Shield west of Hudson Bay (from Aylsworth and Shilts, 1989). The Exeter Lake esker is highlighted in orange, and the Lac de Gras study area is highlighted by the blue box, which approximates the extent of the LiDAR survey. Paleoflow is to the west.

1.2 Bedrock geology

Two main bedrock units occur in the study area: Achaean metaturbidites of the Yellowknife Supergroup, which have an age of 2.71–2.65 Ga (Padgham and Fyson, 1992), and syn- to post-Yellowknife Supergroup Achaean granitoid rocks, which are commonly pegmatitic and were emplaced between 2.65–2.58 Ga (Kjarsgaard et al., 2001). A long, complex history of regional deformation has generated irregular contacts between the two units (Stubley, 2005). Younger (2.33–1.27 Ga; Pell, 1997) and largely

undeformed mafic dykes, mainly of diabase, cross cut these older deformed rock units. In addition, numerous kimberlite pipes are present (Carlson et al., 1999). They have small and commonly circular planform shapes (generally 2–3 Ha, with a maximum of 20 Ha; Scott-Smith, 2008) and range in age from 47.5 to 321 Ma, with the majority falling between 72 and 48 Ma (Davis and Kjarsgaard, 1997; Sarkar et al, 2015). The kimberlites vary in texture and composition but commonly have a fine-grained ultramafic groundmass with olivine, Cr-diopside, pyrope, and ilmenite phenocrysts (Armstrong et al, 2004).

1.3 Surficial geology

The top of the Precambrian Shield is a peneplain: a regional unconformity produced largely during the Precambrian, then modified through Phanerozoic fluvial and Quaternary glacial erosion (Ambrose, 1964). In the study area, land-surface elevation ranges from 430 to 510 metres above sea level, with the highest elevation occurring in the northwest corner of the study area. The terrain is gently undulating, and drainage is poor: small lakes are ubiquitous and large fluvial valleys absent. The bedrock is commonly frost-shattered. Where fresh, it is commonly striated. Striation directions swing clockwise over time: the oldest striations trend southwestward, whereas the youngest dominant striations trend northwestward (Lord and Barnes, 1954; Dredge et al., 1994; Cummings, in review).

Silty sand diamicton overlies bedrock (Ward, 1995; Dredge et al, 1999). It is commonly interpreted as till or, where thick, ice-rich and hummocky, remnant debris-rich

basal ice left over from the last glaciation (Dredge et al., 1999; Cummings, 2016). (For clarity, it will hereafter be referred to as *till*.) The till is composed of angular to sub-rounded pebbles, cobbles and boulders in a silty sand matrix (Dredge et al., 1999). In general, most (>50%) pebbles in till samples share the same lithology as the bedrock beneath (Cummings, in review), suggesting that the till is, for the most part, locally derived, even where thick and hummocky. Rarely, well-defined, elongate dispersal trains of distinctive sand-sized detritus extend northwestward from kimberlite pipes, such as the A21 project pipe at the Diavik diamond mine, located on an island in Lac de Gras (Carlson et al., 1999). This indicates that while older ice-flows must have produced sediment (because they striated and plucked the bedrock), the till in the area was generated almost entirely by the youngest (northwestward moving) ice flow.

The top of the till near Lac de Gras often lacks drumlins and other streamlined features, which contrasts with the till across much of the Canadian Shield west of Hudson Bay (Aylsworth and Shilts, 1989). Rather, large hummocks (5–30 m high) are present locally (Dredge et al., 1999). Industry test holes drilled near Lac de Gras have intersected up to 10 m of massive ground ice in the hummocky till, which Dredge et al (1999) interpret to be buried glacier ice. Most of the till has undergone extensive near-surface (<2 m depth; Hu et al., 2003), post-glacial cryoturbation and is covered in mud boils (such as those described by Shilts (1978)).

Eskers overlie till in the study area. They have been previously described by Wilson (1945), Ward (1993), Ward et al. (1994, 1997), Dredge et al. (1999) and Wolfe et al. (1996) (Figure 1.2). These authors note narrow, peaked-ridge segments and broad, relatively flat, sandy "outwash" segments. In several locations, excavations and

boreholes in eskers near Lac de Gras have revealed massive ground ice, up to 10 m in thickness, that is buried by stratified esker sediment (Wolfe et al., 1996; Dredge et al., 1999). Dredge et al. (1999) suggested that the ice is likely of glacial or glaciofluvial origin. Hu et al. (2003) observed 2 metres of massive, sediment-free ice over bedrock within an esker at the Diavik mine site, located on an island in Lac de Gras, which they interpreted as glacier ice. Wilson (1939) noted a correlation between the size of the eskers and the thickness of the adjacent till: areas of thick till are associated with large, voluminous eskers, whereas areas of thin or no till are associated with fewer and smaller eskers. Wilson (1939) took this to be evidence that the till was the primary source for esker sediment; that the eskers were deposited in short segments as the ice retreated; and that, accordingly, transport distances within the eskers were likely short. Wilson's work was performed using aerial photos; no field work was conducted to test his hypothesis. By contrast, diamond exploration models on the western Canadian Shield have commonly invoked a long-conduit depositional model for eskers, wherein the headwaters of the esker depositing streamsare envisioned to have been located near the Keewatin spreading centre, hundreds of kilometers to the east (Krajick, 2001).

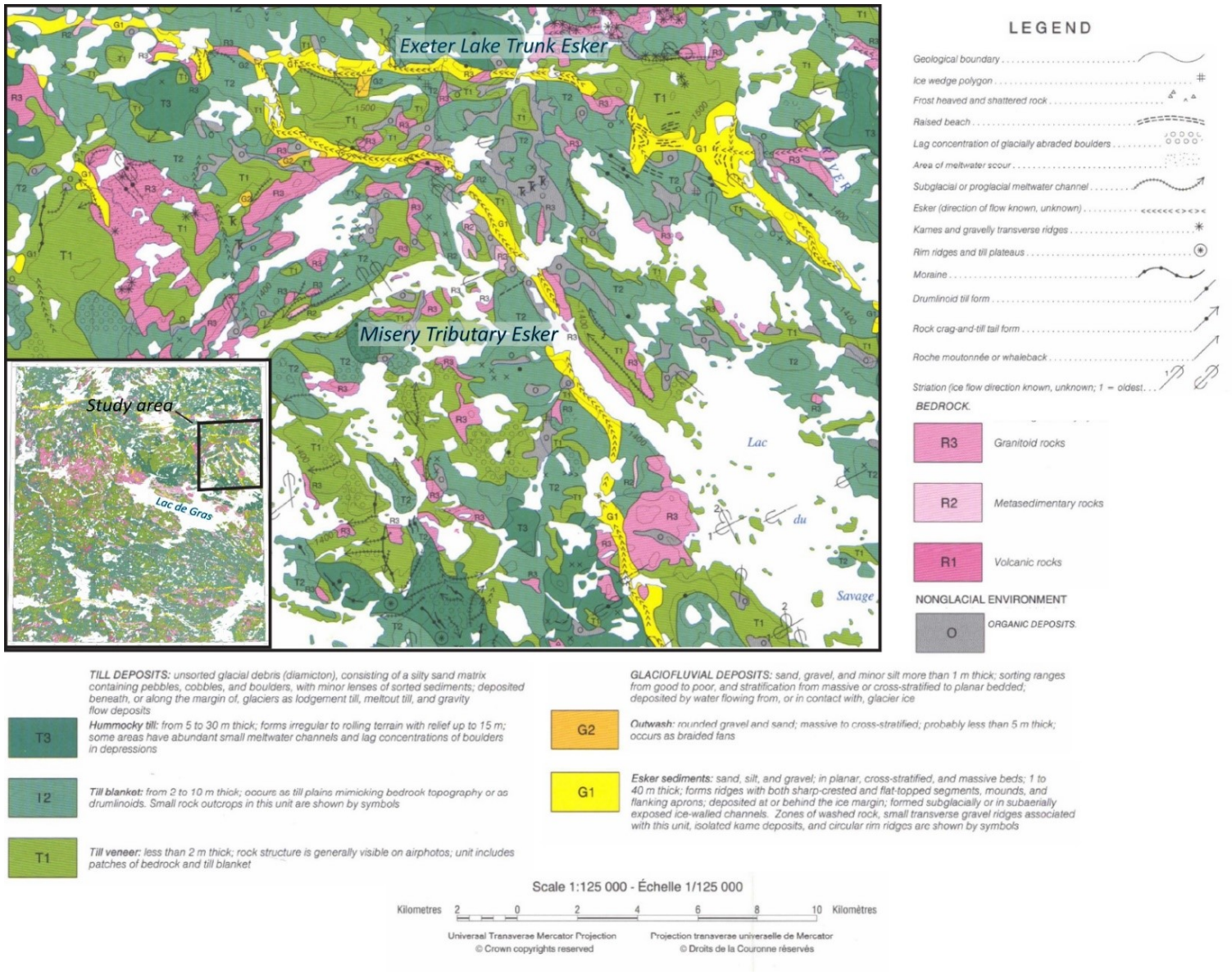

Figure 1.4: Map of surficial sediment in the study area, including eskers (yellow polygons) and till (green polygons) (modified after Ward et al., 1997).

1.4 Glacial hydrology

To provide context for the interpretations presented in this thesis, the principles of glacial hydrology—the origin and flow of meltwater through glaciers—are briefly outlined.

Meltwater in glacial systems tends to be produced in three main ways: by melting of the glacier surface during positive-degree days (above 0° C), by melting of the glacier base where basal ice reaches the pressure melting point, and by melting within the glacier due to strain heating (Lawson, 1993; Fountain and Walder, 1998; Fahnestock, 2001 Eyles, 2006). The first of these processes produces a cyclic supply of meltwater (seasonal, diurnal), whereas the latter two produce a relatively steady supply of meltwater that, in temperate glaciers, is generally subordinate to surface meltwater production by an order of magnitude or more (Benn and Evans, 2010). Once produced, surficial meltwater can pool in supraglacial lakes and form supraglacial streams, but where crevasses exist on the glacier surface—a typical scenario (Post and LaChapelle, 2000)—the bulk of the surficial meltwater is routed into the body of the glacier, where it travels through a network of fractures and conduits to the glacier base (Fountain and Walder, 1998; Fountain et al., 2005). Surface-to-base meltwater-transfer can occur where the ice exceeds 1 km in thickness (Zwally et al., 2002), and becomes more common in areas more proximal to edges of the glacier where ice is thinner, air temperatures higher, and surface meltwater production greater (Fountain and Walder, 1998).

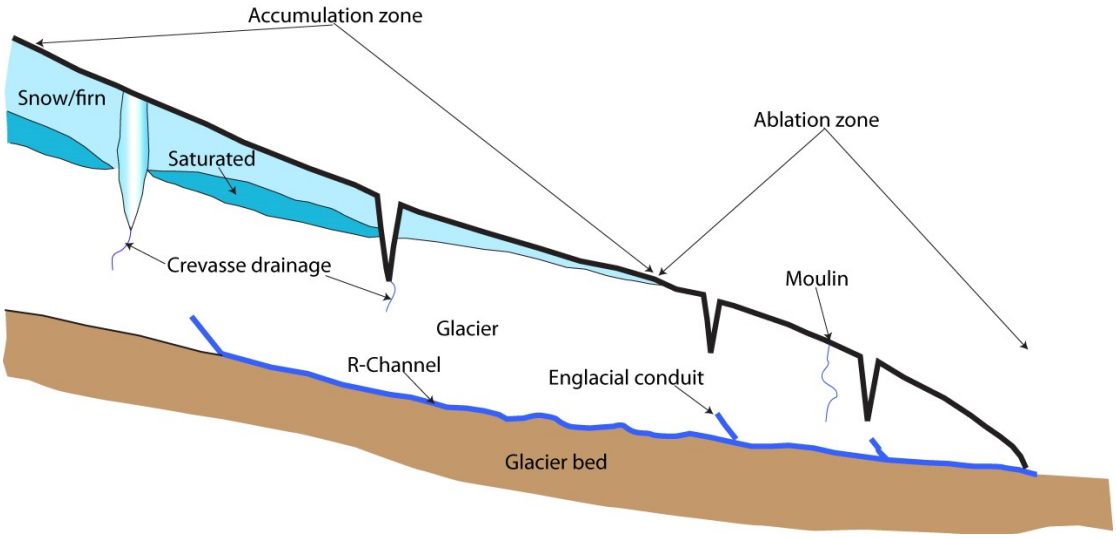

Figure 1.5: Idealized cross-section showing the various water paths within a temperate alpine glacier (modified from Fountain and Walder, (1998); Rothlisberger and Lang (1987)).

Dye experiments and borehole observations in modern glaciers suggests that surface meltwater that reaches the base of a glacier can pass through two different coeval subglacial systems: a network of low-pressure, fast-draining, arborescent (tree-shaped) semi-circular conduits melted up into the ice referred to as R-channels (after Rothlisberger, 1972), and a network of high-pressure, slow-draining, poorly interconnected cavities adjacent to the R-channels (Fountain and Walder, 1998). Water flow within both systems is driven by a hydrostatic pressure gradient that generally parallels the dip of the glacier surface and is far less sensitive to the slope of the substrate (Figure 1.6; Shreve, 1985). The size of R-channels is dictated by the interplay between the rate of channel closure due to creep of surrounding ice (as in Nye, 1953), which increases with ice thickness, and the rate of channel expansion due to melting of the ice, which increases with water discharge (Rothlisberger, 1972). Given that the production of surface meltwater tends to be highly cyclic (seasonal, diurnal), the dimensions of, and

hydraulic pressures within, R-channels also commonly change cyclically. Generally, pressures are highest at the start of the spring melt, when the rate of meltwater production is relatively high and the R-channels are poorly developed. In the height of the summer melt season, conduit dimensions increase with the increased meltwater discharge, and in turn pressures begin to lower. In the winter months, discharge decreases—the only water produced is the steady, year-round flux from basal melting (geothermal heat flux) and strain heating (Boulton et al., 2007)—and channels reduce in size or close completely until spring, when the cycle repeats (Clarke, 2005).

Sudden outbursts of stored meltwater may also augment the seasonal discharge cycle. Rapid drainages of supraglacial or subglacial lakes (termed jökulhlaups) have been documented in modern glaciers (Wadham et al, 2001; Roberts, 2005; Clarke, 2005; Burke et al., 2008). Meltwater is stored by glaciers when sufficient pathways for drainage do not exist. Supraglacial lakes may form in the ablation zone (e.g., Das et al., 2008), and subglacial lakes may develop in bed depressions when the up glacier bed slope exceeds ten times the glacier surface slope (Clarke, 2005). For example, Shoemaker (1992) argues that many of the lake basins on the Shield may have functioned as water storage sites beneath Quaternary ice sheets.

Thermal regime at the glacier bed has also been proposed as a having a strong influence on both glacier movement and routing of internally stored water. Based on studies of modern polythermal glaciers in Svalbard, Murray (2000) puts forth the conceptual model of warm-based ice up-glacier facilitating a surge of fast moving glacial ice, which is inhibited by a frozen, stagnant, cold-based glacier snout. In this model, water travelling along the glacier base through R-channels beneath the thicker, warm-

based ice is routed upward to the glaciers surface over the frozen, cold-based snout as it flows down-gradient toward the ice front. In the glaciers that Murray (2000) studied, this could potentially result in sediment laden efflux from the base of the glacier depositing material on top of the glacier up to 1 km from the ice margin, and generating sediment-rich supraglacial streams.

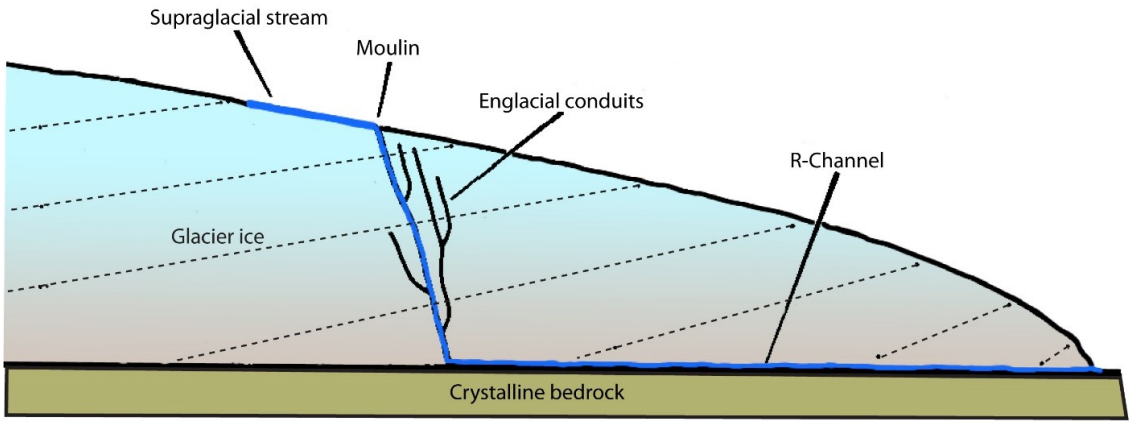

Figure 1.6: Simplified cross-section showing glacial drainage pathways and equipotential lines (dotted lines). Flow is driven by a pressure gradient resulting primarily from the sloping ice front; slope of the substrate is about an order of magnitude less important (Clark, 2005). Hydrostatic pressure increases as ice thickness increases, and flow is from high pressure to low pressure (modified after Shreve, 1985). This figure is typical of water flow through temperate glaciers (i.e. glaciers that are at the pressure–melting point throughout). In polythermal glaciers that transition down-glacier from thick warm-based ice to a thin cold-based glacier snout (e.g., Murray, 2000), the flow of basal meltwater can be different than depicted in that meltwater can be forced to flow from the glacier base up onto the glacier surface causing the terminal portions of R-channels to evolve into supraglacial streams.

1.5 Eskers

Eskers are commonly defined as straight to sinuous glaciofluvial ridges of stratified sand and gravel deposited either in supraglacial, englacial or subglacial streams, or in ice-walled canyons at the glacier terminus (here termed “re-entrants”) (Bannerjee

and MacDonald, 1975; Brennand, 2000; Burke et a.l, 2008). A ubiquitous feature of glaciated terrain, eskers have been studied extensively. European eskers are very similar to their North American counterparts, in both their general morphology, and their regional distribution (Fard, 2002; Fard and Gruzka, 2007). In general, eskers are more abundant on the Canadian and Fennoscandinavian shields than in adjacent areas of Phanerozoic sedimentary rocks (Clark and Walder, 1994; Storrar et al., 2014). The most intensively studied eskers are in populated, easily accessible areas, including New England and southern Ontario and Quebec, where aggregate pits and boreholes provide insight into esker internal heterogeneity (Bannerjee, 1969; Bannerjee and Macdonald, 1975; Buck, 1983; Shreve, 1985a,b; Schulmeister, 1989; Gorrell and Shaw, 1991; Bolduc, 1992; Brennand and Shaw, 1996; Brennand, 1994, 2000; Hooke and Fastook, 2007). Eskers in these regions are commonly tree covered or buried by mud, which can preclude detailed morphological analysis. In Arctic Canada, the opposite tends to be true: aggregate pits and boreholes in eskers are scarce, but geomorphological insight due to absence of trees is unparalleled, and allows for detailed mapping of esker systems (e.g., Aylsworth and Shilts, 1989).

Several main points are generally agreed upon with respect to esker deposition on the Canadian and Fennoscandinavian shields. The lithological similarity between the rounded gravel clasts in eskers and the angular gravel clasts in the subjacent till (e.g., Hellakoski, 1931), along with the fact that eskers commonly reside in corridors eroded discontinuously through the till (variously termed “meltwater corridors” or “esker corridors”; e.g., Kerr et al., 2013), suggest that eskers are eroded from till (Shilts, 1976) by subglacial meltwater and are deposited, at least in part, in subglacial meltwater

conduits (R-channels) (Rothlisberger, 1972; Bannerjee and MacDonald, 1975; Gustavson and Boothroyd, 1987; Gorrell and Shaw, 1991; Brennand, 2000; Delaney, 2002). Not all esker-related sediment is considered to be subglacially deposited, however. For example, flat-topped esker segments can be common in Shield areas (e.g., Dredge et al., 1999) and are generally interpreted to reflect deposition in subaerial conditions. Broader, lobe-like bodies of sediment, typically sandy, are commonly mapped as "outwash" and are typically interpreted to have been deposited where channelized flow expanded and decelerated, with the stream efflux either occurring beneath water level (subaqueous outwash; e.g., Rust 1975), at water level (deltaic outwash; e.g., Dredge et al., 1999), or above water level (subaerial glaciofluvial outwash; e.g., Bolduc, 1992). Some authors have argued that eskers and outwash fans can be deposited entirely or in part supraglacially (Price, 1966; 1969; Shilts et al., 1987; Wolfe et al., 1996), and some esker segments deposited in modern environments are known to be englacial (Burke et al., 2010). Although most authors invoke the need for subglacial meltwater flow through R-channels somewhere within the esker system to explain things like the aforementioned lithological similarity between the till and eskers, a major point of disagreement relates to the length of the R-channels as depicted in Figure 1.1 and discussed previously.

Chapter 2: Esker morphology and surficial sediment cover

2.1 Introduction

Previous surficial geology mapping of remote parts of Northern Canada, including the Lac de Gras region, has tended to rely on 1:60,000 scale stereographic air photos to help interpret landforms and sediment types (Wilson, 1939, 1945; Aylsworth and Shilts, 1989). In many of these studies, little to no ground-truth tests were performed. As such, knowledge of eskers in Northern Canada is largely geomorphological, largely qualitative, and largely macroscopic in perspective (e.g., Prest et al., 1968; Aylsworth and Shilts, 1989; Storrar et al., 2014). Aerial photos are excellent mapping tools, but they provide only a qualitative depiction of three-dimensionality, and therefore cannot easily be used to perform in-depth (quantitative) morphological analyses. Furthermore, esker location and geometry on published maps are reduced to lines (e.g., Wilson, 1939) or chevron symbols (e.g., Ward, 1993) that define the esker axis, with associated polygons denoting areas of "outwash" (e.g., Ward, 1993) (see Figure 1.3). This masks the true complexity of esker morphology and character. Because of the prohibitive cost of establishing comparative ground-truth datasets, almost no systematically collected, well-documented information exists regarding the surficial sediment cover of eskers in Northern Canada.

In this study, a quantitative assessment of the morphology and surficial sediment cover of eskers near Lac de Gras was made possible thanks to high resolution LiDAR data provided by Dominion Diamond Corporation, and to approximately 1870 geo-referenced high-resolution grain-size photographs taken while performing traverses along the Exeter Lake esker and the Misery tributary eskers (Figure 2.1; see digital appendix

for photos and locations). In this chapter, "building block" morpho-sedimentary components that make up the esker are defined based on the LiDAR and surficial sediment datasets.

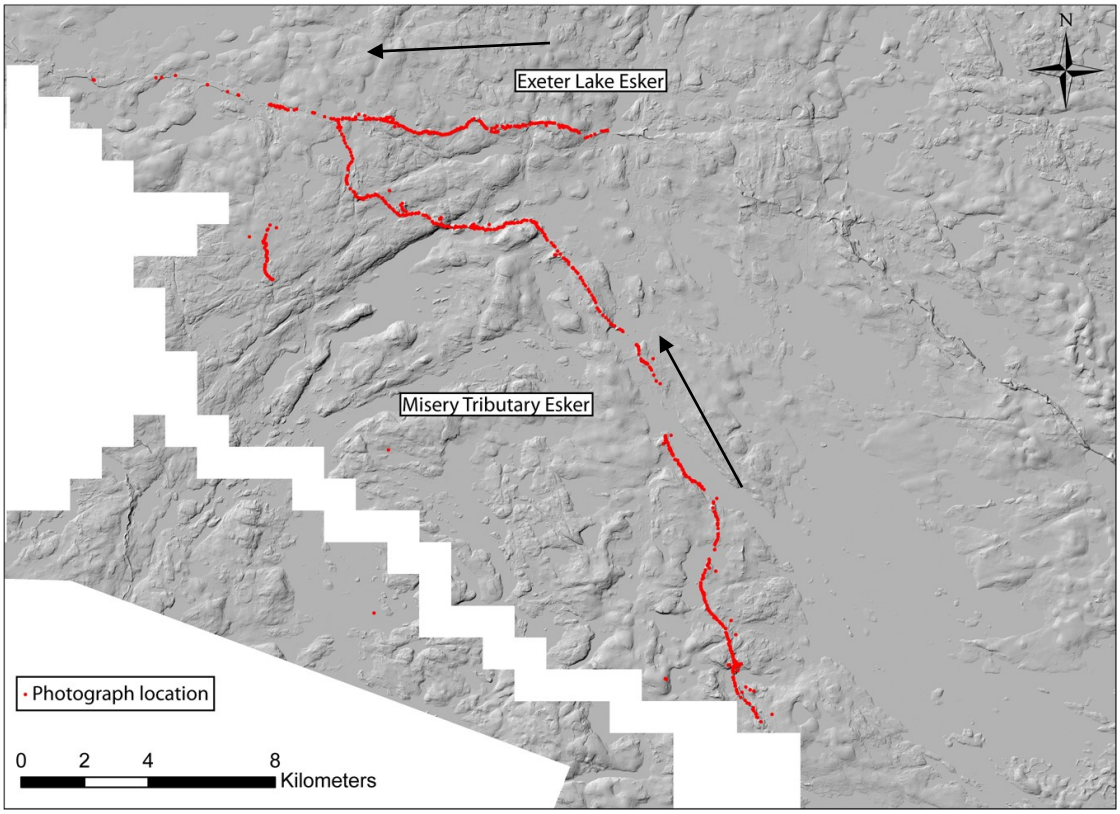

Figure 2.1: LiDAR imagery of study area with locations of grain size photographs (red dots) along the studied portion of the Misery Tributary and Exeter Lake Eskers. Black arrow indicated down esker direction. Detailed maps showing exact grain-size sample locations are presented in Appendix B.

2.2 Methods

The surface morphology of the eskers was studied primarily using LiDAR data. Supplementary insight was gained from aerial orthoimagery and from helicopter fly-overs. The LiDAR data were collected between July 23 and August 1, 2013 by Geodesy Group, prior to my involvement in the project. A Cessna 206 aircraft and a Riegl Q560

laser-scanner were used. The scanner pulsed at 123 kHz resulting in a computed laser point spacing of 0.8 m. In 2014, the owners of the data, Dominion Diamonds, donated the LiDAR data to the Slave Surficial Materials and Permafrost Study (Elliott et al., 2015), and Stephan Gruber (Carleton University) stitched the point cloud data together into a digital elevation model (DEM) with a horizontal and vertical resolution of approximately 1 m per pixel. I obtained the DEM in the spring of 2015 and analyzed it using ArcGIS, along with accompanying aerial orthoimagery obtained during the LiDAR survey (horizontal resolution of 1 m per pixel).

To study sediment forming the surface of eskers, 1874 georeferenced photographs were taken over the course of multiple traverses made while performing the ground-penetrating radar surveys described in Chapter 3. Photography was used to analyze grain size instead of standard lab methods (e.g., sieving) because it was faster and less expensive and, more importantly, because it accurately captured the gravel (>2 mm diameter) fraction, which traditional sampling does not. Photographs were taken at regular ~50 m intervals along the eskers, or wherever a noticeable grain-size change occurred. On sandy esker components, a thin (typically <5 cm) layer of pebbly sediment interpreted to be aeolian deflation lag was typically present that obscured the sandy sediment beneath. At these locations, the lag was brushed away, and the underlying sediment was photographed to capture the representative grain size.

2.3 Results: Morpho-sedimentary components

Four distinct morpho-sedimentary building blocks, here termed esker "components", are identified based on the following criteria: landform width, height, length, and flank slope angle; crest shape in cross-section (flat-crested, sharp-crested or irregular); position (i.e., located along esker ridge or flanking/detached from esker ridge); average grain-size of the surficial sediment; and presence or absence of down-flow-fining trends in the surficial sediment (Table 2.1). These components are described below, whereas interpretation is reserved for later chapters following a description of the internal heterogeneity (sedimentary architecture) of the components and their stratigraphic lap-out relationships. Location maps for the LiDAR images in this section are shown in Figure 2.2.

Table 2.1: Esker components: morphology and surficial sediment

LANDSCAPE ELEMENT	COMPONENT	SURFICIAL SEDIMENTS			MORPHOLOGY					
		Grain size (average, range)	Down-flow fining?	Sparse, angular boulders (absent, rare, common)	Height (average and range)	Width	Length	Slope of flanks	Ice polygons (absent, rare, common)	Crest shape in cross-section (sharp, flat-topped, broadly sloping, or irregular)
ESKER	Type 1. Sharp-crested cobbly to bouldery ridges	Cobble (pebble to Boulder	Rare	Rare	10 – 28 m (15 m average)	25 – 150 m (80 m average)	200 m – 1.3 km (600 m average)	23- 35° (30° average)	Absent	Sharp
	Type 2. Flat-topped cobbly to sandy ridges	Coarse sand to pebbles (fine sand to cobbles)	Common	Rare. Typically concentrated along the margins (sides and distal edge) of the Type 2 component.	2 - 25 m (10 m average)	50 – 200 m (100 m average)	500 m – 1.5 km (800 m average)	6 – 30° (20° average)	Common	Flat topped to broadly sloping
	Type 3. Flat-topped sandy to cobbly pads	Coarse sand to cobble	Common	Absent	4 -25 m (8 m average)	100 – 300 m (150 m average)	200 m – 800 m (400 m average)	4 – 30° (20° average)	Common	Flat topped
ASSOCIATED SEDIMENT	Type 4: Pads	Coarse sand (medium sand to cobbles)	Absent	Absent	4 – 20 m (10 m average)	50 - 200 m (150 m average)	50 - 200 m (150 m average)	15 – 25° (18° average)	Common	Broadly sloping to irregular
	Type 4: Splays	Fine to medium sand (Fine sand to pebbles)	Common	Rare	0 – 10 m 3 m average	50 – 300 m (150 m average)	~ I km	3 - 10° (5° average)	Rare	Flat
ADJACENT TERRAIN	Diamicton (till)	Poorly sorted mixture of sediment (mud to boulders)	N/A	Common	N/A	N/A	N/A	N/A	Absent	Commonly hummocky (hummocks are large → up to 30 m high by 800 m wide)
	Exposed bedrock	N/A	N/A	N/A	N/A	N/A	N/A	N/A	Absent	N/A

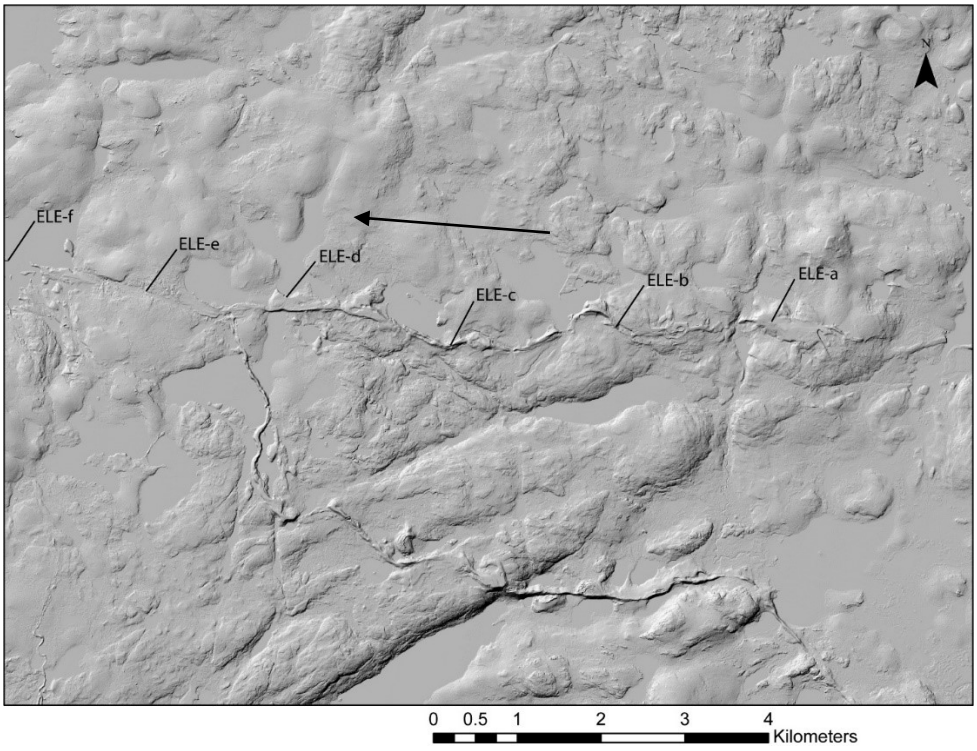

(a)

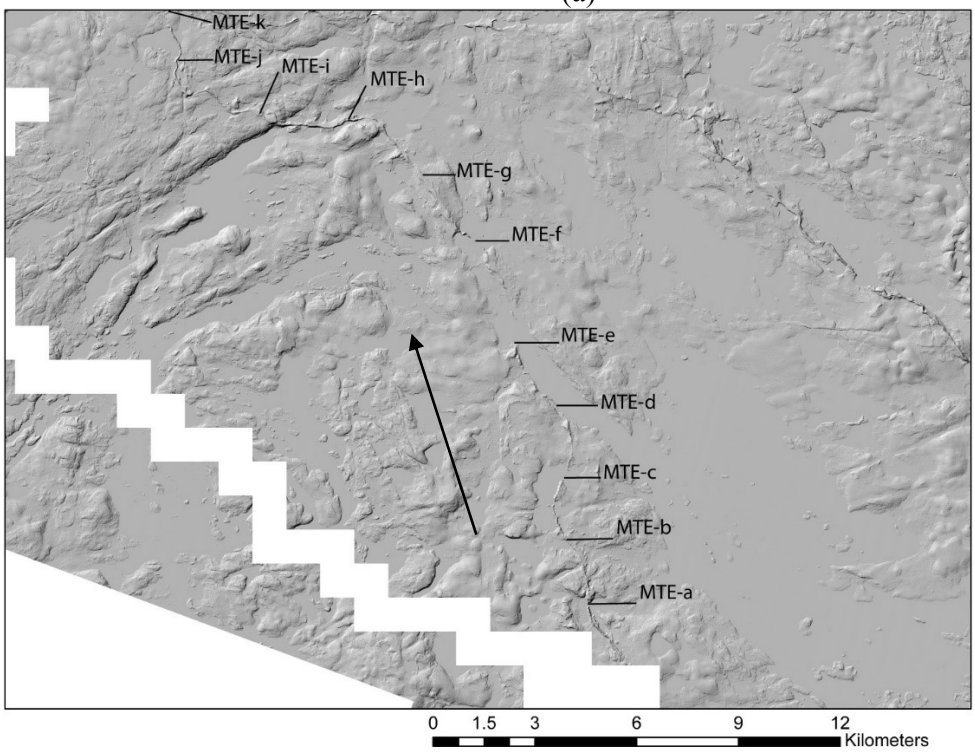

(b)

Figure 2.2: Location maps: (a) The Exeter Lake esker (ELE), and (b) the Misery tributary esker (MTE). Black arrows indicate the down-esker (down-flow) direction. Lines indicate down-esker extent of respective images. Entire studied extent of esker is presented and described in Appendix A.

Type 1 components: Narrow, sharp-crested, gravel ridges

Type 1 components are sharp-crested gravelly ridges that range from 10 to 28 m in height (Figures 2.2, 2.3). They form part of the main esker ridge. Surficial sediment generally consists of well-rounded, clast-supported pebbles to boulders (average grain size is cobbles) with a matrix of sub angular coarse sand to granules. Typically, Type 1 ridges have steep (approximately 25° average) flanks, but in some localities where the landform is lower in height, the flank angles are more gently sloping (see Figure 2.2 vs. Figure 2.3). Type 1 components rarely exceed 120 m in width, and crests are often relatively sharp, which tends to give these components triangular cross-sections. The crests commonly undulate periodically down esker, with wavelengths of 100–200 m and vertical peak-to-trough distances of several meters (maximum 10 m). The overall elevation of surfaces of Type 1 components can either decrease or increase downflow. In places, Type 1 components are punctuated by "hillocks", which are defined as elevated regions (30–300 m long, 20–50 m wide, 5–10 m high) of the Type 1 ridge that rise up above the level of the rest of the ridge. Coarse pebbles to boulders cover the up-esker (stoss) side of hillocks, whereas pebbly coarse sand covers the top and down-esker (lee) side of hillocks. Rare step-like, ridge parallel post-depositional slump features are present on the flanks of Type 1 components. In contrast to Type 2, 3 and 4 components, Type 1 components lack tundra polygons and kettle holes.

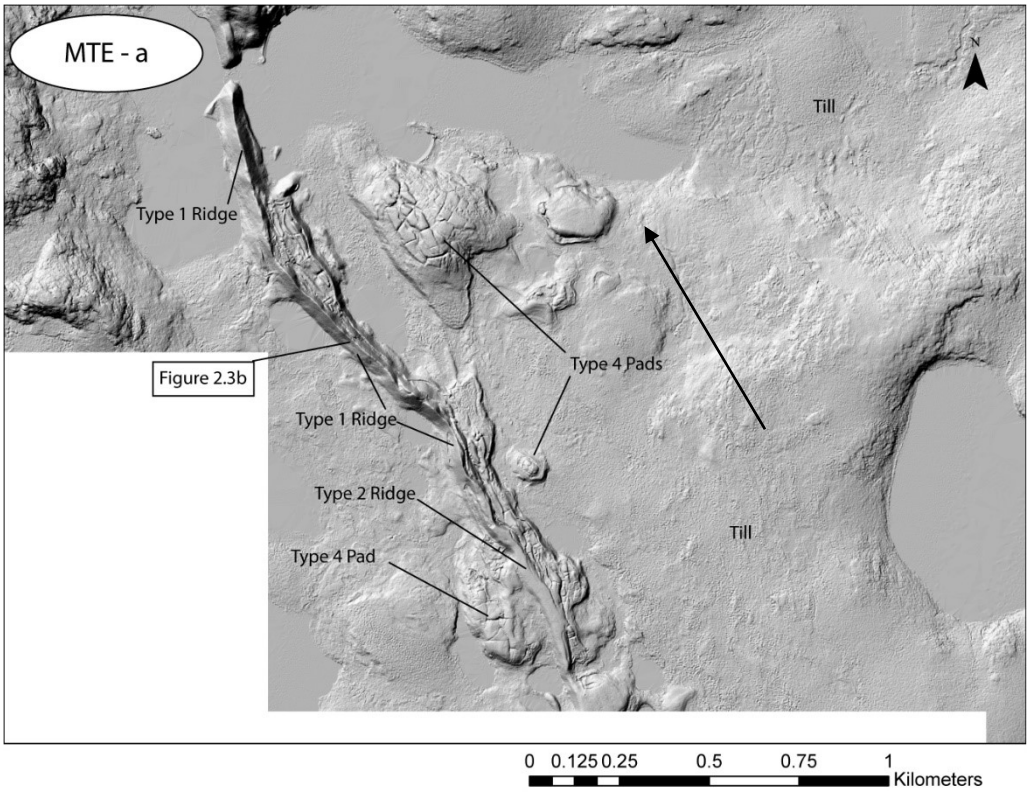

(a)

(b)

Figure 2.3: A typical Type 1 component. (a) LiDAR image showing the location of the Type 1 component in the MTE-a area along the Misery Tributary esker (see Figure 2.2 for location of the MTE-a area). Down-flow direction is to the top of the image. Till surrounding the esker in this area is thin as indicated by the lack of pronounced till hummocks. Post-depositional deformation is interpreted to be related to the melt-out of buried ice as shown along the eastern flank of the main esker ridge. Detached Type 4 pads are present off-esker. (b) Field photo of the sharp crested, boulder-dominated Type 1 component of (a). Down-flow direction is into page.

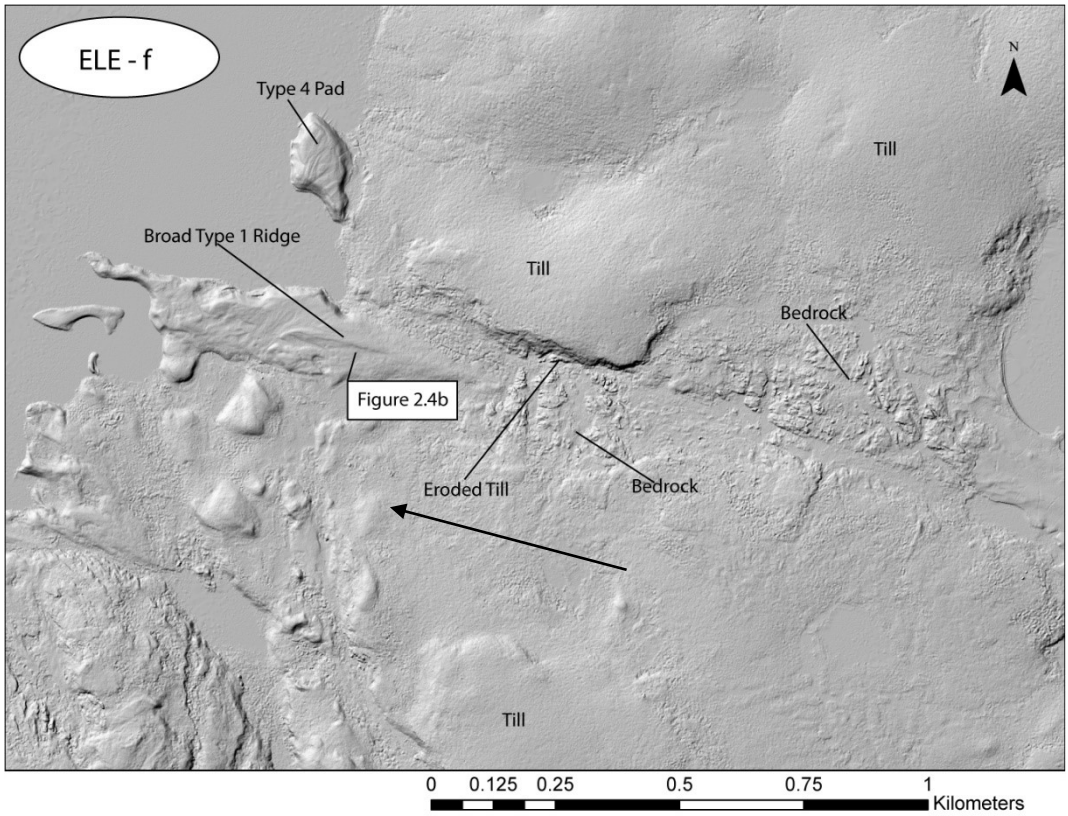

(a)

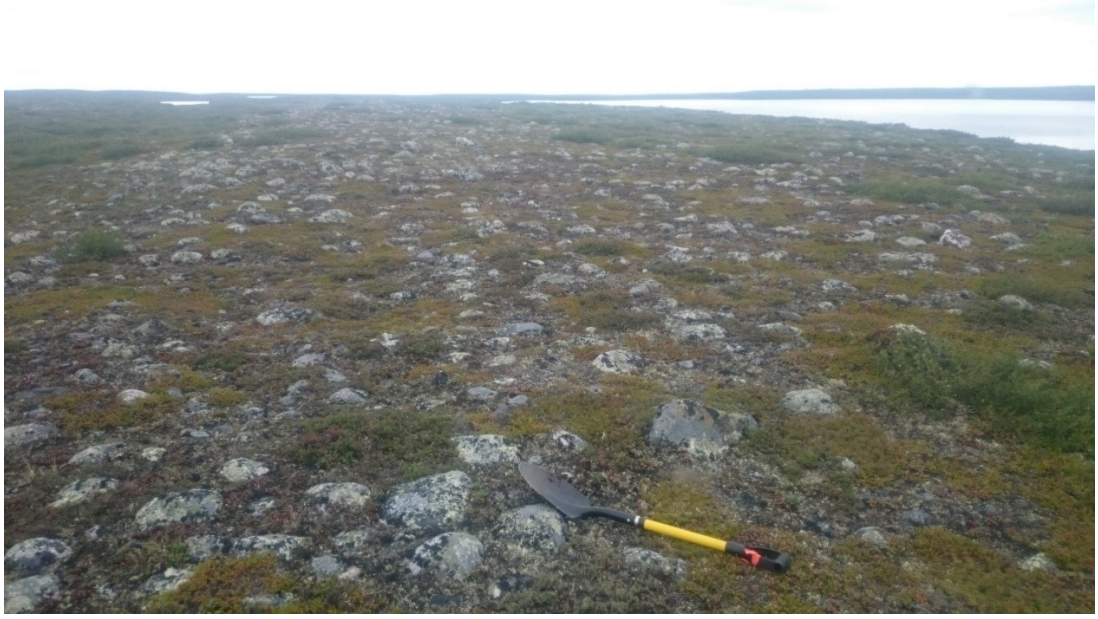

(b)

Figure 2.4: An abnormally low-lying and broad-crested Type 1 component. (a) LiDAR image showing the location of the Type 1 component in the ELE-f area along the Exeter Lake esker (see Figure 2.2 for location of the ELE-f area). Down-flow is to the left. The component occurs downstream of, and within, a zone where till has been eroded and bedrock exposed. (B) Field photo of the Type 1 component in (A). Down-flow is into page.

Type 2 components: Narrow, flat-topped, sand to gravel ridges

Type 2 components consist of narrow (20–200 m, approximately 80 m average), low to high (5–25 m, average 10 m), flat topped to irregular sediment bodies that form part of the main esker ridge (Figures 2.5). Type 2 components often appear flat-topped in LiDAR images, but on the surface, they are commonly marked by very gentle, irregularly spaced undulations (Figure 2.5). Flank slopes range from 5 to 35°, and are on average steep (~20°). Surficial sediment is finer on average than that of the Type 1 components, ranging from clast-supported cobbles with a coarse sand matrix to well sorted fine sand. As with Type 1 components, the cobbles are generally well rounded, whereas sand grains and finer gravel-size clasts (<1 cm diameter) are generally sub-angular. Rarely, sparse accumulations of angular boulders are observed strewn in places along the distal, and in many cases finer-grained, peripheries (the sides and/or distal edges) of Type 2 components. As with Type 1 components, the overall elevation of Type 2 components can either decrease or increase downflow, depending on the locale. In certain locales, post-depositional collapse features are present on Type 2 components: kettle holes are observed in the center of some of the components, and ridge parallel slump features can be present locally at their periphery.

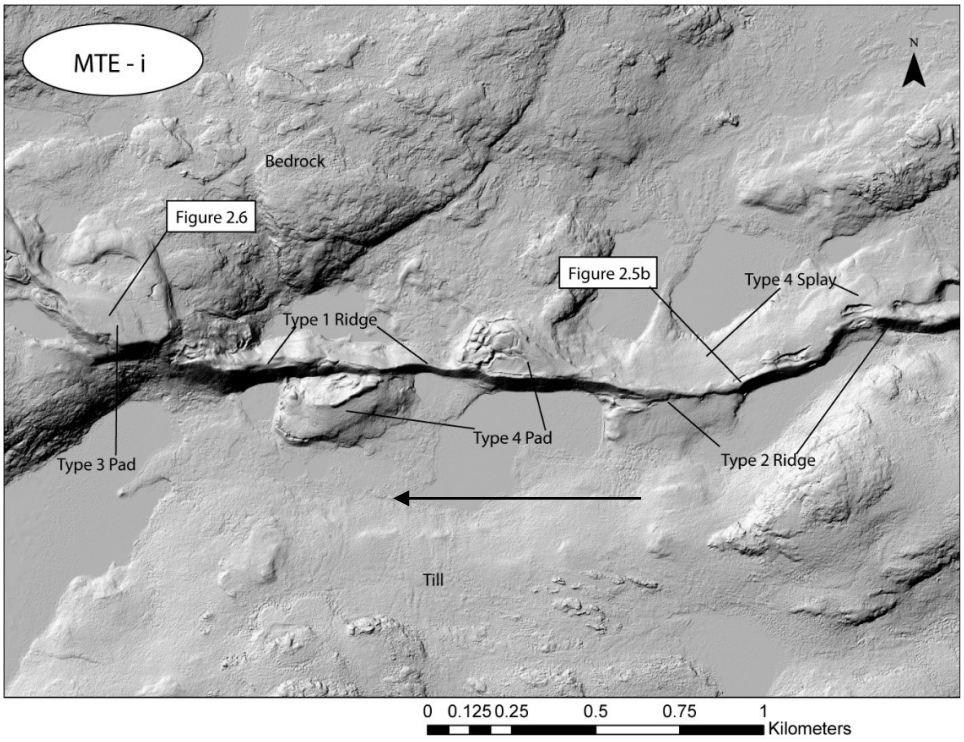

(a)

(b)

Figure 2.5: A typical Type 2 component. (a) LiDAR image showing the location of the Type 2 component in the MTE-i area along the Misery Tributary esker (see Figure 2.2 for location of the MTE-i area). The central ridge in the eastern (upflow) portion of esker in this image is the flat-topped Type 2 component in question. It is flanked on both sides by a sandy Type 4 splay. Down-flow of this, a Type 4 pad, showing evidence of post glacial deformation by ice wedging and melt out, is present at the terminal end of the flanking splay. A large, very irregular Type 1 ridge dominates farther down-flow, flanked to the south by another Type 4 pad. This Type 1 ridge ends and abruptly transitions down-flow into large Type 3 pad at a bedrock high. (b) Field photo of the Type 2 component. Down-flow is into page.

Type 3 components: Wide, flat-topped sand to cobble sediment ridges

Type 3 components are wide (100–250 m), high (up to 25 m above till plain) flat- to irregular-topped sediment bodies ("pads") (figures 2.6, 2.7). They are similar to Type 2 components, but represent a significant widening, and, in some cases, an abrupt increase in elevation, of the main esker ridge. Type 3 components are covered by well-rounded, clast-supported pebble- and cobble-size gravel with a coarse sand matrix. In places, cobbles are imbricated and dip in an up-flow direction. The flanks of Type 3 components range from gently sloping (5–10°) to steep (35°). Over the length of Type 3 components, elevation commonly remains constant, and they generally lack the undulations seen in Type 2 components, although they have irregular top surfaces locally. Post-depositional collapse features are rarely present on the flanks of Type 3 components. Circular, kettle-like depressions, often containing standing water, are common (Figure 2.7) as are tundra polygons.

Figure 2.6: A typical Type 3 component. Note the wide, relatively flat topped, imbricated cobble -covered surface. Down-flow direction is into the page. See the LiDAR image in Figure 2.4A for the location of this Type 3 component along the Misery Tributary esker.

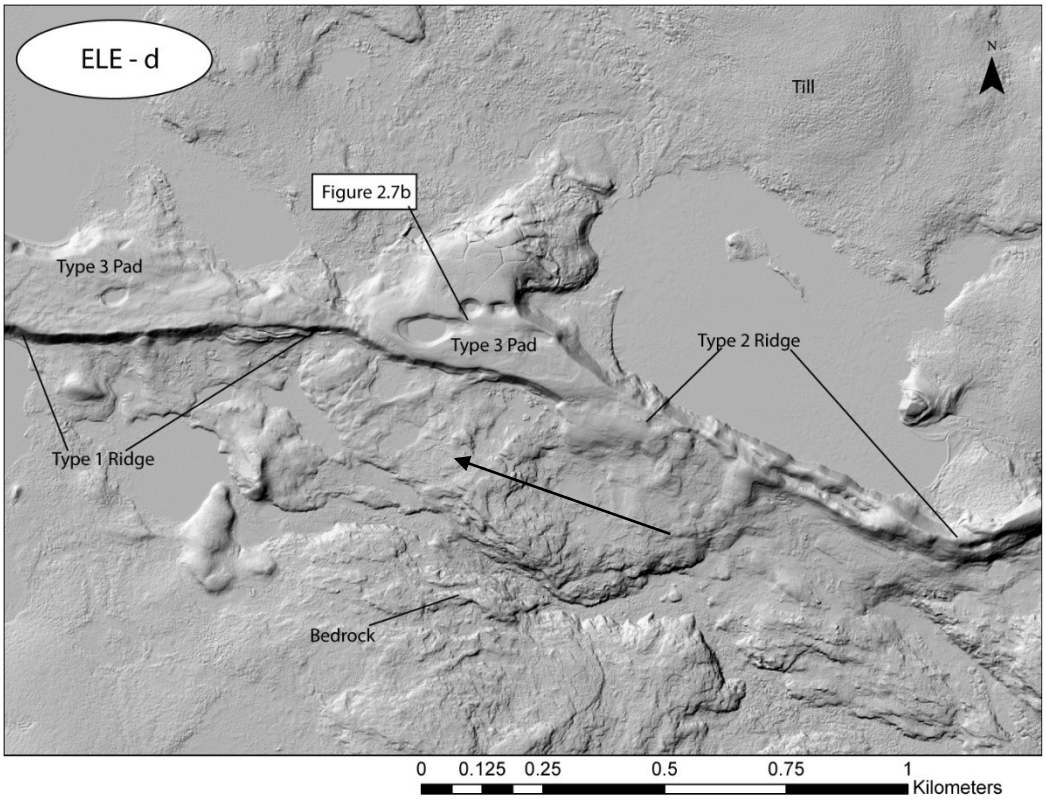

(a)

(b)

Figure 2.7: A kettle on the surface of a Type 3 component. (a) LiDAR image showing the location of several kettle holes, including the one pictured, on a Type 3 component in the ELE-d area of the Exeter Lake esker (see Figure 2.2 for the ELE-d area location). Down-flow is to the left (see black arrow). (b) Photo of one of the kettle holes on the Type 3 component shown in (a). The surface of the Type 3 component and bottom of kettle depression are covered in pebbles and cobbles, whereas the flanks of kettle hole, which expose the underlying strata, are sandy.

Type 4 components: Detached or flanking sand and gravel bodies

Type 4 components are similar to Type 3 components, but, as opposed to forming enlargements of the main esker ridge, they represent sand or gravel bodies that extend out from one side of, or are completely detached from, the main esker ridge. They display two general morphologies. Wide (100–200 m in width), irregular topped sediment bodies that are morphologically similar to Type 3 components but are semi-attached or detached from the main esker ridge by up to 200 m are termed Type 4 ”pads” (Figure 2.8; see also Figures 2.3 and 2.5). Type 4 pads are covered by medium sand or, in places, pebbly coarse sand with rare cobbles (Figure 2.8b). The second type of Type 4 component are termed Type 4 “splays” (Figure 2.5a). Whereas Type 4 pads are elevated sediment bodies, Type 4 splays are low-relief (1–7 m high relative to the adjacent till plain, average 3 m) sediment bodies that flank the main esker ridge. They are 100 to 400 m wide and up to 1 km long, and are covered by well-sorted sediment ranging from fine sand to pebbles. They gently slope and become thinner moving laterally away from the main esker ridge. Type 4 pads and splays share similar post-depositional features, including tundra polygons and landform collapse features often resulting in an undulating, irregular surface (Figures 2.3, 2.8).

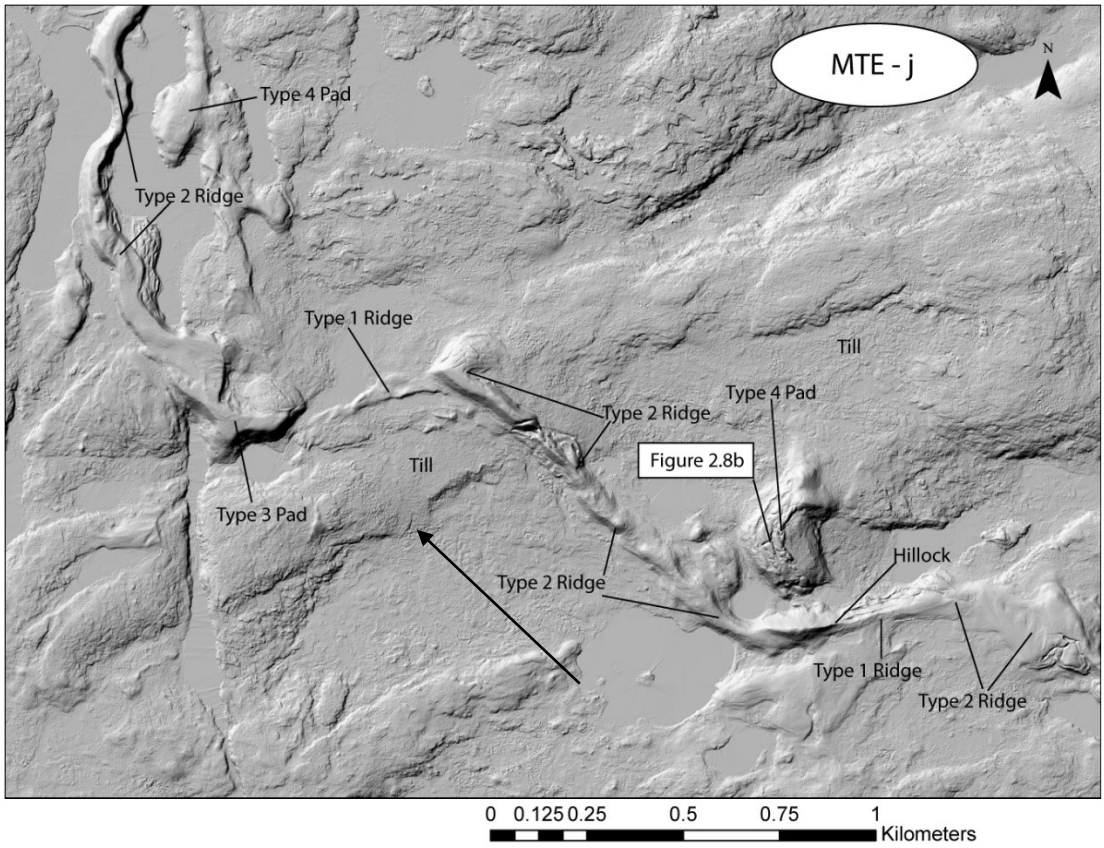

(a)

(b)

Figure 2.8: A typical Type 4 pad component. (a) LiDAR image showing the location of the Type 4 component in the MTE-j area of the Misery Tributary esker (see Figure 2.2 for MTE-j area location). Down-esker is to the left (see black arrow). (b) Field photo showing the surface of the Type 4 component in (a). Down-esker is approximately into the page.

2.4 Results: Relationship between esker and adjacent terrain

Till is the dominant sediment type adjacent to the eskers (Figure 1.3). It was not studied in detail during this project but is described briefly here to provide context. The till is poorly sorted, has a silty sand matrix, and contains angular to subrounded clasts varying in size from pebbles to boulders (Figure 2.8). Drilling conducted by other members of the Slave Province Surficial Materials and Permafrost Study (unpublished results) suggest that the till can contain significant amounts of ice in the form of thin horizontal layers and lenses. In contrast to the esker components, the surface of the till is invariably covered in meter-scale mudboils, similar to those described by Shilts (1978), and these mudboils are visible in LiDAR, which facilitates differentiation of till from esker-associated sediment. The till between eskers near Lac de Gras is generally thick, ice-rich and hummocky (Dredge et al., 1999), and its surface appears smooth in LiDAR data, mudboils notwithstanding. By contrast, in some regions immediately adjacent to the esker, the till is absent or thin (3 – 5 m) and bedrock is exposed (e.g., Figure 2.4A). Where present, these zones extend out between 50 and 500 m in either direction from the main esker ridge. These zones of thin till and exposed bedrock adjacent to eskers are commonly referred to as "esker corridors" or "meltwater corridors" (e.g., Craig, 1964; Rampton, 2000). Corridors can be difficult to define because they are discontinuous over 100s of meters to kilometers down-esker, and they typically pass imperceptibly into thicker hummocky till moving outward from the eskers, although, rarely, cutbank-like scours define their edges (Figure 2.9).

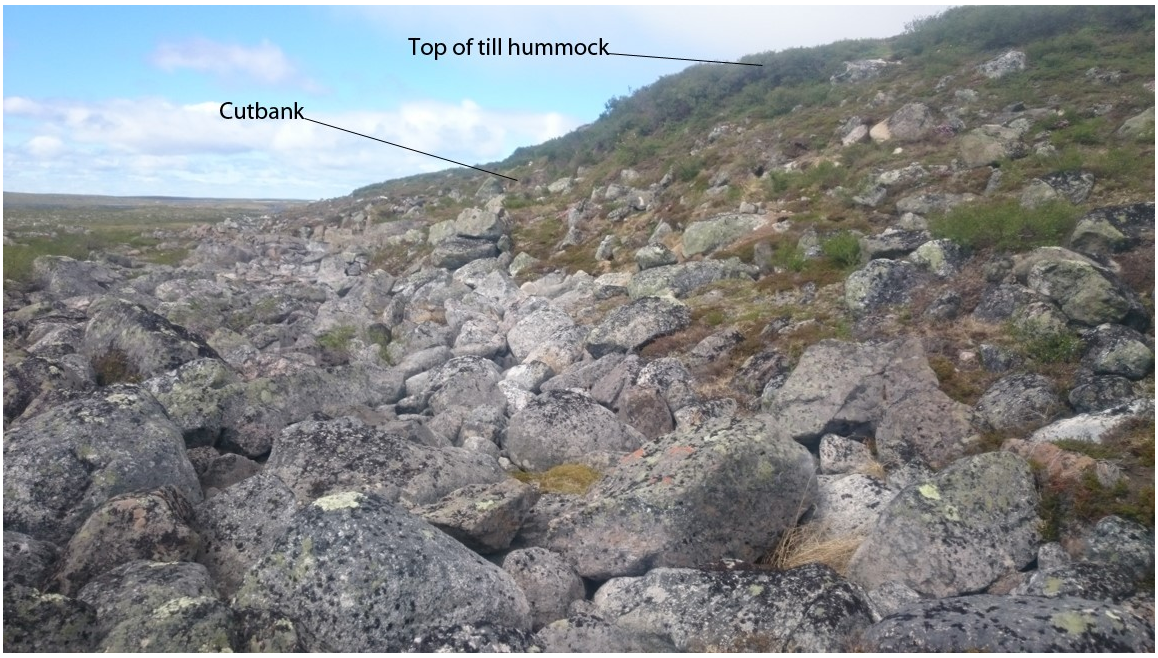

Figure 2.9: Cutbank eroded into a till hummock at the north edge of the esker corridor shown in Figure 2.2A. Note large subangular boulders comprising a large fraction of the till in this location. The subangular boulders in foreground have been eroded from the till cutbank but have not been displaced significantly in a down-flow direction. They are on average 50 cm in diameter. Down-flow is into the page.

2.5 Results: Downflow trends in morphology and surficial sediment

a) Small-scale down-esker trends

The surficial sediment that covers Type 1 components generally does not fine or coarsen systematically in a down-flow direction (Figures 2.10, 2.11). The one exception to this occurs just down-flow of the tributary junction between the Misery and Exeter Lake eskers (Figure 2.12). Here, a zone of scoured bedrock passes down-flow into a low and flat Type 1 ridge. The surface of the Type 1 ridge fines down-flow over a distance of 800 m, from well-rounded boulders to well-rounded cobbles, before gradually transitioning into a broad, flat Type 2 ridge (which in turn continues to fine down-flow,

for a total distance of 3 km; not shown in Figure 2.12). In contrast to this example, non-systematic variations in grain size along other Type 1 ridges are common, and are typically due to the presence of skiffs of pebbly coarse sand that drape the ridge.

The surficial sediment on Type 2 and Type 3 components commonly fines systematically in a down-flow direction (Figures 2.10, 2.11). The fining tends to be gradual, although the rate of fining and the horizontal extent over which it occurs are not always consistent. Type 4 splays and pads do not have clear down-flow fining trends. Where splays of sediment drape the main esker ridges, sediment texture remained consistent along their length.

In many places a predictable down-esker succession of component types is observed. Type 1 components commonly transition down-esker into Type 2 or Type 3 components. In some places, wave-like "hillocks" mark these transitions. Type 2 components commonly either terminate down-esker at a water body, or pinch out onto till, bedrock, or an emerging Type 1 ridge. Less commonly, they abruptly widen to a Type 3 component. The locations of Type 3 components is difficult to predict. They appear to follow no distinct trend with respect to preceding esker components, but are always characterized by an abrupt widening of the landform. The location of Type 4 components is likewise difficult to predict, although one large, prominent ice-wedge-covered Type 4 pad in the MTE-a area (Figure 2.2) appears to shoot off and form a continuation of the main ridge of the esker, but one that is separated from the main ridge by 200 m of exposed till plain.

b) Larger-scale down-esker trends

Across the study area, no net down-flow grain-size fining trend is observed along either the Misery tributary esker (28 km) or Exeter Lake esker (13 km). Likewise, no progressive, net down-flow change in cross-sectional area (width or height) of the landforms is apparent.

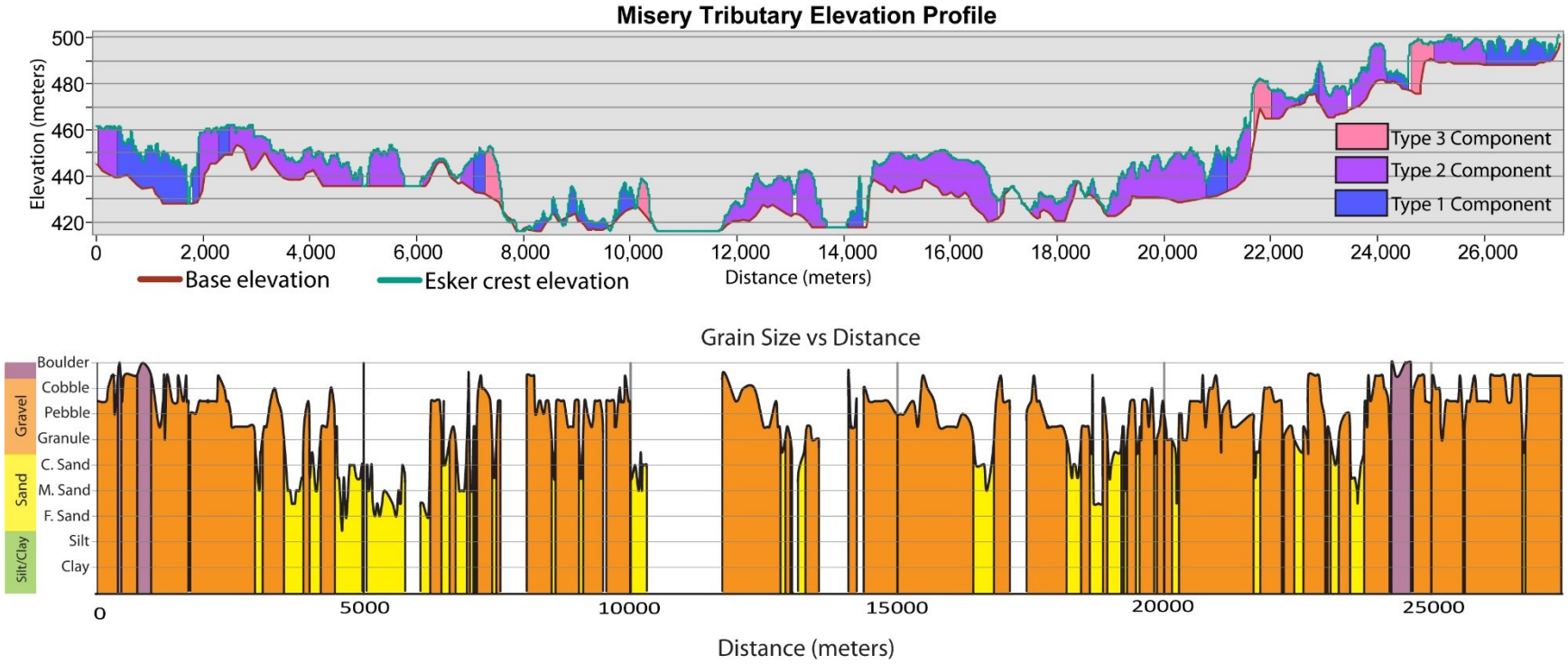

Figure 2.10: Elevation profile and grain size chart of the Misery tributary esker showing position of esker components. Down-flow is to the right. White areas along profile correspond to segments where esker material is absent, obscured by heavy vegetation, submerged beneath a lake, or otherwise indiscernible from the surrounding till. See Appendix B for detailed maps showing surficial grain size over the studied extent of the Misery Tributary Esker. Base elevation corresponds to the elevation of the ground and lakes adjacent to the esker (lakes occur where base elevation is flat).

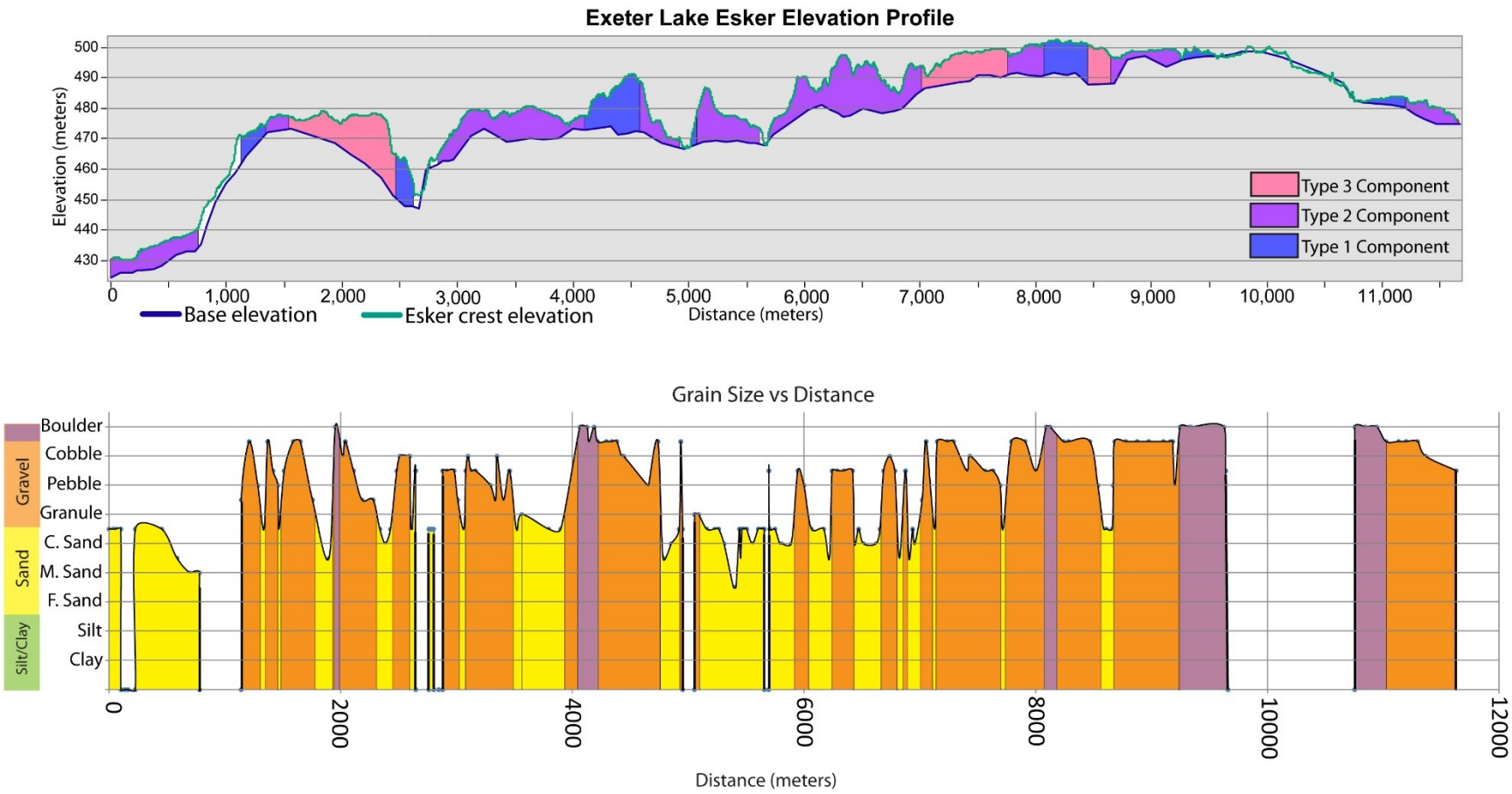

Figure 2.11: Elevation profile and grain size chart of the Exeter Lake Esker showing positions of esker components. Down-flow is to the right. White areas along profile correspond to segments where esker material is absent, obscured by heavy vegetation, submerged beneath a lake, or otherwise indiscernible from surrounding till. See Appendix C for detailed maps showing grain size over the studied extent of the Exeter Lake Esker. Base elevation corresponds to the elevation of the ground and lakes adjacent to the esker (lakes occur where base elevation is flat).

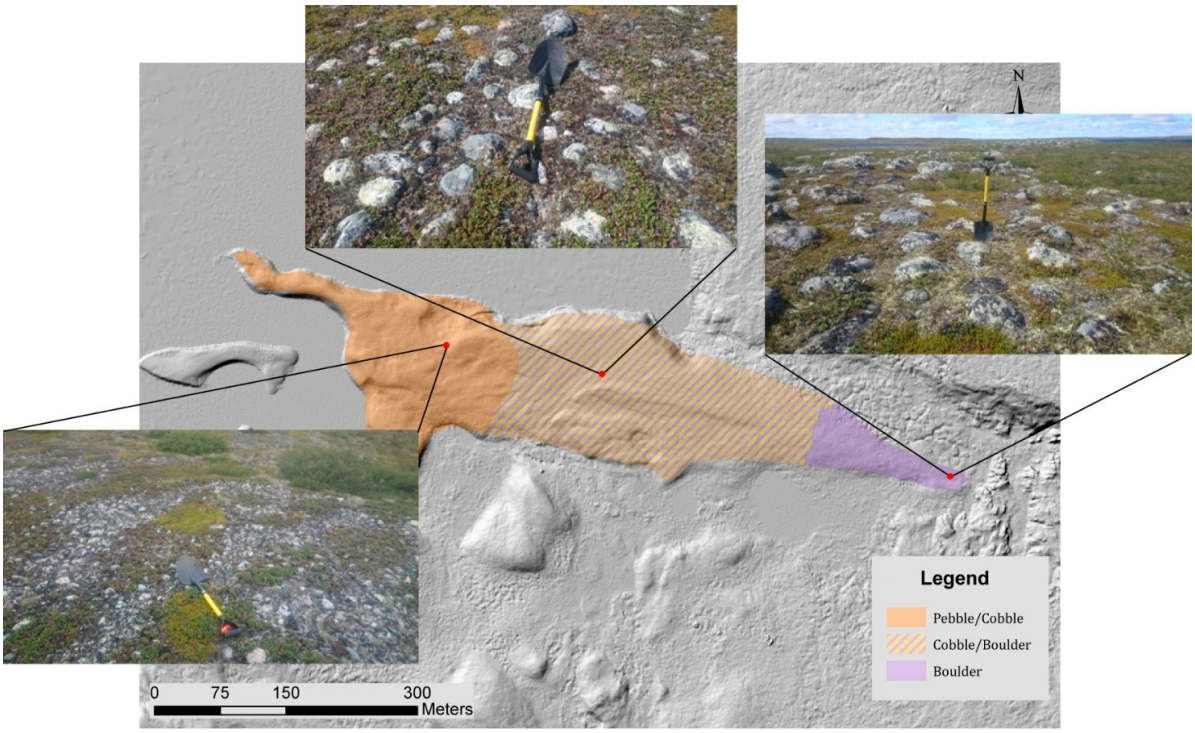

Figure 2.12: Down-flow fining segment from ELE-f area (Figure 2.2) with inset photographs showing surface texture. Down-flow is to the left. Segment continues to fine down-esker to coarse sand after break in esker at lake, for a total length of 3 km long (down-flow portion not shown here).

Chapter 3: Sedimentary architecture - Ground penetrating radar and augered boreholes

3.1 Introduction

A ground penetrating radar (GPR) survey was performed and several boreholes were drilled to gain insight into the sedimentary architecture of the eskers. Ground penetrating radar (GPR) is a geophysical sensing technique used to image cross-sections of the shallow subsurface. Although primarily used in industrial applications in urban areas where accurate knowledge of the subsurface is required and excavation is not possible, such as utility locating and infrastructure evaluation, numerous studies have also proven GPR effective at imaging the extent, shape, orientation and lap-out relationships of packages of beds within sedimentary bodies (i.e., "sedimentary architecture"; see Smith and Jol, 1997; Neal, 2004; Burke et al., 2010). The ability of GPR to image bedding in sedimentary deposits stems from the order-of-magnitude greater dielectric permittivity (K) (often referred to as relative permittivity) of water relative to most other subsurface materials (e.g., sand, gravel, air and ice; see Cassidy, 2009b), and to the fact that the amount of water present tends to vary from bed to bed in conjunction with variables like grain size, sorting, packing and porosity. Dielectric permittivity (K) is a measure of a material's resistance to becoming polarized by an external electric field: materials with high dielectric permitivities, like water, readily become polarized. Radar waves reflect off of interfaces between media with different dielectric permitivities. Conductivity of a material is also important because materials with high conductivities contain free charges that, when subjected to an applied

electromagnetic field, will flow through the material, causing loss of energy and attenuation of the GPR signal. Highly conductive media, such as clay-rich sediment or salt-water aquifers, are therefore unsuitable for imaging with GPR. Esker sediments derived from crystalline bedrock are an ideal medium for GPR (e.g., Burke et al., 2010) because they generally consist of well-sorted (clay-poor) sand and gravel, and have pores that are saturated with fresh water, air, and/or ice. In addition to sedimentary bedding, which is imaged primarily due to the above-mentioned variations in water content, another major feature that one commonly images in sedimentary media is the groundwater table, or in polar settings the permafrost table, provided a film of water is pooled on top of it, because significant jumps in dielectric permittivity tend to occur across these surfaces (e.g., Arcone et al., 1998; Annan, 2004).

At its most basic, a GPR imaging system consists of a transmitter antenna and a receiver antenna at a fixed distance apart (Annan, 2004). The transmitter emits a radio-wave pulse of a given frequency into the ground and the receiver listens for reflections of this radiation coming back from the ground at the same frequency. At each position on the survey line, a pulse is emitted and travels through the ground. When these waves encounter a difference in K, some of the energy is reflected back towards the surface, and some of the energy is permitted through the material. This takes place until all of the energy from the original pulse has dissipated. The time between transmission and reception is measured and recorded, and an image of the reflections can be generated by plotting horizontal distance (x axis) versus two-way travel time (y axis).

Following acquisition, the y-axis of GPR transects can be converted from two-way travel time to depth if the velocity at which the radar waves travel through the ground is

known. The method employed in this study to determine velocity is a process called hyperbola fitting (see Annan, 2004). This method can be used if there are hyperbola-shaped reflections in the GRP transects, such as those generated by point-source reflectors like buried wires, pipes, or boulders (e.g., Annan, 2004). Because the emitted pulse has a hemispherical wave front, and because point-source reflectors will reflect some energy back towards the source, the receiver will begin recording reflections from point-source reflectors before the receiver antenna is directly over top of them. As the unit moves closer, reflection time decreases, reaches a minimum above the buried object, then increases again as the unit moves beyond this point. The net effect is a downward-opening hyperbola-shaped reflection in the GPR transect, the opening angle of which is dictated by the velocity that the waves travel through the ground. A narrow hyperbola (small angle) indicates a low velocity material, and a wide hyperbola (large angle) indicates a high velocity material (which, in the extreme, will approach the speed of light in air, approximately 0.3 m/ns). Software can be used to approximate the curve of the hyperbola and to determine velocity, which can then be used to convert the transects from time to depth.

3.2 Methods

Two separate GPR surveys were conducted, one using 100 MHz antennas, which image the ground to greater depth but at a lower resolution, and one using 500 MHz antennas, which image the ground at a higher resolution but to a shallower depth.

Between the two surveys, 151 GPR transects were collected and processed, for a total of 150 line kilometers.

The 100 MHz survey (Figure 3.1a) was performed using a MalaGS Rough Terrain Antenna. The objective of the 100 MHz survey was to image the internal sedimentary architecture of the building-block components that make up the esker (Type 1 to 4 components), and to ascertain the stratigraphic lap-out relationships between these components. Survey parameters were as follows: 832 ns time window and 1048 MHz sample frequency, with time triggered sample acquisition every 0.25 seconds. Handheld GPS readings were automatically recorded and attached to the collected data at a 2 second interval. To reduce noise, samples were stacked using MalaGS autostacking function. Selected locations were surveyed multiple times to ensure results were reproducible and of good quality. Survey transects were collected by walking along the crest of the esker in a down-esker (down flow) direction. Transects that cross the esker perpendicularly were also collected at numerous locations. At total of sixty one 100 MHz GPR transects were collected.

The 500 MHz GPR survey (Figure 3.1b) was performed over selected parts of the esker using a MalaGS 500 MHz shielded antenna. The objective of the 500 MHz survey was to image the near-surface sedimentary architecture of sandier portions of esker in greater detail. The survey consisted of 90 shorter transects collected primarily over flat-topped Type 2, 3 and 4 esker components. Due to the nature of the 500 MHz antenna, rough, undulating ground (e.g., bouldery Type 1 components) could not be surveyed. Sampling frequency was 6355 MHz over a time window of 105 ns, stacked 4 times. Data acquisition was triggered by a measuring wheel every 2 cm. Position was recorded by a

handheld GPS and automatically synched to the GPR data at approximately 4 second intervals.

Data processing was performed with ReflexW software. All 100 and 500 MHz transects were subjected to the same processing steps, with slightly varying parameters (see Annan (2004) and Cassidy (2009a) for details on these processing steps). The processing steps were recommended by Aurora Geoscience, owners of the GPR equipment, and are similar to those used by Matthew Burke, who succesfully imaged sedimentary architecture of eskers in Iceland and Alaska (Burke, personal communication, 2015). A dewow filter was first applied, then a start-time correction. Trace samples were then interpolated using the GPS data to have a spacing of 25 cm for the 100 MHz, and 2 cm for the 500 MHz. For the 100 MHz survey, traces were back-stepped 5 metres down the transect path vector to compensate for the distance between the GPS device and the midpoint between the transmitter and receiver antennas. This processing step relied on a tailor-made program written by Stephan Gruber (Carleton University) using R software. Next, bandpass and background removal filters were applied, followed by a divergence compensation gain adjustment. The final step was an elevation correction, using elevation values extracted from the LiDAR data. The resulting images show elevation corrected transects that preserve the hyperbola-shaped reflections generated by buried boulders, and the relative strengths of reflections at different depths. Velocity of the material was calculated by the aforementioned hyperbola-fitting method, and was in places modified slightly by information obtained by drilling augered boreholes. Velocity for the bulk of the medium being imaged (frozen

sediment) was calculated to be approximately 0.13 m/ns, and this closely aligns with drilling results.

Using the LiDAR data as a guide, 39 potential borehole locations were selected to target Type 1 to 4 components along both the Exeter Lake esker and Misery tributary esker. Points West Heritage Consulting Ltd performed an archaeological assessment, and they concluded that eight of the locations, all along the Misery tributary esker, had a sufficiently low risk of encountering an archeological site to justify drilling (Ross, 2015). All eight of these locations were approved for drilling by the Prince of Wales Northern Heritage Centre in Yellowknife prior to the summer 2015 field season (Figure 3.1). Drilling was completed with a custom designed, light-weight, low RPM drill that was moved from location to location by helicopter. Of the equipment available to the program, the auger bit proved most effective at drilling the eskers. Although this meant that there was no core recovered, useful information was still gathered by analyzing the sediment returned to the surface, and by questioning the drillers about the speed and feel of drill penetration. The auger bit was rejected if it encountered clasts larger than approximately 10 cm diameter. Due to these constraints, only seven of the eight approved holes—and, only Type 2, 3, and 4 components—were drilled.

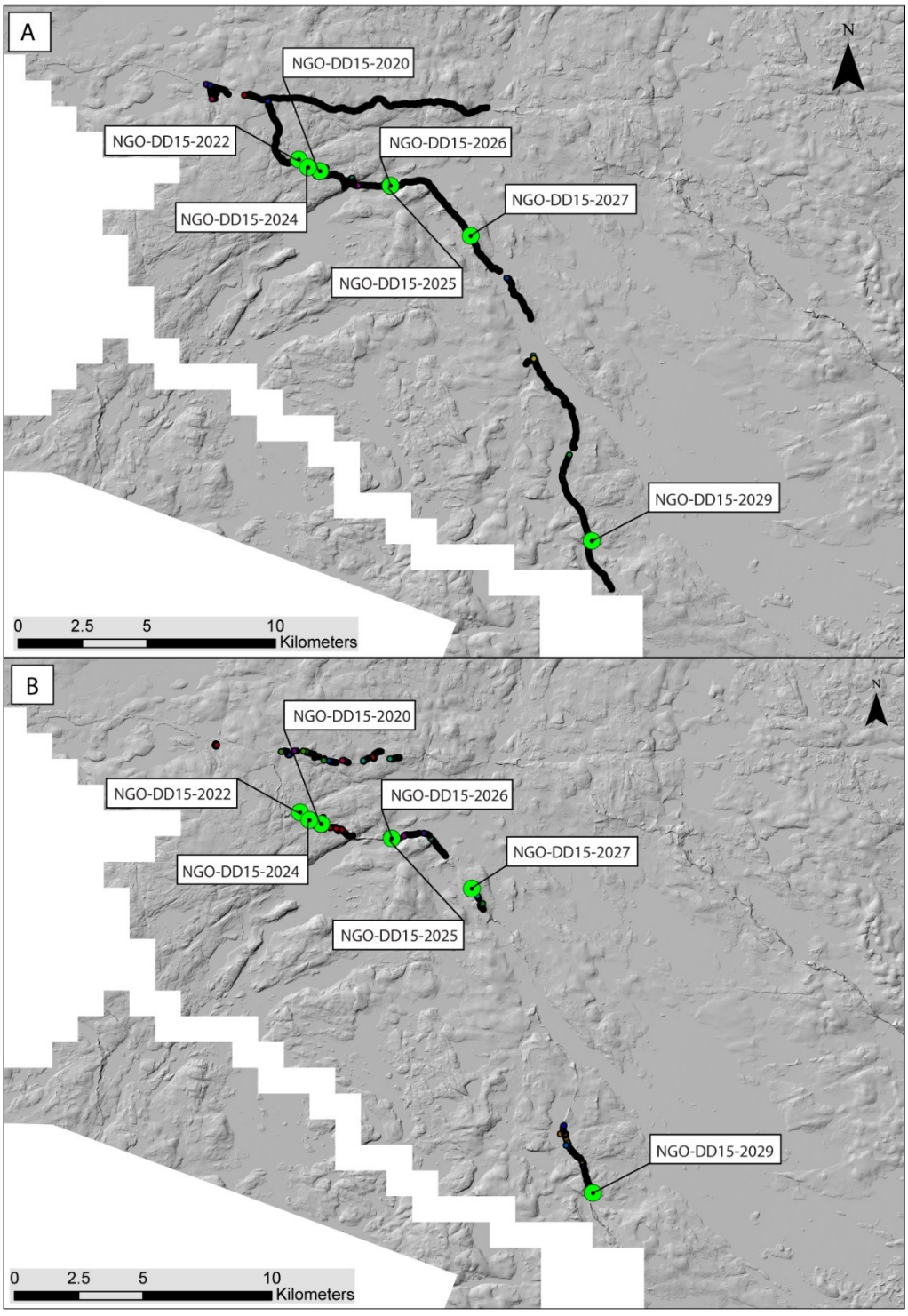

Figure 3.1: Locations of the seven auger boreholes (green dots) and extent of the 100 MHz (a) and 500 MHz (b) GPR surveys (black lines).

3.3 Results: Auger boreholes

The seven auger boreholes provide a first-order approximation of the sediment texture at various locations along the esker. Overviews of each hole are presented below, with sedimentary logs shown in Figure 3.2. These data are integrated with GPR data later in the chapter.

NGO-DD15-2024
UTM Zone 12: 527987N 7178628E

Hole NGO-DD15-2024 was drilled into a coarse sand-covered Type 2 component (Figures 3.1, 3.2). Drilling ceased at 7.4 m depth when a large cobble was encountered. From bottom to top, the vertical succession consisted of (1) a layer of rounded pebbles and cobbles from 7.4 to 7 m depth, (2) an upward-coarsening pebbly sand unit from 7 to 2.9 m depth, and (3) an upward-coarsening sandy unit from 2.9 m depth to surface. Water content in the returned material gradually increased downhole from the surface until the permafrost table was encountered at a depth of 1.8 m.

NGO-DD15-2022
UTM Zone 12: 527631N 7178941E

Hole NGO-DD15-2022 was drilled into a pebble and cobble covered Type 2 component (Figure 3.1, 3.2). Drilling ceased at 10 m depth when resistance on the auger bit became too great for the drill rig to overcome. From bottom to top, the vertical succession consisted of (1) coarse sand with sparse pebbles from 10 to 1 m depth, which is sharply overlain by (2) a unit of small (< 10 cm) cobbles and pebbles with a coarse sand and granule matrix from 1 m depth to surface, which, based on the drilling feel and

returned material, likely transitioned from matrix- to framework-supported moving upward. Water content in the returned material gradually increased from the surface until the permafrost table was encountered at a depth of 2 m, below which all further encountered sediment was frozen.

NGO-DD15-2029
UTM Zone 12: 539024N 7164144E

Hole NGO-DD15-2029 was drilled into a pebble covered Type 3 pad (Figure 3.1, 3.2). Drilling ceased at 12.1 m depth when resistance on the auger bit became too great for the drill rig to overcome. From bottom to top, the vertical succession consisted of (1) a unit of medium sand with sparsely distributed pebbles from 12.1 to 1.6 m depth, and (2) pebble gravel with a coarse sand matrix and rare cobbles from 1.6 m depth to surface. Water content in the returned material gradually increased with depth, from 0% at the surface to near saturated at the permafrost boundary at 2 m depth.

NGO-DD15-2020
UTM Zone 12: 528485N 7178484E

Hole NGO-DD15-2020 was drilled into a pebbly coarse sand covered Type 4 pad (Figure 3.1, 3.2). Drilling ceased at 4.6 m depth when resistance to the auger bit became too great for the drill rig to overcome. From bottom to top, the vertical succession consisted of (1) silty diamicton with abundant cobbles from 4.6 to 4.1 m depth, sharply overlain by (2) coarse sand with ~20% gravel (granules, pebbles and cobbles) distributed throughout from 4.1 m depth to surface. The diamicton is similar in texture to the till adjacent to the esker, and is distinct from the overlying sandy unit because of its high silt content and the greater angularity of its gravel clasts. The permafrost table was

encountered at a depth of 2 m, with water content approaching complete saturation at this depth.

NGO-DD15-2027
UTM Zone 12: 534312N 7175981E

Hole NGO-DD15-2027 was drilled into a pebble and cobble covered Type 2 component (Figure 3.1, 3.2). Three drill attempts were made in the immediate vicinity before penetration below a depth of 30 cm was achieved. Drilling ceased at 6.1 m depth when bedrock was likely encountered. From bottom to top, the vertical succession consisted of (1) bedrock at 6.1 m depth, (2) an upward-coarsening medium sand unit from 6.1 to 2 m depth (contains sparse pebbles and cobbles above 4.5 m), and (3) pebble gravel with rare cobbles from 2 m depth to surface. Water content in the returned sediment increased with depth, nearing saturation at the permafrost table at a depth of 2 m.

NGO-DD15-2026
UTM Zone 12: 531200N 7177920E

Hole NGO-DD15-2026 was drilled into a vegetated, fine-sand covered Type 4 splay, adjacent to the main esker ridge where hole NGO-DD15-2025 was drilled (Figures 3.1, 3.2). A depth of 1.6 m was reached before the drill bit was rejected when it encountered diamicton, the cobbly nature of which prevented further drilling. From top to bottom, the vertical succession consisted of (1) a sandy silt diamicton at the base of the hole (1.6 m depth) sharply overlain by (2) fine sand from 1.6 m depth to surface. Permafrost was encountered at a depth of 1.5 m. Similar to all other holes in this study,

water content increased downward from surface to near saturation just above the permafrost table.

NGO-DD15-2025
UTM Zone 12: 531149N 7177840E

Hole NGO-DD15-2025 was drilled into a coarse sand covered Type 2 component (Figures 3.1, 3.2). Drilling ceased at 4 m depth when cobbles were encountered. From bottom to top, the vertical succession consisted of (1) a unit of pebbles with a coarse sand matrix and rare cobbles from 2.8 to 4 m depth, sharply overlain by (2) coarse sand with sparsely distributed pebbles from 2.8 m to surface. A pebble layer was intersected in the coarse sand unit from 2.2 to 2.3 m depth. Permafrost was encountered at a depth of 1.7 m. Water content increased downward from surface, reaching near saturation at the permafrost boundary.

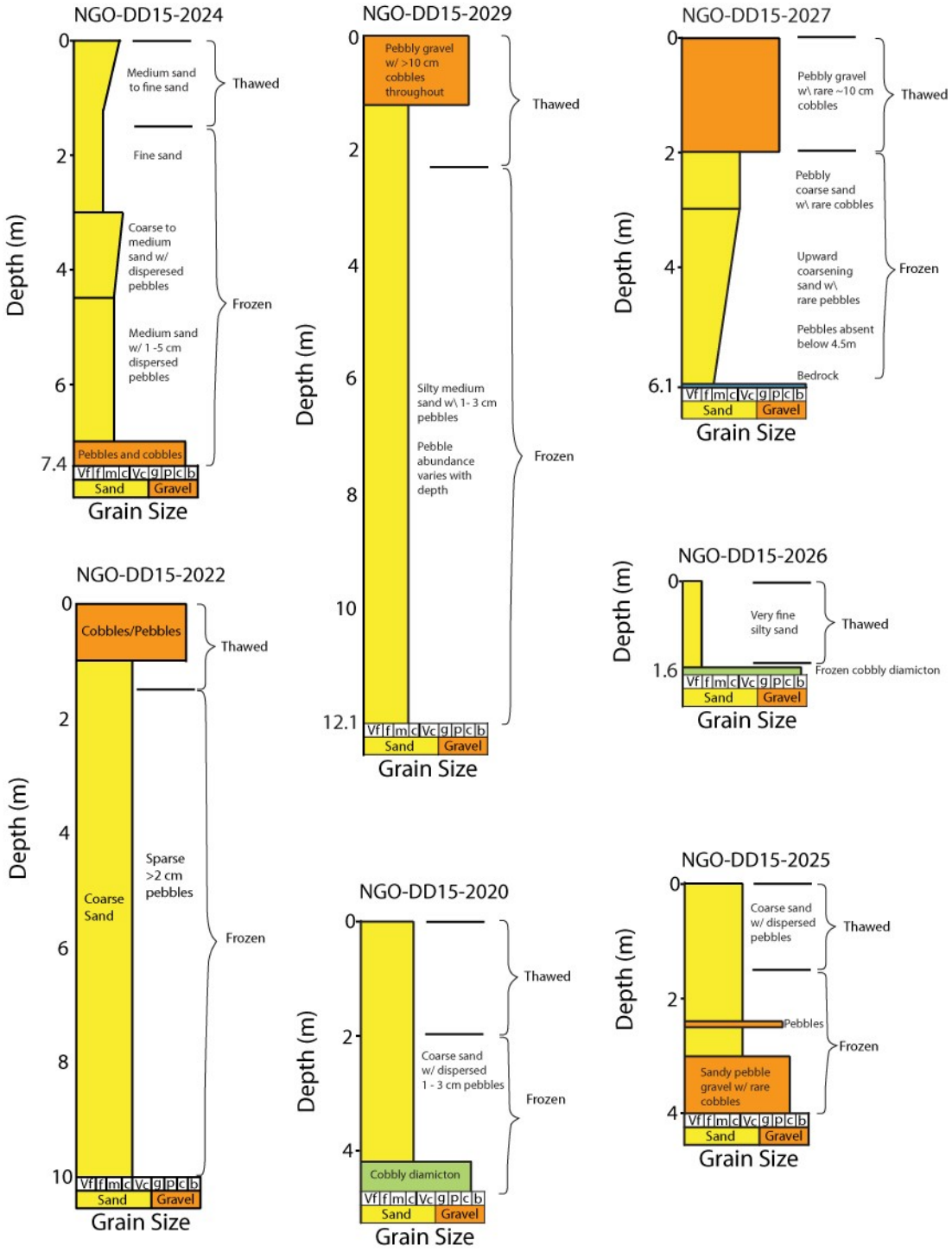

Figure 3.2: Sedimentary logs of the seven auger boreholes. See Figure 3.1 for locations.

3.4 Results: Exposures

Sediment within the esker is only well exposed at a single location, where a stream cut through a Type 1 component along the Misery Tributary esker, directly to the south of drill hole NGO-DD15-2029 (Figures 3.1, 3.3, 3.4). The exposure is approximately 15 m high, and in-situ, round, clast-supported cobbles and boulders in a coarse sand and pebble-gravel matrix are present through its entire extent beneath a thin cover of sandy detritus. The stream is lined with similar round cobbles and boulders, and it lies at or below the elevation as the surrounding till plain, suggesting that most if not all of this Type 1 component consists of rounded cobbles and boulders. This observation is important, as drilling the coarse Type 1 material was not possible. If this exposure is representative, Type 1 ridges may commonly have a relatively consistent cobble to boulder texture from base to crest.

Figure 3.3: Exposure of Type 1 component at stream cut, with 100 MHz GPR device in foreground. Digging into sandy slumped material on flanks revealed in-situ rounded cobbles and boulders close to surface. Similar cobbles and boulders formed the base of the stream.

Figure 3.4: Aerial photograph of exposure location. Down-esker is into the page.

3.5: Results: Radar facies (RFs)

In general, the GPR data obtained are of very high quality. Duplicate survey lines show nearly identical results. In the 100 MHz transects, distinct reflections are visible over the entire 832 ns time window, giving a penetration depth of approximately 40 m at the calculated 0.13 m/ns radar velocity. This depth exceeds the maximum esker height in the area. The 500 MHz transects have a penetration depth of approximately 6 m, approaching the theoretical maximum values for this type of medium given the parameters and equipment used (Annan, 2004).

In the 500 MHz transects, a strong, continuous reflection is commonly visible that trends parallel to the ground surface and is located consistently between 1.5 and 2 m below ground surface. Boreholes (Section 3.4) show this reflection to be associated with the permafrost table, the surface across which the ground transitions from being thawed and air- to water-saturated to frozen and ice-saturated. The thin water-saturated layer

above the permafrost table (Section 3.4) is likely integral in generating the strong reflection (e.g., Hinkel et al. 2001). Reflections interpreted to be generated by sedimentary bedding are almost ubiquitously apparent above the permafrost table, especially in sandier esker sediment, presumably due to variation in the amount of pore water from bed to bed (e.g., Cassidy, 2009). Reflections generated by sedimentary bedding are present but muted in the ice-saturated sediment beneath the permafrost table, presumably due to reduced variation in water content from bed to bed (e.g., Bristow and Jol, 2003; Neal, 2004).

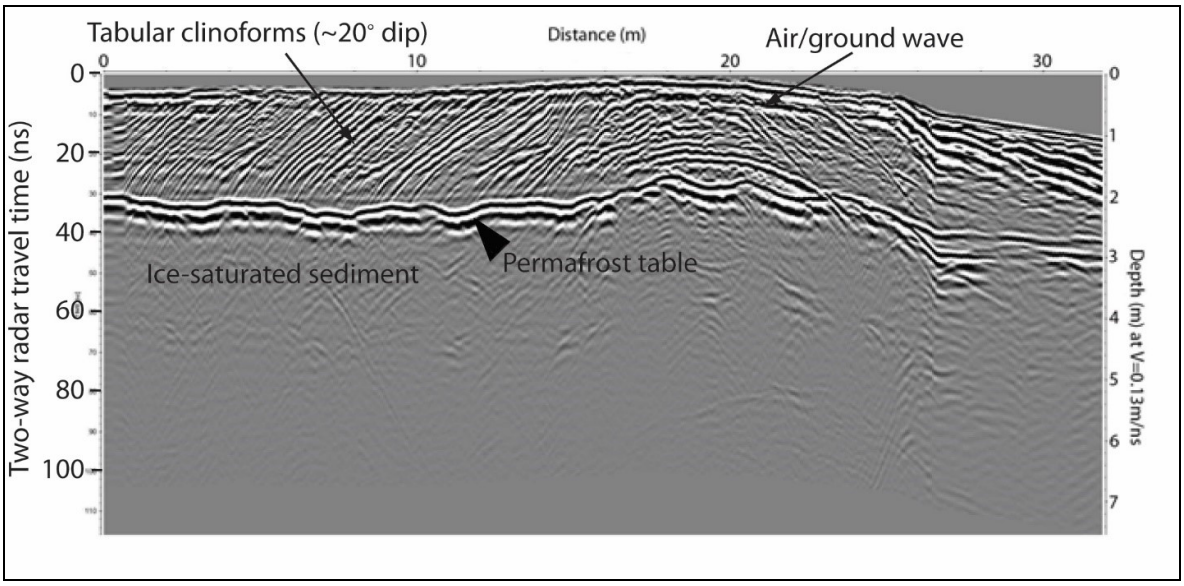

Figure 3.5: Example of a 500 MHz GPR transect illustrating some of the common features seen in the 500 MHz GPR data. Down esker is into page. Vertical exaggeration = 4.3.

In all 100 MHz transects, the uppermost 4–6 m invariably consists of a package of ground-parallel, high-amplitude events (Figure 3.6). These are artifacts of the collection process. They are produced by radar waves travelling directly from source to receiver through the air (i.e., the air wave) and the ground (i.e., the ground wave) (e.g., Fisher et

al., 1992), and they partially to completely obscure reflections generated by sedimentary bedding and the permafrost table. Similar artifacts are observed in the 500 MHz data (Figure 3.2), but, given the shorter distance between source and receiver antennas and thus shorter air and ground wave travel time, they only obscure the upper ~20 cm of the transects. Because the permafrost table falls within the interval containing ground-wave and air-wave artefacts in the 100 MHz data, the 100 MHz transects exclusively image ice-saturated sediment. As with the 500 MHz transects, bedding reflections in the ice-saturated sediment are commonly visible, but are relatively weak. Boosting the gain can increase contrast and help resolve these weak reflections.

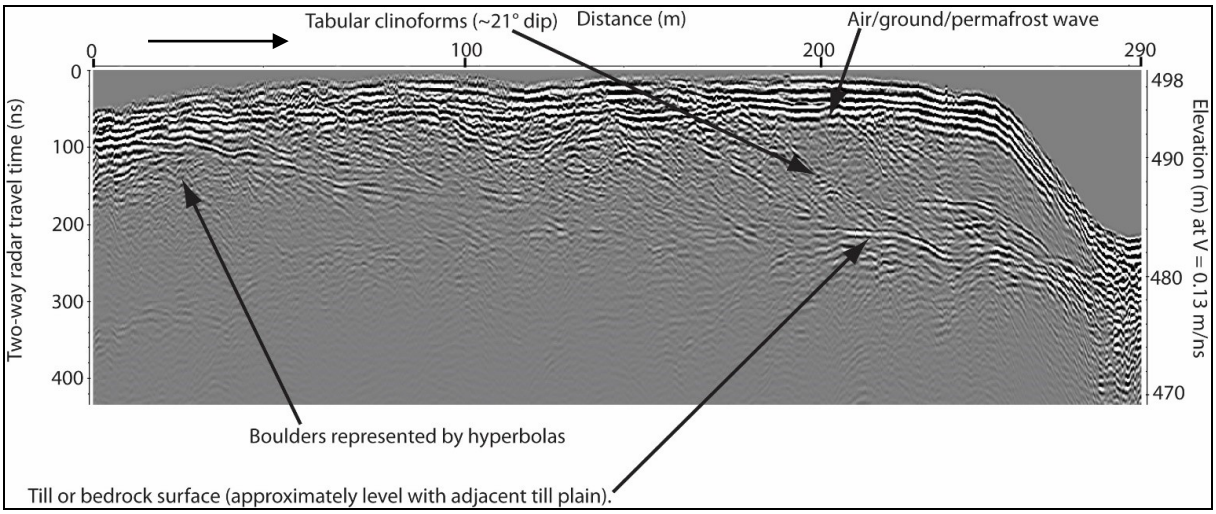

Figure 3.6: Example of a 100 MHz GPR transect illustrating some of the features common to the 100 MHz GPR data. Down esker is to the right. Vertical exaggeration = 10.3.

By calibrating the GPR data with the borehole and surficial-sediment data, different radar facies (RFs)—distinct portions of the GPR that can be differentiated from adjacent portions of the GPR based on their appearance and sediment texture—can be identified, each interpreted to be indicative of a specific depositional process and, in

some cases, a specific depositional environment (e.g., Burke et al., 2010). Because the 100 MHz and 500 MHz surveys image strata at different scales and resolutions, and because most of the strata imaged in the 500 MHz transects (i.e., the strata above the permafrost table) is obscured in the 100 MHz transects due to air- and ground-wave artifacts, to facilitate analysis, two different sets of radar facies are established here, one for the 100 MHz survey, and one for the 500 MHz survey.

Table 3.1: 500 MHz radar facies. The representative images cover a vertical depth of ~ 1 m and a horizontal distance of 2 m. Flow direction is left to right.

Radar Facies	Representative image	Description	Sediment texture	Interpretation
RF500-1		Relatively small-scale (0.5–2 m thick) tabular units bounded by flat upper and lower surfaces (reflections). Internally composed of a set of inclined, tabular- to trough-shaped reflections that dip moderately to steeply (25-35°) in a down-esker direction.	Fine to coarse sand, with minor granule to pebble sized clasts	Dune or barform deposits
RF500-2	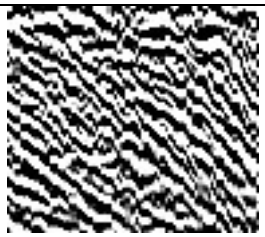	Relatively large-scale (2–6 m thick) tabular to wedge-shaped units bounded above by a flat, horizontal, near-surface reflection and below by a reflection at depth that is commonly near-horizontal, but can vary from flat to irregular. Internally composed of moderately to steeply inclined (13-35°) down-esker dipping tabular to trough-shaped reflections. Always occurs as a single set.	Fine to coarse sand with rare pebbles and cobbles throughout	Deltaic foresets
RF500-3		Gently to moderately inclined (5-15°) up-flow dipping parallel reflections	Fine to coarse sand with rare pebbles and cobbles throughout	"Backset" (upflow-dipping) beds formed at jet efflux (subglacial–subaerial transition). Where shallow-dipping, possibly large-scale anti-dune cross-stratification.
RF500-4	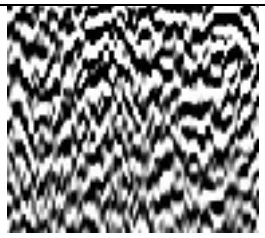	Irregular, non-parallel hyperbolic reflections	Pebbles, cobbles and boulders, in a coarse sandy matrix	Cobble and boulder-rich sediment;
RF500-5	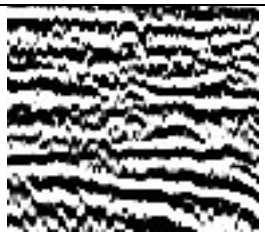	Sub parallel to parallel planar reflections with rare hyperbolic reflections. -	Coarse sand to pebbles with rare cobbles throughout	Lower plane bed sand and gravel, gravelly topset beds

RF500-1: Cross-stratified beds (dune or barform deposits)

RF500-1 is characterized by steeply inclined planar reflections that dip down-esker at 15–35° (Table 3.1). The inclined reflections form cross-stratified sets that are 0.5–2 m thick, and are bounded by planar bounding reflections, forming tabular units that are commonly stacked on top of each other. RF500-1 is typically found in medium to coarse sand, and rarely in granule and pebble sized sediment.

Two interpretations seem possible for RF500-1: either these features were produced by gravelly bars (see Figure 3.9; e.g., Lunt and Bridge, 2004; MacDonald et al., 2009; Reesink et al., 2014) or that they were produced by dunes. Gravel dunes rarely form in rivers (Dinehart, 1992), but are known to form during exceptional discharges in a variety of gravel-rich depositional environments (e.g., jökulhlaups in proglacial areas; Marren and Schuh, 2009).

RF500-2: Large-scale foreset packages (deltaic deposits)

RF500-2 is characterized by tabular- to wedge-shaped packages of down-flow dipping inclined reflections. The facies is therefore similar to RF500-1, but the packages are much thicker, ranging from 2 m to over 6 m, the latter value representing the limit of penetration for the 500 MHz survey. Also unlike RF500-1 units, RF500-2 units always occur in isolation, and are never stacked upon one another. Dip angles of the reflections range from 10 to 35°. Drilling results indicate that sediment of RF500-2 is largely composed of medium to coarse sand with rare pebbles.

RF500-2 is interpreted to represent foreset bedding generated by progradation of coarse-grained (Gilbert-type) deltas (e.g., Smith and Jol., 1997; Burke et al., 2010).

RF500-3: Backset beds (high to low angle—jet-efflux deposits; low angle—antidune deposits)

RF500-3 is characterized by shallowly to moderately inclined (5–15°) reflections that dip in an up esker direction. Packages of these reflections rarely exceed 2 m in thickness, and are commonly interstratified with other packages of up- and down-esker dipping reflections. RF500-3 was not intersected by any of the boreholes. However, sediment texture is suspected to consist of medium to coarse sand with rare pebbles, given the texture of surface sediment in areas where RF500-3 is present.

RF500-3 is interpreted to represent the deposits of supercritical bedforms, such as antidunes,, where the dip is shallow and sediment is finer grained (e.g., Burke et al., 2011; Cartigny et al., 2014). Coarser material in RF500-3 could be indicative of up-flow accretion of jet efflux deposits at the head of an ice contact delta (e.g., Nemec et al., 1999; MacDonald et al., 2009).

RF500-4: Pebble-, cobble- and boulder-rich sediment (high-energy bedload deposit)

RF500-4 is characterized by a "noisy" or chaotic texture, marked by abundant overlapping hyperbolas, and the absence of any distinct continuous planar reflections. Thickness of RF500-4 units ranges from >1 m to 6 m. The sediment associated with RF500-4 is inferred to be rich in gravel (pebbles to boulders) based on the drilling results, the single stream-cut exposure, which occurs in a gravelly part of the esker (Figure 3.3), and the gravel-rich surficial sediments typical of areas where RF500-4 is observed.

RF500-4 is interpreted to have formed by vertical aggradation of gravelly bedload under high-energy conditions. The till in off-esker locations generates a similar chaotic, hyperbola-rich signature.

RF500-5: Planar stratification (vertically accreted deposits)

RF500-5 is characterized by packages of parallel to sub parallel, planar, horizontal reflections that generally range from 1 to 3 m thick. Drilling results show that RF500-5 is composed of sediment ranging in size from medium sand to pebble gravel with sparse cobbles.

Although planar stratification can be generated under either upper and lower flow regime conditions, and upper and lower plane bed could conceivably be difficult to differentiate in GPR, RF500-5 is interpreted to have more likely been generated by bedload sheets under lower flow regime conditions given that it appears to generally have a coarser grain size (e.g., Whiting et al., 1988; Marren and Schuh, 2009). Alternatively, RF500-5 could potentially be generated by thin, discontinuous dune cross-stratified beds (eg, Facies 2 of Reesink et al., 2014)

Table 3.2: 100 MHz radar facies. Texture image covers a depth of ~ 10 m and a horizontal distance of 15 m. Flow direction is left to right.

Radar Facies	Texture	Description	Composition	Interpretation
RF100-1	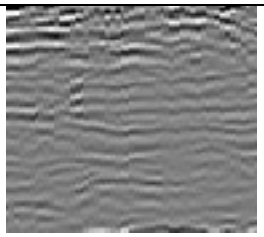	Sub parallel to parallel reflections, w/ small irregularities and breaks	Fine to coarse sand, w/ minor granule to cobble sized clasts	Traction-transport deposits
RF100-2	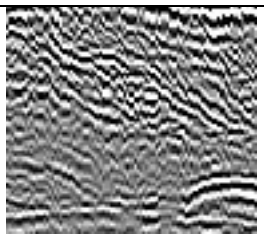	Continuous, moderately to steeply (13-35°) down flow dipping parallel reflections	Fine to coarse sand w/ rare pebbles and cobbles throughout	Foreset beds generated by deltaic progradation (equivalent to RF500-2)
RF100-3	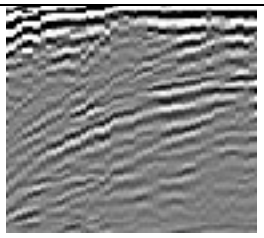	Continuous shallow to moderately (5-15°) up flow dipping parallel reflections	Fine to coarse sand w/ rare pebbles and cobbles throughout	Backset beds deposited at mouth of debouching R-channel
RF100-4	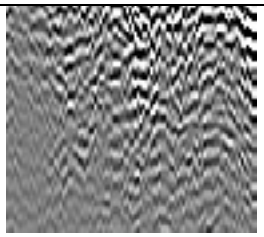	Irregular, non-parallel hyperbolic reflections	Cobbles and boulders, in a coarse sandy matrix	High energy, cobble- and boulder-rich horizontal(?) bedding
RF100-5	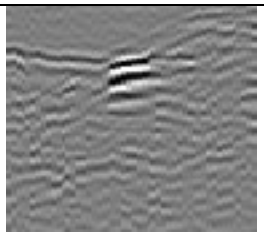	Hyperbolic reflections, with weak subparallel reflections.	Silty cobbly diamicton / Bedrock	Till/bedrock Radar basement

RF100-1: Planar stratification (Traction transport deposits)

RF100-1 is characterized by parallel to subparallel, planar to near-planar, horizontal reflections. Hyperbolic reflections are absent. The thickness of RF100-1 packages typically ranges from 2 m to 5 m Boreholes that penetrate RF001-1 intersected sediment ranging from medium sand to pebbles.

Given the vertical resolution of the 100 MHz data, which is calculated using the method outlined in Annan (2004) to be approximately 1 m, it is possible that RF100-1 represents beds that accreted vertically, but that could have been generated by a range of different processes. For example, aggradation of both upper and lower plane might be expected to generate a GPR signature similar to RF100-1, as might the stacking of thinner (<1 m) dune cross-stratified beds.

RF100-2: Large scale foreset packages (deltaic deposits)

RF100-2 is characterized by tabular to wedge-shaped packages (several meters to >10 meters thick) of moderately to steeply dipping inclined (15–35°), down-esker dipping reflections. Drilling reveals that RF100-2 is composed primarily of medium to coarse sand, with rare pebble sized clasts.

RF100-2 is directly analogous to RF500-2. It is interpreted that this radar facies represents progradational Gilbert-type deltaic foreset bedding (e.g., Smith and Jol, 1997; Burke et al., 2008, 2010;).

RF100-3: Backset beds (jet efflux deposits)

RF100-3 consists of shallowly to moderately up-esker dipping (5–15°) inclined reflections. While drilling did not encounter this radar facies, it can be inferred from the radar texture (sub-parallel reflections, lack of large hyperbolas) that the material likely consists of crudely stratified coarse sand to pebbles, though this does not rule out the possibility that beds of finer material may be present. The thickness of RF100-3 units typically ranges from 2 to 10 m.

It is interpreted that RF100-3 formed by up-flow accretion of jet efflux deposits at the transition from subglacial stream to proglacial ice contact delta settings (e.g., Nemec et al., 1999; MacDonald et al., 2009). RF100-3 is partly analogous to RF500-3, where parallel inclined reflections are present at a moderate angle and extend for several meters in thickness.

RF100-4: Cobble- and boulder-rich sediment (high-energy bedload deposit)

RF100-4 is characterized by abundant hyperbolic reflections. Although RF100-4 was not drilled, it is inferred that the radar signature is generated by relatively coarse gravel (pebbles, cobbles and boulders), given that the esker is commonly covered in cobbles and boulders where RF100-4 is observed, and from rounded cobbles and boulders observed in an exposure (Figure 3.3) at a location where RF100-4 is present. Thickness of RF100-4 units ranges from 5 to > 20 m.

RF100-4 is interpreted to have been deposited by vertical aggradation of pebble to boulder bedload beneath high-energy subaqueous flows (e.g., Burke et al., 2010). The facies is analogous to RF500-4.

RF100-5: Esker base (till/bedrock)

RF100-5 is varied in its appearance, though commonly it is characterized by muted, discontinuous reflections in general, with weak hyperbolic reflections and weak, non-hyperbolic high angle planar reflections locally. The radar facies was not intersected by boreholes. Discontinuous, subparallel reflections with varying densities of hyperbolas suggest that RF100-5 is likely composed of poorly sorted, unstratified material.

RF100-5 is observed only at significant depth in esker GPR transects or in off-esker areas of till or exposed bedrock, and is therefore interpreted to represent either diamicton (till) or bedrock. High angle non-hyperbolic reflections are interpreted to be generated by water or ice filled fractures in bedrock. This radar facies was sometimes difficult to differentiate from RF100-4, especially at depth. As such, determining the depth to the esker base was often difficult.

3.6 Results: Sedimentary architecture

This section examines the sedimentary architecture of the esker at the borehole locations, where data control is most substantial.

a) Sedimentary architecture of Type 2 component at Borehole NGO-DD15-2022

Borehole NGO-DD15-2022 was drilled into a pebble and cobble covered (<10 cm diameter clast size) flat-topped Type 2 component that forms part of the main ridge of the Misery tributary esker (Figure 3.1). In the 500 MHz GPR profile (Figure 3.7a), the two different sedimentary packages observed in the borehole are characterized by two different radar facies. Approximately planar reflections with small hyperbolic reflections in the upper 1 m are associated with pebble to cobble gravel (RF500-5). This unit truncates large-scale, steep (20° dip), down-esker dipping foresets (RF500-2). When first viewing the 500 MHz GPR transect (Figure 3.7a), the scale of the foresets is difficult to discern because, below the 2 m depth mark, reflection strength abruptly decreases across the permafrost table. Still, weakly visible inclined reflections indicate that foreset beds continue well below the permafrost table, and below the maximum depth of penetration (~6 m) for the 500 MHz data. At the far left of the 500 MHz profile, the radar texture appears "noisy", with no coherent bedding reflections. This noisy texture is likely artificial, a result of the 500 MHz GPR device moving over an uneven cobble surface, an interpretation supported by the observation of coherent large-scale foreset reflections at this location in the 100 MHz data (see next).

The 100 MHz GPR profile (Figure 3.7b) is more varied than the 500 MHz GPR profile, and the upper 4-6 m of strata is obscured by the airwave, the groundwave, and the

permafrost reflection. As with the 500 MHz transect, large-scale, steep (20° dip), down-esker dipping reflections (RF100-2) are associated with the coarse sandy sediment package at the base of the borehole. The foreset reflections downlap a strong uneven horizontal reflection at a 15–20 m depth that is below the base of the borehole and is interpreted to be either bedrock or till, given that it is approximately at the same level as the till covered off-esker ground surface. The foresets have the same dip and orientation as the down-flow face of the Type 2 landform, a relationship visible on the right hand side of Figure 3.7b.

Whereas the Type 2 component at the NGO-DD15-2022 borehole location is flat-topped and contains continuous, coherent reflections, the esker up-flow of this (0 to 220 m in Figure 3.7b) has an irregular top surface and contains reflections that are less continuous and commonly disrupted in appearance.

The large-scale sandy foresets and gravelly topset that make up the Type 2 component at the NGO-DD15-2022 borehole location are interpreted to be deltaic in origin (e.g., Smith and Jol, 1997). Given its narrow, steep sided shape, the Type 2 component is interpreted to have formed by progradation of a delta into a narrow ice-walled re-entrant at the ice front. The irregularity of the Type 2 component up-esker of the borehole site (0 to 220 m in Figure 3.7b) is interpreted to reflect post-depositional deformation of the deltaic body, possibly related to melt-out of buried ice (e.g., Price, 1969; Wolfe, 1998).

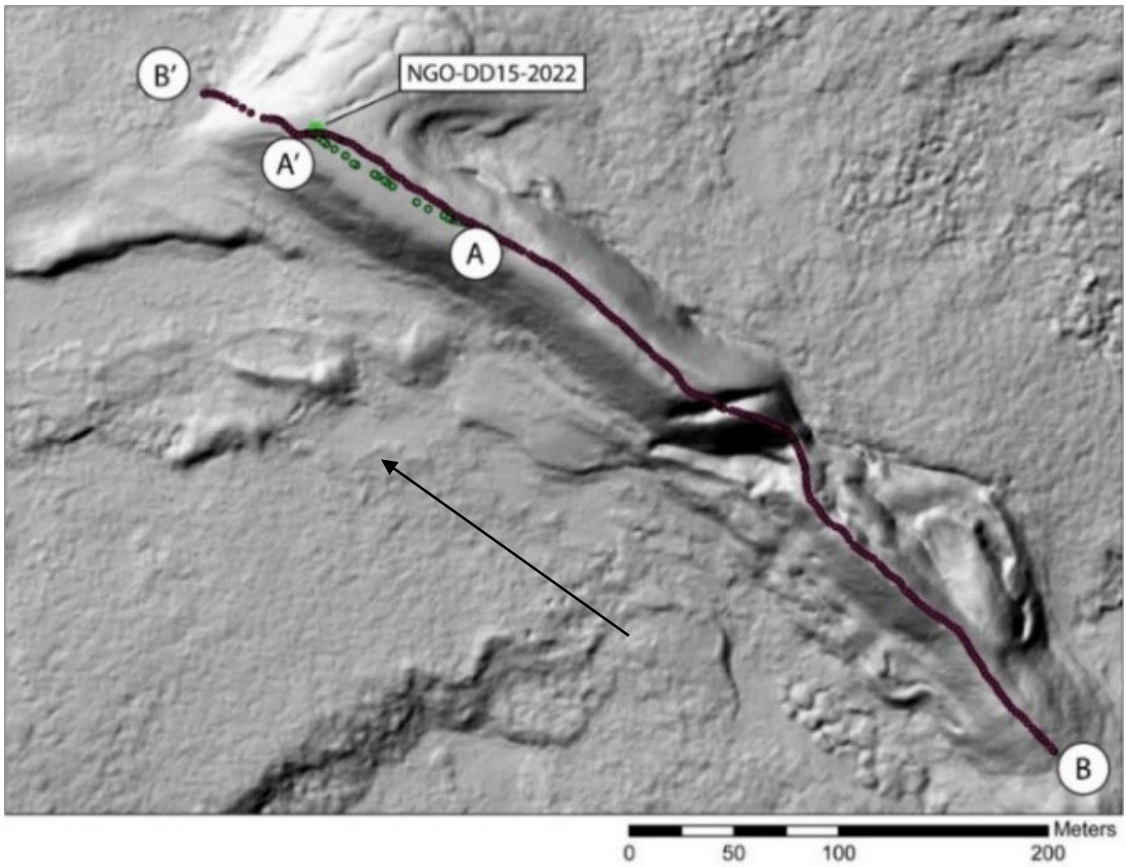

Figure 3.7a: LiDAR image of drill hole NGO-DD15-2022 location.

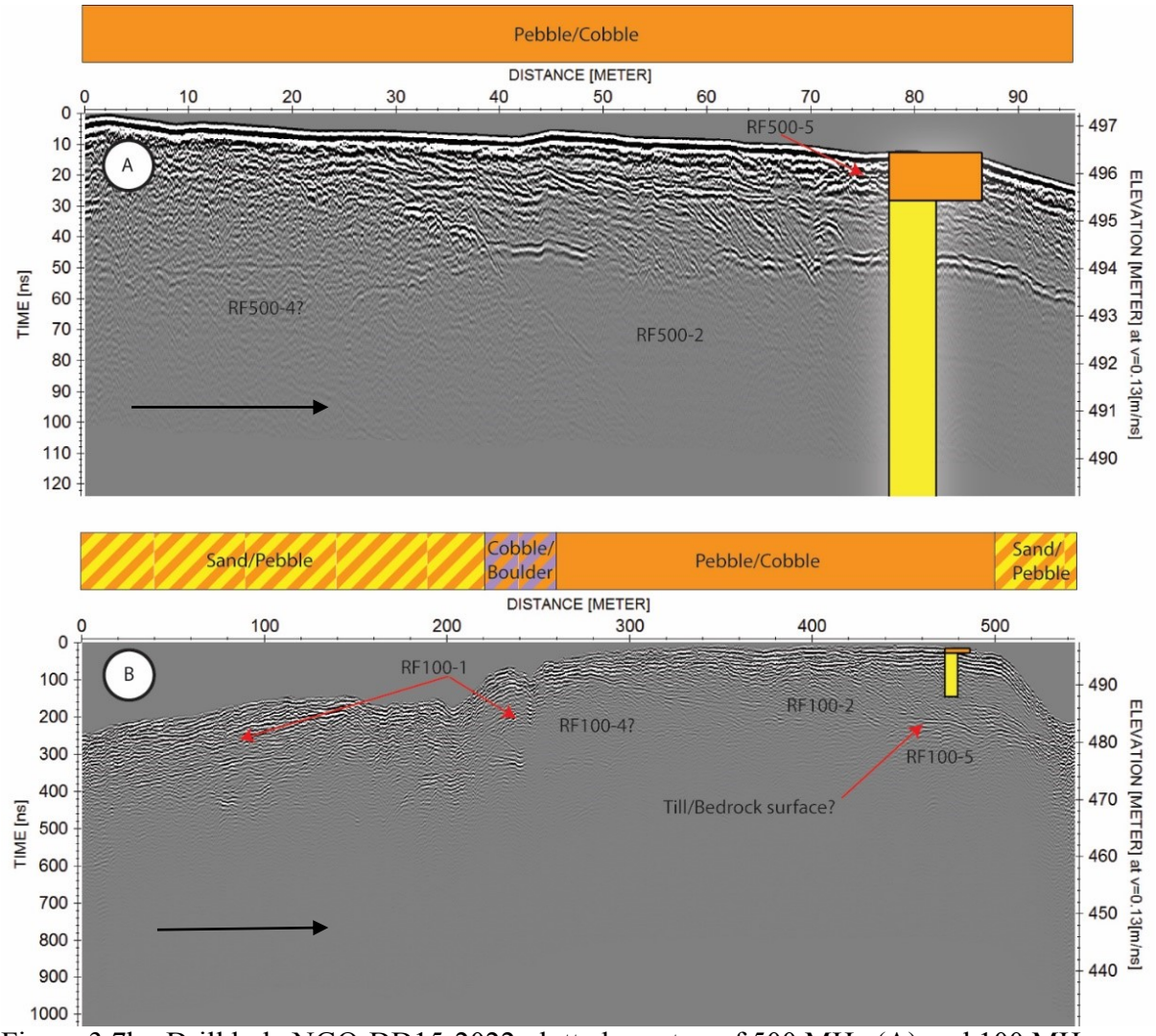

Figure 3.7b: Drill hole NGO-DD15-2022 plotted overtop of 500 MHz (A) and 100 MHz (B) GPR transects. See Figure 3.1 for drill hole location. NGO-DD15-2022 is drilled into a pebble and cobble covered Type 2 component. A to A' and B to B' are left to right. The coloured horizontal bars in (A) and (B) indicate sediment grain size on the esker surface. In (A), the strong reflection ~2 m below ground surface is the permafrost table. In (B), the airwave and groundwave obscure stratal reflections from ground surface to a depth of ~5 m. Down-esker (down-flow) is toward the NE in the LiDAR image, and toward the right in (A) and (B). In the sedimentary log, yellow indicates coarse sand with sparse pebbles and orange indicates pebbles and cobbles. Vertical exaggeration (A) = 11.8. Vertical exaggeration (B) = 7.9.

b) Sedimentary architecture of Type 2 component at Borehole NGO-DD15-2024

Borehole NGO-DD15-2024 was drilled into a sand-covered Type 2 component that forms part of the main ridge of the Misery tributary esker (Figure 3.1). Parts of the esker near the borehole are distinctly flat topped, including the part into which the borehole was drilled, but overall, the esker at this location has an irregular surface, and the flat-topped portions do not necessarily dip down-esker (Figure 3.8). At normal gain settings, the 500 MHz GPR transect (Figure 3.8a) illustrates an abrupt change in reflection strength at the permafrost table ~2 m below ground surface, with only weak reflections visible in the frozen sediment below. Variation in the strength of the permafrost table reflection may indicate variable water saturation above this level. When the gain is increased, the permafrost boundary becomes more clearly visible, as do weaker reflections in the underlying frozen sediment (Figure 3.5b). As with reflections beneath the irregular-topped portion of the Type 2 component at the previous borehole location (Figure 3.7), reflections beneath the highly irregular Type 2 component at the NGO-DD15-2024 borehole location have a low lateral continuity and commonly appear disrupted. Radar facies are commonly hard to define, and a clear correlation between radar facies the transect and sediment texture in the borehole is not obvious. Packages of inclined reflections (RF500-1,2) are present at various locations along the length of the transect, as are packages of surface parallel reflections (RF500-5). Reflection packages tend to be short (<40 m long) and thin (< 2 m thick), and they tend to have boundaries that are difficult to map out.

Given the relatively fine (medium sand to pebbles) surface material, the presence of flat-topped areas in an overall irregular portion of the esker, and the disrupted nature of

reflections, the Type 2 component at the NGO-DD15-2024 borehole location is suspected to have been deposited in open channel conditions and then deformed during melt out of buried ice (e.g. Price, 1969; Wolfe et al, 1996).

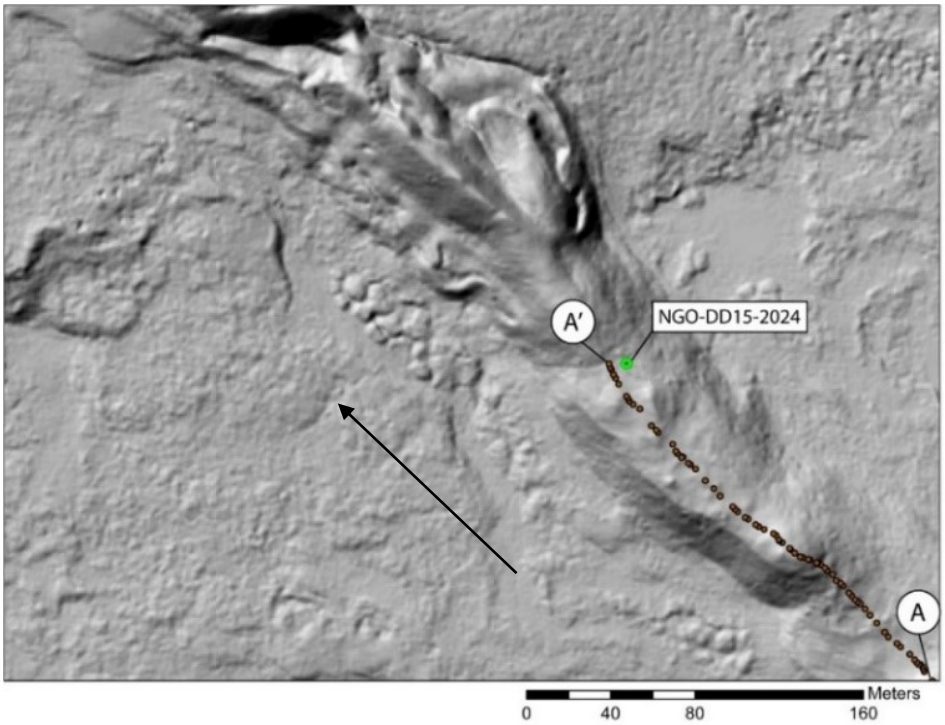

Figure 3.8a: LiDAR image of drill hole NGO-DD15-2024 location.

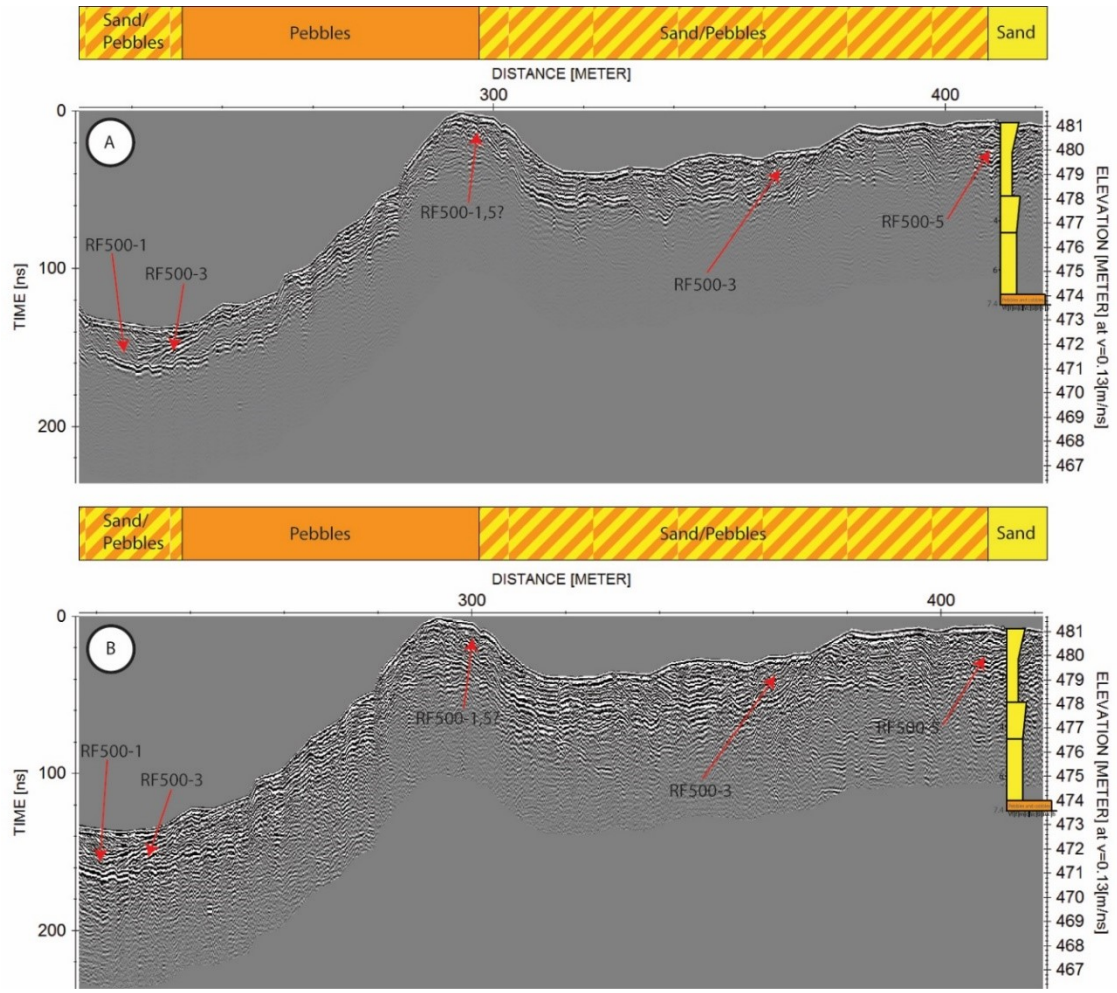

Figure 3.8b: Borehole NGO-DD15-2024, which is drilled into a sand-covered Type 2 component, plotted over top of normal (A) and gain-increased (B) 500 MHz GPR profiles. A to A' is left to right. The coloured horizontal bars over (A) and (B) show sediment grain size on the esker surface. The strong reflection ~2 m below ground surface is the permafrost table. Down-esker (downflow) is toward the NE in the LiDAR image, and toward the right in (A) and (B). In the sedimentary log, orange indicates pebbles and cobbles and yellow indicates fine to coarse sand. Vertical exaggeration = 14.8.

c) Sedimentary architecture of Type 4 detached pad at Borehole NGO-DD15-2020

Borehole NGO-DD15-2020 was drilled into a Type 4 detached pad adjacent to the main ridge of the Misery tributary esker (Figure 3.1). In a nearby 500 MHz GPR transect (Figure 3.9), the permafrost table is immediately evident (strong reflection at ~1.5 m depth) and closely parallels the undulating ground surface. Several prominent diffraction

hyperbolas are interpreted to be generated by high angle normal faults within the sediment (e.g., Jol, 2009). This interpretation is further supported by the collapsed appearance of the landform in the LiDAR imagery. Faults likely developed to accommodate for volume loss as buried glacial ice melted out.

Radar facies are difficult to define at this location, likely due to the deformation and faulting mentioned above. Coarse sand intersected in the borehole between ground surface to 4 m depth is associated with a package of disrupted, planar reflections. Below this, frozen silty diamicton with a high percentage of cobbles sized clasts was intersected. Coherent reflections are not associated with this unit.

The Type 4 pad at this location is interpreted to have been deposited on an ice-rich, sediment-rich substrate, possibly dirty glacier ice, which has subsequently melted out in part, generating the irregular top surface and disrupted sedimentary architecture.

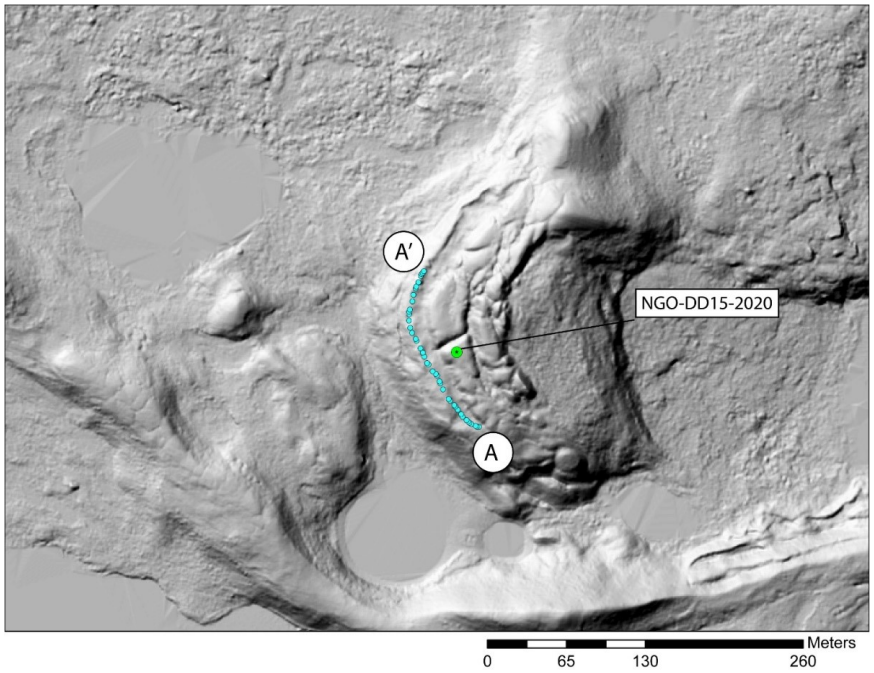

Figure 3.9a: LiDAR image of drill hole NGO-DD15-2020 location.

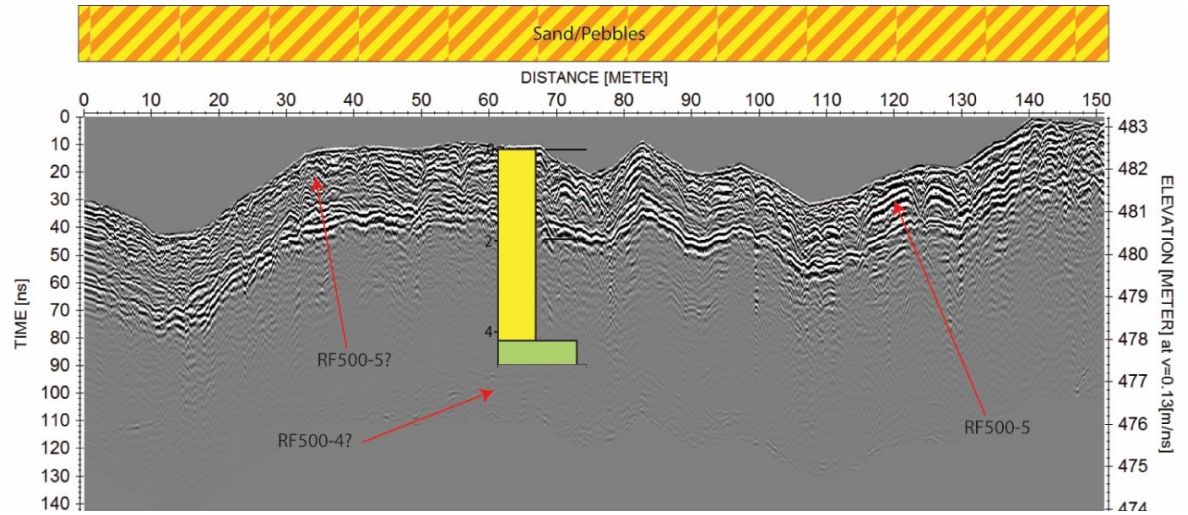

Figure 3.9b: Borehole NGO-DD15-2020, which is drilled into a sand-covered, esker-detached Type 4 pad, plotted over a 500 MHz GPR transect. A to A' is left to right. The coloured horizontal bar above the GPR transect shows sediment grain size on the esker surface. The strong reflection ~2 m below ground surface is the permafrost table. Down-esker direction is to the left (west) in the LiDAR, and is into the page in the GPR transect. (It is less clear which direction is down-flow for this Type 4 component because it is detached from the main ridge and clear paleoflow indicators (e.g., dune cross-sets in near-surface sediment) were not observed.) In the sedimentary log, green indicates diamicton (till) and yellow indicates coarse sand with dispersed pebbles. Vertical exaggeration = 15.8.

d) Sedimentary architecture of Type 2 component at Borehole NGO-DD15-2025

Borehole NGO-DD15-2025 is drilled into a coarse sand and pebble covered flat-topped Type 2 component that forms part of the main ridge of the Misery tributary esker (Figure 3.1). The GPR transects from this location (Figure 3.10) are similar in character to those near borehole NGO-DD15-2022 (Figure 3.7), with discontinuous packages of inclined (RF500-1 and RF500-2) and planar, surface parallel reflections (RF500-5). Boundaries between radar facies are difficult to discern. The flat top of the esker at this location has a distinct up-esker dip. Both normal (Figure 3.10a) and gain increased 500 MHz GPR transects (Figure 3.10b) are shown here, the latter of which images weaker reflections in the frozen zone beneath the permafrost table. The radar texture is fairly consistent over the GPR transect, showing several irregular, strong inclined reflections that begin at the surface and dip at approximately 20° down esker. In the normal GPR transect, these inclined reflections appear to intersect the permafrost reflection and then stop. However, in the gain boosted GPR (Figure 3.10b) it can be seen that these beds continue below the permafrost table, forming large-scale (5 m high), steep (20°), down-esker dipping tangential foresets (RF500-2) that appear to downlap a poorly resolved substrate, which is below the base of the borehole.

Given the substantial thickness of the down-esker-dipping foresets, coupled with the narrowness and the flat top of the landform, it is interpreted that the Type 2 component at NGO-DD15-2025 was generated by progradation of a coarse grained Gilbert-type delta into a subaerial ice-walled conduit. The up-esker dip of the flat-topped Type 2 component at this location, coupled with the locally disrupted appearance of the GPR, suggests that the sediment body was deposited supraglacially, in a subaerial, down-

glacier dipping ice-walled conduit, and that it became tilted and slightly deformed following ice melt out (e.g., Price, 1969; Wolfe, 1996).

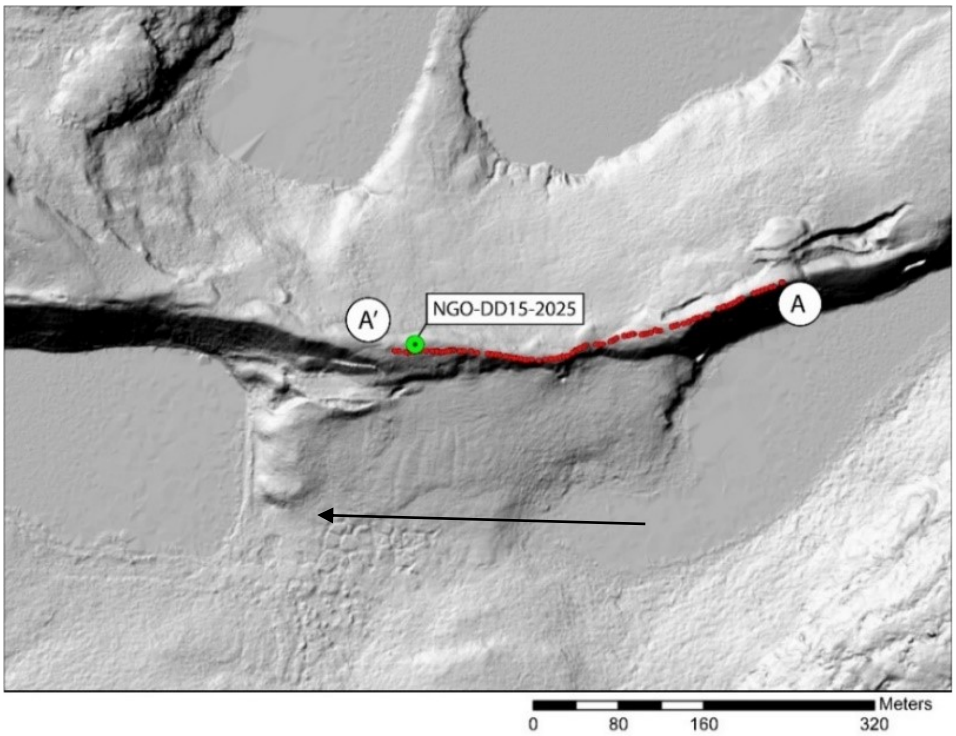

Figure 3.10a: LiDAR image of drill hole NGO-DD15-2025 location

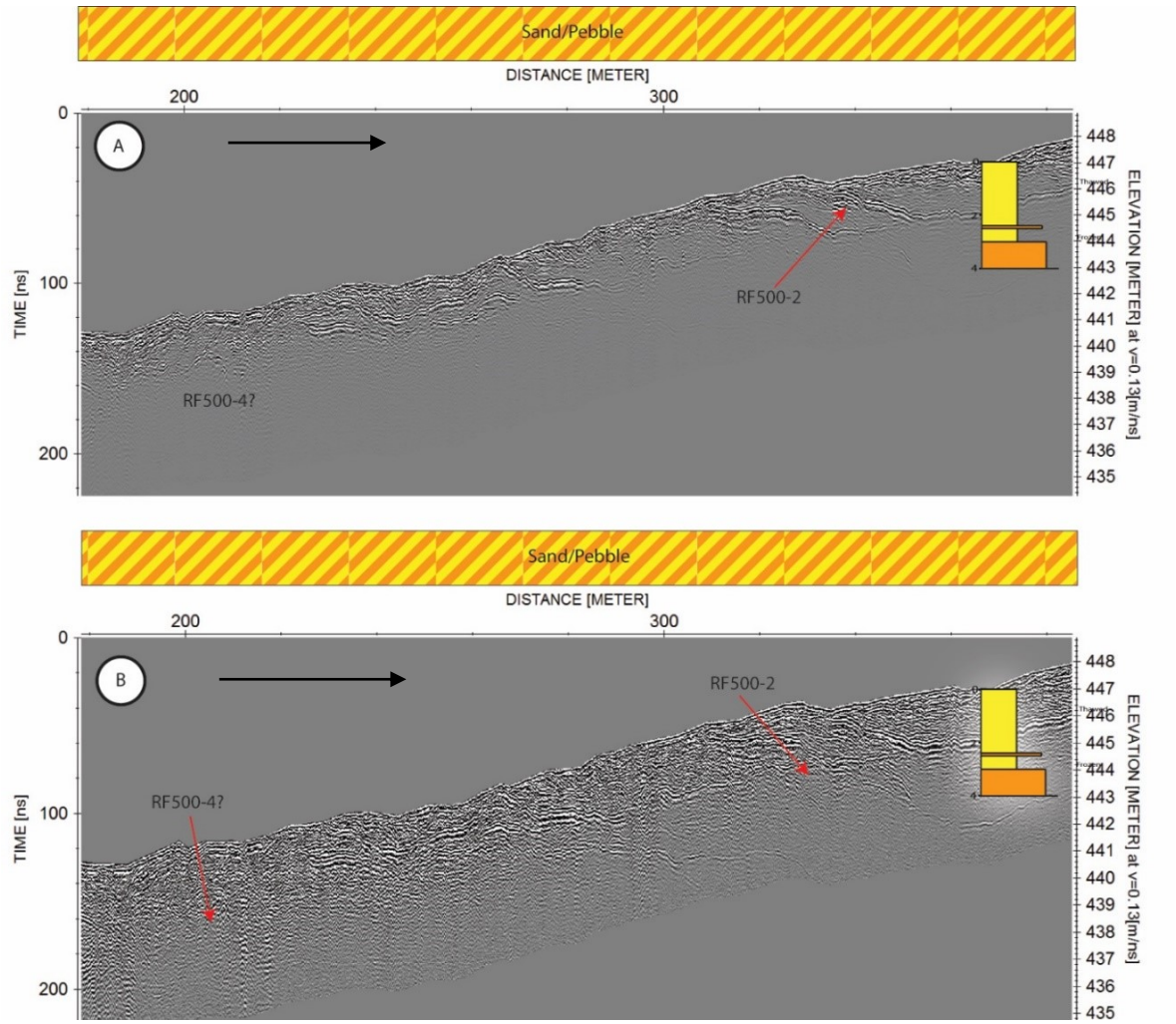

Figure 3.10b: Borehole NGO-DD15-2025, which is drilled into a pebbly coarse sand covered Type 2 component, plotted overtop of normal (A) and gain increased (B) 500 MHz GPR transects. A to A' is left to right. The coloured horizontal bars above (A) and (B) show sediment grain size on the esker surface. The strong reflection ~2 m below ground surface is the permafrost table. Down esker is left in LiDAR and right in GPR figures, as indicated by black arrows. Vertical exaggeration = 14.6.

e) Sedimentary architecture of Type 4 splay component at Borehole NGO-DD15-2026

Borehole NGO-DD15-2026 is drilled into a broad, fine sand covered Type 4 splay (Figure 3.1), 100 m north of the location on the central ridge of the Misery tributary esker where NGO-DD15-2025 was drilled. The 500 MHz GPR transect from this location has a smooth, sloping surface and an irregularly undulating permafrost table reflection

(Figure 3.10). The ground surface was highly vegetated, and the vegetation was organized into small mounds that caused the GPR device to undulate during data collection. Likely as a result, the GPR texture is irregular and noisy, similar to the up esker portion of Figure 3.7 described previously.

The drill hole at this location consisted of well-sorted fine sand overlying a silty diamicton with large cobbles that prevented further drilling (Figure 3.10). Up-esker on the side of a small collapse feature visible on the right hand side of the LiDAR image (Figure 3.11) is fine- to medium sand exposed that contains climbing ripples. It is interpreted that the Type 4 component here is a splay-like body of fine sandy outwash that was deposited supraglacially, perhaps as a result of a flooding of the main adjacent esker channel, resulting in fine sediment being deposited on adjacent glacier ice. This would be analogous to an overbank splay deposit in a modern fluvial system (e.g., North and Davidson, 2012).

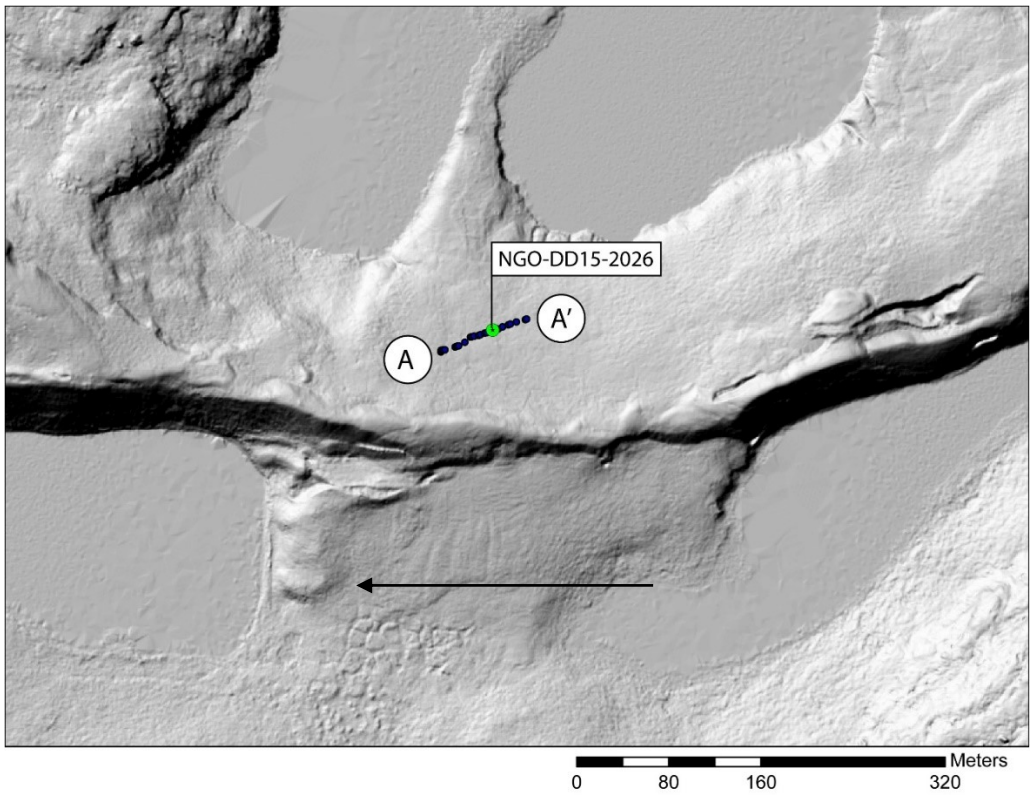

Figure 3.11a: LiDAR image of drill hole NGO-DD15-2026 location. Black arrow indicates down-esker direction.

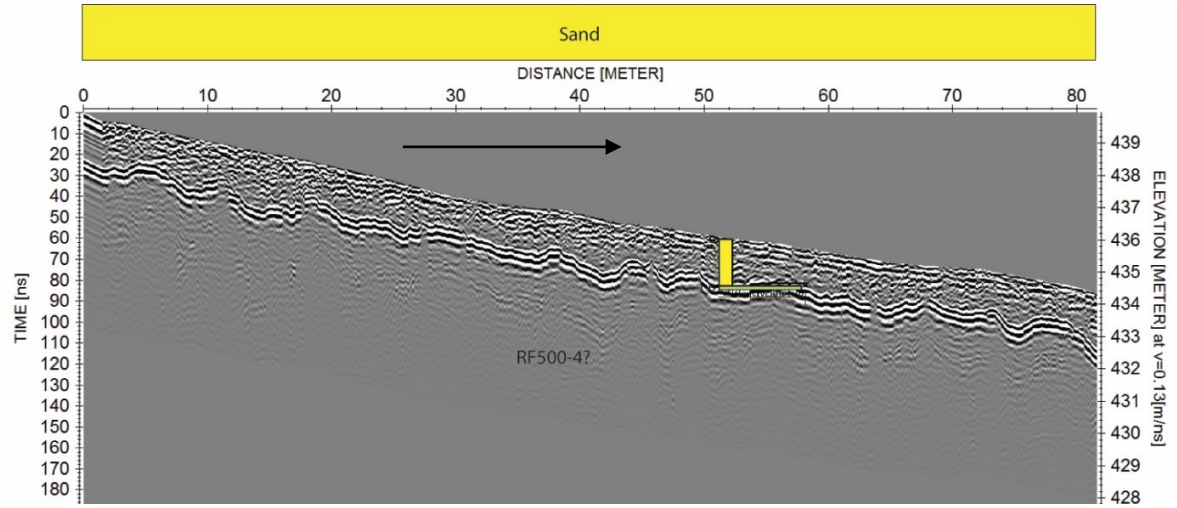

Figure 3.11b: Borehole NGO-DD15-2026, which is drilled into a heavily vegetated fine sand Type 4 splay, plotted overtop of normal 500 MHz GPR imagery. The coloured horizontal bar above the GPR transect shows sediment grain size on the esker surface. The strong reflection ~2 m below ground surface likely records both the permafrost table and the transition from sand to diamicton. A to A' is left to right in the GPR transect. Down-esker is right to left in LiDAR and GPR transect, as indicated by the black arrows.. Vertical exaggeration = 6.7.

f) Sedimentary architecture of Type 2 component at Borehole NGO-DD15-2027

Borehole NGO-DD15-2027 was drilled into a pebble and cobble covered Type 2 component along the Misery tributary esker (Figure 3.1). The upper 2 m of the 500 MHz GPR transect from this location (Figure 3.12) correlates with a package of gravel at the top of the borehole. At this level, discrete 0.5–1 m thick tabular packages of down-esker dipping reflections (~25° dip), each bounded by planar reflections, are observed (RF500-1) that are interpreted to represent braid bars (e.g., Lunt and Bridge, 2004). The gravel unit sharply overlies an upward-coarsening pebbly sandy unit that in turn directly overlies bedrock (Figure 3.12). The upward-coarsening pebbly sand unit is associated with a package of weak, irregular, large-scale (>4 m thick) down-esker dipping (~15° dip) reflections below the permafrost table (RF500-2), interpreted to be sandy deltaic foreset beds. The succession is interpreted to reflect progradation of a coarse-grained delta into standing water that occupied a re-entrant of the ice front. Collapsed depressions up-esker of the borehole location, which are visible in the LiDAR image in Figure 3.12, could indicate this segment of esker was deposited over ice that subsequently melted out locally (e.g., Price, 1969), or possibly that ice blocks were deposited in the deltaic package that have subsequently melted out (e.g., Maizels, 1997).

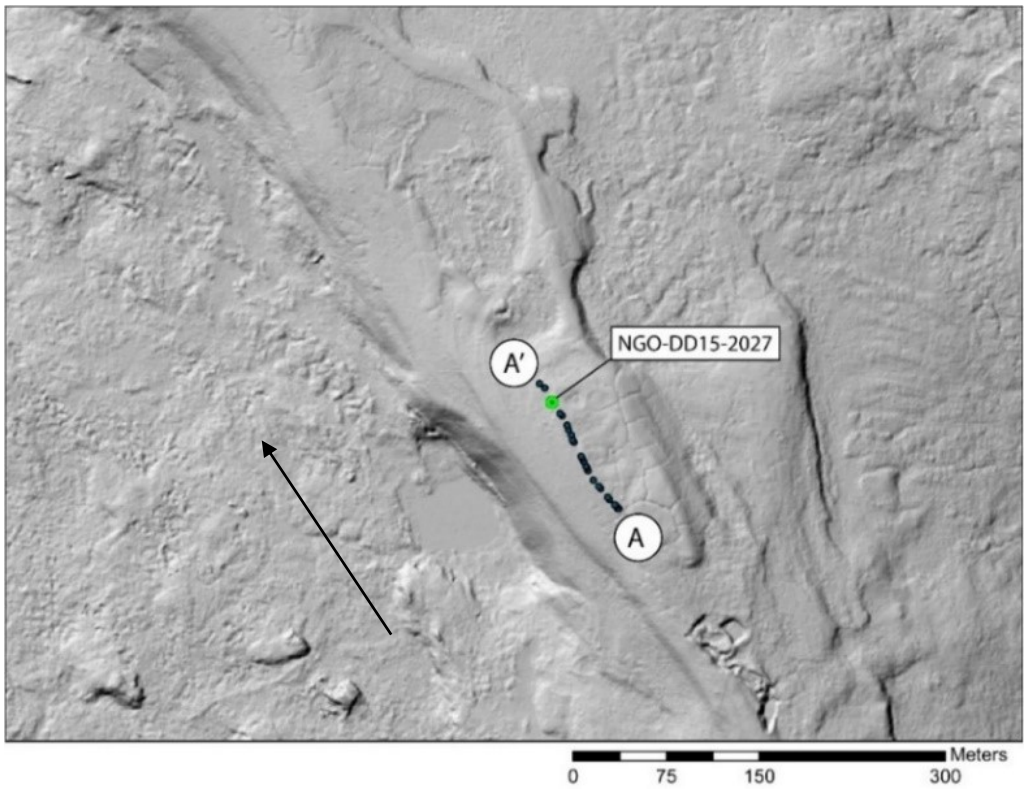

Figure 3.12a: LiDAR image of drill hole NGO-DD15-2027 location. Black arrow indicates down-esker direction.

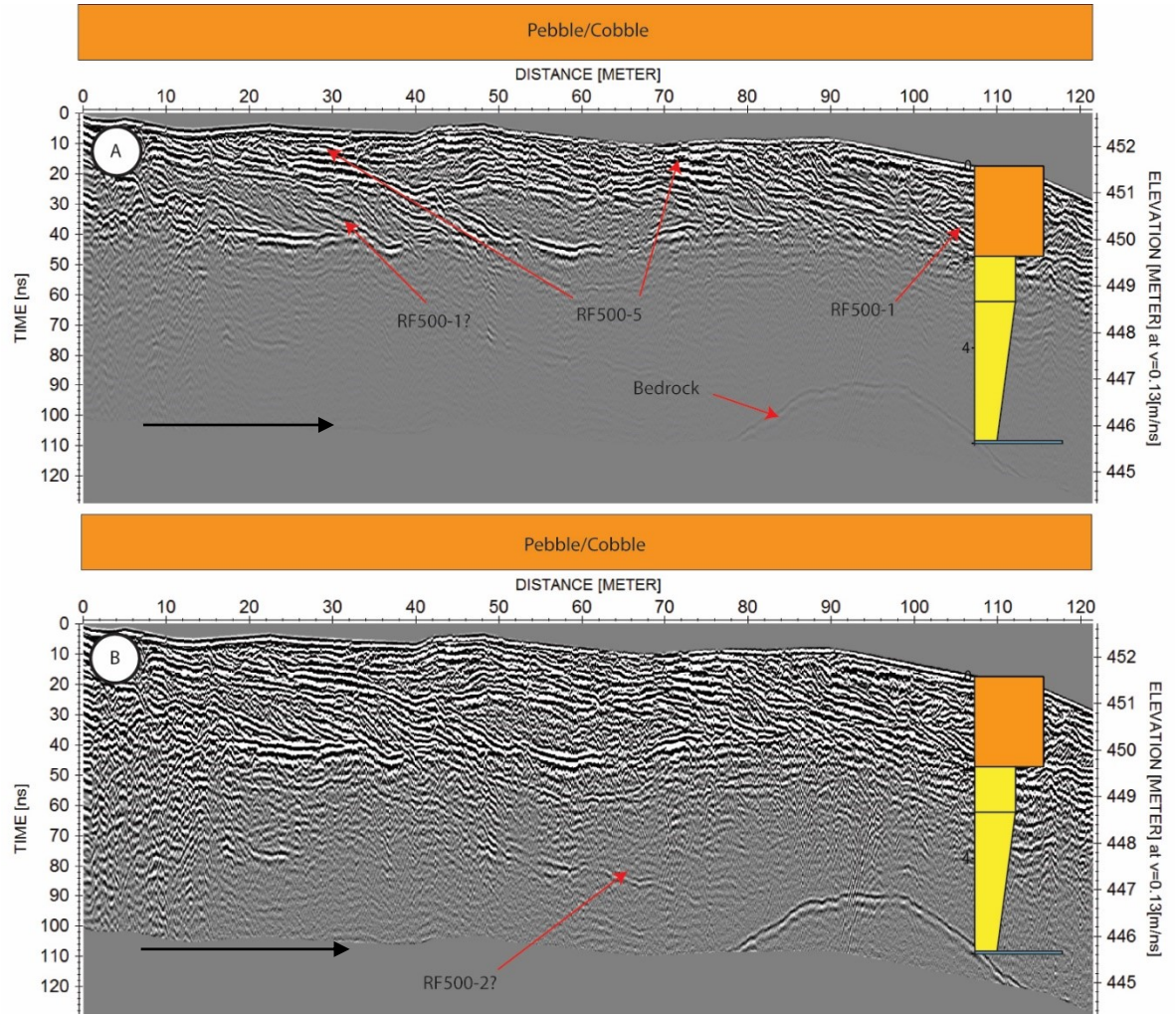

Figure 3.12b: Borehole NGO-DD15-2027, which is drilled into a pebble and cobble covered Type 2 component, plotted overtop of normal (A), and gain increased (B) 500 MHz GPR transects. A to A' is left to right. The coloured horizontal bar shows sediment grain size on the esker surface. The strong reflection ~2 m below ground surface is the permafrost table. Down esker direction is northwest in the LiDAR, and right in the GPR transect, as indicated by the black arrows. Vertical exaggeration = 14.2.

g) Sedimentary architecture of Type 3 component at Borehole NGO-DD15-2029

Borehole NGO-DD15-2029 was drilled into a pebble covered, flat-topped Type 3 component along the Misery tributary esker (Figure 3.1). The borehole consists of an upper 1 m thick package of pebbles and small (<10 cm diameter) cobbles overlying >10 m of pebbly coarse sand.

The 500 MHz GPR transect from this location (Figure 3.13a) is similar to the 500 MHz transect collected from the Type 4 detached pad where borehole NGO-DD15-2020 is located (Figure 3.9). Pseudo-horizontal reflections above the permafrost table (~2 m depth) are disrupted and irregular (Figure 3.13a), and coherent reflections below the permafrost table are absent. Undulations in the permafrost table are likely the result of patches of raised vegetation, resulting in an effect similar to what was observed in Figure 3.11.

The up-esker end of the 100 MHz GPR transect from the NGO-DD15-2029 borehole location (Figure 3.13b) begins at a low elevation, where the landform surface is highly irregular and the GPR data are "noisy" and characterized by short, irregular, pseudo-horizontal reflections. These features are interpreted to reflect post-depositional slumping along the south eastern edge of the landform, an interpretation reinforced by the slumped appearance of the landform in the LIDAR data (Figure 3.13). On the elevated flat plateau that forms the bulk of the Type 3 landform, the appearance of the GPR transect changes. Here, a package of weak, relatively continuous planar reflections (RF100-1) associated with the sand unit at the base of the borehole overlies a package of stronger, irregular reflections (RF100-5) below the base of the borehole. A reflection defining the contact between these two units rises in a down-esker direction. This reflection has a similar elevation as the surrounding till plain suggesting that it corresponds to the top of the till.

The sedimentary succession in this drill hole appears similar to other holes where coarse gravelly topsets overlie sand-bearing foreset beds (Figures 3.7, 3.12). However, the large-scale inclined reflections that characterize these other locations are not present.

Small tundra polygons that are present on the surface at this location, but are not visible in LiDAR images, could be responsible for disturbing the primary bedding, and produce the disrupted GPR texture. Additionally, surface vegetation tends to trap and stabilize fine sediment, and this may also play a role in obscuring bedding in the 500MHz transect. Steep sides of the landform in this location (~35°) likely indicate ice confinement during deposition. The presence of a large kettle hole (see LiDAR in Figure 3.13) suggests either that deposition of this component occurred on an ice-rich substrate that has since melted out in places (e.g., Price, 1969; Wolfe, 1998), or that ice blocks were deposited in the sediment body, and subsequently melted out (e.g., Maizels, 1997).

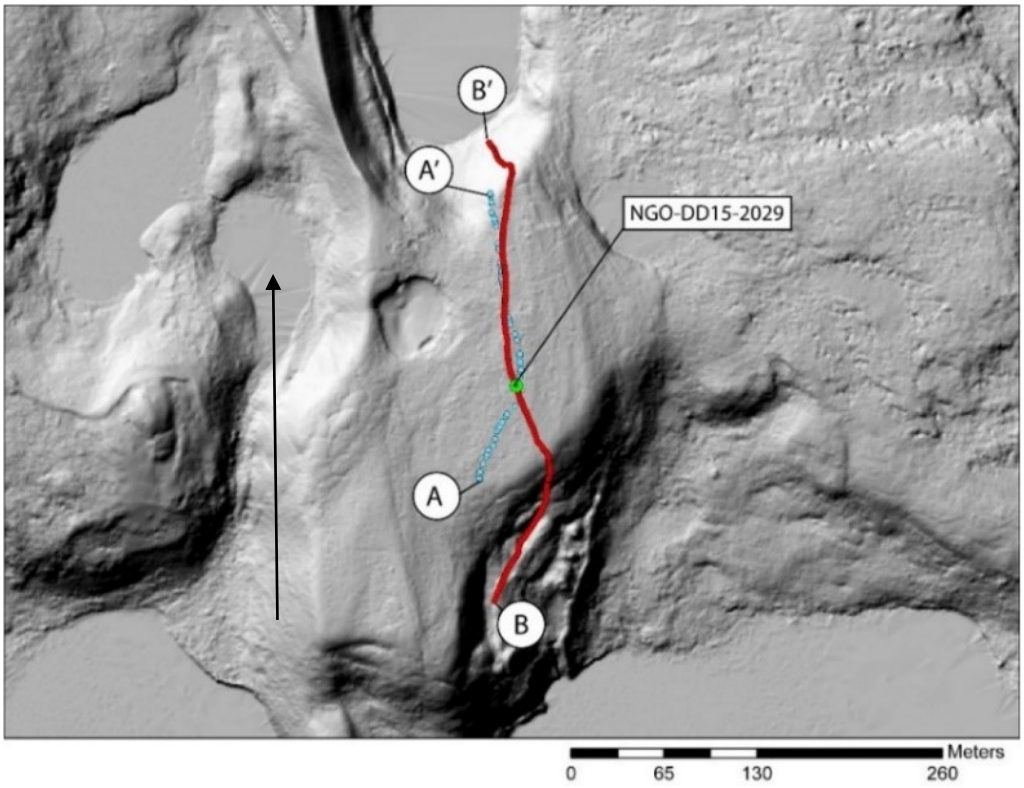

Figure 3.13a: LiDAR image of drill hole NGO-DD15-2029 location. Black arrow indicates down-esker direction.

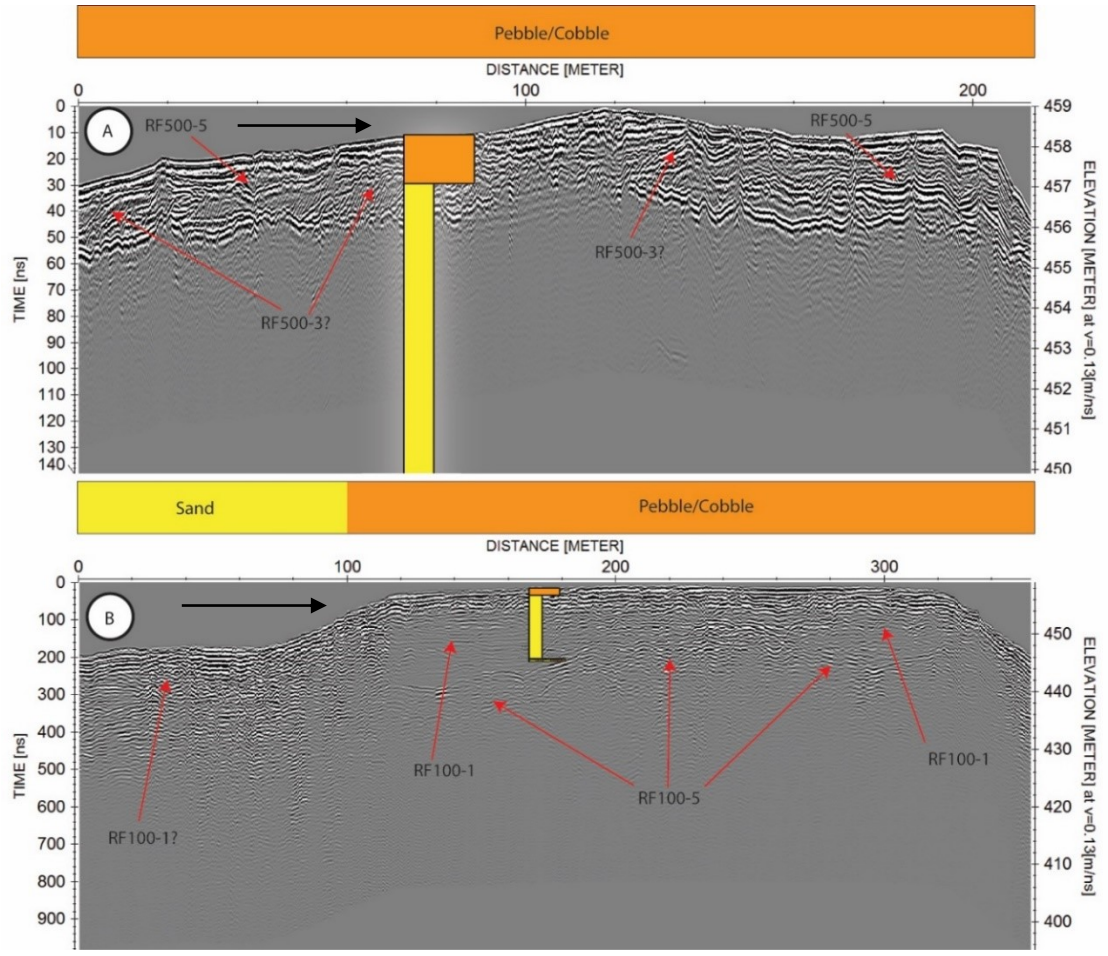

Figure 3.13b: Borehole NGO-DD15-2029, which is drilled into a flat-topped, ridge-attached Type 3 component, plotted overtop of 500 MHz (A) and 100 MHz (B) GPR transects. A to A' and B to B' are left to right. The coloured horizontal bars in (A) and (B) show sediment grain size on the esker surface. In (A), the strong reflection ~2 m below ground surface is the permafrost table. In (B), the airwave and groundwater obscure reflections generated by strata from ground surface to a depth of ~5 m. Down-esker is north in the LiDAR, and to the right in the GPR transects, as indicated by black arrows. Vertical exaggeration (A) = 23.3. Vertical exaggeration (B) = 5.7

3.7: Results: Depositional environments and stratigraphic relationships of esker components

In this section, all data types—LiDAR, surficial sediment samples, GPR transects, boreholes, and the single outcrop—are integrated in order to uncover relationships between the external characteristics (i.e., surficial sediment, morphology) and the internal characteristics (i.e., sedimentary architecture) of the Type 1 to 4 morpho-sedimentary components that make up the esker (Table 3.3), which are used as a basis for interpreted the environments within which the components were deposits. Stratigraphic contacts and lap-out relationships between the different components are discussed.

Table 3.3: Summary of GPR characteristics of the identified esker components.

LANDSCAPE ELEMENT	COMPONENT	100 MHz GPR				500 MHz GPR			
		Radar Facies (Dominant, Subordinate	Depth of effective penetration	Reflections conformable or disconformable with surface	Clinoforms (rare common, absent)	Radar Facies (Dominant, Subordinate	Depth of effective penetration	Reflections conformable or disconformabe with surface	Clinoforms (rare common, absent)
ESKER	Type 1. Sharp-crested cobbly to bouldery ridges	RF100-4 (Dominant) RF100-5 (Subordinate)	~40 m	Conformable	absent	RF-500-4	~6 m	n/a	absent
	Type 2. Flat-topped cobbly to sandy ridges	RF100-2 (Dominant) RF100-1 (Subordinate)	~40 m	Conformable to disconformable	common	RF500-1 RF500-1 (Dominant) RF500-5 (Subordinate)	~6 m	Conformable to disconformable	common
	Type 3. Flat-topped sandy to cobbly pads	RF100-1 RF100-2 (Dominant) RF100-3 (Subordinate)	~40 m	Conformable to disconformable	common	RF500-2 Dominant RF500-5 (Subordinate)	~6 m	Conformable to disconformable	common
ASSOCIATED SEDIMENT	Type 4: Pads	RF100-1 (Dominant) RF100-5 (Subordinate)	~40 m	Conformable	absent	RF500-5	~6 m	Conformable	absent
	Type 4: Splays	n/a	~40 m	Conformable?	absent	RF500-5 (Dominant) RF500-4 (Subordinate)	~6 m	Conformable?	absent
ADJACENT TERRAIN	Diamicton (till)	RF100-5	~40 m	Conformable	absent	RF500-4	~6 m	Conformable	absent
	Exposed bedrock	RF100-5	~40 m	Dsconformable	n/a	n/a	n/a	n/a	n/a

Type 1 components (R-channel deposits)

Type 1 components have triangular cross sections and are invariably covered in rounded cobbles and boulders (e.g., Figure 3.14). They lack obvious features related to post-depositional deformation. The only significant exposure along the esker—a 15 m high stream cut through a Type 1 component (Figure 3.3)—reveals rounded, framework-supported cobbles and boulders with a pebbly coarse sand matrix from top to bottom. Ground penetrating radar transects show radar facies with short, irregular, pseudo-horizontal reflections and abundant hyperbolic reflections believed to be indicative of coarse gravelly sediment (RF100-5 and RF500-4). The GPR transects often show little to no variations in radar facies. Based on these observations, it is inferred that Type 1 components are composed of crudely stratified framework-supported cobbles and boulders, likely with a coarse sandy matrix.

The basal contact of Type 1 components is not well imaged by GPR and is below the elevation of the base of the exposure (Figure 3.3). However, insight into its nature can be obtained from the LiDAR data. In several locations, cobble and boulder dominated Type 1 components appear to directly overlie thin till or bedrock in esker corridors. This relationship is perhaps most evident at the down-flow fining esker segment described in detail in Chapter 2 (Figures 2.3, 2.12), where a Type 1 component at the up-flow end of the segment appears to directly overlie scoured bedrock. In addition to suggesting that Type 1 components may commonly erosively overlie the top of the till, this image suggests that the sediment in esker segments can be locally sourced from scour zones located underneath, and immediately up esker, of Type 1 components.

Type 1 components are interpreted to have aggraded in subglacial meltwater tunnels (R channels), and to have been sourced from the local subglacial till, and possibly from debris-rich glacial ice. Larger sediment (large pebbles, cobbles and boulders) likely commonly travelled as bedload and became rounder in the process, whereas finer grains (mud, sand and possibly granules and finer pebbles) likely commonly travelled in suspension and remained relatively angular in the process, commonly bypassing the R-channel to the conduit terminus. In this study, evidence for a subglacial interpretation comes from several sources. LiDAR imagery shows that the till tends to be relatively thin or absent in the surrounding esker corridors, and several GPR lines and a drill hole show that esker material can directly overlie bedrock (hole NGO-DD15-2017, Figure 3.12).

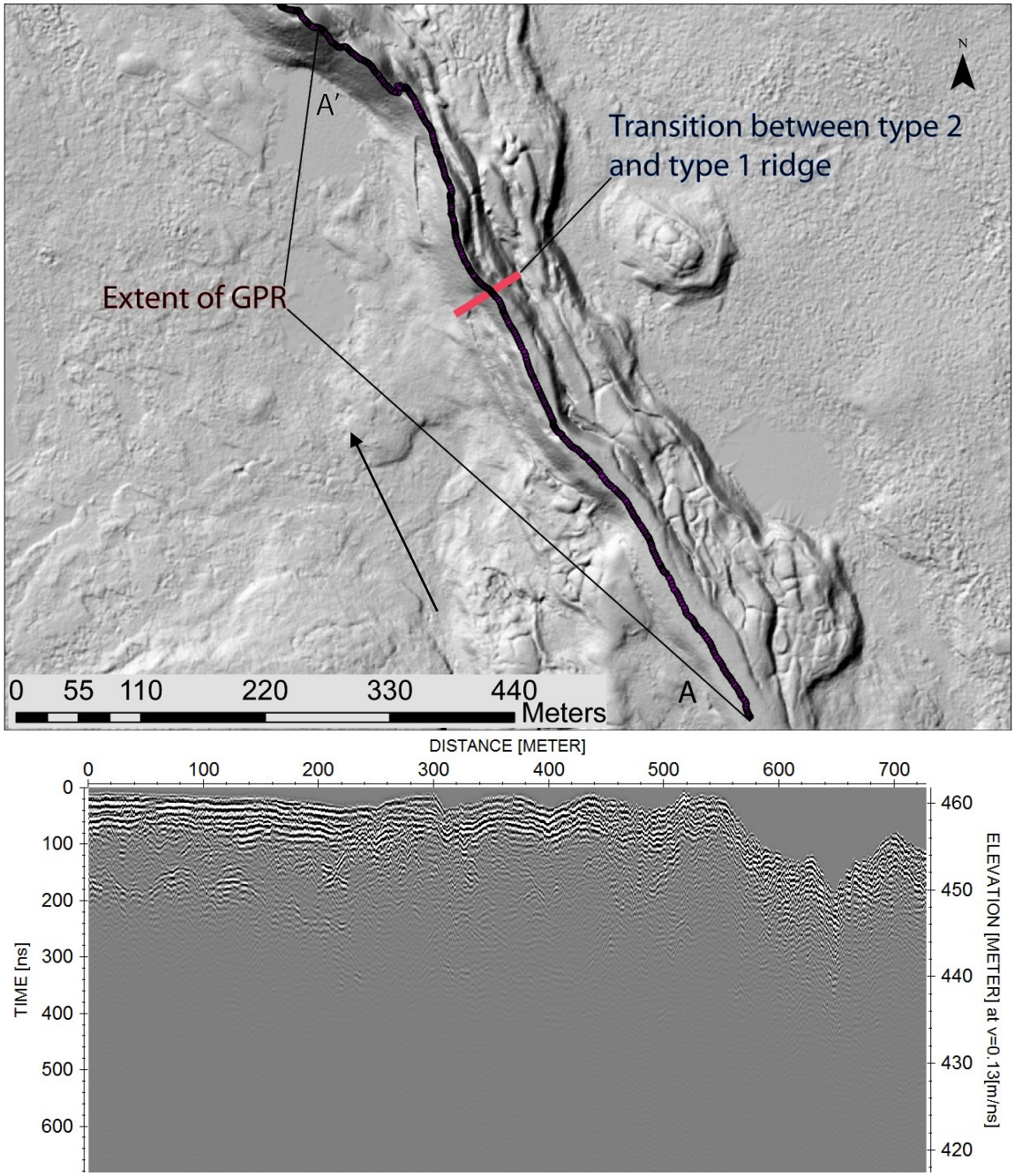

Figure 3.14: LiDAR imagery and un-interpreted 100 MHz GPR from MTE-a area (fig 2.2). Black arrown indicates down-esker direction.

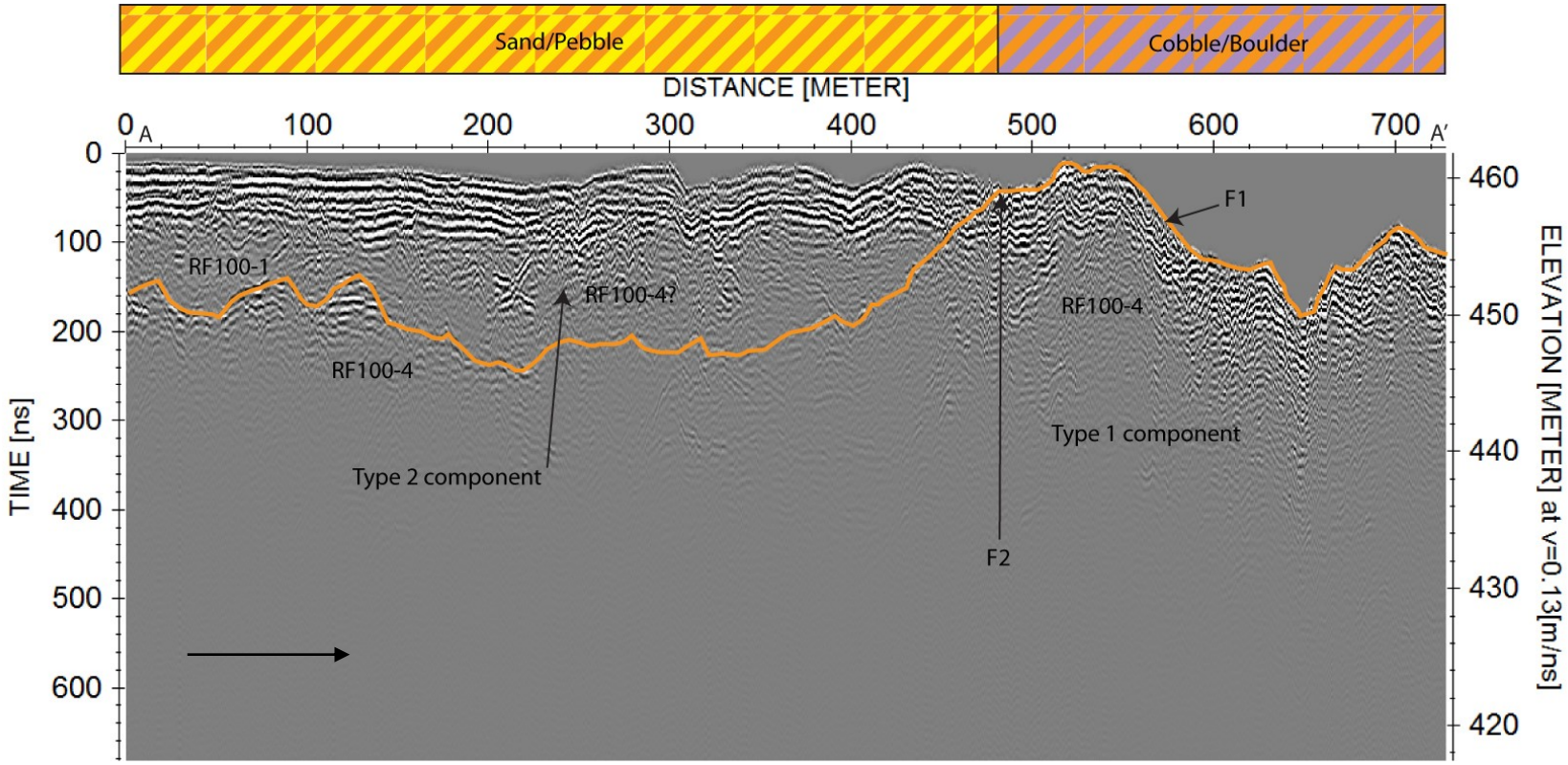

Figure 3.15: Interpreted 100 MHZ GPR profile over Type 2 and Type 1 components (from Figure 3.14). F1 indicates upper surface of cobble and boulder-dominated Type 1 component. F2 indicates approximate surface location of the abrupt transition between the broad crested, coarse sandy gravel Type 2 component and the sharp crested, boulder-dominated Type 1 component. While individual beds are not evident in this GPR profile, a relatively strong reflection at a depth of 10–15 m from 0 to 350 m and gradually rising to surface from 350–480 m is traced, and interpreted to represent buried Type 1 component material. This shows that in this locale, the Type 2 component overlies the Type 1 component. Black arrow indicates down-esker direction. Vertical exaggeration = 16.5.

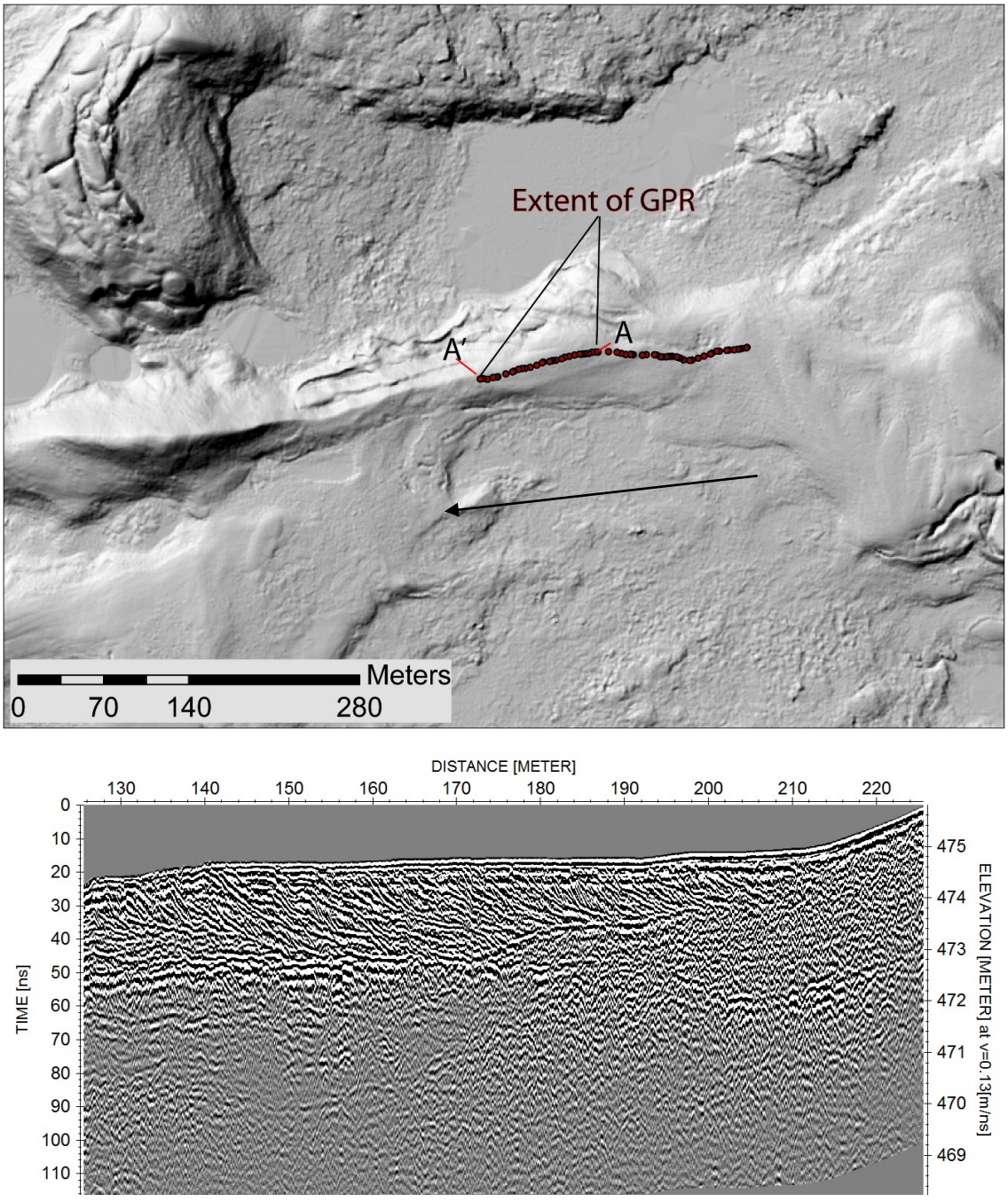

Figure 3.16: LiDAR imagery and un-interpreted 100 MHz GPR from MTE-j area (Fig 2.2). Down-esker (black arrow) is to the left in the LiDAR image, and to the right in the GPR transect.

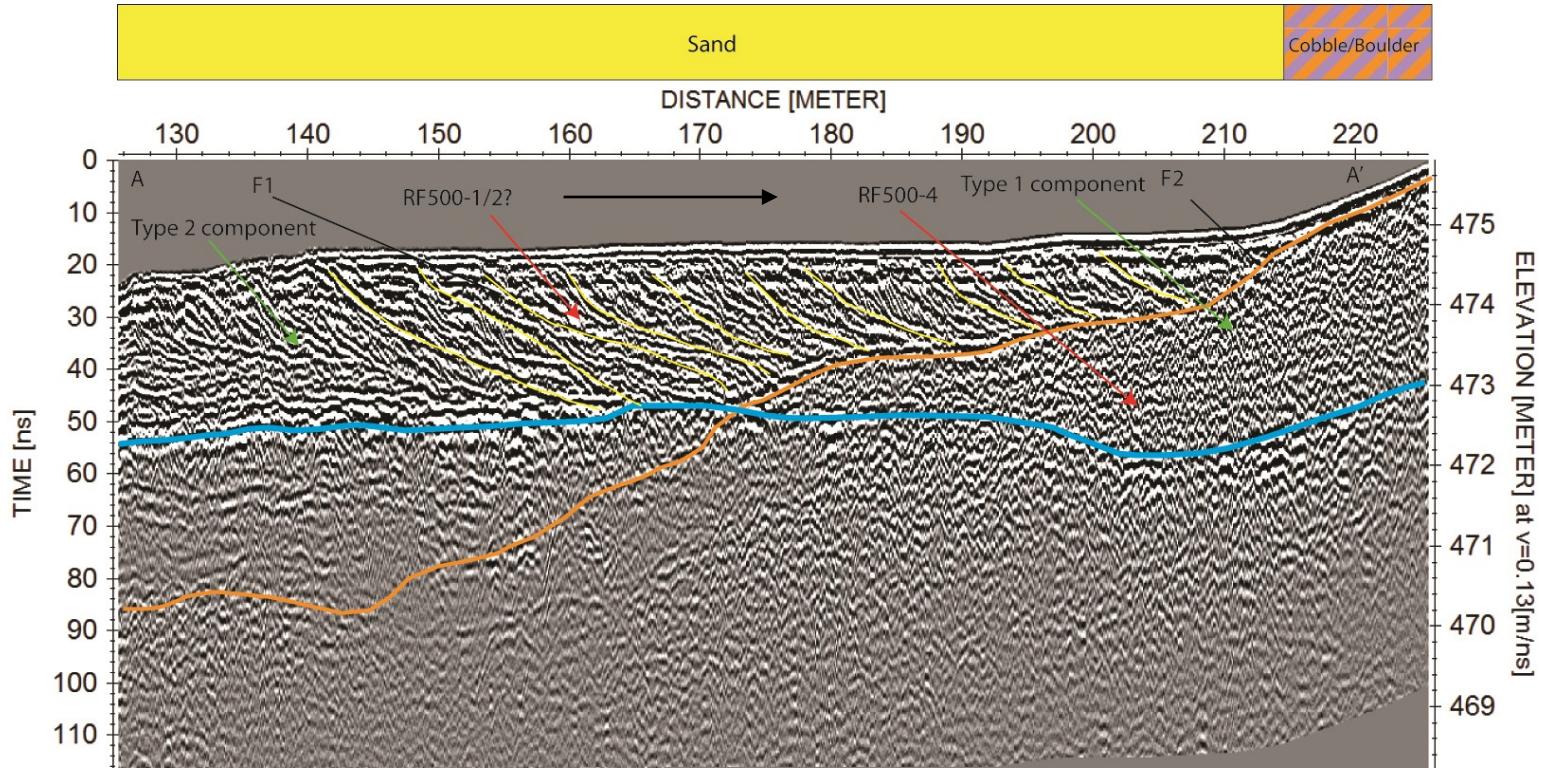

Figure 3.17: Interpreted version of the 500 MHz GPR profile in Figure 3.16, which shows a typical down-flow transition from a Type 2 component to a Type 1 component. Down-esker is to the right, as indicated by the black arrow. The blue line indicates the permafrost table. From 128 to 214 m, inclined reflections (10–15°) are observed within the flat-topped Type 2 component (indicated by F1 and traced in yellow) and the sediment at surface consists of coarse sand. The inclined reflections, interpreted to be deltaic foresets, down lap the top of a hyperbola rich cobble-boulder gravel Type 1 component the downlap surface (F2) is traced in orange, which comes to surface at 214 m. Down-esker of this, the surface sediment is cobble- and boulder-dominated (214–226 m in GPR transect), and the landform develops the sharp-crested profile typical of Type 1 components, which is clearly visible in the LiDAR in Figure 3.13. This is typical of downflow transitions from Type 2 to Type 1 components: the former tend to overlie, downlap, and pinchout against the latter moving downflow. An excavation was made, approximately 1 m in depth at the 200 m mark, confirming the presence of underlying cobbles and boulders. Vertical exaggeration = 11.8.

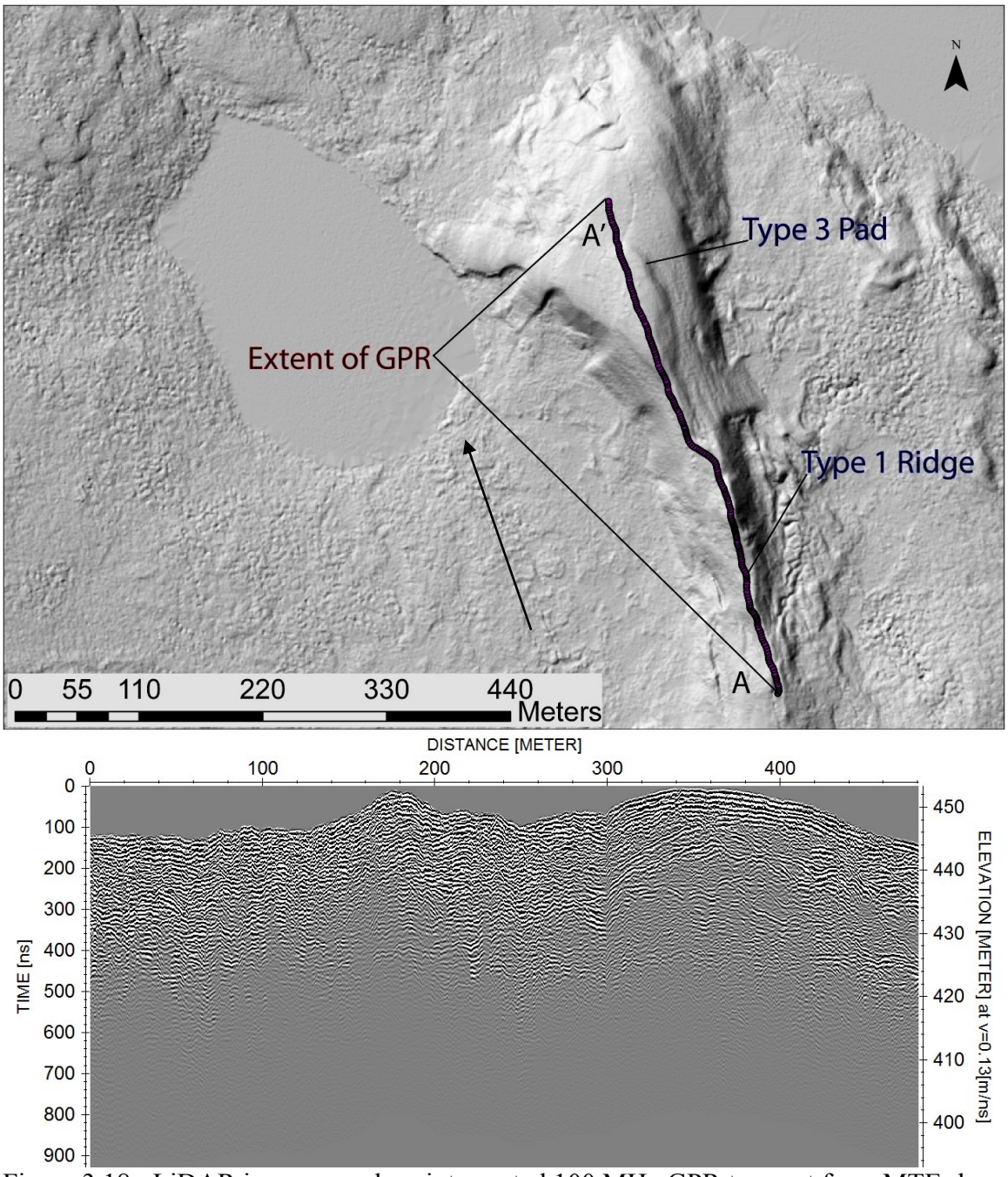

Figure 3.18: LiDAR imagery and un-interpreted 100 MHz GPR transect from MTE-d area (Figure 2.2). Down-esker is to the north in the LiDAR image (black arrow), and to the right in the GPR transect

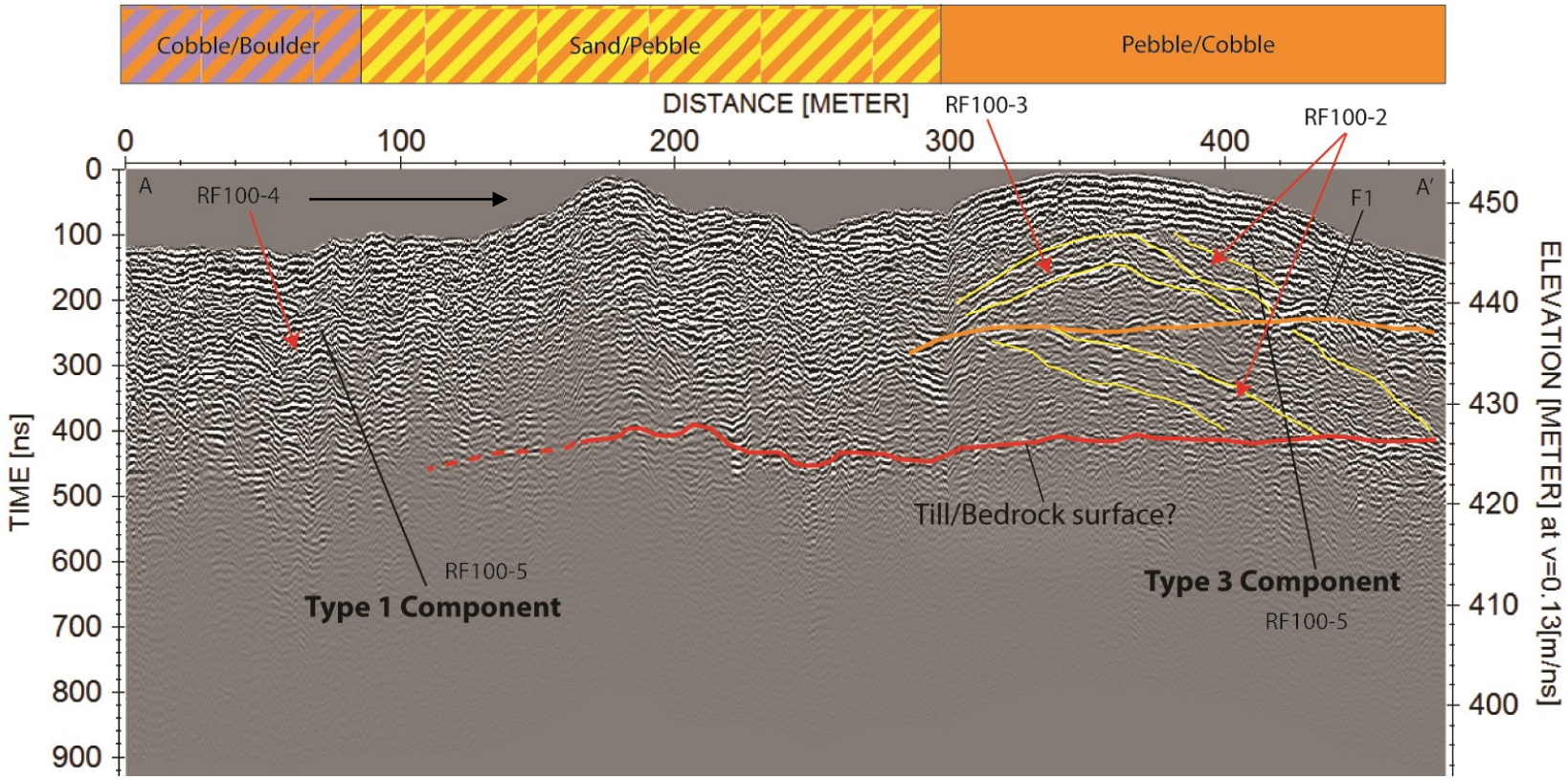

Figure 3.19: Interpreted version of the 100 MHz GPR profile in Figure 3.18, showing a down-flow transition from a cobble and boulder-dominated Type 1 component to a sandy, fan-like Type 3 pad. Down-esker direction is to the right, as indicated by the black arrow. The coloured horizontal bar represents sediment grain size at surface. The airwave and groundwater combine to obscure strata from ground surface down to a depth of ~5 m. At a depth of 20–25 m beginning at the 120 m mark, a relatively strong reflection (traced in red) is present that extends to the down-esker end of the transect. Its elevation is similar to that of the adjacent till plain, suggesting it represents the boundary between esker material and the underlying till or bedrock. Beyond the 300 m mark, individual beds can be traced in the Type 3 material. F1 indicates a planar reflection (traced in orange) that truncates underlying approximately parallel inclined (between 5 and 10 degree dip) beds (traced in yellow). Above F1, at the 300 m mark, backset beds transition into foreset beds. This figure illustrates two potential phases of progradational deposition at the terminus of the feeding Type 1 conduit. A lower package of inclined beds is interpreted to have been deposited within an ice-walled accommodation space, limited by water depth. A subsequent rise in water level within the ice-walled confined space resulted in the second phase of progradational deposition. Vertical exaggeration = 8.0

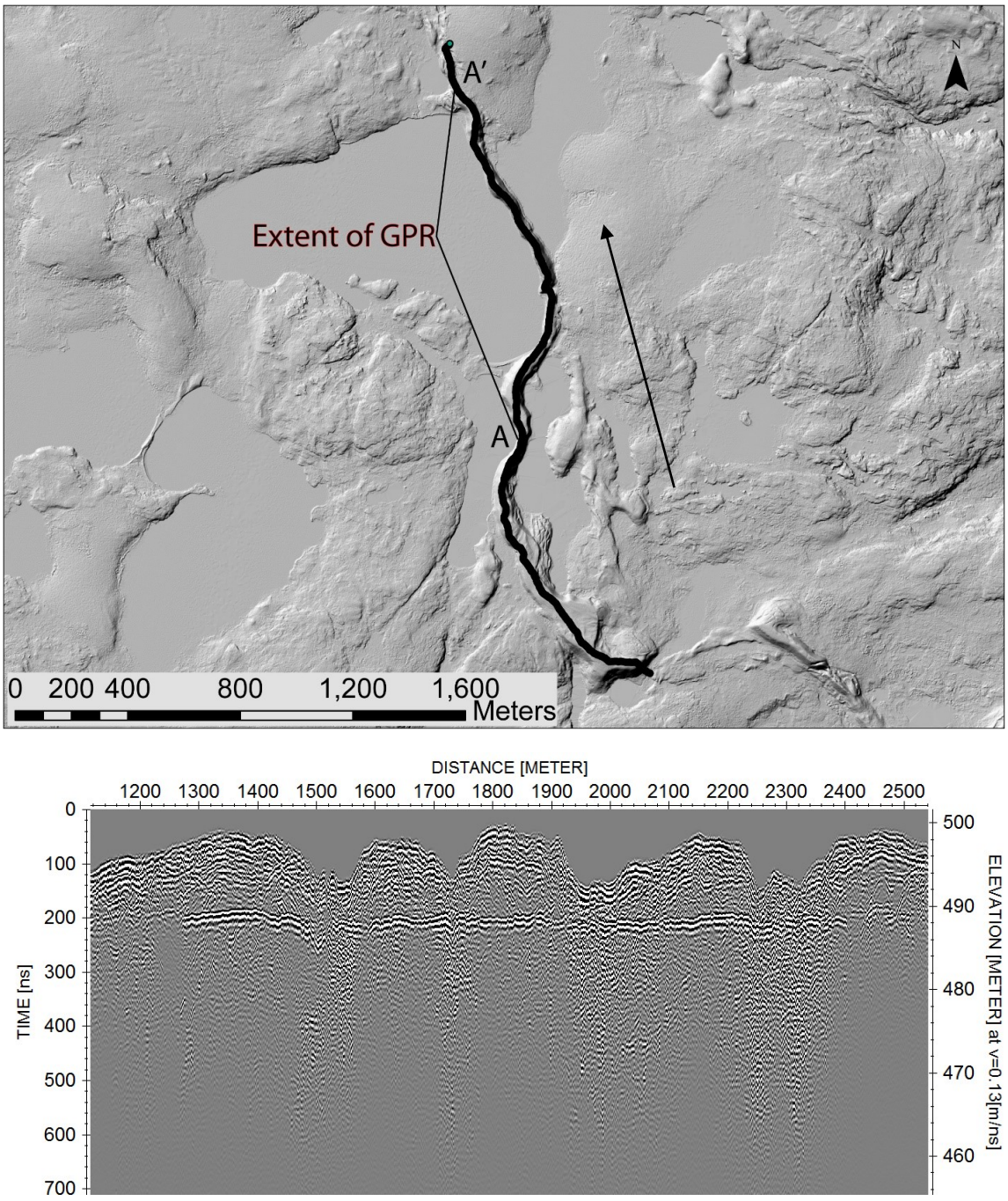

Figure 3.20: LiDAR imagery and un-interpreted 100 MHz GPR line from MTE-j and MTE-k areas (Figure 2.2). Black arrow points down-esker.

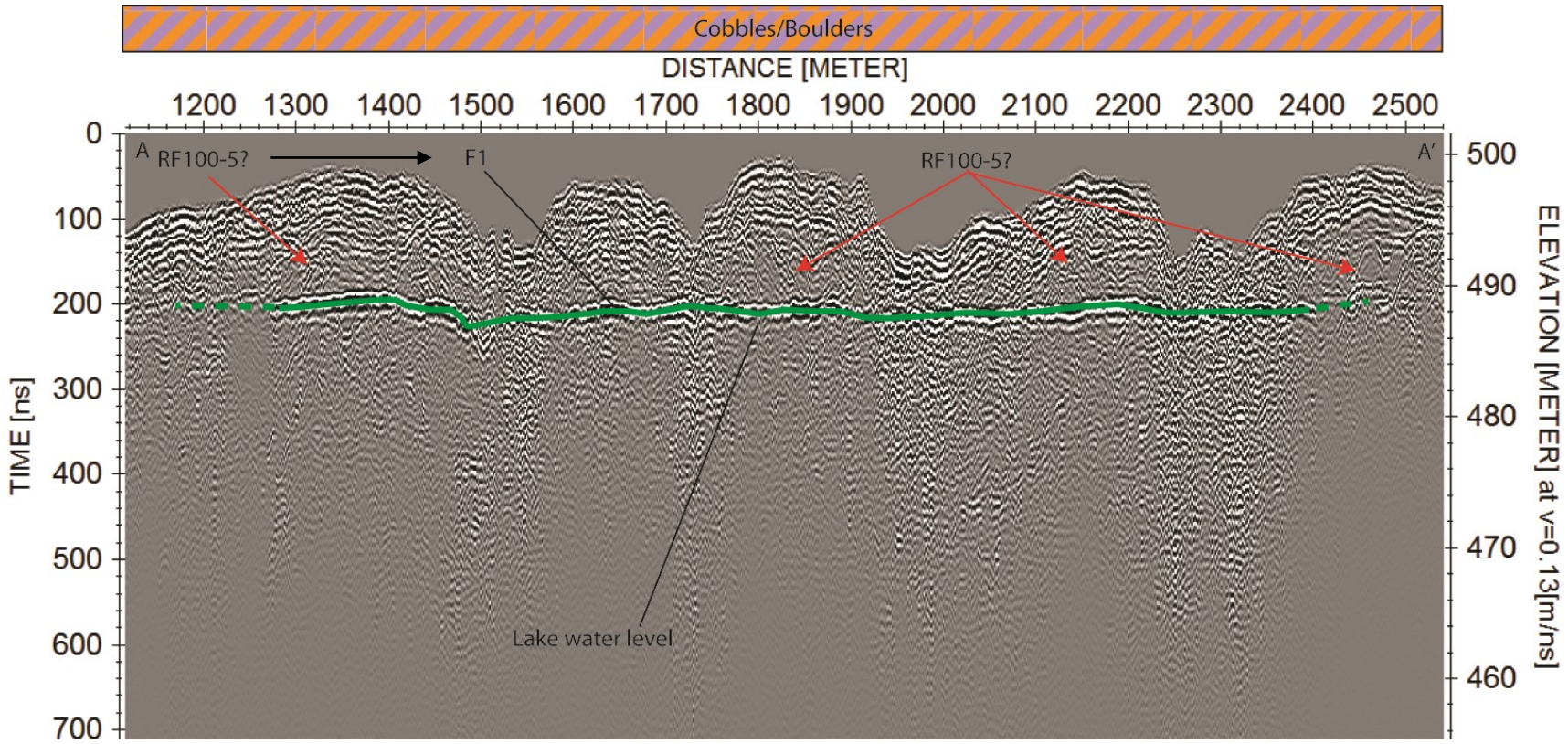

Figure 3.21: Interpreted 100 MHz GPR profile of an undulating, cobble-dominated Type 1 component (Figure 3.20). Black arrow points down-esker. Strong reflection surface indicated by F1 and traced in green is interpreted to represent a water-table reflection. This segment of esker is unique in the study area as it is relatively thin (20–30 m) and bounded by lakes on both sides. Where the esker becomes suitably thin, lake water has permeated the esker material, and a strong water table reflection results at the approximate elevation of the bounding lakes. This figure illustrates the effectiveness of the LiDAR assisted elevation correction applied to the GPR data used in this study. Vertical exaggeration = 30.9.

Type 2 components (narrow ice-confined deltaic deposits)

Type 2 components are relatively narrow (50–100 m), flat- to irregular-topped sediment bodies that form part of the main esker ridge. Their surface texture is finer grained than Type 1 components, ranging from fine sand to pebbles and cobbles. The slope of their flanks ranges from 5° to 35°, but is more commonly steep than gentle. Although their top surfaces commonly appear "flat" in LiDAR, they are observed to undulate irregularly and subtly on the ground. The flat tops can dip down-esker or up-esker. Tundra polygons are common features on the surface of Type 2 components (Figure 3.22). In boreholes, sedimentary successions often consist of sand at depth that is sharply overlain by a thin (typically 1–2 m thick) package of pebbles and cobbles at surface. Type 2 components have a specific radar-facies association. In the 500 MHz survey, planar reflections (RF500-5) dominate in the upper 0–2 m associated with the near-surface gravel, overlying continuous packages of downflow-dipping reflections (RF500-2) associated with the sand at depth. In the 100 MHz survey, Type 2 components are commonly characterized by thick (5–15 m) packages of planar to down-flow-dipping inclined reflections (RF100-1 or RF100-2).

Stratigraphically, Type 2 components are observed to downlap and commonly pinch out downflow onto either Type 1 components (Figures 3.15, 3.17) or till or bedrock (Figure 3.12).

It is interpreted that Type 2 components were generally deposited by deltaic progradation at locations where subglacial streams debouched into standing open water within re-entrants of the ice front. Analogous foresets and topsets are observed in GPR transects from flat-topped glacial deltaic deposits described by Smith and Jol (1997) and

Nemec et al (1999) (see also Bannerjee and MacDonald (1975) and Boulduc (1992)). Variation in morphology and sedimentary architecture of Type 2 components was likely a function of varying conditions at the site of deposition, including re-entrant width, flow depth, and the magnitude of water and sediment discharge. Additionally, there is strong evidence that supraglacial deposition followed by ice melt out occurred in locales where reflections are disrupted and the surface of Type 2 components either undulates irregularly (Figure 3.8) or gains in elevation down esker, suggesting post-depositional deformation and tilting (Figure 3.10).

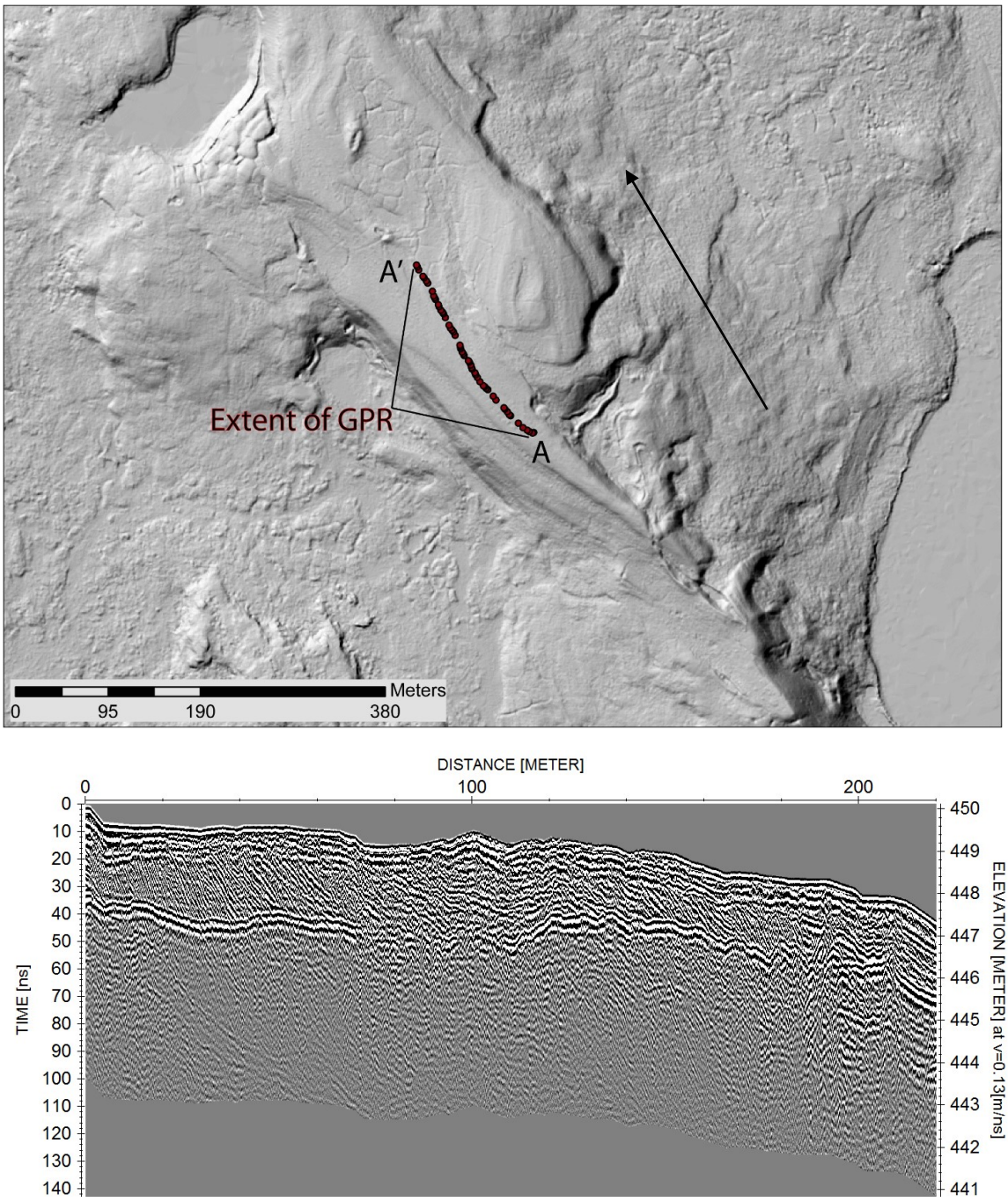

Figure 3.22: LiDAR imagery and un-interpreted 500 MHz GPR transect from at Type 2 component in the MTE-g area (see Figure 2.2 for location of this component along the esker). Down-esker is northwest in the LiDAR image (black arrow) and right in the GPR transect.

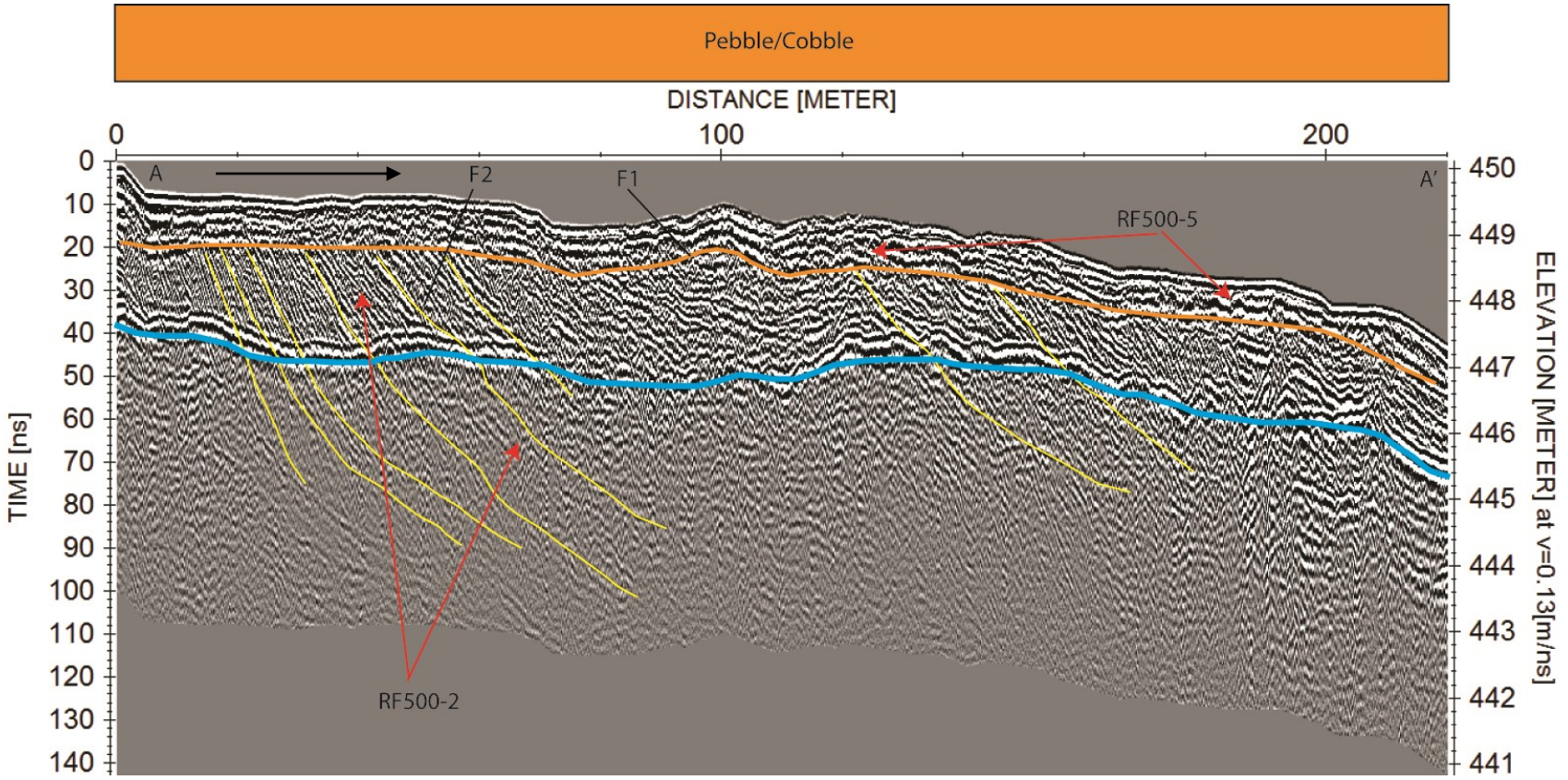

Figure 3.23: Interpreted increased-gain 500 MHz GPR profile of Type 2 component (Figure 3.22). Down-esker is to the right, as indicated by the black arrow. F1 indicates an upper truncation surface (traced in orange) of underlying inclined (15–20°), down-esker dipping reflections (traced in yellow). This is interpreted to be indicative of a coarser, gravel-dominated topset overlying deltaic foreset beds. The deltaic foresets indicated by F2 can be observed to extend below the permafrost table (traced in blue), likely exceeding a depth of 6 m. Vertical exaggeration = 24.4.

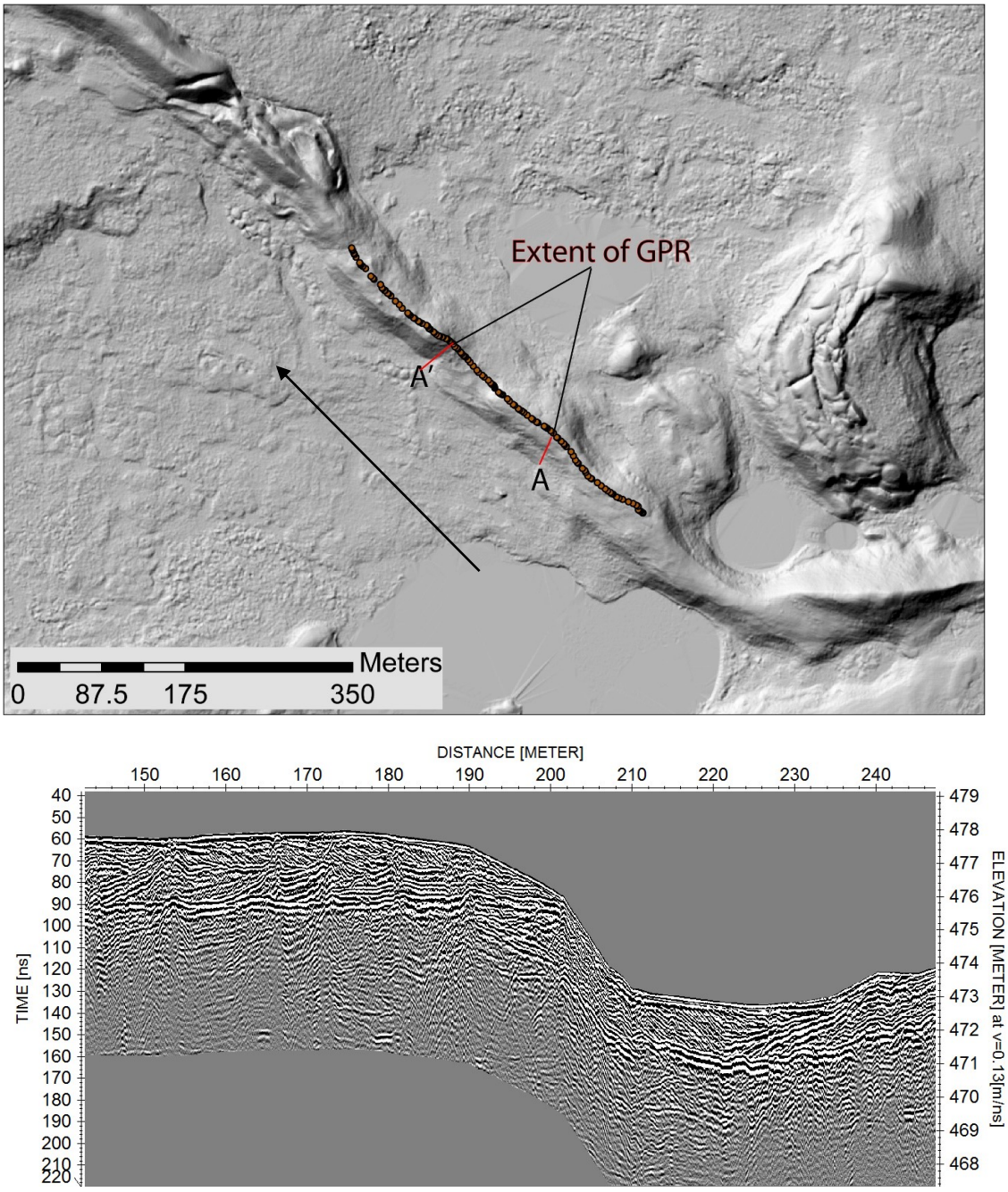

Figure 3.24: LiDAR imagery and uninterpreted 500 MHz GPR from MTE-j area (Figure 2.2). Down-esker direction toward the upper left in LiDAR (black arrow), and toward the right in the GPR transect.

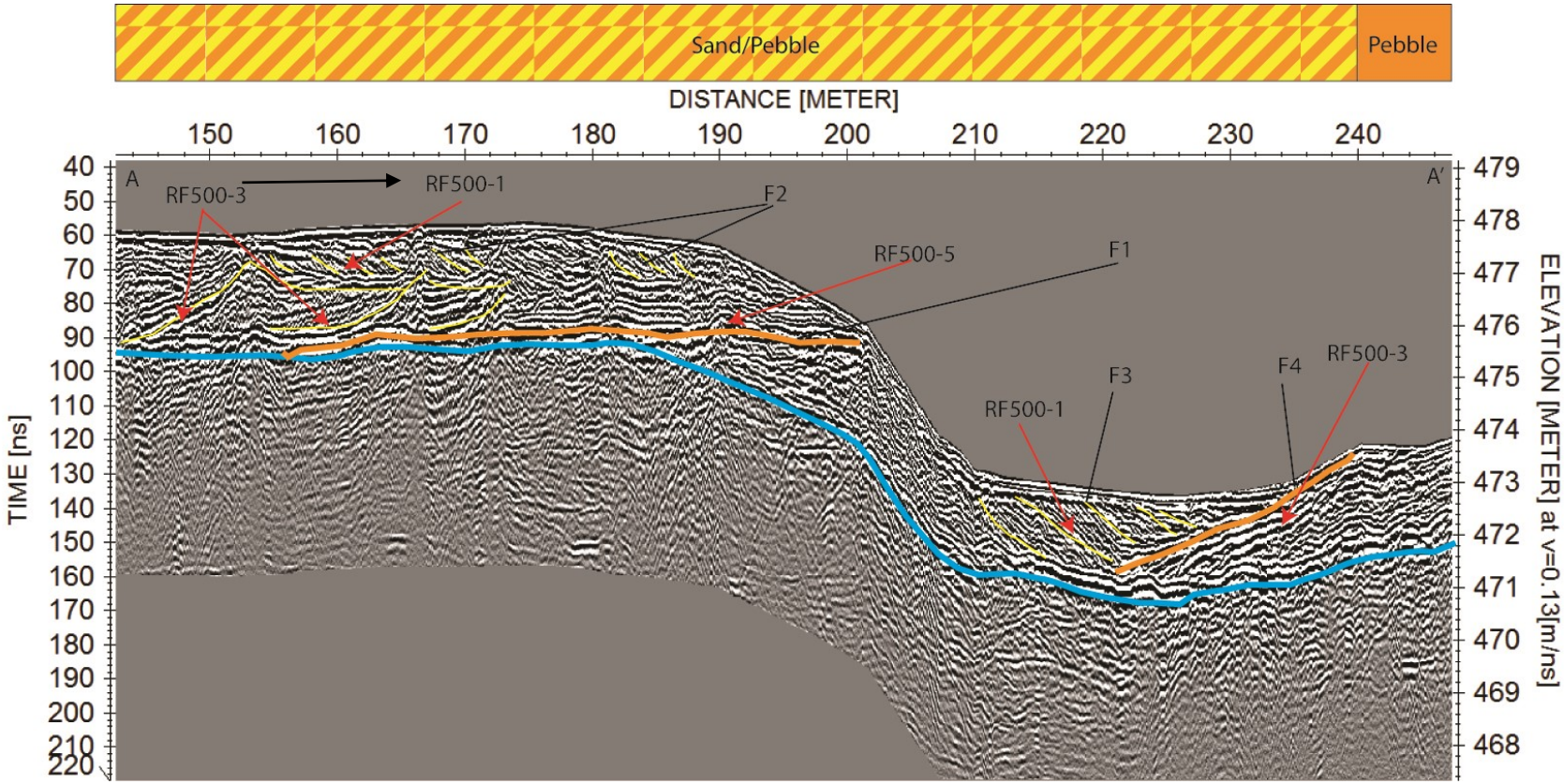

Figure 3.25: Interpreted increased-gain 500 MHz GPR profile of Type 2 component (Figure 3.24). Black arrow indicates the down-esker direction. F1 and F4 (traced in orange) indicate reflections that are bounded by up-esker-dipping (in the case of F1) and down-esker-dipping packages of inclined reflections. It is interpreted that the inclined reflections indicated by F3 stratigraphically overlie F4, and F1 stratigraphically overlies F3. The undulating esker surface could be a result of melt out of buried ice. Vertical exaggeration = 8.8.

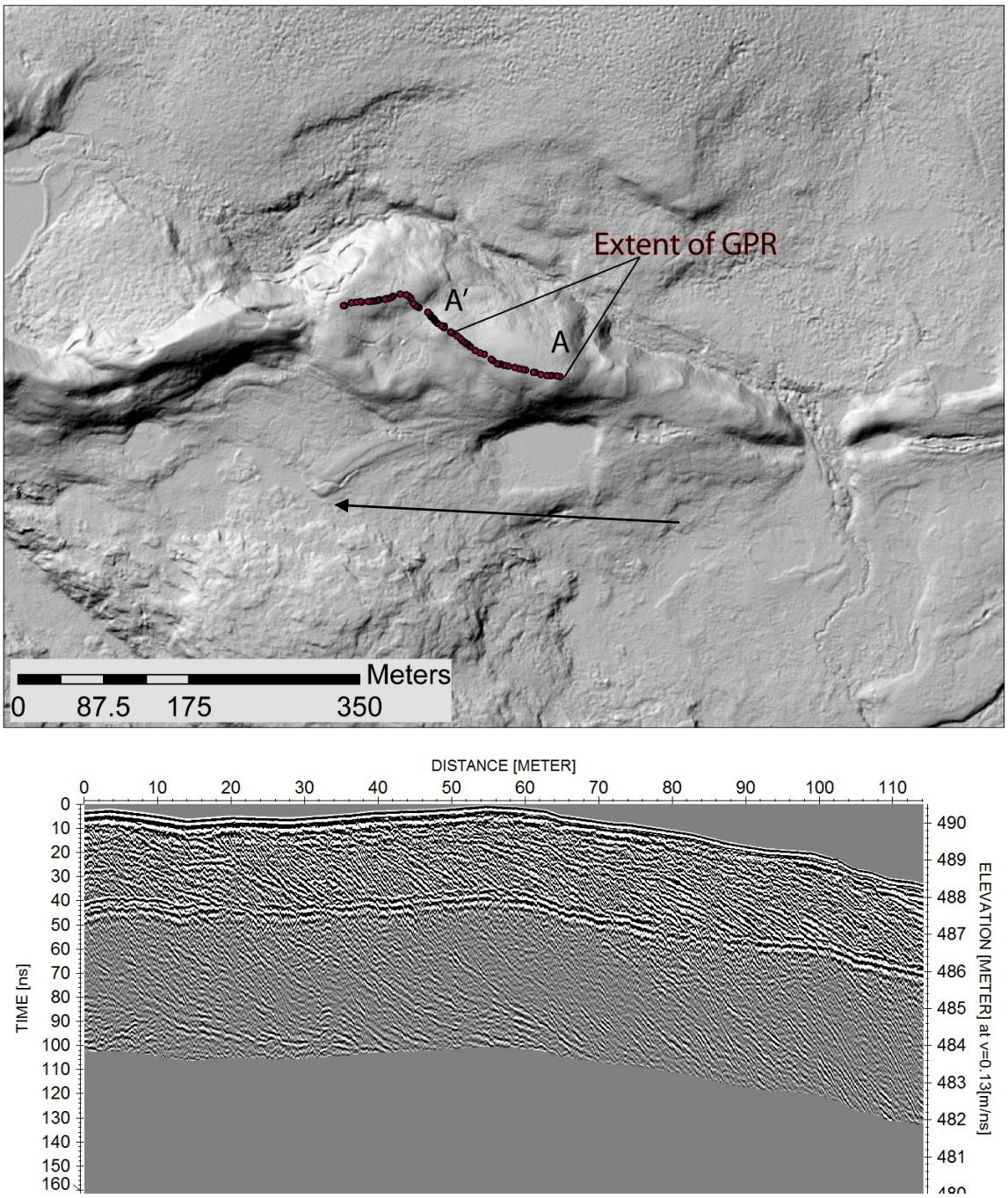

Figure 3.26: LiDAR imagery and uninterpreted 500 MHz GPR transect from a Type 2 component from the ELE-c area (see Figure 2.2 for location of this component along the esker). Down-esker is left in the LiDAR image (black arrow), right in the GPR transect.

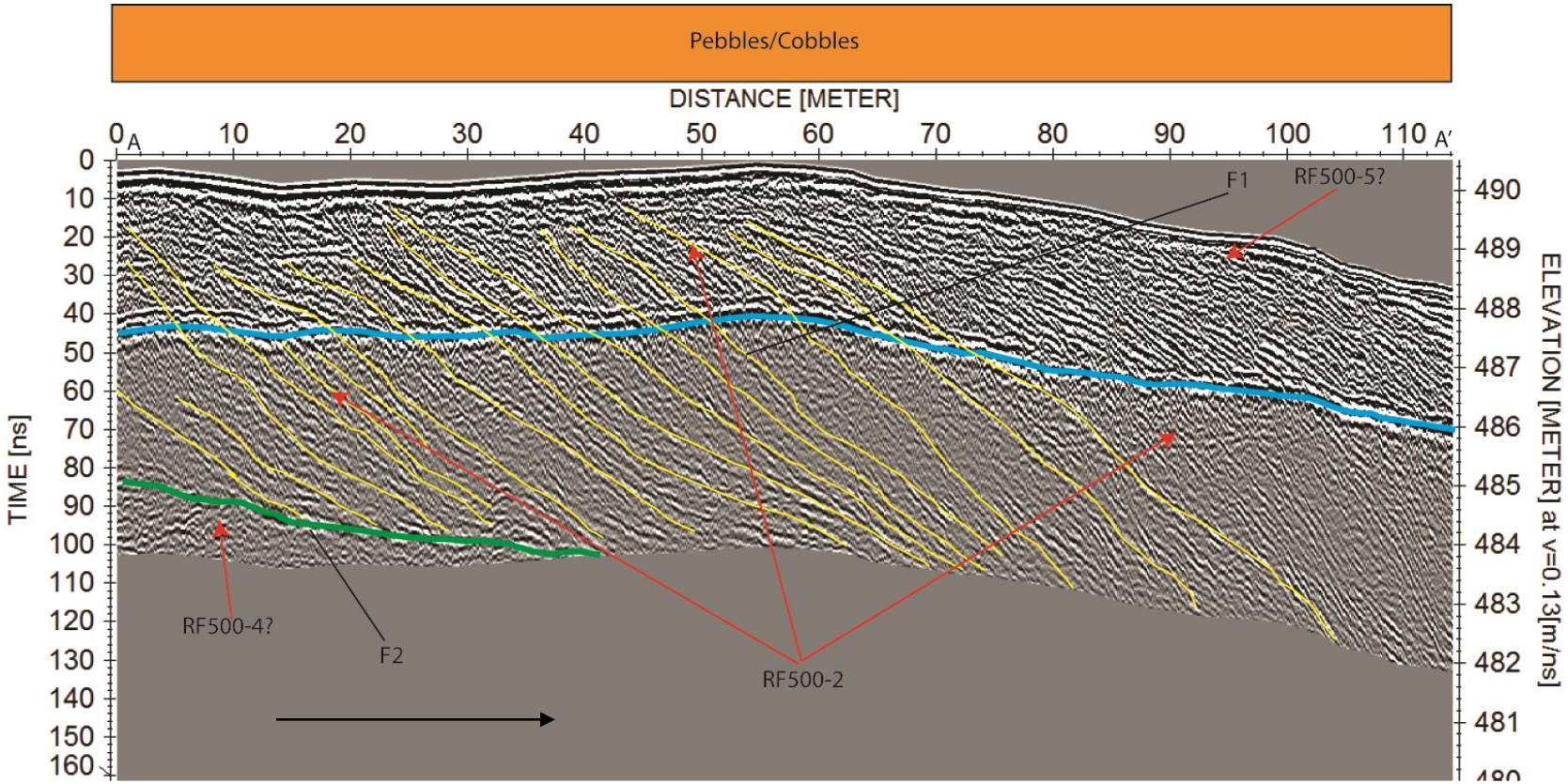

Figure 3.27: Interpreted 500 MHz GPR profile of the Type 2 component shown in Figure 3.26. Down-esker direction is to the right (black arrow). F1 points to long, continuous inclined parallel reflections that dip between 12 and 15° in a down-esker direction and extend visibly below the permafrost table. F2 points to a downlap surface (traced in green) below the inclined reflections. The foreset beds are interpreted to be deltaic in nature, and the material underlying the downlap surface is interpreted to be an older, coarser, Type 1 component based on GPR texture. See Figure 3.29, 5400–5500 m for 100 MHz GPR imagery covering the same area. Vertical exaggeration = 10.8.

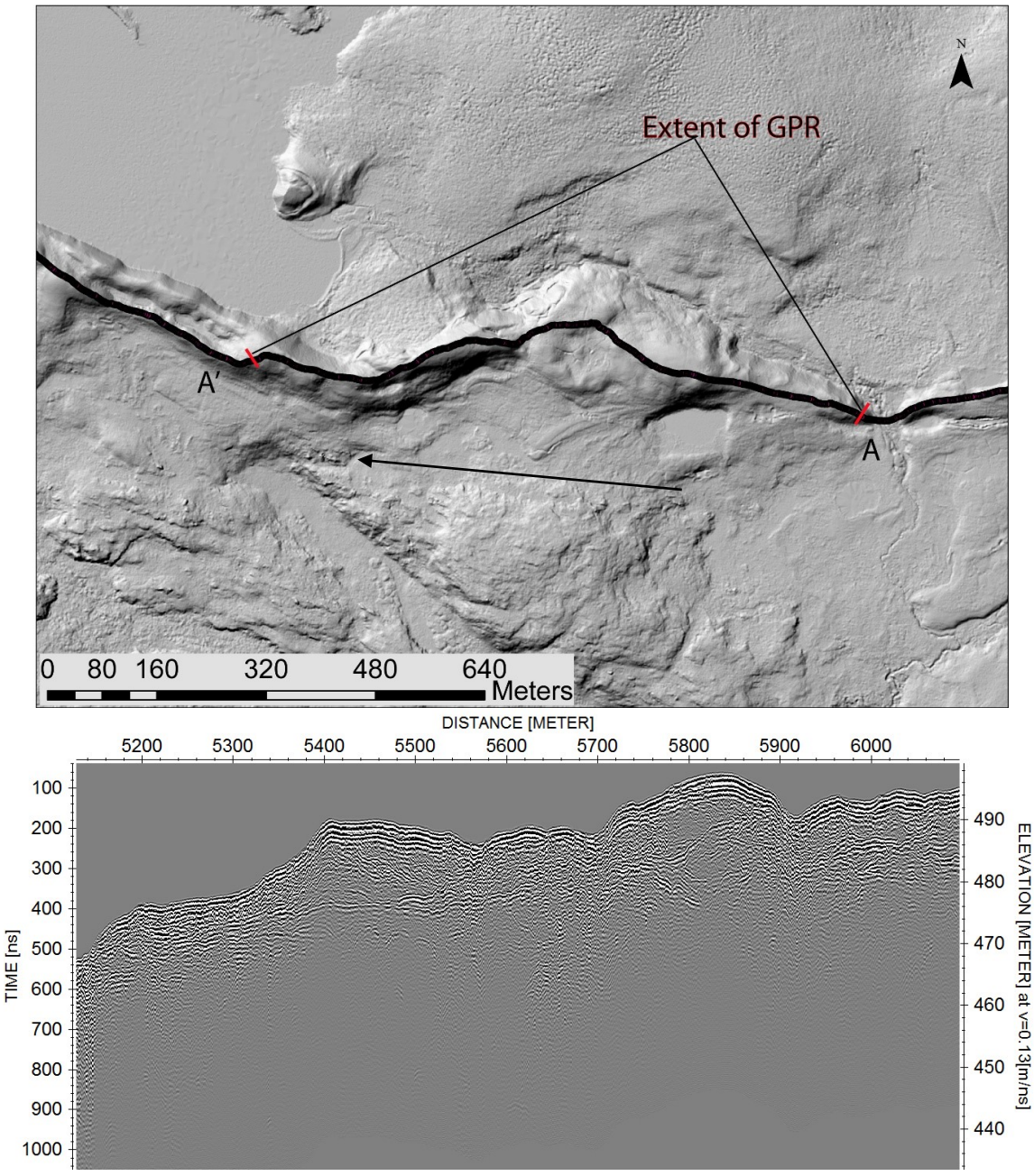

Figure 3.28: LiDAR imagery and un-interpreted 100 MHz GPR transect from an irregular topped Type 2 component from the ELE-c area (see Figure 2.16 for location of this component along the esker). Down-esker direction is left in the LiDAR image (black arrow), right in the GPR transect.

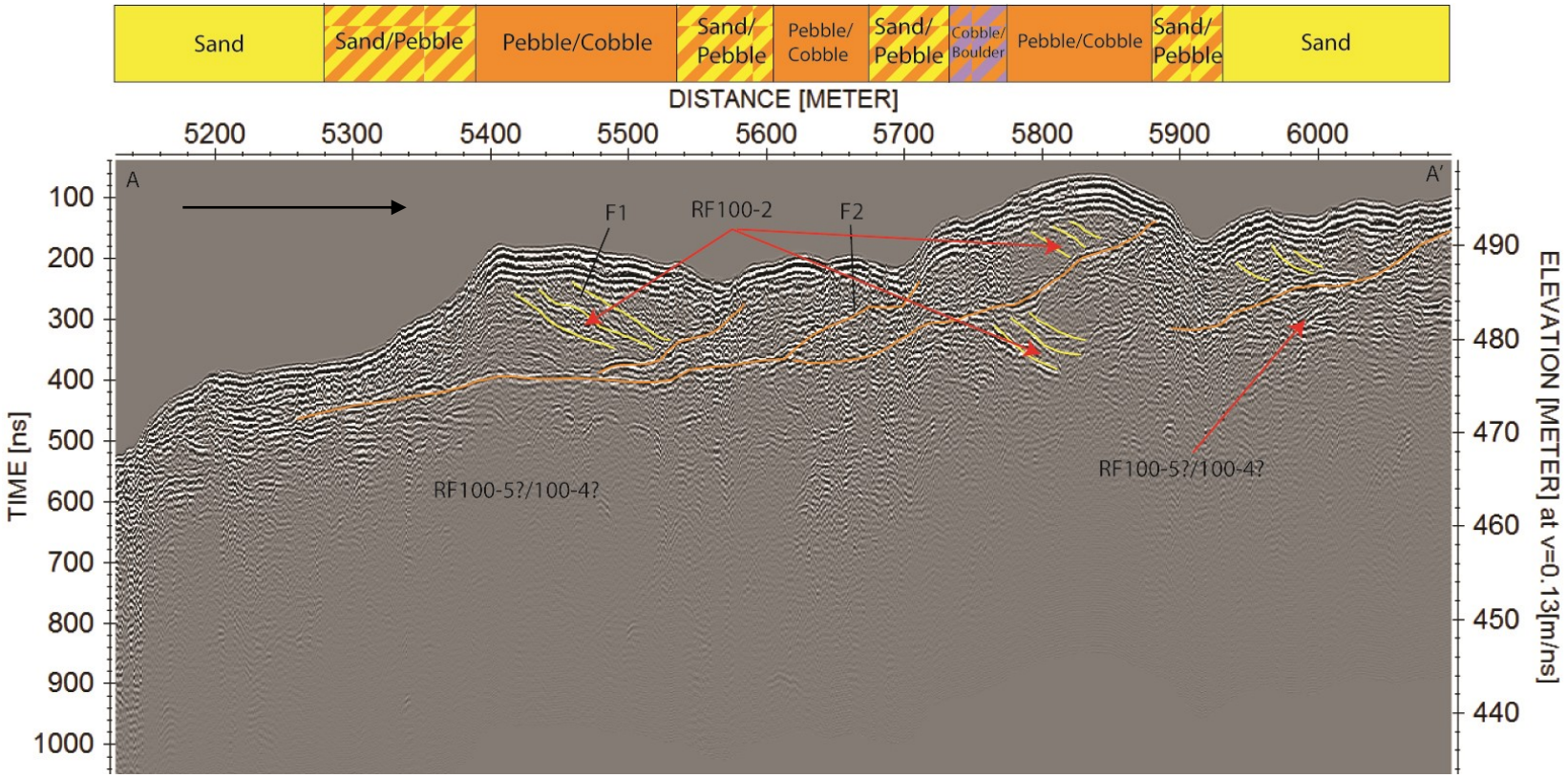

Figure 3.29: 100 MHz GPR profile of a variable-width Type 2 component (from Figure 3.28), with a cobble-dominated hillock between 5700 and 5900 m. The black arrow points down-esker. This GPR profile follows a general trend of up-esker dipping reflections (F2, traced in orange) with down-esker dipping reflections that downlap these surfaces. Given that these reflection packages have a relatively large scale (~10 m high, 100s of meters long), their "shingled" and "backstepped" stacking pattern is interpreted to be the result of a larger, longer-term process, namely "time transgressive" deposition during ice retreat over a short (<1 km) distance. Vertical exaggeration = 14.7.

Type 3 components (broad ice-confined deltaic deposits)

Type 3 components are broad (>100 m wide), flat- to irregular-topped, sandy pebble to cobble covered sediment bodies with steep flanks (10 to 30°). The single borehole drilled into a Type 3 component, NGO-DD15-2029, revealed a coarse, pebble and cobble upper 1.5 m overlying a >10 m thick package of coarse sand. Type 3 components generally have a consistent appearance in GPR transects. At the 500 MHz resolution they are most commonly observed to be similar in character to Type 2 components, and as such consist of surface parallel planar reflections (RF500-5) overlying parallel inclined reflection packages (RF500-2) (Figures 3.31–3.36). At the 100 MHz resolution, parallel planar reflections (RF100-1) are commonly observed to overlie 2 to 10 m thick up esker dipping inclined reflections (RF100-3), transitioning into a more vertically continuous package of planar (RF100-1) and inclined (RF100-2) further down-esker within the component (Figures 3.27–3.30). Large backset beds commonly occur near the heads of Type 3 components (e.g., Figure 3.32), whereas large foresets commonly characterize their downflow portions (Figure 3.30). On the Exeter Lake esker, it was observed that planar bedded RF500-5 was overlying RF500-4 at the peripheries of large Type 3 pads, likely indicating buried coarser material associated with Type 1 ridges locally at depth (Figure 3.32).

The depositional environment of Type 3 components is interpreted to be similar to that of Type 2 components, differing mainly in dimensions of their lateral confinement. Large-scale, steep, down-esker dipping reflections are interpreted to be deltaic clinoforms. The large-scale backset beds in the up-esker portion of 100 MHz GPR transects match observations by Nemec et al. (1999) in modern ice contact deltas. They

are interpreted to have formed by deposition during hydraulic jump processes (see MacDonald et al. 2009) at the outlet where R-channels debouched into larger, ice-confined proglacial basins. The internal architecture in several Type 3 components (Figures 3.28, 3.30) is similar to that of an esker-associated ice-walled canyon fill generated recently during a subglacial outburst flood in Iceland (Burke et al., 2008). In many cases, Type 3 components start abruptly, and appear to have no upflow equivalent, which might suggest limited accommodation in the feeder R-channels during deposition. However, at one locale (Figures 3.15, 3.16), a Type 1 ridge appears to grade into a Type 3 pad in a down-flow direction, suggesting that a variety of depositional scenarios may have occurred.

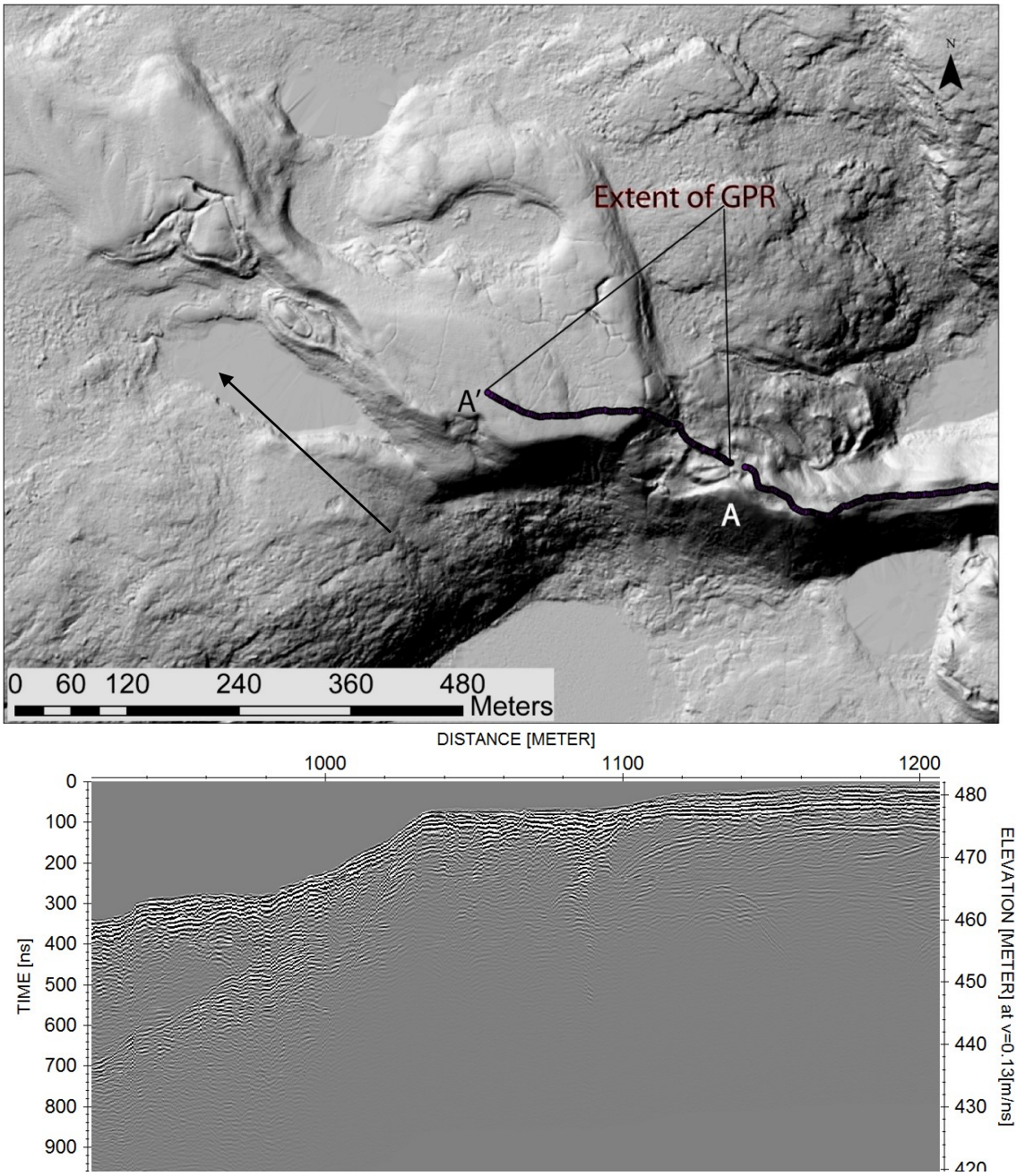

Figure 3.30: LiDAR imagery and un-interpreted 100 MHz GPR from MTE-i area (Figure 2.2). Down-esker is toward upper left in LiDAR (black arrow), toward right in GPR transect. In the LiDAR, note the braid-bar-like feature and, farther downflow, the recurved spits that ornament the Type 3 component at this location.

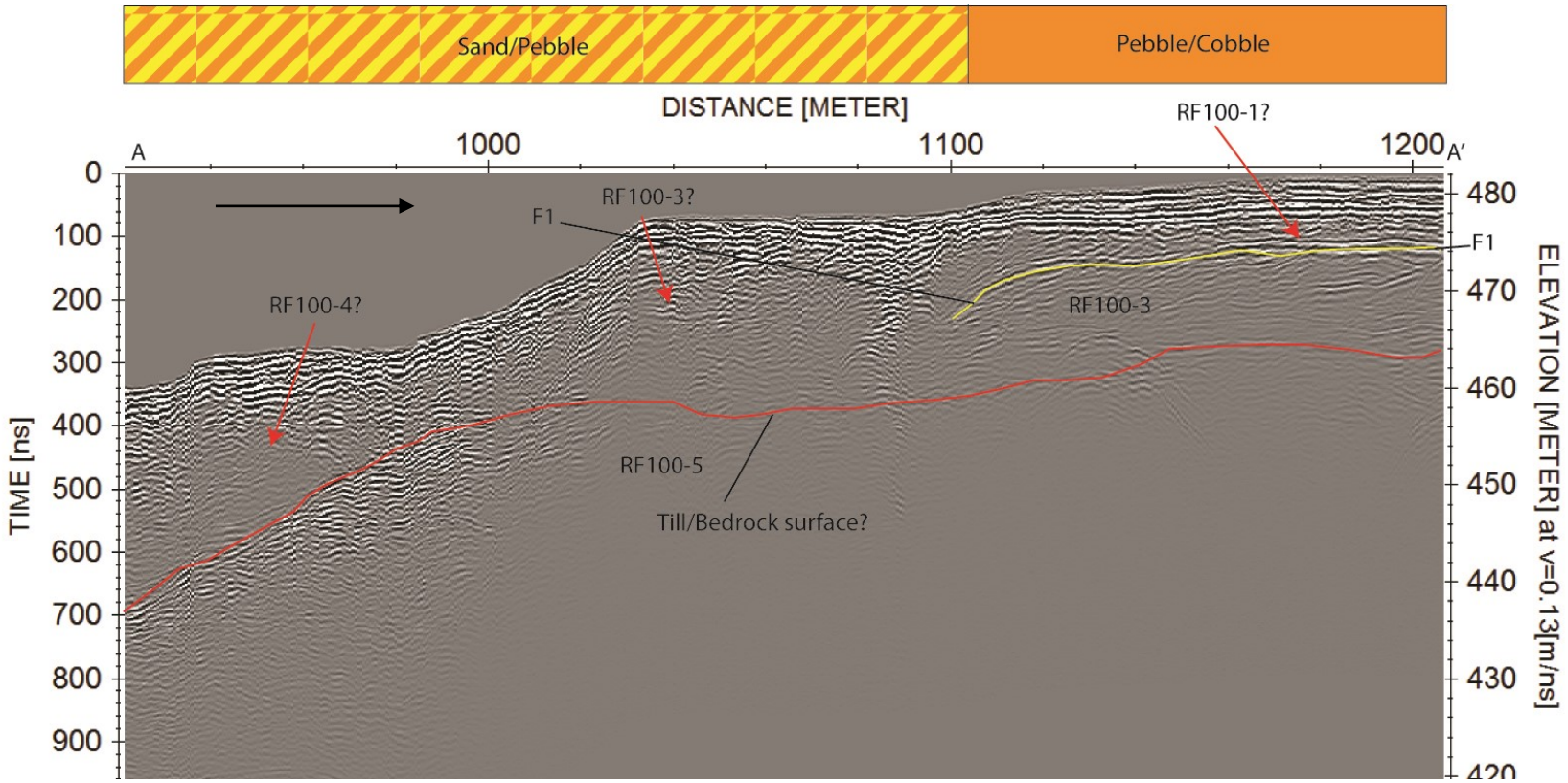

Figure 3.31: Interpreted 100 MHz GPR profile showing down-esker transition from sand and gravel of Type 1 component from 920–1030 m to Type 3 pad from 1030–1200 m. Black arrow points down-esker. Red line indicates inferred radar basement. Weak up-esker-dipping reflections at F1 are interpreted to represent backset beds, potentially analogous to those described in MacDonald et al. (2009). Surficial material of the Type 3 portion is an imbricate cobble pavement, likely a coarse deltaic top set. At the 100 MHz resolution, associated foreset beds are not visible. Vertical exaggeration = 4.7.

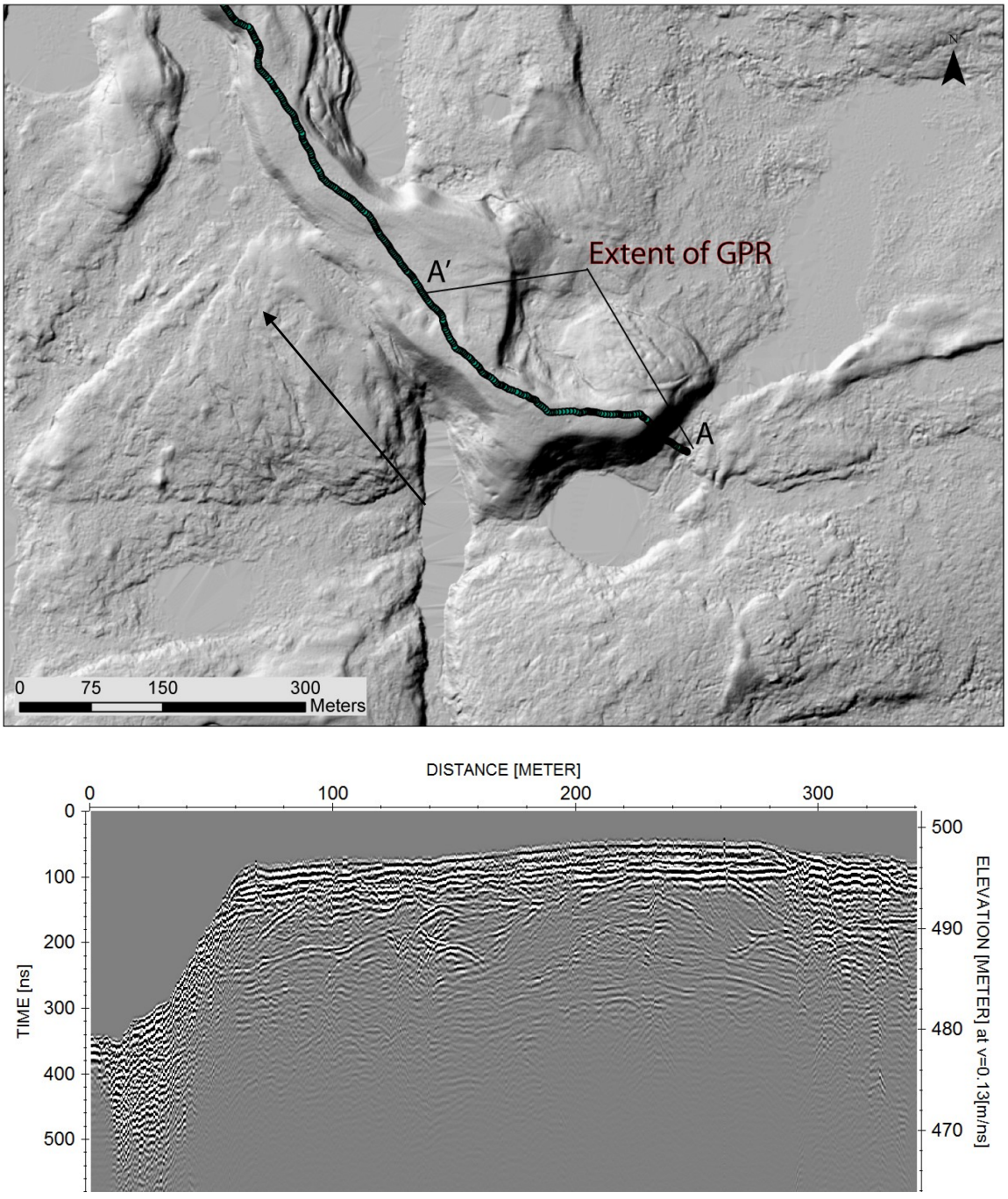

Figure 3.32: LiDAR imagery and un-interpreted 100 MHz GPR of a Type 3 component from MTE-j area (Figure 2.2). Down-esker is toward the upper left in LiDAR (black arrow), and toward the right in the GPR transect.

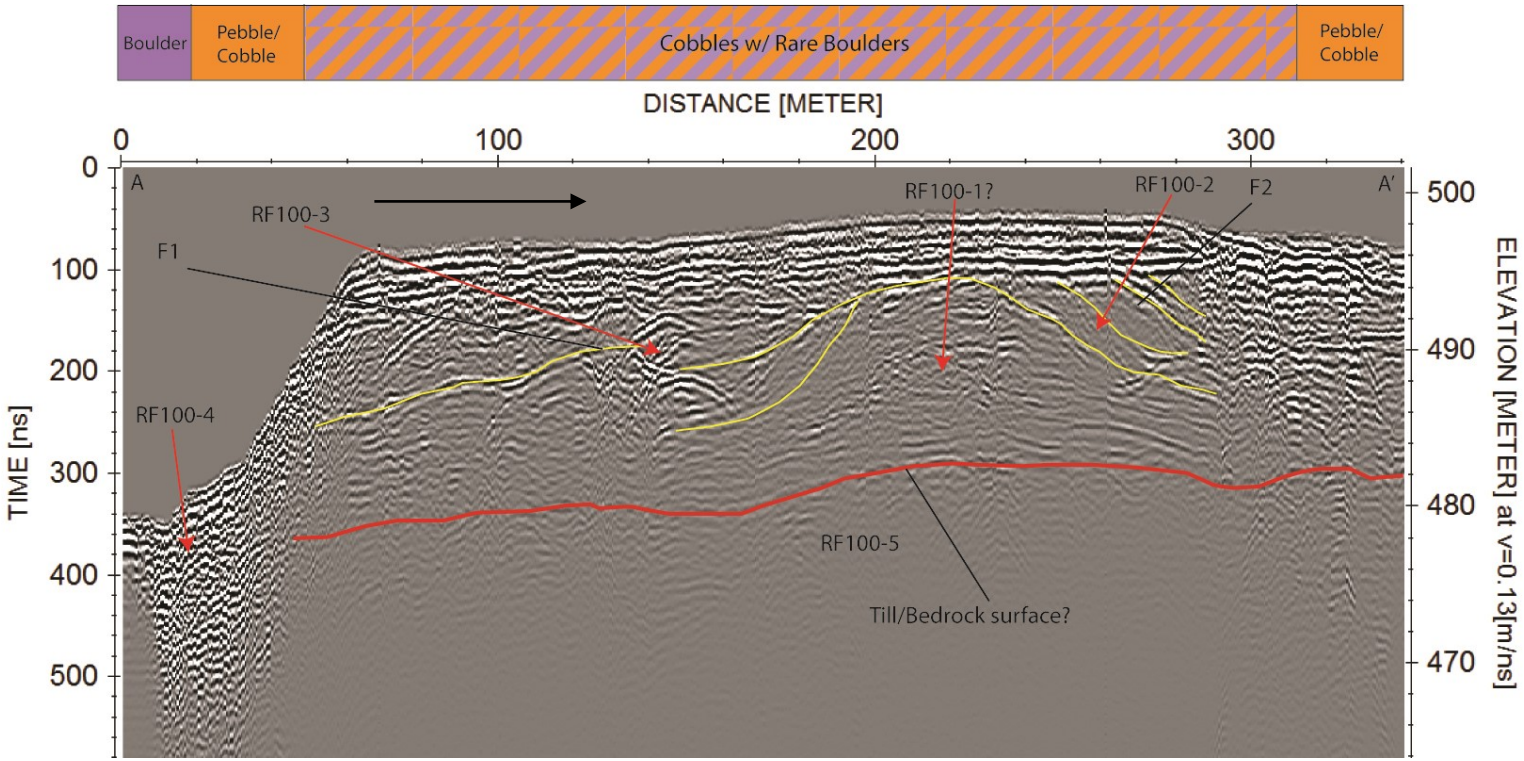

Figure 3.33: Interpreted 100 MHz GPR profile of the abrupt transition from low relief boulder-dominated Type 1 component to elevated, wide Type 3 pad (from Figure 3.32). Black arrow points down-esker. This GPR profile images a similar down-esker progression presented in Figure 3.31, and the resulting imagery is markedly similar. Up-esker-dipping reflections interpreted to be the result of backset beds (F1), potentially associated with hydraulic jump deposits (see MacDonald et al., 2009), are present, along with a transition to down esker dipping foreset reflections (denoted by F2). This is interpreted to be evidence for deltaic progradation within ice-confined accommodation space, concurrent with ice-confined up-flow accretion at the up-esker end of the component. Vertical exaggeration = 9.2.

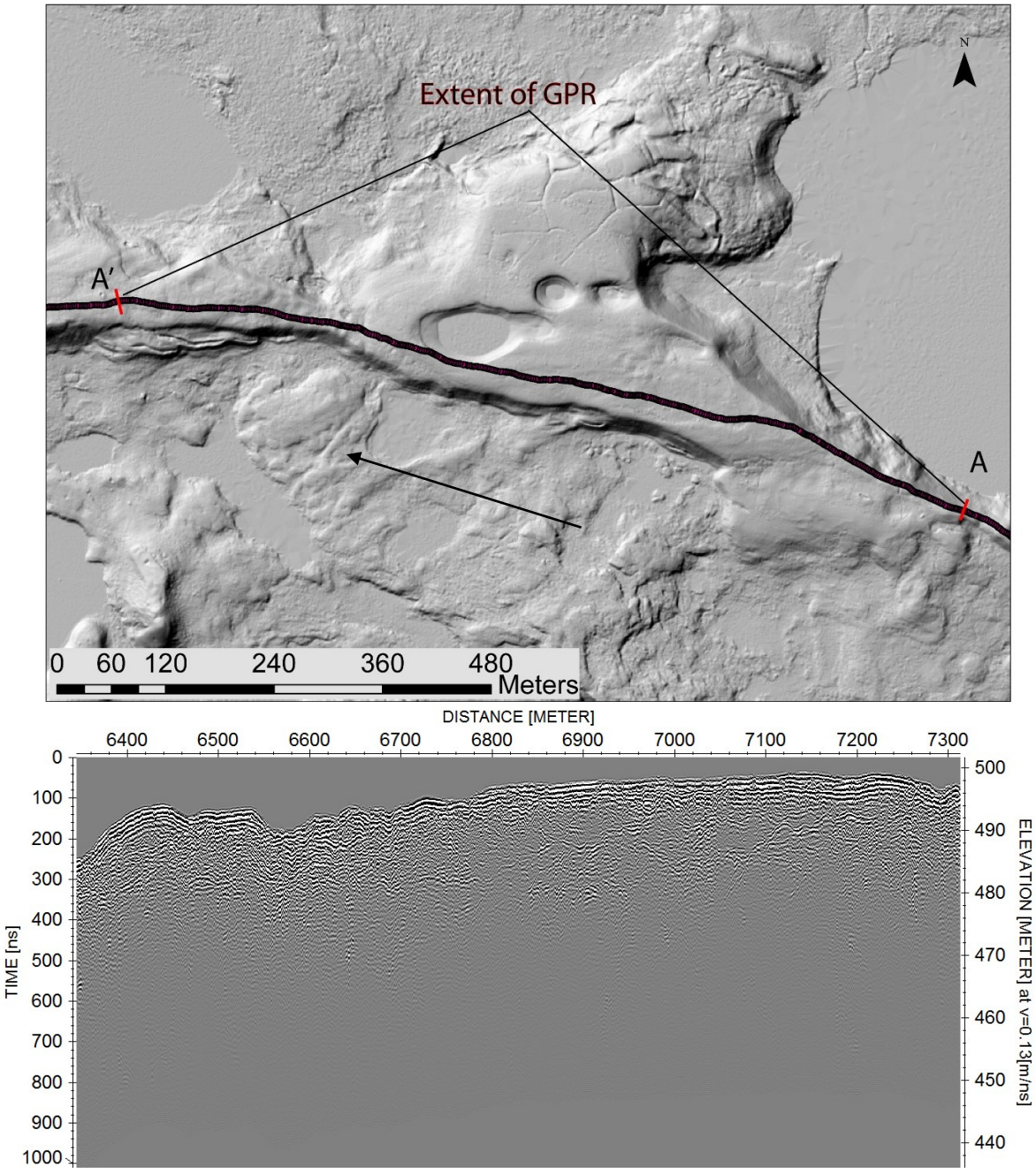

Figure 3.34: LiDAR imagery and uninterpreted 100 MHz GPR transect from a broad, flat-topped Type 3 component from the ELE-d area (see Figure 2.2 for location of this component along the esker). Down-esker direction is to the left in the LiDAR image (black arrow), to the right in the GPR transect.

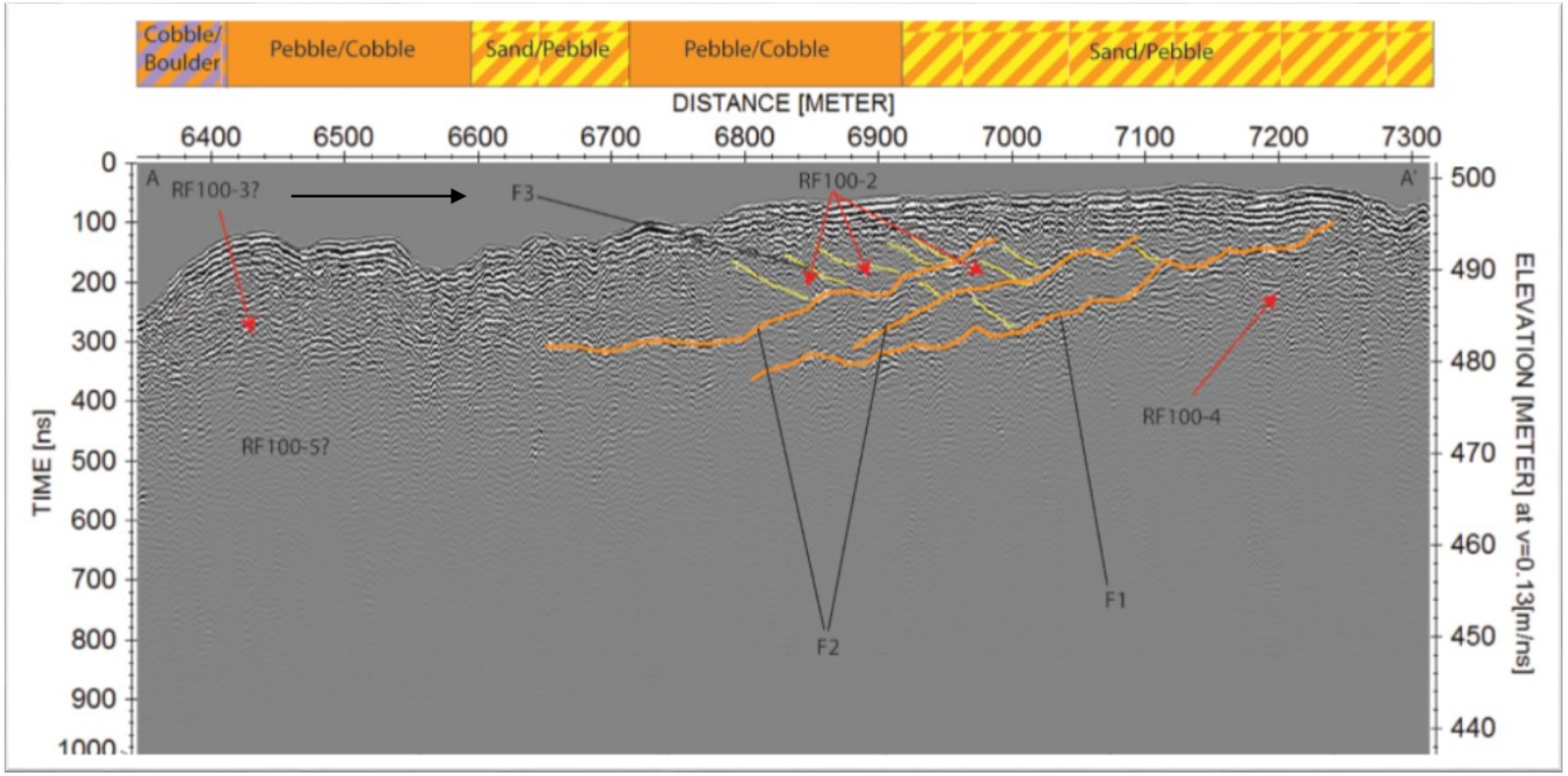

Figure 3.35: Interpreted 100 MHz GPR profile of the wide Type 3 pad shown in Figure 3.34. Black arrow points down-esker. This GPR profile is similar in nature to Figure 3.29, showing the same back-stepped shingled appearance of up-esker-dipping reflection surfaces (F1, F2, traced in orange) with downlapping, inclined reflections between 7 and 10 degrees (F1, traced in yellow). These features may be large-scale equivalents of the hydraulic jump bars generated experimentally by MacDonald et al. (2009). Additionally, this figure shows finer grained Type 3 sediments overlying what is interpreted to be cobble and boulder-dominated Type 1 material (RF100-4) (surface denoted by F1). This is interpreted to indicate time-transgressive deposition during ice retreat, whereby older, subglacial deposits located down-esker are overlain by younger proglacial sediments located up-esker (see Chapter 4). Vertical exaggeration = 15.7.

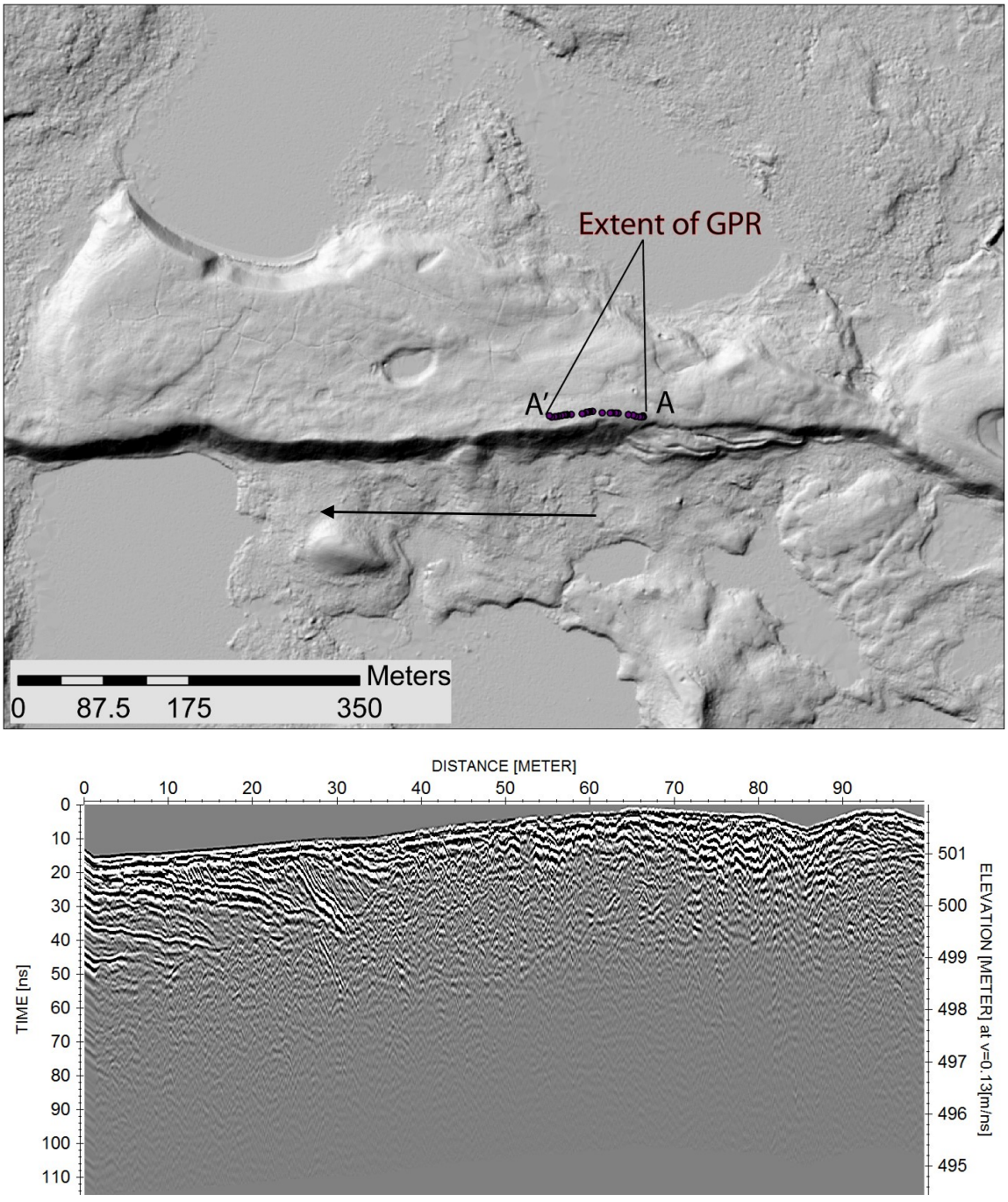

Figure 3.36: LiDAR imagery and uninterpreted 500 MHz GPR of a broad flat-topped Type 3 component from ELE-d area (see Figure 2.2 for location of this esker segment). Down-esker direction is to the left in the LiDAR image (black arrow), and to the right in the GPR transect.

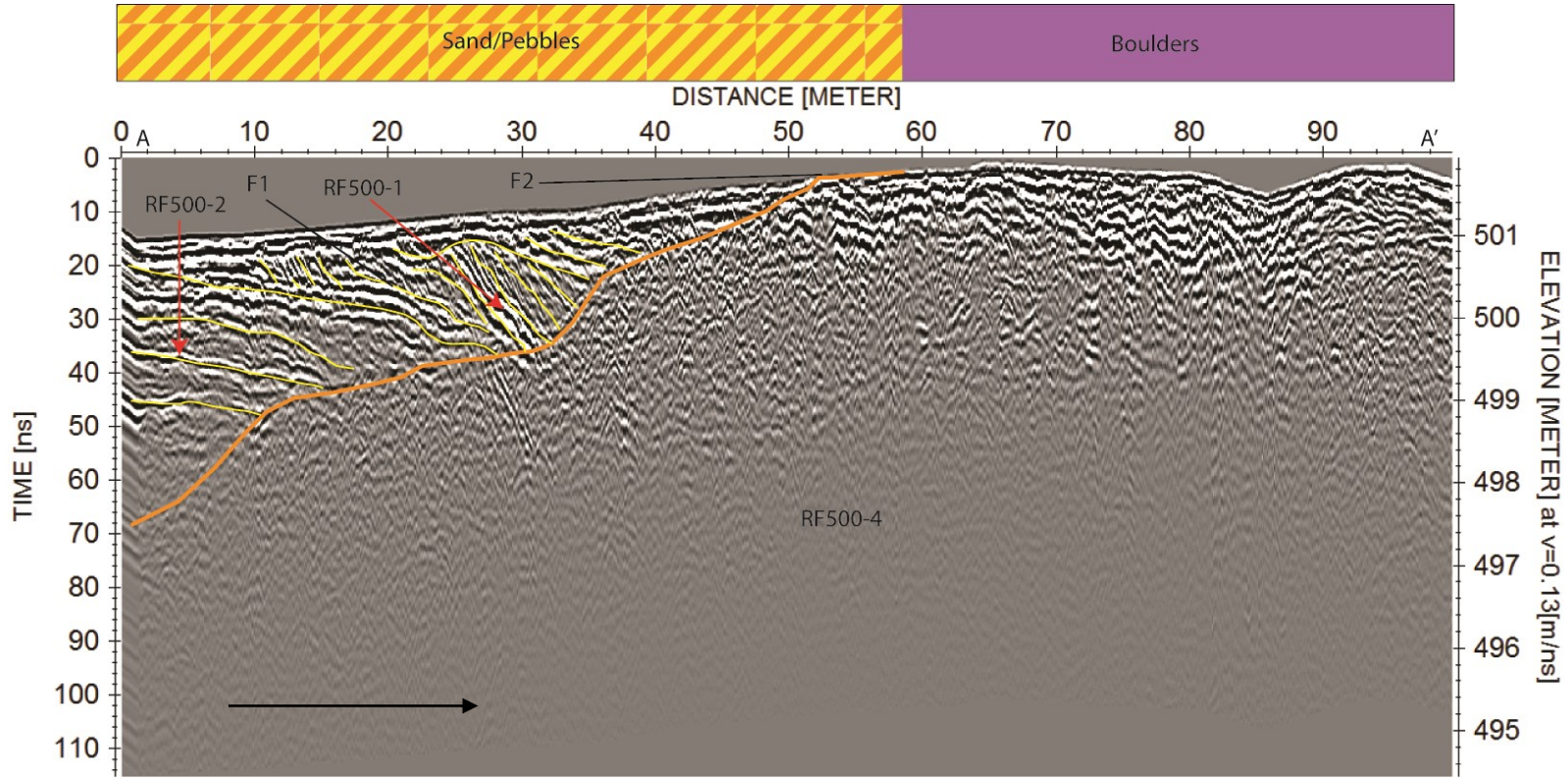

Figure 3.37: Interpreted 500 MHz GPR transect from Figure 3.36 showing that a boulder-dominated Type 1 ridge (60–100 m) underlies the Type 3 component, even though the Type 1 component has little to no surface expression (see LiDAR in Figure 3.36). Down-esker direction is to the right, as indicated by the black arrow. The inclined reflections within the Type 3 component, which are highlighted in yellow and denoted by F1, that are interpreted to be deltaic foresets. These foresets downlap the top of the Type 1 component (downlap surface shown in orange and denoted by F2). In the LiDAR data, the southernmost flank of the flat-topped Type 3 component is more prominent, and has a noticeably different surface texture: it is covered in cobbles and boulders, whereas the surface of the rest of the Type 3 component is covered in finer grained sediment (coarse sand, pebbles and cobbles). This, along with GPR transects from this location, attests to the presence of a buried Type 1 ridge beneath the entire southern edge of the Type 3 component (see also Figure 3.38, 3.39). Vertical exaggeration = 13.8.

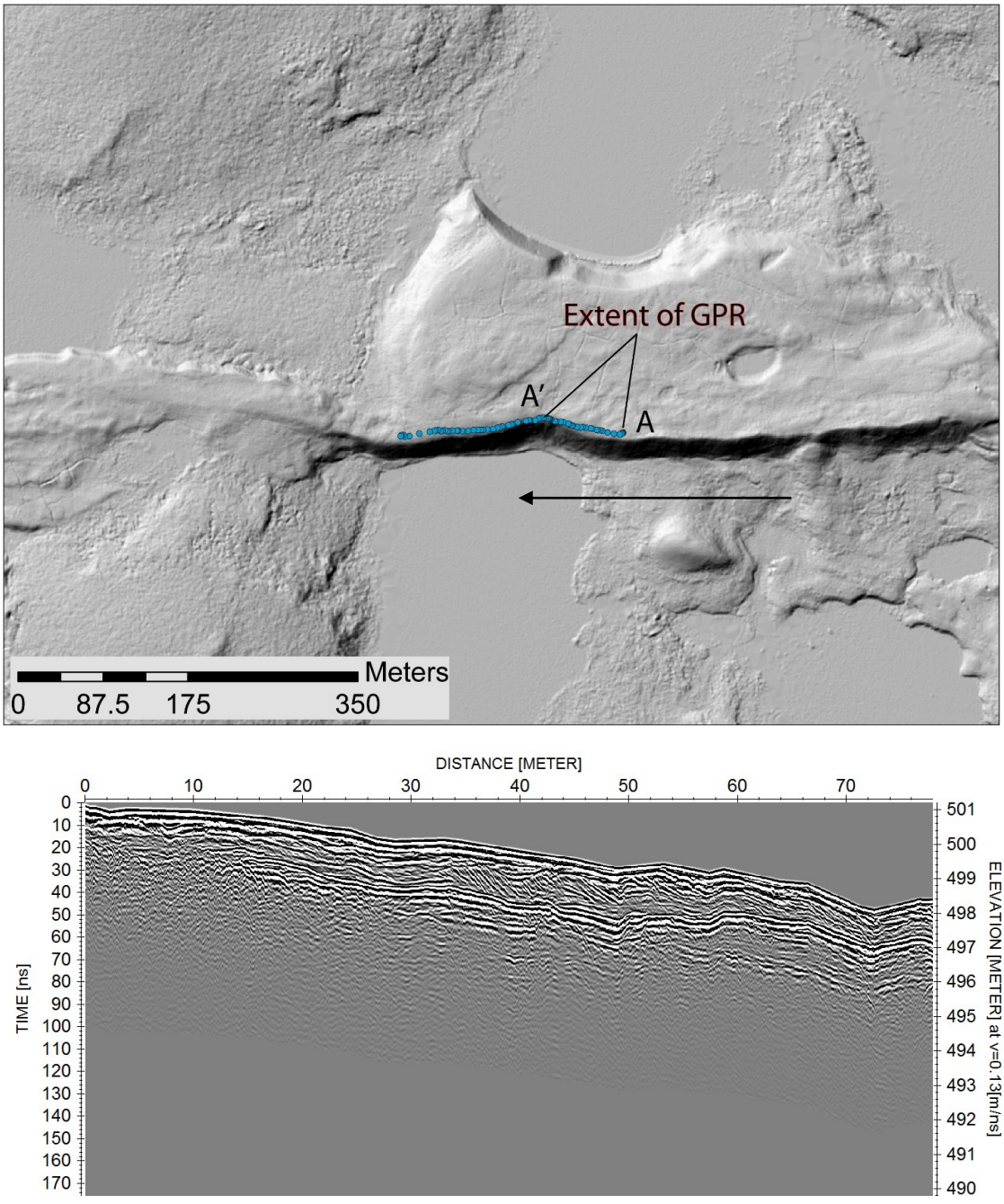

Figure 3.38: LiDAR imagery and uninterpreted 500 MHz GPR from the same Type 3 component shown in Figure 3.36 and 3.37. Down-esker direction is to the left in the LiDAR image (black arrow), and to the right in the GPR transect.

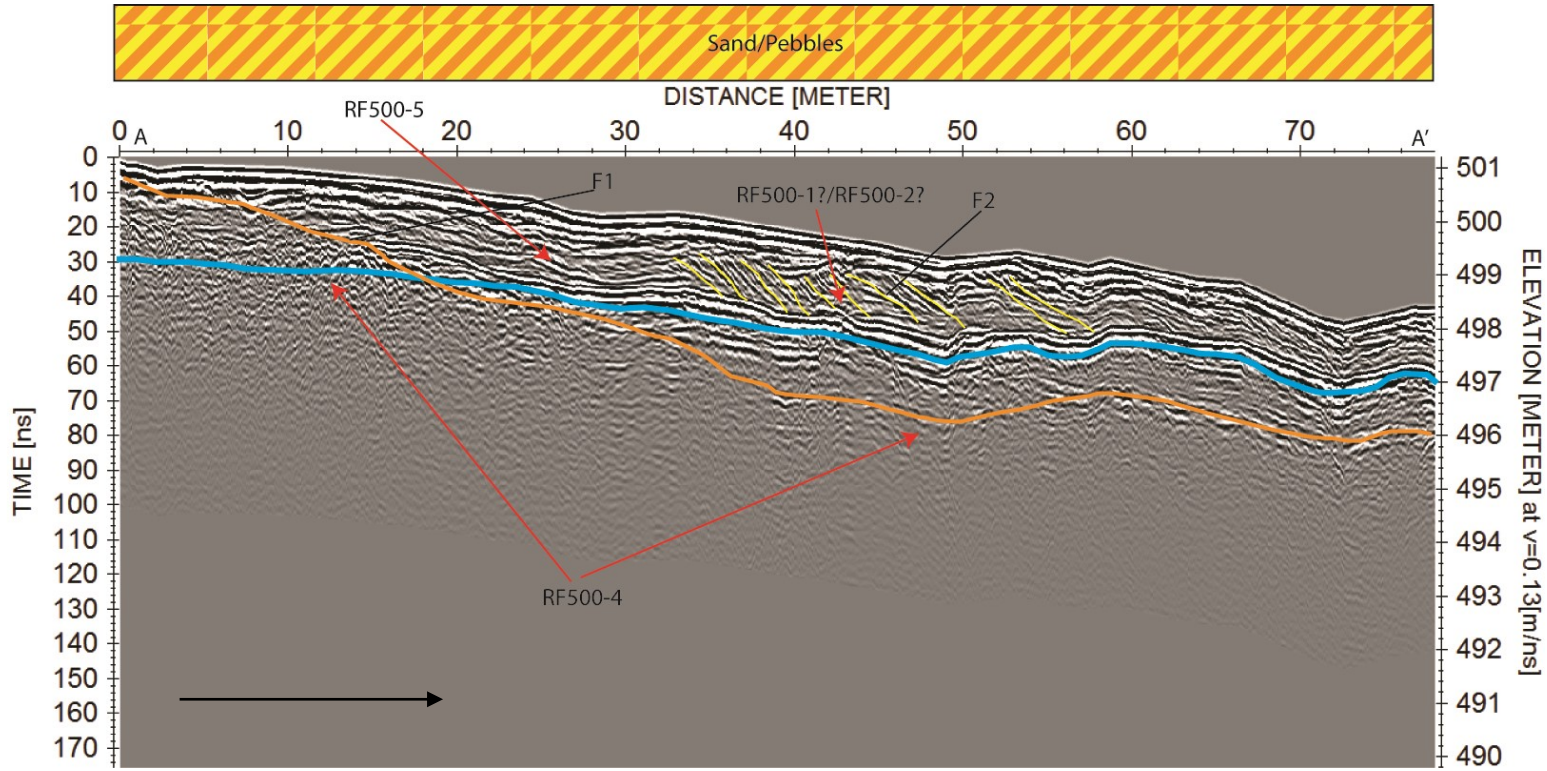

Figure 3.39: Interpreted 500 MHz GPR profile from Figure 3.38 showing a boulder-dominated Type 1 ridge (beneath orange line) buried beneath a broad, flat-topped Type 3 pad. The blue line indicates the permafrost table. Black arrown points down-esker. Vertical exaggeration = 7.1.

Type 4 components (Supraglacial fan deposits)

Type 4 components form irregularly undulating, elevated detached pads (Type 4 pads), or wide splays of fine sandy sediment that flank the main esker ridge (Type 4 splays). Detached pads are elevated landforms, commonly with steep sides, that have a surface sediment texture consisting of pebbles and coarse sand with rare cobbles. Splays are low elevation landforms composed of well sorted fine sand. Boreholes from both pads and splays intersected a silty diamicton with a high proportion of cobble clasts beneath these sediment bodies, between 2 and 4 m below the ground surface. Radar facies in Type 4 components are commonly disrupted.

The irregularly undulating surfaces and disrupted stratigraphic architectures of Type 4 pads are interpreted to be indicative of deposition onto debris-rich glacial ice. Type 4 pads could be the result of a rerouting of sediment-laden melt water from the main conduit onto the adjacent surface of the glacier, where it accumulated in water-filled depressions or fractures on the surface of the adjacent glacial ice. This is perhaps most clearly suggested by a detached Type 4 pad along the Misery Tributary esker (Figure 2.2A). It is interpreted here that splays are also deposited supraglacially, but in a relatively unconfined fashion, potentially as a result of a flooding of a Type 2 component ice-walled channel, resulting in what would be analogous to splay type overbank deposition in a modern fluvial setting (North and Davidson, 2012). Fine sediment deposited as thin sheets onto adjacent ice would result in the landform association (fine sediment flanking Type 2 ridges) observed in this study.

Chapter 4: Discussion

4.1 Introduction

The data gathered in this study permitted an investigation of the morphology, the surficial sediment cover and the sedimentary architecture of the eskers at a greater level of detail than previously possible. Through the course of this investigation, numerous questions were raised by the data that at first appeared difficult to answer. What is the precise nature of esker deposition in the Lac de Gras area? What are the implications of the variably undulating nature of different esker components? To what extent has the esker been reworked and deformed after initial deposition? And finally, what can be inferred about transport distance of sediment within the esker, based off the above interpretations? This chapter will discuss the data collected in this study with the goal of providing potential solutions to these questions, and proposing, where applicable, appropriate methodologies to better investigate these problems in the future.

4.2 Deposition of Lac de Gras eskers

Viewed macroscopically from above (e.g., Aylsworth and Shilts, 1989), the significant lengths and tributary-like planform geometries of the eskers in the Lac de Gras area was interpreted by prospectors sampling for kimberlite indicator minerals (KIMs) during the diamond boom in the early 1990s to be indicative of synchronous deposition in long conduits (i.e., Figure 1.1B). If correct, KIMs and other bedrock fragments could have been transported 100s of kilometers from the point where they were eroded through the esker system to the point where they were deposited (Krajick,

2001). The data gathered in this study provide evidence that this may not be the case. Aerial imagery with the resolution of the LiDAR used in this study was unavailable to early prospectors, as was insight into the internal architecture and stratigraphic relationships of esker components from GPR and borehole data. This section will lay out the evidence for a short conduit model of deposition for the portions of the Exeter Lake and Misery tributary eskers studied, by integrating results from LiDAR, surface grain size trends, boreholes, and GPR imagery.

In previous studies, authors generally agree that eskers are composed of two main depositional components: narrow, sharp-crested gravelly ridges interpreted to be R-channel deposits, and wider, broader-crested pebbly to sandy sediment bodies interpreted to be "fans" (e.g., subaqueous, deltaic or subaerial outwash fans) deposited where flow from the R-channels expanded and decelerated at the ice front (Banerjee and Macdonald, 1975; Rothsilberger, 1972; Brennand, 1994, 2000; Storrar et al, 2007; Buck, 1983 Schulmiester, 1989; Lundqvist, 1999). In this study, all esker material encountered is interpreted to fit into these two categories.

Figure 4.1 presents a conceptual model of how the eskers near Lac de Gras formed. Segmental deposition in short conduits during ice retreat, as depicted, is interpreted to bring together and explain many of the features observed. Each segment consist of (1) a Type 1 ridge that correlates downflow into a Type 2/3/4 fan (most segments), or (2) a Type 3 fan that lacks a Type 1 ridge upflow, presumably due to lack of accommodation in the R-channel during deposition. Abrupt changes in surficial grain size are interpreted to commonly be stratigraphic in nature, in that they can be explained by overlapping of different esker components that became superimposed during ice

retreat. Longer down-esker fining segments (maximum 3 km; see Figure 2.29) are interpreted to have escaped superposition by younger segments as the ice retreated. Abrupt widening of landforms in aerial photographs and LiDAR are explained by the presence of Type 3 components marking the presence of a broader (but still ice confined) basin.

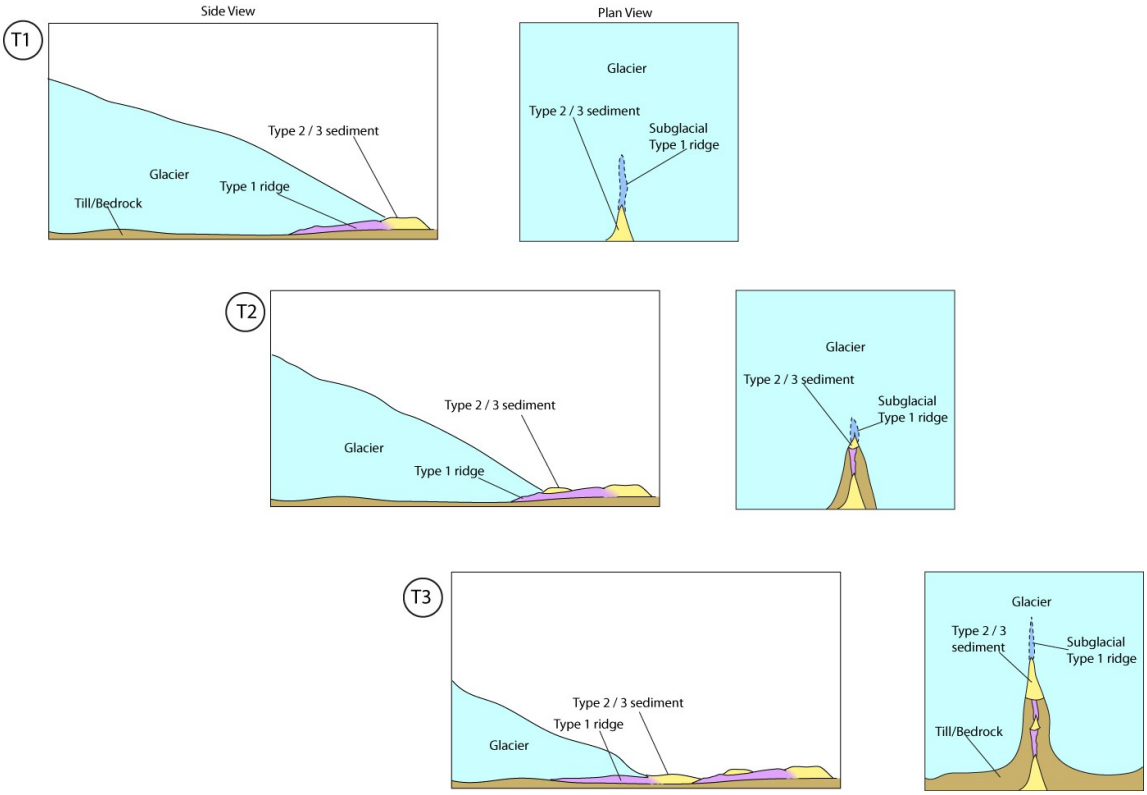

Figure 4.1: Highly simplified conceptual model of esker deposition in the study area. Time 1 (T1) points to an initial stage of esker deposition, wherein a subglacial Type 1 component is deposited that grades downflow into a proglacial sediment body (Type 2 or 3 component) that downlaps its substrate. Time 2 (T2) and Time 3 (T3) follow, illustrating the concept of segmented deposition during ice-front retreat. Note that in T2, the Type 2/3 component is portrayed without an associated Type 1 component upflow, a scenario that appears to have been relatively common during esker deposition in the study area, presumably reflects little accommodation in the R-channel feeder channel during sedimentation. Many variations of this simplified framework are possible. A multitude of variables—level of standing water in the re-entrant, rate of ice retreat, duration of sedimentation, underlying base topography, potential for temporary ice advance— have the potential to add complexity to this and likely account for the wide variety of landform expression observed. One scenario not depicted here is supraglacial deposition, whereby sediment delivered by R-channels is deposited onto the surface of the glacier at or near the ice front. This scenario is interpreted to be at the root of the melt out features and undulating profiles seen in many of the esker components in this study.

If the esker was deposited time transgressively in short segments,why does the overall esker system retain a dendritic patter over 100s of kilometers? Several different proponents of the short conduit model have proposed solutions to this problem. As the

ice front retreats, Boulton et al (2009) suggests that the short esker segments follow a template set by long, tree-shaped subglacial drainage pathways thatextend deep beneath the ice sheet. The pathways are mainted perennially by the small amounts of meltwater generated by basal melting, and their downflow portions, where the esker segments form, swell during summer as surface melt descends through moulins and crevasses and intersects them. Shilts (1984) envisions a similar model, but with long, supraglacial streams providing the template. Hook and Fastook (2007) argue that the long supraglacial streams envisioned by Shilts (1984) are too dynamic to form stable configurations over thousands of years. Rather, they argue that dynamic opening and closing of surface-to-base pathways (moulins, crevasses) eventually results in a tree-shaped esker forming. Which of these models, if any, best explains the Exeter Lake esker is a topic for future research.

4.3 Variation in thickness and width of the esker components

For Type 1 ridges, sudden outburst floods from subglacial or supraglacial lakes, superimposed over seasonal variations in meltwater supply, may have had considerable impact on the dimensions of R-channels, the sediment supplied to them, and the ability for sediment to accumulate within them (Gustavson and Boothroyd, 1987). Drainage of such lakes may have routed considerable volumes of water into the R-channel networks (e.g., Das et al., 2008; Burke et al., 2008). This would have expanded the dimensions of the R-channels, eroded sediment from the subjacent till and debris-rich basal ice, potentially scoured the R-channels of previously deposited sediment, and/or, especially

during waning stages, deposited abundant sediment in the R-channel (Roberts, 2005). Is there evidence from Type 1 components that such outbursts may have occurred? The fact that large rounded boulders in excess of 1 m in diameter are observed in some of the Type 1 ridges in this study suggests that flow velocities may have been high, possibly in the range of 5.0 m/s based on observations from modern settings (Costa, 1983). Combining this flow velocity with a cross-sectional area of 800 m^2 (assuming average R-channel cross-sectional area was equal to the average triangular cross-section (80 m wide by 20 m high) of a Type 1 ridge) yields a discharge rate of approximately 4,000 m^3/s. This discharge rate is similar to average discharge rates calculated during supraglacial lake drainage events in Greenland (e.g., 8700 m^3/s; Das et al., 2008) and subglacial lake drainage events in Iceland (e.g., 1000 to 10,000 m^3/s; Marren and Schuh, 2009; see also Burke et al., 2008).

For Type 2, 3 and 4 "fan" components, the width of the ice walled conduit (Type 2 or 3 components) or water-filled depression on the glacier surface (Type 4 components) into which the sediment bodies were deposited, and the water depth at the time of deposition, were likely the two most significant variables that controlled the morphology of the landform, at least initially. The level of standing water at the mouth of a re-entrant was likely controlled by the elevation of the sill of the proglacial lake where ice impinged on bedrock, and by meltwater supply to the proglacial lake. Melting or lowering of confining ice could cause lake drainage, which would rapidly force regression of the shoreline, causing the locus of deltaic deposition to shift downward and basinward. Conversely, sudden input of floodwater could rapidly raise water levels within a re-entrant, resulting in normal regression or, in areas of low sediment supply, transgression.

The local water level may also have increased significantly beneath hydraulic jumps at the conduit efflux during sudden increases in discharge, facilitating deposition of hydraulic jump bars and backset beds (e.g., MacDonald et al., 2009) at the upflow ends of Type 3 components. The width of the re-entrant could also potentially have be influenced by such sudden increases in discharge. Kettle holes, common on Type 3 components, are interpreted to be the result of melt out of ice blocks completely or partially buried during high magnitude flow events (Marren and Schuh, 2009). Although re-entrant width and water depth likely dictate the initial morphology of Type 2 and 3 components, the nature of the substrate onto which these sediments were deposited will also dictate its final morphology. Specifically, as discussed below, if deposition occurred completely or partially on glacier ice, melt out of that ice could cause significant post-depositional modification of the landform.

4.4 Post-depositional deformation and reworking of esker sediments

One implication of a time-transgressive esker depositional model that involves ice retreat, a proglacial lake with a varying water level, variable meltwater discharge, and, in places, ice-melt out following deposition, is that older esker components, once deposited, may have been reworked by littoral, glaciofluvial, and aeolian processes. Insights from LiDAR, GPR data and grain-size samples gathered in this study seem to indicate that post-depositional modification of esker sediments is a common feature of these deposits. Beach ridges and spits are present locally on sandier esker components (Figure 4.2), indicative of littoral reworking of the components. A braid-bar-like feature is observed

on a Type 3 component in one location (Figure 3.30), just upflow of several spits, indicating glaciofluvial action. Aeolian processes may have been much more significant immediately following deposition, where a sloping continental ice sheet would likely have driven strong, sustained katabatic winds. This could have resulted in a rapid winnowing of surficial material, a process that is relatively common throughout the Arctic (e.g., Mackay and Burn, 2005), with associated dispersal of fine material off esker and onto the adjacent till plain. In addition to post-depositional winnowing by wind and water, many locales along the studied eskers show evidence of post-depositional deformation that is interpreted to be related to melt-out of buried ice. A previous survey of the Misery tributary esker revealed buried massive ice with an oxygen isotope signature suggestive of glacial ice in a drill hole approximately 2 km to the south of the study area (Wolfe et al, 1996). As reviewed in Chapter 1, other studies have encountered similar glacial ice beneath eskers near the study area (Dredge et al., 1999; Hu et al., 2003). These observations support the conclusion that some of the undulations in the esker profile are likely due to ice melt-out. The prevalence of post-depositional deformation and erosion in finer grained portions of the eskers is striking: such deformation is rare in Type 1 components but common in Type 2, 3 and 4 components (Figures 4.3, 4.4), lending support to the interpretation that Type 1 components were typically deposited subglacially, as opposed to englacially or supraglacially.

The mechanisms that trigger the melting of buried ice within esker sediments is an area for further investigation. There is no strong geothermal source of heat to trigger melting of buried ice in this part of the Shield (e.g., Jaupart and Mareschal, 2007). This leaves two options: climatic warming or submergence beneath water. The latter option

seems plausible, at least locally, given the observations that some esker segments are ornamented by beach ridges and spits, and that permanently unfrozen ground exists beneath the larger of the modern lakes and streams in the immediate area (Hu et al, 2003). Additionally, the water table from adjacent lakes can permeate the esker, as observed in some GPR profiles (see figure 3.21). The former option, climatic warming, also seems plausible. Like the rest of the Arctic, the Lac de Gras region experienced a warm period following deglaciation, the Holocene Thermal Maximum, from 6.9 to 3.2 ka BP, during which mean annual temperatures are interpreted to have been warmer than today by an average of 1.6 +/- 0.8°C (Kaufman et al, 2004). Depth to permafrost can be quite sensitive to air temperature: Burn and Zhang (2009) showed that an increase in air temperature by 1°C over 25 years can increase active layer thickness by up to 25 cm. As such, it would not be unreasonable to suspect that the Holocene Thermal Maximum, possibly coupled with submergence following esker deposition, contributed to the melting out of buried ice within the esker.

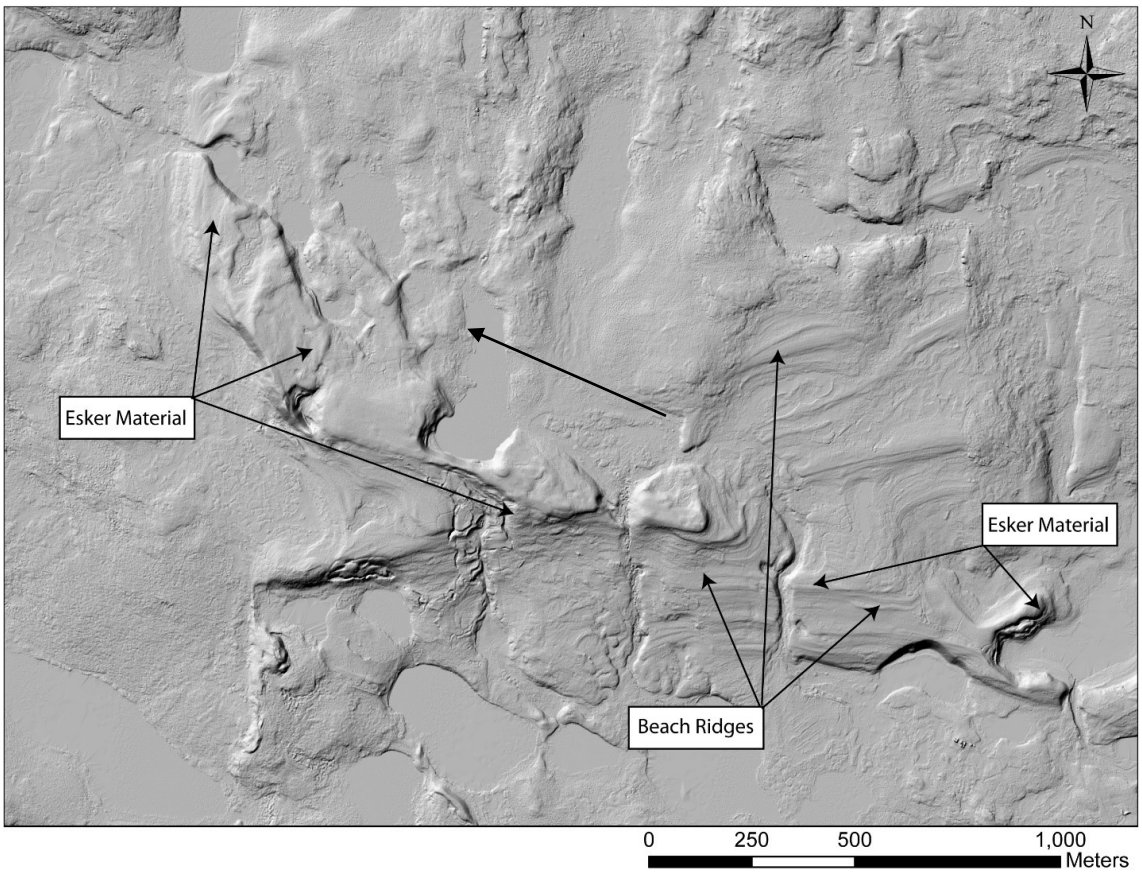

Figure 4.2: LiDAR imagery of Exeter Lake Esker, approximately 5 km up esker of the ELE-a area (Figure 2.2), showing raised beaches.

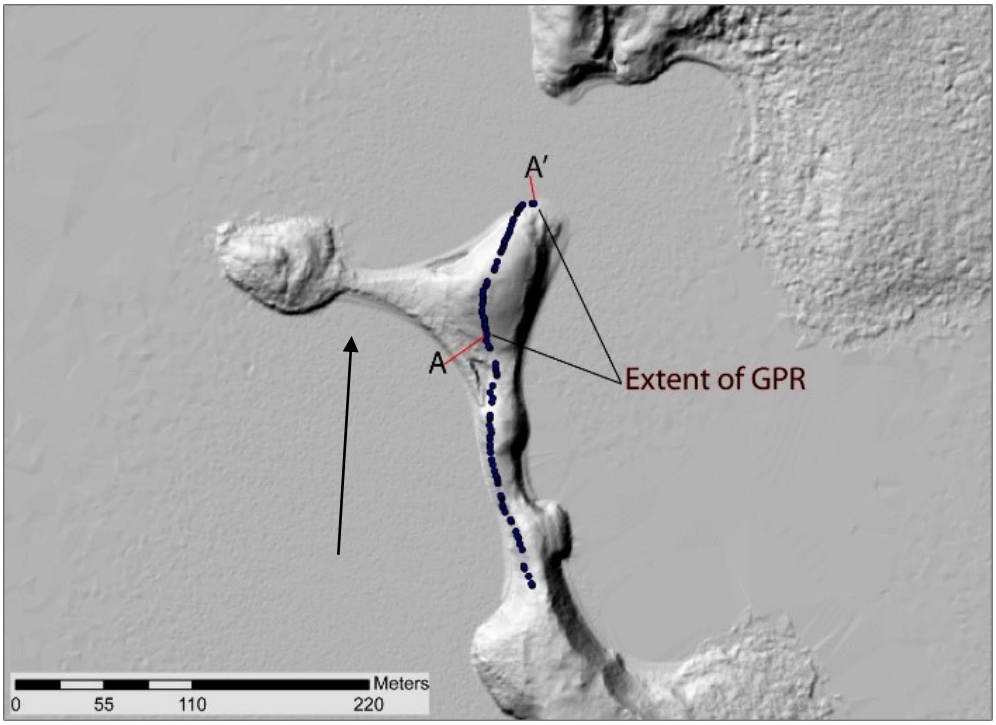

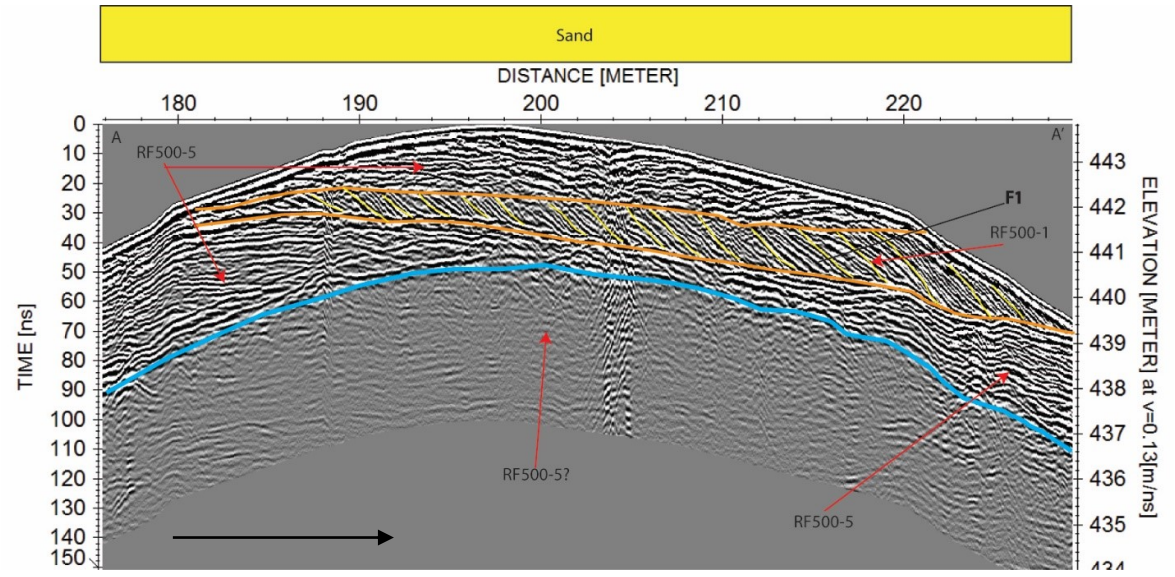

Figure 4.3: Increased-gain processed 500 MHz GPR profile of sandy hillock on Type 2 component. The black arrows point down esker. Sub parallel, planar reflections above and below the permafrost table (blue line) are overlain by a down-flow thickening package of inclined reflections (25 degree dip) interpreted to be clinoforms as a result of sand bar accretion (F1). Vertical exaggeration = 5.2

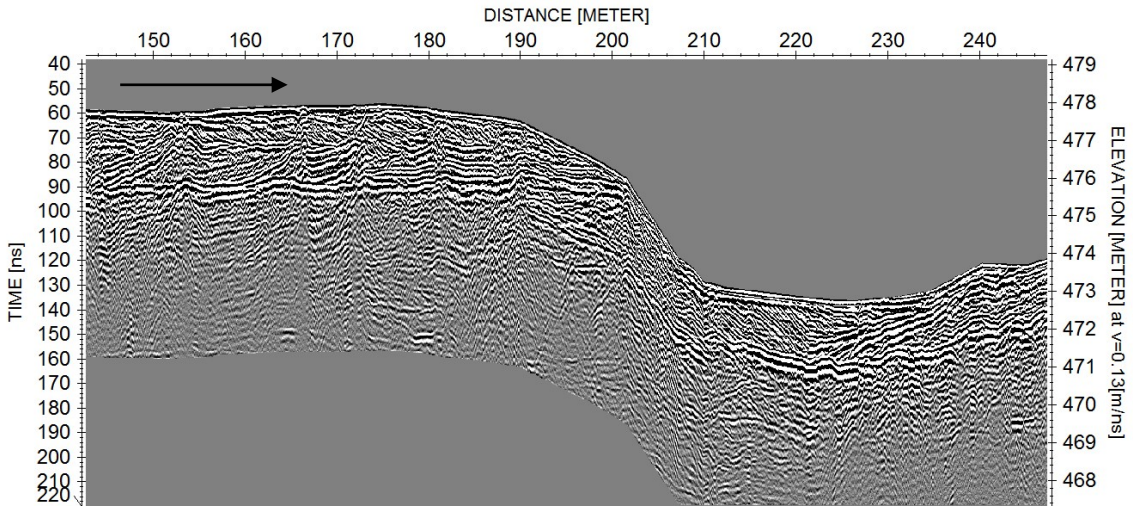

Figure 4.4: GPR profile (see Figures 3.21 and 3.22 for location and detailed interpretation) showing the undulating profile of a Type 2 component of the Misery Tributary Esker. The black arrow points down-esker. The figure illustrates another example of horizontal strata terminating at the eskers surface. At approximately the 200 m mark, clearly identifiable horizontal reflections terminate abruptly at the point where the surface enters a 5 m depression. This is likely an example of subsidence caused by melt-out of buried ice. Vertical exaggeration = 8.8.

Boreholes from the Exeter Lake esker indicate that a grain-size difference exists between deltaic foresets and topsetswithin Type 2 and 3 components: the foresets typically consist of pebbly coarse sand, whereas the topsets typically consist of framework-supported pebbles and cobbles with a coarse sand matrix. This difference in gain size between foreset and top set could conceivably reflect a combination of primary and secondary processes. Coarse pebbles and cobbles are commonly transported as bedload in gravel bed streams, whereas sandy material, and especially finer sandy material, is commonly transported as suspended load (e.g., Wilcock, 2004). If this was also true in the esker system in question, the sand would have had a tendency to bypass the topset and deposit on the foreset slope, where an abrupt decrease in energy would have allowed it to settle out.However, as argued previously, post depositional reworking by wind and water also likely occurred in places on the esker, and this could have

winnowed sandy material from the topset. It seems likely, therefore that in many places along the esker some combination of primary and secondary processes generated the observed grain-size difference between topsets and foresets. .

4.5 Transport distance within eskers

The question of transport distance is a complicated one, and one of great importance to mineral exploration. The primary factor controlling transport distance in esker systems downflow of the sediment source—which is typically a till dispersal train, not the bedrock itself (e.g., Bolduc, 1992)—would be the overall length of the meltwater conduit within which esker material was deposited. In the two end-member scenarios discussed in Chapter 1 (Figure 1.1), only the long conduit model has the potential for long distance transport downflow of the till dispersal train source (Cummings et al, 2011). In this study, a time-transgressive, short-conduit esker depositional model is favoured. Segments in this study were measured from the proximal end of a Type 1 ridge to the distal end of their corresponding Type 2 or 3 component or, in cases where Type 1 components are absent, from the up-flow end of a Type 3 component to the downflow end of the grain-size-fining trend. Complications in identifying segments arise, however, because coarse-grained Type 1 ridges, interpreted to have been deposited in R-channels, are frequently overlain by more recently deposited, sandier Type 2 and 3 components. Segments that can be confidently identified in the study area have variable lengths. The shortest segment is approximately 800 m in length (Figure 2.5, MTE-d area) and the longest is approximately 3 km (Figure 2.29). Previous authors have interpreted segments of similar length in other eskers based mainly on morphological analysis (e.g., Shilts,

1973; St. Onge, 1984; Hooke and Fastook, 2007). Furthermore, dispersal trains in eskers rarely extend more than several kilometers past the till dispersal train sources (Cummings et al., 2011), which may lend credence to this model. As such, it is hypothesized that for the length of the studied eskers, the maximum transport distance of sediment eroded from a subjacent till source might be no longer than several kilometers. This hypothesis could be tested by studying dispersal trains of distinct sand (e.g., KIMs) or gravel particles in the esker, provided a distinct dispersal train could be located in the subjacent till across which the esker passed. Given the paucity of studies integrated till-esker dispersal train studies (see review in Cummings et al., 2011), it is unclear whether transport distances on this order are the norm or the exception for eskers in general.

Chapter 5: Conclusions and recommendations for further studies

Overall, this study was effective in mapping and classifying the studied extent of the targeted eskers, and using GPR imagery and boreholes to make inferences on the depositional history of the eskers. It is concluded that the studied esker can be broadly categorized into four main components types, based on their morphology and sedimentary composition. Type 1 components are coarse, generally peaked ridges, and are interpreted to have formed subglacially in R channels. Type 2 components are broad to flat-topped, generally sandy ridges that are interpreted to be deposited by deltaic progradation into proglacial ice-walled channels. Type 3 components are broad, sand- to cobble-dominated surfaced bodies that are expansions of the main esker ridge. Type 3 components are interpreted to be deposited as prograding, proglacial deltaic sediments, often developing a coarse, pebbly to cobbly topset. Type 4 components are interpreted to be deposited supraglacially when sediment-laden meltwater was diverted from the main sediment transporting conduit and onto the surface of the glacier.

As an entire landform, the studied eskers are interpreted to be deposited time transgressively, in relatively short (0.8 km - 3 km) segments. This conclusion is supported by GPR imagery that shows proglacially deposited sediments down lapping older subglacial sediments, abrupt surficial grain size changes at component transitions, and post depositional erosive features indicative of a sequentially back-stepping point of meltwater discharge, and melt out of buried ice. This has important implications for mineral exploration using eskers in the Lac de Gras area. A short conduit model of formation implies that transport distances for eskers in the region is likely on the order of

several kilometers, rather than hundreds of kilometers as has commonly been assumed (e.g., Krajick, 2001).

For subsequent studies, I recommend several ways to build and improve upon the results from this investigation. To improve the understanding of the sedimentary architecture of eskers, a new GPR survey should be conducted, ideally using a 200 MHz rough terrain antenna, using a differential GPS system for location and elevation tracking. At a frequency of 200 MHz, there would be an ideal balance between the penetration depth required to image the bulk of esker material, and resolution needed to effectively see sedimentary strata. The differential GPS system would provide a much more accurate elevation correction and would be essential for areas with no LiDAR coverage. Extracting elevation data from the LiDAR imagery is time consuming, and having accurate elevation data directly applied to the survey lines would be invaluable.

To better constrain transport distance within eskers, setting up a study to purely investigate till vs esker dispersal trains would be ideal. Finding a location where a known, till-sample-delineated dispersal train is crossed by an esker would allow for the accurate determination of transport distance within an esker relative to till. Bulk esker samples taken from different esker components could be compared, and it may be possible to determine the most effective sampling medium for locating kimberlite indicator minerals in eskers.

REFERENCES

Ambrose, J.W. 1964. Exhumed paleoplains of the Precambrian Shield of North America. American Journal of Science. 262. p. 817-857.

Annan, A. P. 2004. Ground Penetrating Radar: Principles, Procedures, and Applications. Sensors and Software Inc.

Arcone, S.A., Lawson, D.E., Delaney, A.J., Strasser, J.C. and Strasser, J.D. 1998. Ground-penetrating radar reflection profiling of groundwater and bedrock in an area of discontinuous permafrost. Geophysics, v. 63, p. 1573–1584.

Armstrong, J.A., Wilson, M., Barnett, R.L, Nowicki, T., Kjarsgaard, B.A. 2004. Mineralogy of primary carbonate-bearing hypabyssal kimberlite, Lac de Gras, Slave Province, Northwest Territories, Canada. Lithos, 76 (1-4). p. 415-433.

Atkinson, W.J. 1989. Diamond exploration philosophy, practice, and promises: a review. In: O'Reilly, S.Y. (Ed.), Kimberlites and Related Rocks: Their Mantle/Crustal Setting, Diamonds and Diamond Exploration. Proceedings of the 4th International Kimberlite Conference, Perth, Australia. GSA Special Publication Number 14, pp. 1075–1107.

Averill, S.A. 2011. Viable indicator minerals in surficial sediments for two major base metal deposit types: Ni-Cu-PGE and porphyry Cu. Geochemistry: Exploration, Environment, Analysis, v. 11, p. 279–291.

Aylsworth, J. and Shilts, W. 1989. Glacial features around the Keewatin ice divide: Districts of Mackenzie and Keewatin. Geological Survey of Canada, Paper 88–24, 21 p.

Banerjee, I. 1969. Sedimentology of an esker north of Peterborough, Ontario. Project 670036, Quaternary Research and Geomorphology, Geological Survey of Canada. pp. 2.

Banerjee, I. and MacDonald, B.C. 1975. Nature of esker sedimentation. In Jopling, A.V. and MacDonald, B.C. (eds.), Glaciofluvial and Glaciolacustrine Sedimentation, SEPM Special Publication 23, pp. 132–154.

Benn, D.I., Evans, D.J.A. 2010. Glaciers and Glaciation, 2nd edition. Hodder Education. pp. 801.

Bolduc, A. 1992. The formation of eskers based on their morphology, stratigraphy, and lithologic composition, Labrador, Canada. Unpublished PhD thesis, Lehigh University, 190 p.

Boulton, G.S., Lunn, R., Vidstrand, P., Zatsepin, S. 2007. Subglacial drainage by groundwater–channel coupling, and the origin of esker systems: part 1 — glaciological observations. Quaternary Science Reviews 26, 1067–1090.

Boulton, G.S., Hagdorn, M., Maillot, P.B., Zatsepin, S. 2009. Drainage beneath ice sheets: groundwater–channel coupling, and the origin of esker systems from former ice sheets. Quaternary Science Reviews xxx p. 1-18.

Brennand, T.A. 1994. Macroforms, large bedforms and rhythmic sedimentary sequences in subglacial eskers, south-central Ontario: implications for esker genesis and meltwater regime. Sedimentary Geology 91, 9–55.

Brennand, T.A. and Shaw, J. 1996. The Harricana glaciofluvial complex, Abitibi region, Quebec: its genesis and implications for meltwater regime and ice-sheet dynamics. Sedimentary Geology, v. 102, p. 221–262.

Brennand, T.A., 2000. Deglacial meltwater drainage and glaciodynamics: inferences from Laurentide eskers, Canada. Geomorphology 32, 263–293.

Bristow, C., Jol, H. 2003. An introduction to ground penetrating radar (GPR) in sediments. In: Ground Penetrating Radar in Sediments, Geological Society special publication.

Buck, S. 1983. Transport distances of bedrock particles in the Tweed esker. Unpublished MSc thesis, Brock University, 83 p.

Burn, C. R., Zhang, Y. 2009. Permafrost and climate change at Herschel Island (Qikiqtaruq), Yukon Territory, Canada, J. Geophys. Res. 114. pp. 2156-2202.

Burke, M.J., Woodward, J., Russell, A.J., Fleisher, P.J., Bailey, P.K. 2008. Controls on the sedimentary architecture of a single event englacial esker: Skeidararjokull, Iceland. Quaternary Science Reviews 27, 1829–1847.

Burke, M.J., Woodward, J., Russell, A.J., Fleisher, P.J., Bailey, P.K. 2010. The sedimentary architecture of outburst flood eskers: A comparison of ground-penetrating radar data from Bering Glacier, Alaska and Skeiðarárjökull, Iceland. Geological Society of America Bulletin. 122: 1637-1645.

Carlson, J.A., Kirkley, M.B., Thomas, E.M, Hillier, W.D. 1999. Recent Canadian kimberlite discoveries. In: Proceedings of the VIIth international kimberlite conference. Ed(s) Gurney, J.J., Gurney, J.L., Pascoe, M.D., Richardson, S.H., 1 p. 81-89.

Carrigy, M. 1970. Experiments on the angles of repose of granular materials. Sedimentology 14, 147-158.

Cartigny, M.J.B., Ventra, D., Postma, G., Van Den Berg, J.H. 2014. Morphodynamics and sedimentary structures of bedforms under supercritical-flow conditions: New insights from flume experiments. Sedimentology, 61. pp. 712-748.

Cassidy, N.J. 2009. Ground penetrating radar data processing, modelling and analysis. In: Jol, H.M. (ed), Ground Penetrating Radar Theory and Applications, p. 141-176.

Cassidy, N.J. 2009. Electrical and magnetic properties of rocks, soils and fluids. In: Jol, H. (ed.), Ground Penetrating Radar Theory and Applications. Elsevier, p. 41–72.

Clark, P.U. and Walder, J.S. 1994. Subglacial drainage, eskers, and deforming beds beneath the Laurentide and Eurasian ice sheets. Geological Society Bulletin of America, v. 106, p. 304–314.

Clarke, G.K.C, 2005. Subglacial processes. Annual Reviews, Earth and Planetary Science. 33. pp. 247-276.

Costa, J.E. 1983. Paleohydraulic reconstruction of flash-flood peaks from boulder deposits in the Colorado Front Range. Geological Society of America, 94. pp. 986-1004.

Craig, B.G. 1964. Surficial geology of east-central District of Mackenzie. Geological Survey of Canada, Bulletin 99, 41 p.

Craigie, E. 1993. Sampling techniques and the distribution of kimberlite indicator minerals in glacial tills and sediments *in* Diamonds: Exploration, Sampling and Evaluation Short Course. Prospectors and Developers Association of Canada Conference, Toronto, March 27, 1993, p. 237–247.

Cummings, D.I., Kjarsgaard, B., Russell, H., Sharpe, D. 2011. Eskers as mineral exploration tools. Earth-Science Reviews. 109: 32-43.

Cummings, D.I. 2012. Quaternary geology of the 2012 Diavik Diamond Mines Inc till sample grid, Lac de Gras, Northwest Territories (NTS 76C). Unpublished technical report submitted to Diavik Diamond Mines Inc, October 18, 2012, 86 p.

Das, S.B., Joughin, I., Behn, M.D., Howat, I.M., King, M.A., Lisarralde, D., and Bhatia, M.P. 2008. Fracture propagation to the base of the Greenland ice sheet during supraglacial lake drainage. Science, v. 320, p. 778–781.

Davis, W.J., Kjarsgaard, B.A. 1997. A Rb-Sr isochron age for a kimberlite from the recently discovered Lac de Gras Field, Slave Province, Northwest Canada. The Journal of Geology, 105. p. 503-510.

De Geer, G. 1912. A geochronology of the last 12000 years. Congres Géologique Internationale Stockholm 1910, 241–253.

Delaney, C. 2002. Sedimentology of a glaciofluvial land system, Lough Ree area, Central Ireland: implications for ice margin characteristics during Devensian deglaciation. Sedimentary Geology, Sedimentary Geology 149: 111-126

Dinehart, R.L. 1992. Evolution of coarse gravel bed forms: field measurements at flood stage. Water Resources Research, v. 28, p. 2667–2689.

Dredge, L., Kerr, D., Wolfe, S. 1999. Surficial materials and related ground ice conditions, Slave Province, N.W.T., Canada. Canadian Journal of Earth Science. 36: 1227-1238.

Dredge, L.A., Ward, B.C. and Kerr, D.E. 1994. Glacial geology and implications for drift prospecting in the Lac de Gras, Winter Lake, and Aylmer Lake map areas, central Slave Povince, Northwest Territories *in* Geological Survey of Canada, Current Research 1994-C, p. 33–38.

Dreimanis, A. 1989. Tills: their genetic terminology and classification. In Goldthwait, R.P., Matsch, C.L. (eds), Genetic classification of glacigenic deposits. p. 17-84.

Elliott, B. 2015. Slave Province Surficial Materials and Permafrost Study—Concluding presentation. 43rd Annual Yellowknife Geoscience Forum, Yellowknife, Northwest Territories.

Eyles, N. 2006. The role of meltwater in glacial processes. Sedimentary Geology. 190. p. 257-268.

Fahnestock, M., Abdalati, W., Joughin, I., Brozena, J., Gogineni, P. 2001. High geothermal heat flow, basal melt, and the origin of rapid ice flow in central Greenland. Science, 294, pp. 2338–2342

Fard, A.M. 2002. Large dead-ice depressions in flat-topped eskers: evidence of a Preboreal jokulhlaup in the Stockholm area, Sweden. Global and Planetary Change, 35. pp. 273-295.

Fard, A.M., Gruszka, B., 2007. Subglacial conditions in a branching Saalian esker in north-central Poland. Sedimentary Geology, 193. pp. 33-46.

Fisher, S.C., Steward, R.R. and Jol, H.M. 1992. Processing ground penetrating radar (GPR) data. CREWES Research Report, v. 4, p. 11-1 to 11-22.

Flint, R.F., 1930. The origin of the Irish “eskers”. Geographical Review 20 (4), p. 615–630.

Fountain, A.G. Walder, J.S., 1998. Water flow through temperate glaciers. Reviews of Geophysics 36 (3), 299–328.

Fulton, R.J. 1995. Surficial materials of Canada, Map 1880A. Geological Survey of Canada. 1:5,000,000 scale.

Gorrell, G., Shaw, J. 1991. Deposition in an esker, bead and fan complex, Lanark, Ontario, Canada. Sedimentary Geology. 72: 285-314.

Gustavson, T. C., Boothroyd, J. C. 1987. A depositional model for outwash, sediment sources, and hydrologic characteristics, Malaspina Glacier, Alaska: A modern analog of the southeastern margin of the Laurentide Ice Sheet. Geological Society of America Bulletin 99: 187-200

Hellaakoski, A. 1931. On the transportation of materials in the esker of Laitila. Fennia 52, 282–311.

Hinkel, K., Doolittle, J., Bockheim, J., Nelson, F., Paetzold, R., Kimble, J., Travis, R. 2001. Detection of subsurface permafrost features with ground penetrating radar, Barrow, Alaska. Permafrost and Periglacial Processes. 12: 179-190

Hooke, R., Fastook, J. 2007. Thermal conditions at the bed of the Laurentide Ice Sheet in Maine during deglaciation: implications for esker formation. Journal of Glaciology, 53: 646-658.

Hu, X., Holubec, I., Wonnacott, J., Lock, R., Olive, R. 2003. Geomorphological, geotechnical and geothermal conditions at Diavik Mines. In: Phillips, M., Springman, S., Arenson, L. (Eds.) Proceedings of the Eighth International Conference on Permafrost. 6 pp.

Jaupart, C., Mareschal, J.C. 2007. Heat flow and thermal structure of the lithsosphere. 6.05 Elsevier Brochures. pp. 218-251.

Jol, H.M. 2009. Ground penetrating radar theory and applications. Elsevier.

Kaufman, D. S., Ager, T. A., Anderson, N. J., Anderson, P. S., Andrews, J. T., Bartlein, P. J., Brubaker, L. B., Coats, L. L., Cwynar, L. C., Duvall, M. L., Dyke, A. S., Edwards, M. E., Eisner, W. R., Gajewski, K., Geirsdóttir, A., Hu, F. S., Jennings, A. E., Kaplan, M. R., Kerwin, M. W., Lozhkin, A. V., MacDonald, G. M., Miller, G. S., Mock, C. J., Oswald, W. W., Otto-Bliesner, B. L., Porinchu, D. F., Rühland, K., Smol, J. P., Steig, E. J., Wolfe, B. B. 2004. Holocene thermal maximum in the western Arctic (0–180°W). Quaternary Science Reviews. 23. pp. 529-560

Kerr, D.E., Knight, R.D., Sharpe, D.R., Cummings, D.I. 2013. Surficial geology, Artillery Lake, Northwest Territories, NTS 75-O. Geological Survey of Canada, Canadian Geosciences Map 110.

Kjarsgaard, B.A., Wilkinson, L., Armstrong, J.A. 2001. Geology, Lac de Gras kimberlite field, central Slave province, Northwest Territories–Nunavut. Geological Survey of Canada, Open File 3238, scale 1:250 000

Krajick, K., 2001. Barren Lands: An Epic Search for Diamonds in the North American Arctic. Freeman, W.H. 442 pp.

Lawson, D.E. 1993. Glaciohydrologic and glaciohydraulic effects on runoff and sediment yield in glacierized basins. Monograph 93-2, US Army Corps of Engineers. pp. 108.

Levasseur, D., 1995. Les eskers: Essai de synthese bibliographique. Géographie physique et Quaternaire 49 (3), 459–479.

Lord, C.S. and Barnes, F.Q. 1954. Aylmer Lake, District of Mackenzie, Northwest Territories. Geological Survey of Canada, Map 1031A.

Lundqvist, J. 1999. Periodical sedimentation in Scandinavian eskers. GFF, 121. pp. 175-181.

Lunt, I.A., Bridge, J.S. 2004. Evolution and deposits of a gravelly braid bar, Sagavanirktok River, Alaska. Sedimentology, 51. pp. 415-432.

MacDonald, R.G., Alexander, J., Bacon, J.C., Cooker, M.J. 2009. Flow patterns, sedimentation and deposit architecture under a hydraulic jump on a non-eroding bed: defining hydraulic-jump unit bars Sedimentology, 56. pp. 1346-1367.

MacKay, J, R., Burn, C. R. 2005. A long-term field study (1951-2003) of ventifacts formed by katabatic winds at Paulatuk, western Arctic coast, Canada. Canadian Journal of Earth Sciences, 42. pp. 1615-1635.

Maizels, J. K. 1997. Jokulhlaup deposits in proglacial areas. Quaternary Science Reviews, 16. pp. 793–819.

Marren, P.M., Schuh, M. 2009. Criteria for identifying jökulhlaup deposits in the sedimentary record. In: Megaflooding on Earth and Mars, Ed(s). Burr, D.M., Carling, P.A., Baker, V.R. Cambridge University Press. pp. 225-242.

Martini, I. P. 1990. Pleistocene glacial fan deltas in southern Ontario, Canada. Special publication number 10 of the International Association of Sedimentologists. 1990. pp. 281-296.

Murray, T., Stuart, G.W., Miller, P.J., Woodward, J., Smith, A.m., Porter, P.R., Jiskoot, H. 2000. Glacier surge propagation by thermal evolution at the bed. Journal of Geophysical Research, 105. pp. 13491-13507.

Neal, A. 2004. Ground Penetrating Radar and its use in Sedimentology: principles, problems and progress. Earth Science Reviews. 66: 261-330.

Nemec, W. 1990. Aspects of sediment movement on steep delta slopes. In: Colella, A. and Prior, D. B. (Eds). Special publication number 10 of the International Association of Sedimentologists. 1990. pp. 29-73.

Nemec, W., Lonne, I., Blikra, L.H. 1999. The Kregnes moraine in Gauldalen, west-central Norway: anatomy of a Younger Dryas proglacial delta in a palaeofjord basin. Boreas, 28. pp. 454-476.

Nichols, H. 1976. Historical aspects of the North American treeline. Arctic, v. 29, p. 38–37

North, C.P., Davidson, S.K. 2012. Unconfined alluvial flow processes: Recognition and interpretation of their deposits, and the significance for palaeogeographic reconstruction. Earth Science Reviews, 111. pp. 199-223.

Padgham, W.A., Fysonm W.K. 1992. The Slave Province: a distinct Archean craton. Canadian Journal of Earth Science. 29. p. 2072-2086.

Pell, J.A. 1997. Kimberlites in the Slave Craton, Northwest Territories, Canada: a preliminary review. Russian Geology and Geophysics, 38. p. 5-16.

Post, A., LaChapelle, E.R. 2000. Glacier Ice, Revised Edition. University of Toronto Press. p. 145.

Prest, V.K., Grant, D.R., Rampton, V., 1968. Glacial Map of Canada. Map 1253A, Scale 1:5000000, Geological Survey of Canada.

Price, R.J. 1966. Eskers near the Caseent Glacier, Alaska. Geografiska Anneler, 48. pp. 111-125.

Price, R.J. 1969. Moraines, sandar, kames and eskers near Breidamerkurjökull, Iceland. Transactions of the Institute of British Geographers, 46. pp. 17-43.

Rampton, V.N., 2000. Large-scale effects of subglacial meltwater flow in the southern Slave Province, Northwest Territories, Canada. Canadian Journal of Earth Sciences 37. pp. 81–93.

Rampton, V.N. and Sharpe, D.R. 2009. Glaciofluvial processes and mineral exploration in southern Slave Province, Northwest Territories, Canada [Abstract]. GAC-MAC Conference, Toronto, May 24–27.

Reesink, A. J. H., Ashworth, P.J., Sambrook Smith, G. H., Best, J. L., Parsons, D. R., Amsler, M. L., Hardy, R. J. 2014. Scales and causes of heterogeneity in bars in a large multi-channel river: Río Paraná, Argentina. Sedimentology 61. pp. 1055-1085.

Roberts, M.J. 2005. Jokulhaups: a reassessment of floodwater flow through glaciers. Reviews of Geophysics, 43. pp 21.

Ross, J. 2015. Summer addendum to archeology overview assessment for the Slave Province Surficial Materials and Permafrost Study, Lac de Gras area. Unpublished technical report prepared by Point West Heritage Consulting Ltd for Barrett Elliot, Northwest Territories Geological Survey, 13 p

Röthsilberger, H. 1972. Water pressure in intra and sub-glacial channels. Journal of Glaciology, 11. pp. 177-202.

Rothsilberger, H., Lang, H. 1987. Glacial Hydrology. In: GLavio-fluvial Sediment Transfer. Ed(s) Gurnell, A.M., Clark, M.J. John Wiley and Sons Ltd. pp. 207-284.

Rust, B.R. 1977. Mass flow deposits in a Quaternary succession near Ottawa, Canada: diagnostic criteria for subaqueous outwash. Canadian Journal of Earth Sciences, 14. pp. 175-184.

Sarkar, C., Heaman, L. M., Pearson, D. G. 2015. Duration and periodicity of kimberlite volcanic activity in the Lac de Gras kimberlite field, Canada and some recommendations for kimberlite geochronology. Lithos, 218-219: 155-166.

Scott-Smith, B.H. 2008. Canadian kimberlites: geological characteristics relevant to emplacement. Journal of Volcanology and Geothermal Research, 174. pp. 9-19.

Schulmeister, J. 1989. Flood deposits in the Tweed Esker (southern Ontario, Canada). Sedimentary Geology, 65. pp. 153-163.

Shilts, W.W. 1973. Drift prospecting; geochemistry of eskers and till in permanently frozen terrain: District of Keewatin, Northwest Territories. Geological Survey of Canada, Paper 72-45. 34 pp.

Shilts, W. 1978. Nature and genesis of mudboils, central Keewatin, Canada. Canadian Journal of Earth Science. 15: 1053-1068.

Shilts, W.W. 1976. Glacial till and mineral exploration. In: Legget, R.F. (Ed.), Glacial Till: An Interdisciplinary Study, Royal Society of Canada, Special Publication 12. p. 205–224.

Shilts, W.W., 1984. Esker sedimentation models, Deep Rose Lake map area, district of Keewatin. Current Research, Part B, Geological Survey of Canada, Paper 84-1B, pp. 217–222.

Shoemaker, E.M. 1992. Water sheet outburst floods from the Laurentide Ice Sheet. Canadian Journal of Earth Sciences, v. 29, p. 1250-1264.

Shreve, R.L., 1985a. Esker characteristics in terms of glacier physics, Katahdin esker system, Maine. Geological Society of America Bulletin 96, 639–646.

Shreve, R.L. 1985b. Late Wisconsin ice-surface profile calculated from esker paths and types, Katahdin esker system, Maine. Quaternary Research, v. 23, p. 27–37.

Smith, D., Jol, H. 1997. Radar Structure of a Gilbert-type delta, Peyto Lake, Banff National Park, Canada. Sedimentary Geology. 113: 195-209.

Sollas, W.J. 1896. A map to show the distribution of eskers in Ireland. Scientific Transactions of the Royal Dublin Society 5 (13), 785–822.

St. Onge, D. 1984. Surficial deposits of the Redrock Lake area, District of Mackenzie *in* Current Research, Part A, Geological Survey of Canada, Paper 84-1A, p. 271–276.

Storrar, R., Stokes, C., Evans, D. 2014. Morphometry and pattern of a large Sample (>20,000) of Canadian eskers and implications for subglacial drainage beneath ice sheets. Quaternary Science Reviews, 105: 1-25.

Stubley, M. 2005. Bedrock geology of the Slave Craton. Northwest Territories Geological Survey.

Sutherland, D.G. 1982. The transport and sorting of diamonds by fluvial and marine processes. Economic Geology 77, 1613–1620.

Wadham, J.L., Hodgkins, R., Cooper, R.J., Tranter, M. 2001. Evidence for seasonal subglacial outburst events at a polythermal glacier, Finsterwalderbreen, Svalbard. Hydrological Processes, 15. p. 2259-2280.

Ward, B. 1993. Surficial geology, Lac de Gras (NTS 76D), Northwest Territories. Geological Survey of Canada, Open File 2680, 1:125,000 scale.

Ward, B., Dredge, L. and Kerr, D. 1994a. Ice flow indicators, Winter Lake–Lac de Gras–Aylmer Lake, District of Mackenzie, Northwest Territories, Geological Survey of Canada, Open File 2808, 1:250,000 scale.

Ward, B., Dredge, L. and Kerr, D. 1994b. Surficial geology, Lac de Gras, District of Mackenzie, Northwest Territories. Geological Survey of Canada, Open File 2926, 1:125,000 scale.

Ward, B. 1997. Surficial geology, Lac De Gras, District of Mackenzie, Northwest Territories. Geological survey of Canada, Series A Map.

Whiting, P.J., Dietrich, W.E. and Leopold, L.B. 1988. Bedload sheets in heterogeneous sediment. Geology, v. 16, p. 105–108.

Wilson, J. 1939. Eskers north east of Great Slave Lake. Transactions and Proceedings of the Royal Society of Canada, Section IV, 1939. 12 p.

Wilson, J. 1945. Further eskers north of Great Slave Lake. Transactions and Proceedings of the Royal Society of Canada, Section IV, 1945. 4 p.

Wolfe. S., Burgess, M. Douma, M., Hyde, C., Robinson, S. 1996. Geological and geophysical investigations of the BHP Airstrip Esker and Misery Lake Esker, Slave Geological Privince, NWT. Report of Field Activities Conducted in March 1996, Geological Survey of Canada. pp. 32.

Zwally, H.J., Abdalati, W., Herring, T., Larson, K., Saba, J., Steffen, K. 2002. Surface melt-induced acceleration of Greenland Ice Sheet flow. Science, 297. pp. 218-222.

Appendix A: LiDAR of Studied Esker Segments

The following figures are interpreted LiDAR maps of the studied esker. This appendix acts as a supplement to the figures in Chapter 2.

In the following figures, the overall extent of the studied esker is presented as LiDAR imagery, with interpretations of components and surficial materials (Figures 2.9 – 2.27). For clarity, grain-size photograph locations were omitted, but are presented along with relevant grain size information in Appendix C.

Misery Tributary Esker

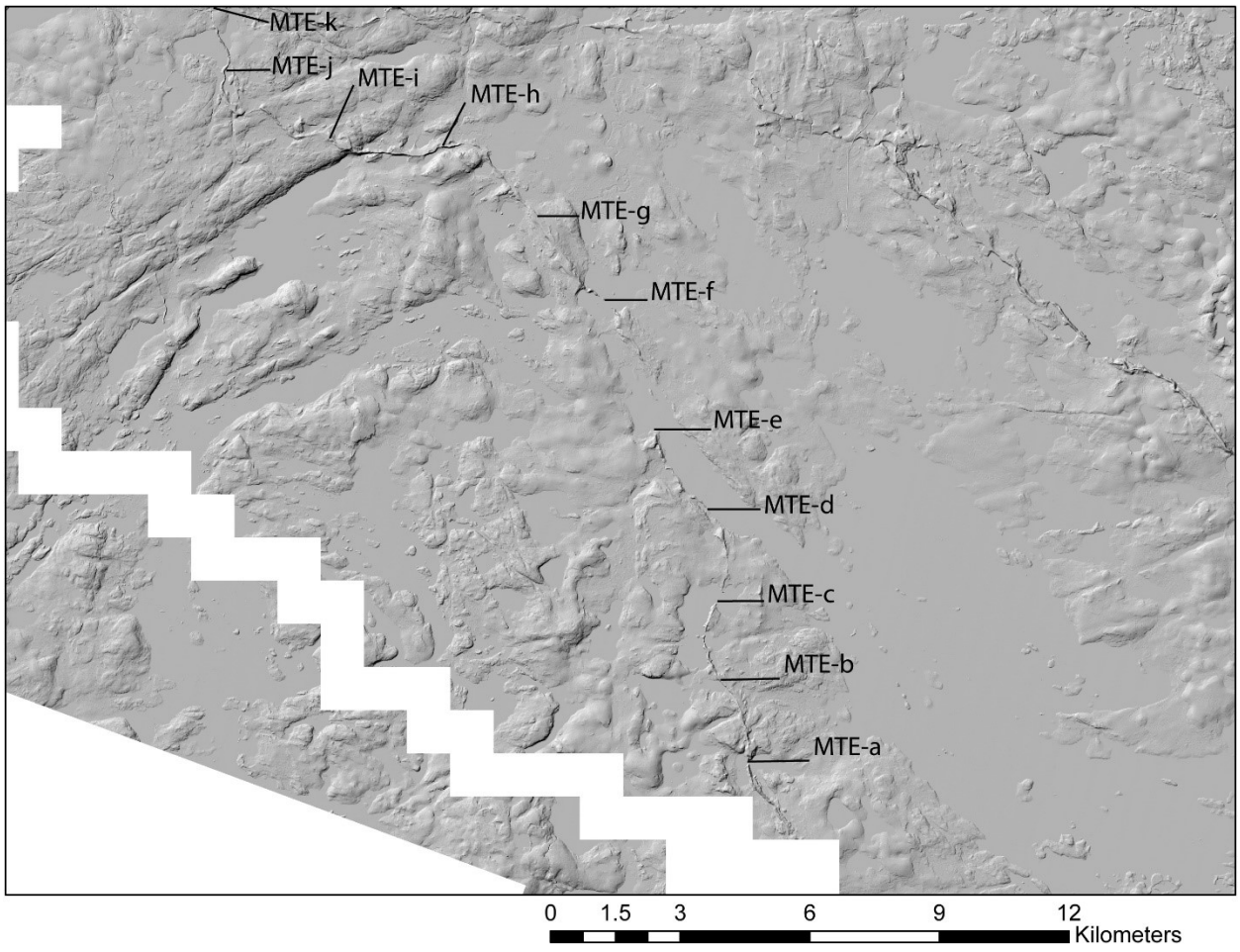

Figure A1: Misery Tributary Esker (MTE) overview. Figures 2.10-.2.20 depict locations MTE-a to MTE-k, with lines pointing to the down-esker extent of respective images. Paleoflow direction is broadly south to north.

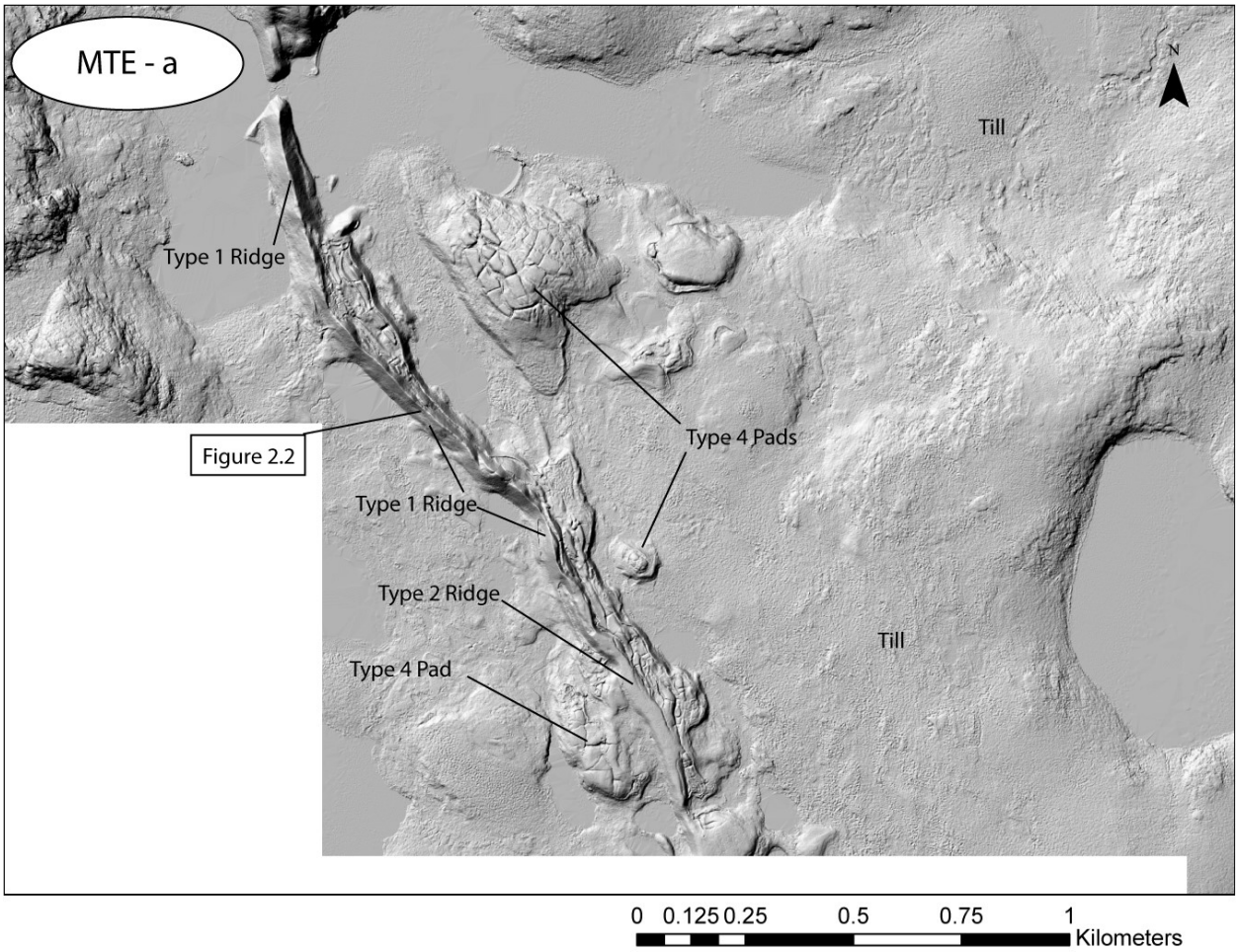

Figure A2: LiDAR imagery showing the esker and its various morphological components. Till surrounding the MTE-a area appears to be thin, as indicated by the lack of pronounced till hummocks in the area. Thaw slumping is evident on the eastern flank of the main esker ridge. Polygonal patterned ground interpreted to be associated with ice wedging and ice melt out is visible in the northern-most large Type 4 component.

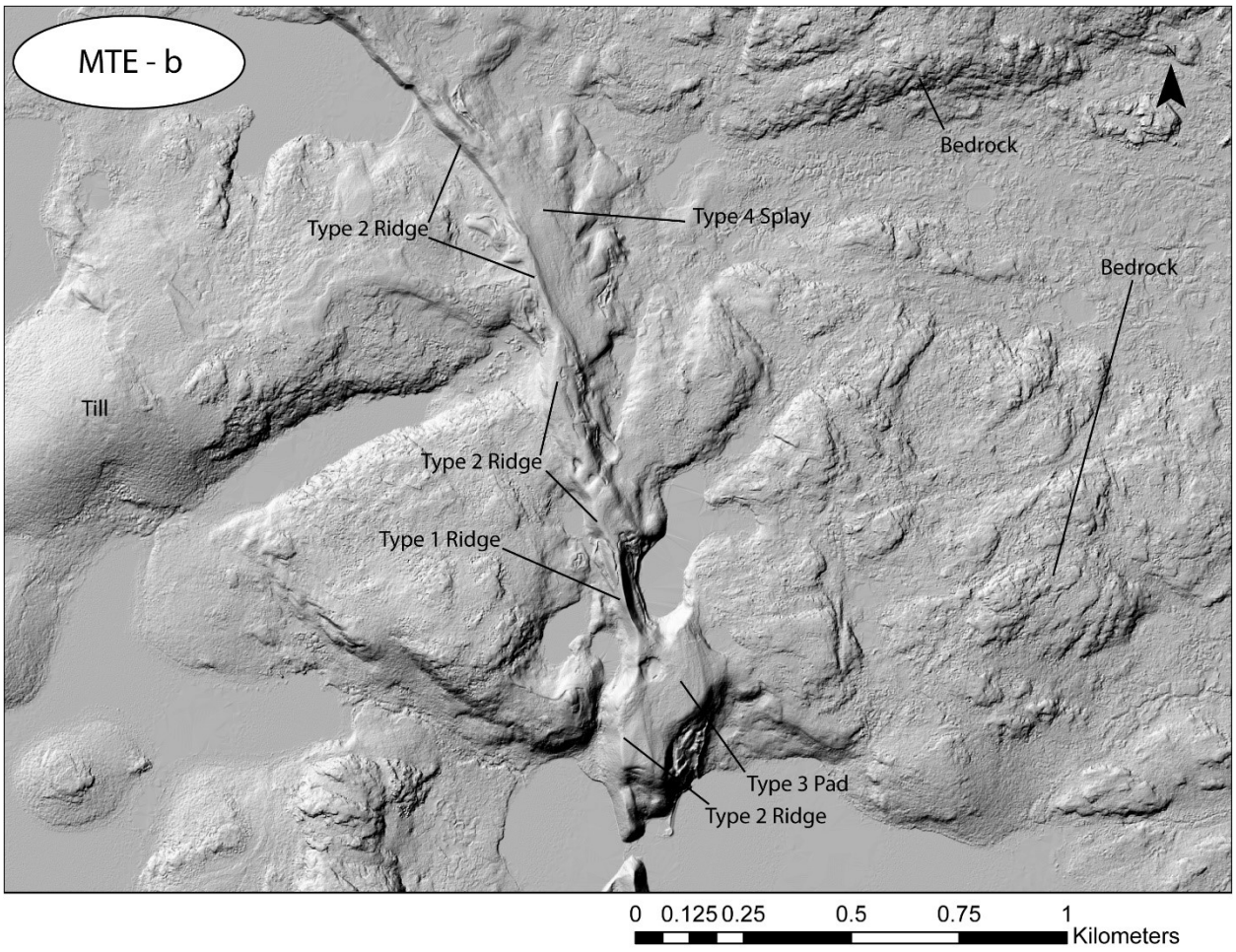

Figure A3: 1:8000 Scale LiDAR image of MTE-b area. Esker overlies a portion of elevated bedrock present in the southeastern portion of the map. West of the esker, till is thinner adjacent to the main ridge but appears to thicken to the west as illustrated by the presence of a large till hummock. The Type 3 component extends east of the main ridge and is slightly lower in elevation. Kettle hole and thaw slumping are interpreted to represent melt out of buried ice.

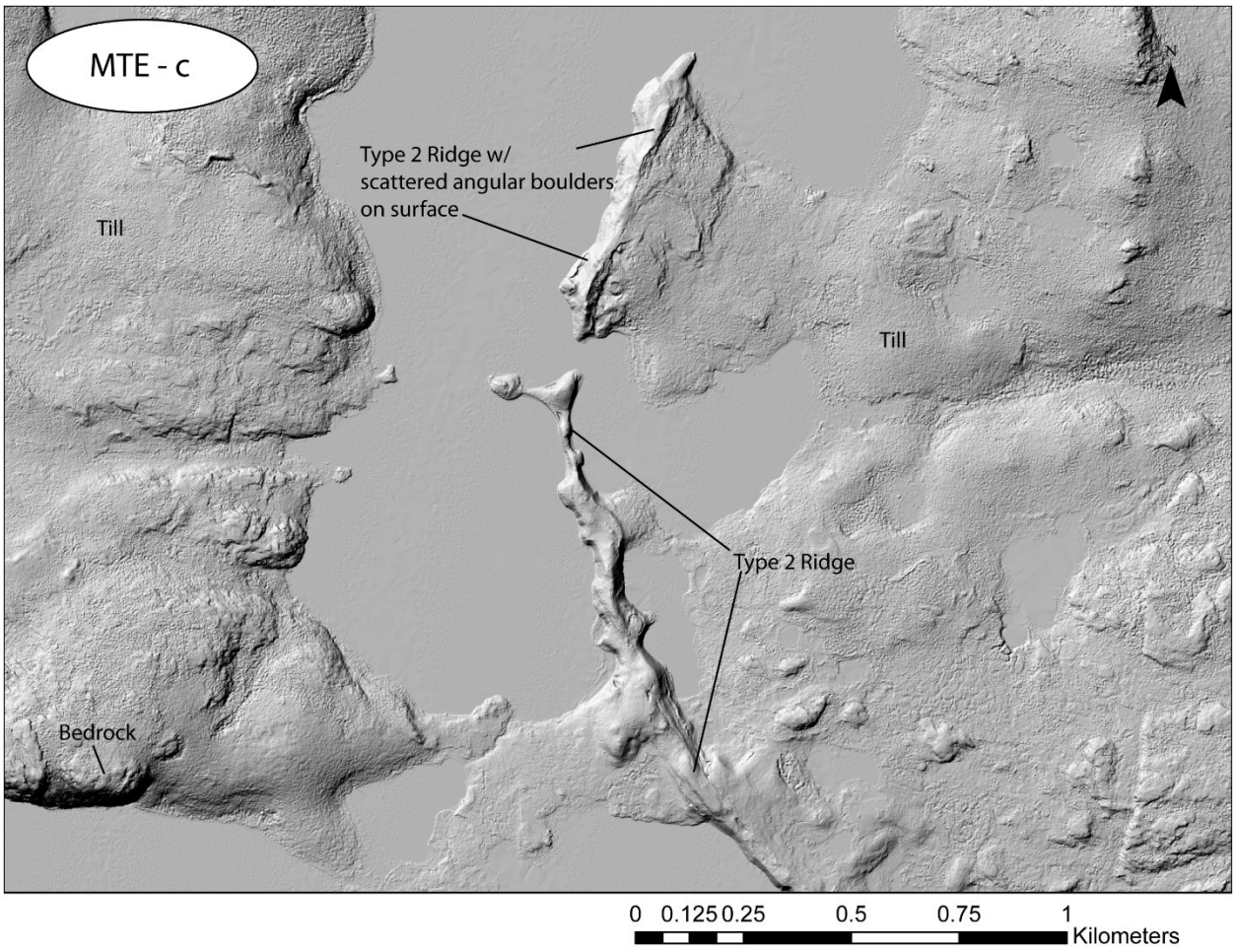

Figure A4: Southern portion of esker in MTE-c is a fine-grained (coarse to fine sand), broadly crested thin, Type-2 ridge. Peninsular body protruding into the lake is coarser grained similar to a small Type 4 pad. Northern portion of esker in this figure is unique within the study area: very fine sand is mounded and scattered with very large (>1.5 m) angular boulders and cobbles. Boulders become sparser to the north and the segment appears to be a standard Type 2 ridge at the very northern-most point.

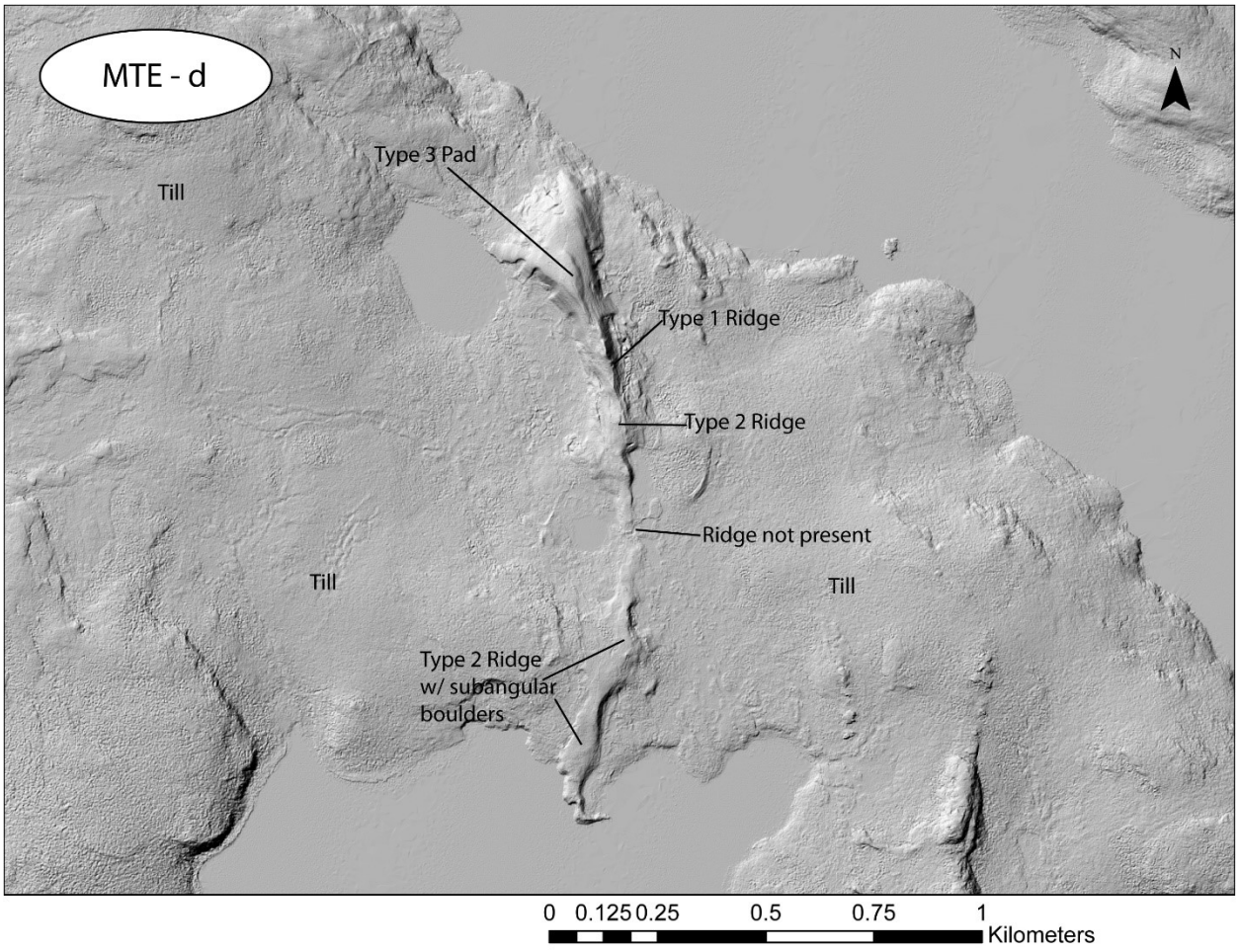

Figure A5: Southern portion of MTE-d area esker is similar to northern portion of MTE-c, with more-rounded boulders. A gap in the ridge is present as heavily vegetated, cryoturbated diamicton, similar in appearance to the surrounding till. Type 2 ridge begins after break in esker that quickly transitions to a sharp crested Type 1 ridge. Type 1 ridge transitions into a fan shaped Type 3 pad that appears to mark the limit of esker sediment in this figure. Adjacent till is thin.

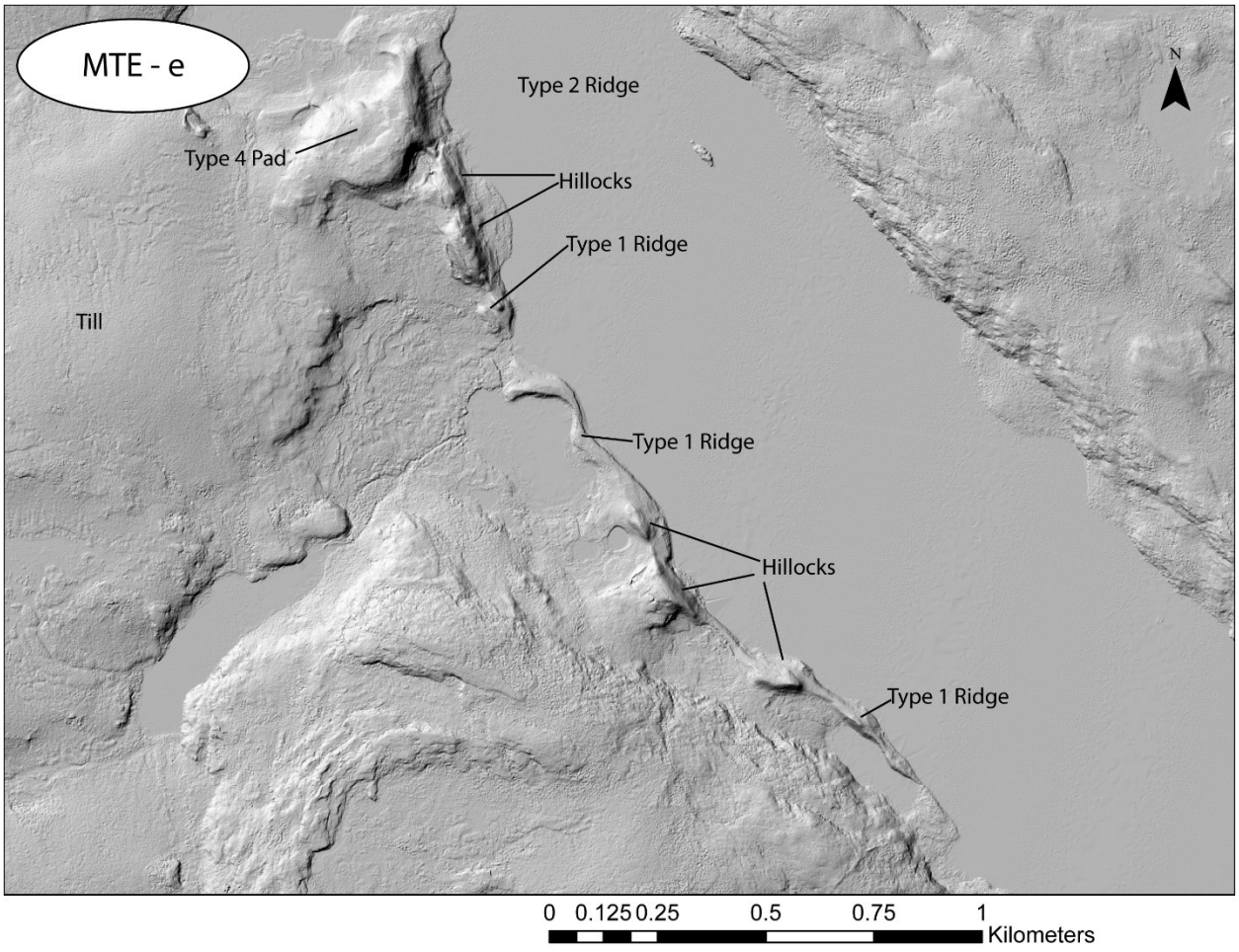

Figure A6: After a gap of 500 m, the esker re-appears along trend of segment in Figure A5. Esker in MTE-e area is a cobbly Type 1 ridge punctuated by several elongate hillocks that fine in grain size down-flow. In the northern portion of this figure, the esker terminates at a water body (Lac Sauvage) as a Type 2 ridge flanked by a gently sloping Type 4 pad. Till adjacent to esker is thin but appears to thicken to the west evidenced by the large till hummock.

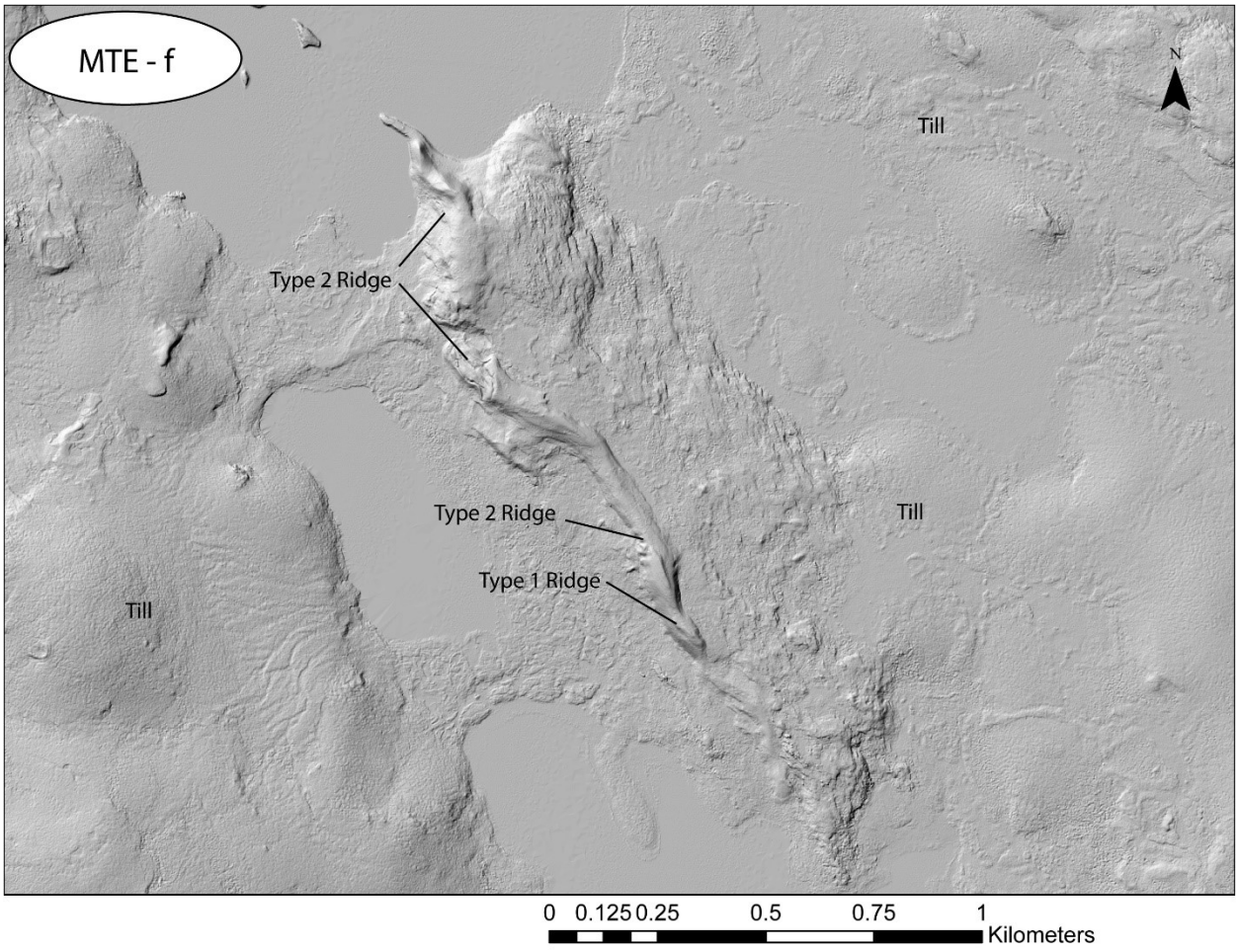

Figure A7: The MTE-f area is located approximately 1.2 km north of the MTE-e area (Figure A7). The esker is present as a relatively large Type 1 ridge that transitions into a Type 2 ridge to the north. Till adjacent to esker is thin, and the whole landform in this area appears to be situated on a bedrock high flanked by thicker, boggy, low lying till to the east, and hummocky till to the west.

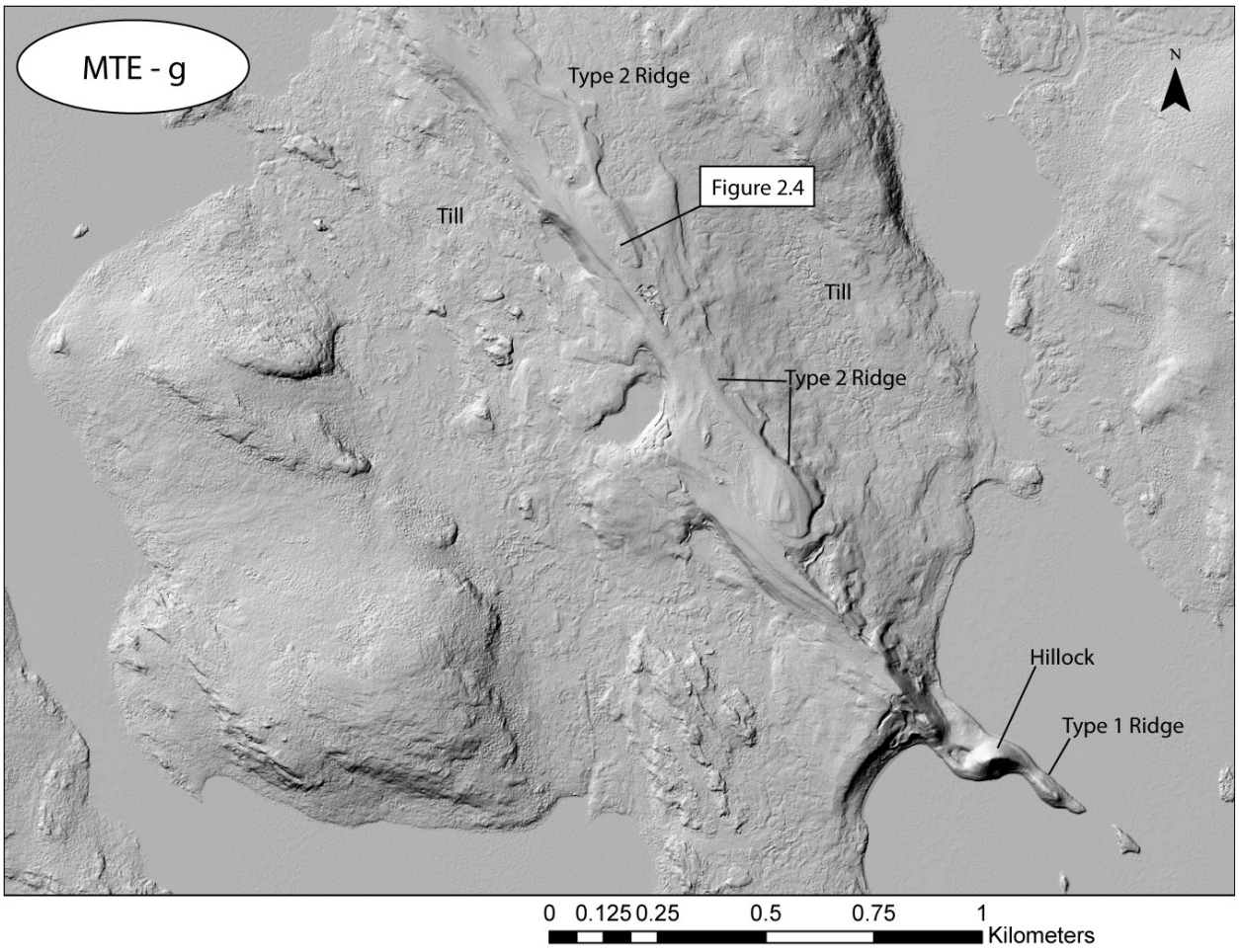

Figure A8: In southeastern portion of MET-g area, the esker emerges from a water body as a Type 1 ridge quickly followed by a large hillock and an abrupt break. A Type-2 ridge follows a steep uphill slope on what appears to be a bedrock high. The Type-2 ridge is broad and low relief with a fan-like appearance that makes a case for this component being classified as a Type 3 pad. However, a coarse-pebble- and cobble-surface-texture that gradually fines down flow to coarse sand, combined with the low relief and gently undulating profile is more consistent with the Type 2 classification. It could also be interpreted that in this figure, parallel lines on the flanks of the land are due to beach re-working by a proglacial waterbody.

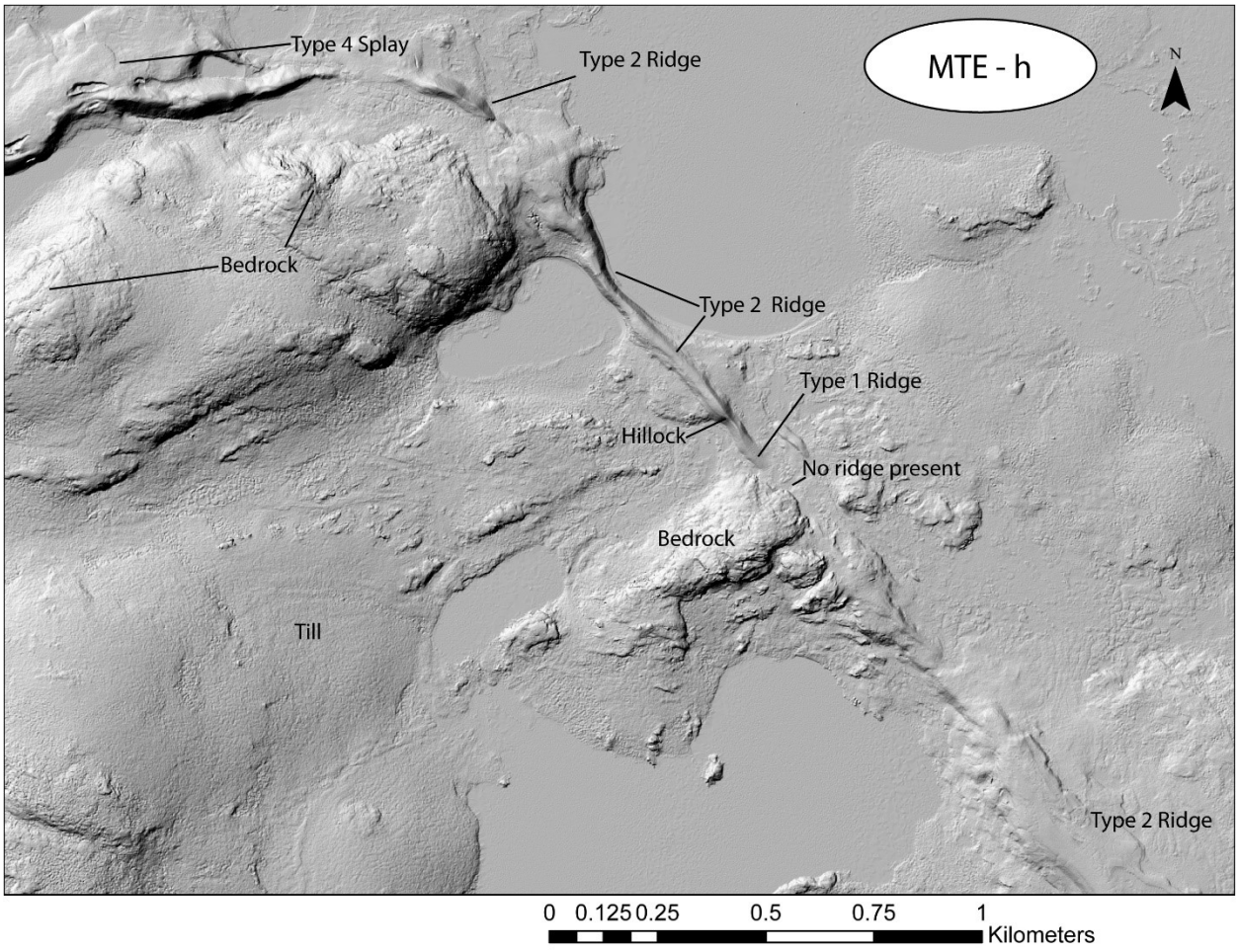

Figure A9: Type-2 Ridge in southeastern portion of MTE-h area terminates on a bedrock high, followed by an apparent break in the esker. Esker re-emerges as a Type-1 ridge, transitioning abruptly into a broad crested Type 2 ridge. At a point where esker bends to the west, esker material is obscured by heavy vegetation. Type 2 ridge re-appears and is flanked by a vegetated fine sand outwash, with rare kettle holes, comprising a type 4 splay component. Till in the immediate vicinity of the esker is thin, and often boggy.

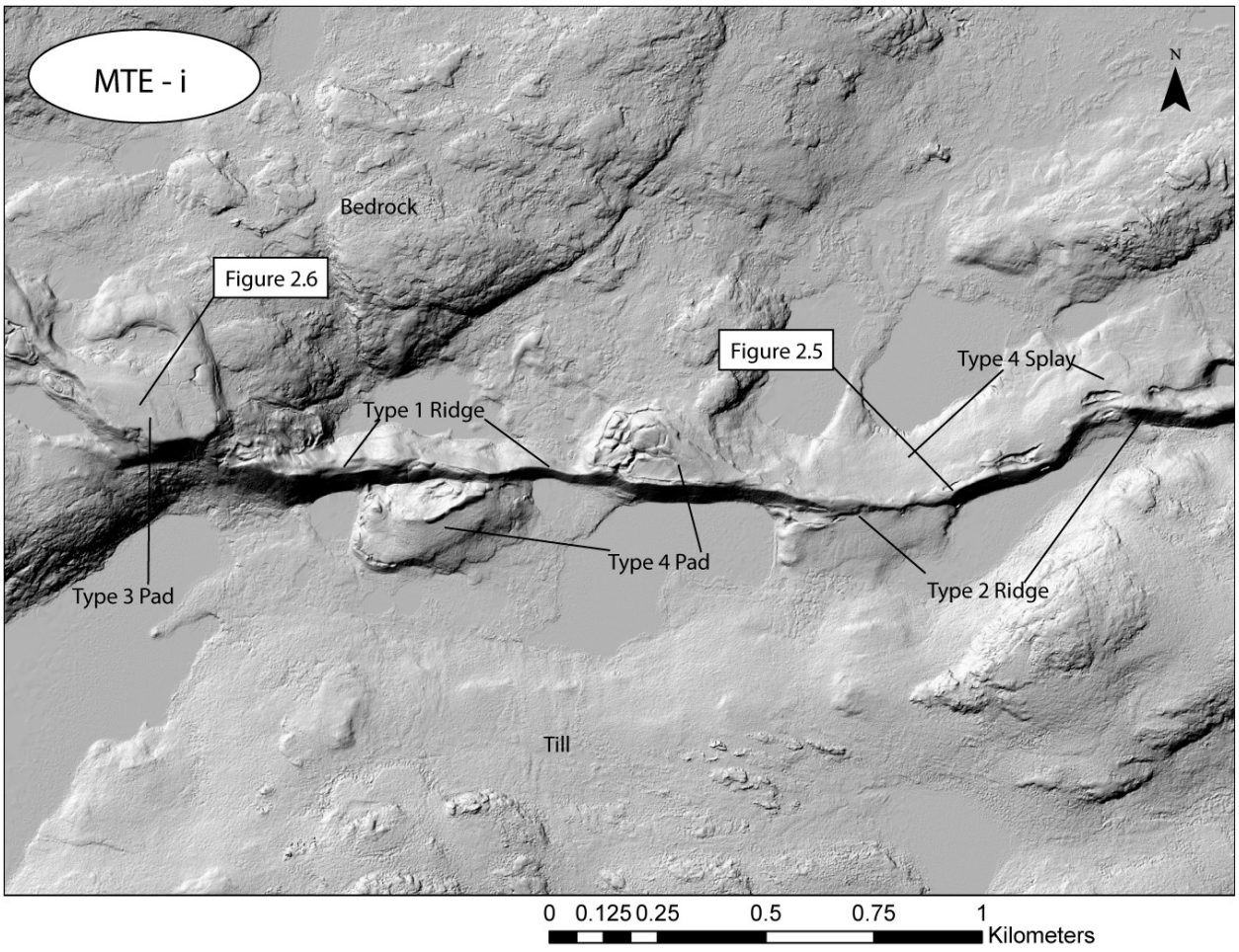

Figure A10: The esker has shifted from a north north-west trend in the south (figs 2.10 – 2.17), to a west-oriented direction in the MTE-i area. The eastern portion of esker is present as a Type 2 ridge flanked by a fine sandy Type 4 splay with rare angular boulders on the surface. In the center of the figure, a Type 4 pad, showing evidence of post glacial deformation by ice wedging and melt out, is present at the terminal end of the flanking sediment. A large, very irregular type 1 ridge dominates to the west, flanked to the south by another Type 4 pad. This Type 1 ridge ends and abruptly transitions into large Type 3 pad. The type 3 pad is located overlying a steep increase in bedrock elevation.

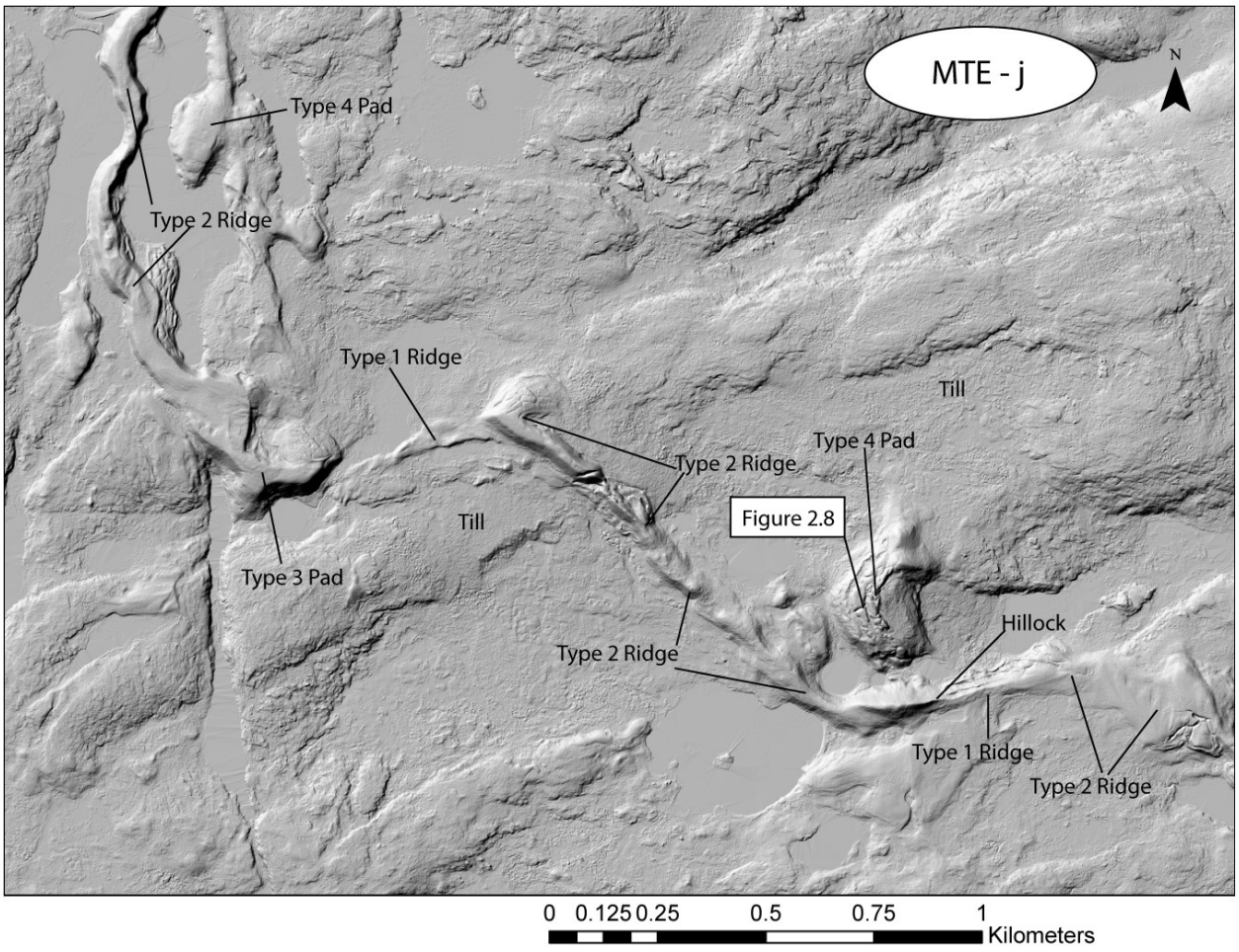

Figure A11: The esker in the MTE-j area has a step-like pattern in plan view perhaps suggesting an external control of channel development. Parallel-stepping segments could indicate meltwater paths confined to fractures. Of potential additional significance is the Type 2 ridge in the central portion of the figure that terminates in a fan like fashion. This sediment body appears to terminate in a direction oblique to the regional paleoflow of the esker, giving strong evidence to segmented deposition.

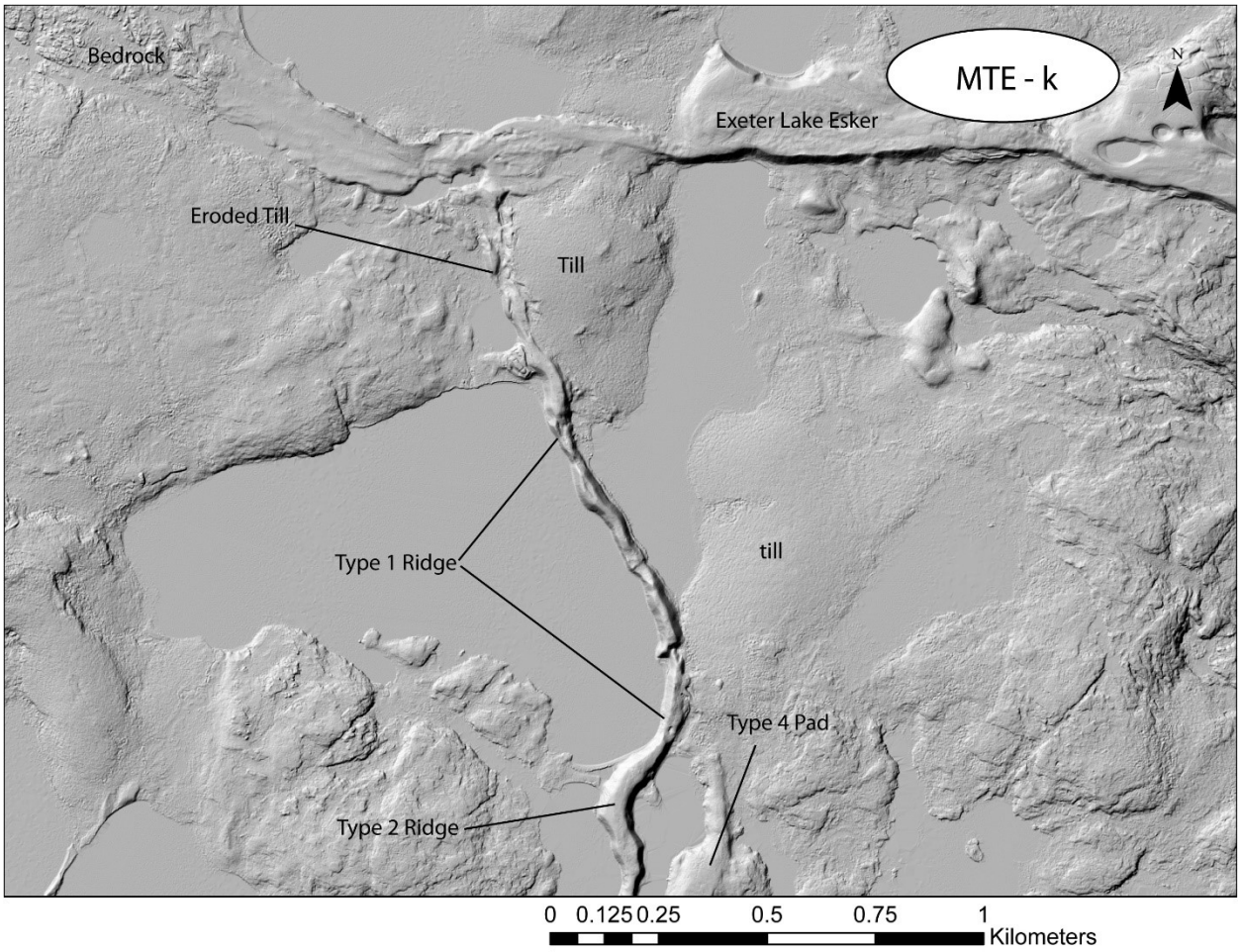

Figure A12: The esker in MTE-K area resumes its northward trajectory until in intersects and terminates at the main Exeter Lake trunk esker. In the southern portion of the figure, the broad crested, gently undulating, cobbly Type 2 ridge transitions to a narrower, highly undulating, cobbly Type 1 Ridge. This Type 1 ridge continues until it meets the larger Exeter Lake Esker. Near the terminus, a till hummock appears to have been cut by the esker, and eroded cut banks are present. In this area, the till is higher than the esker, and the esker appears to have been deposited in a narrow, eroded corridor.

Exeter Lake Esker

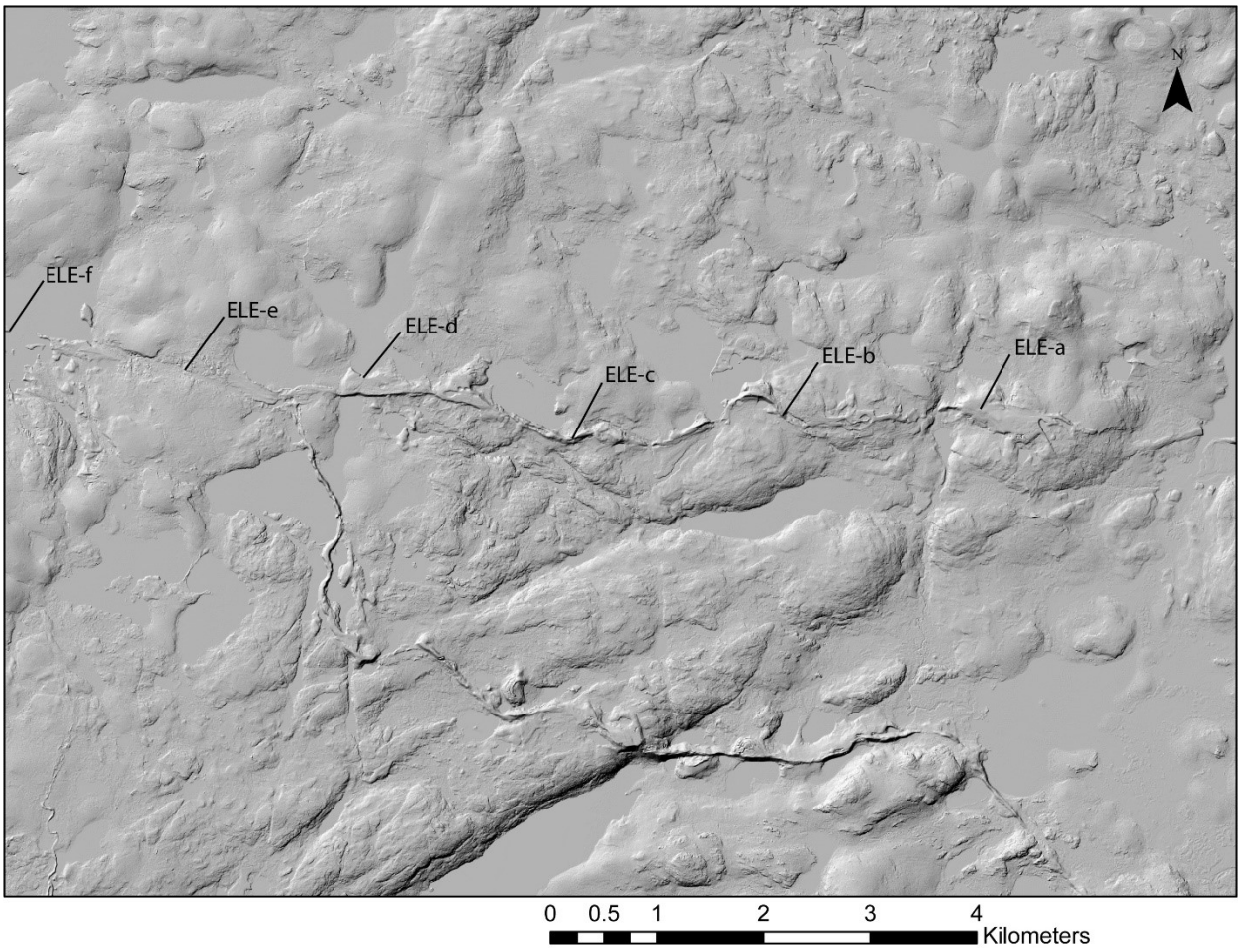

Figure A13: Exeter Lake Esker (ELE) overview, Figures A14-A19 depict locations ELE-a to ELE-f, with lines indicating down-esker extent of respective images.

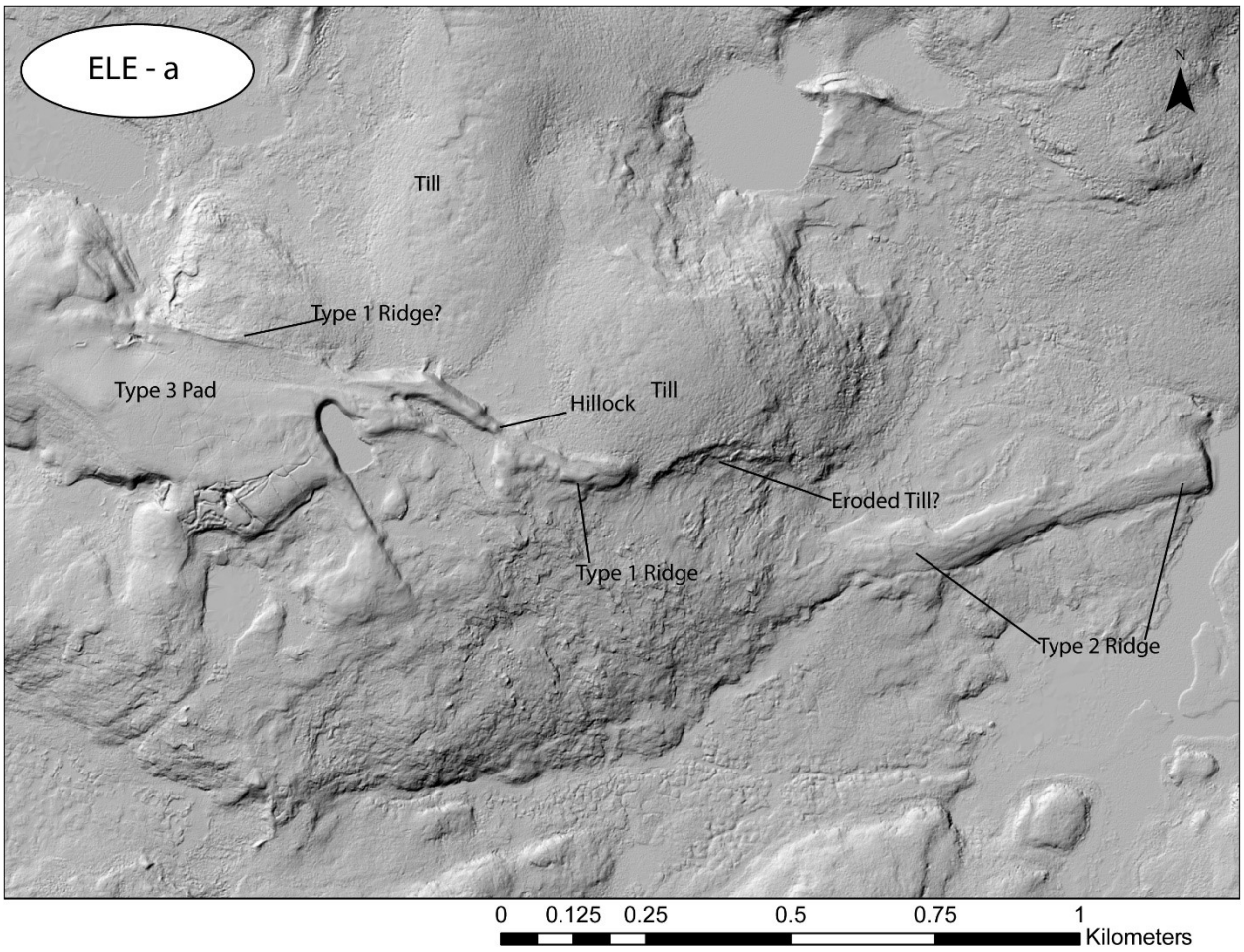

Figure A14: The ELE-a area marks the start of the studied extent of the Exeter Lake Esker. It begins as a low, flat Type 2 component that terminates at the onset of a steep hill. This break in esker is characterized by what appears to be relatively thin till overlying some poorly exposed bedrock. At the top of this hill, the esker resumes, first as a bouldery, low Type 1 ridge, then rapidly transitioning into at very wide (>200m) flat topped Type 3 pad. The northern flank of the broad esker is slightly more prominent, and composed of rounded cobbles and boulders, indicating a Type 1 ridge may be present, underlying the adjacent Type 2 material.

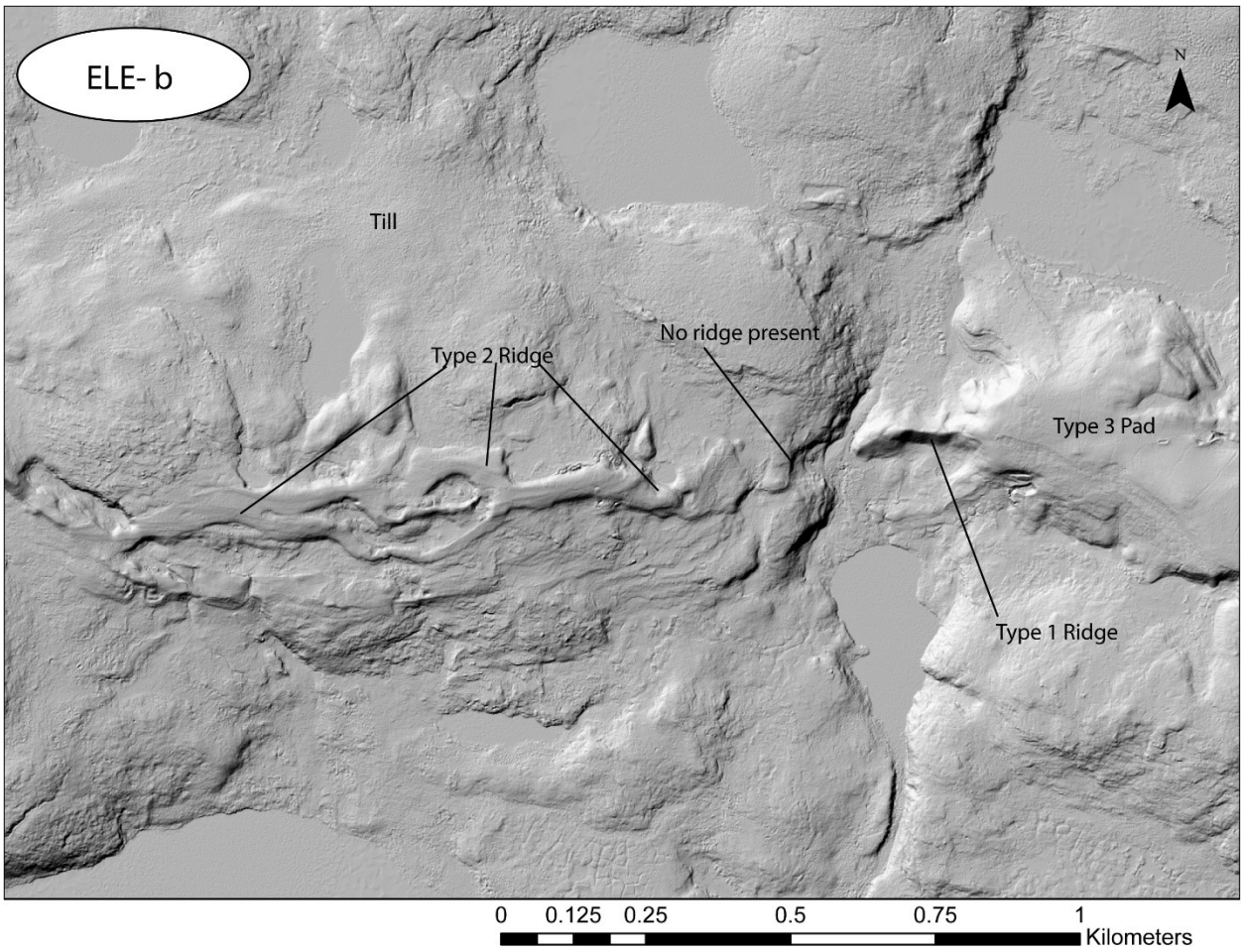

Figure A15: In the eastern portion of the ELE-b area, the broad Type 3 pad continues from ELE-a and transitions down slope to a cobbly Type 1 ridge. A stream cuts this ridge, revealing cobbles in a coarse sandy matrix. The esker reappears on the other side of the stream as a Type 2 ridge that has an anastomosing, sinuous appearance, interpreted to be the result of stagnant ice preventing deposition, and directing the meltwater channel.

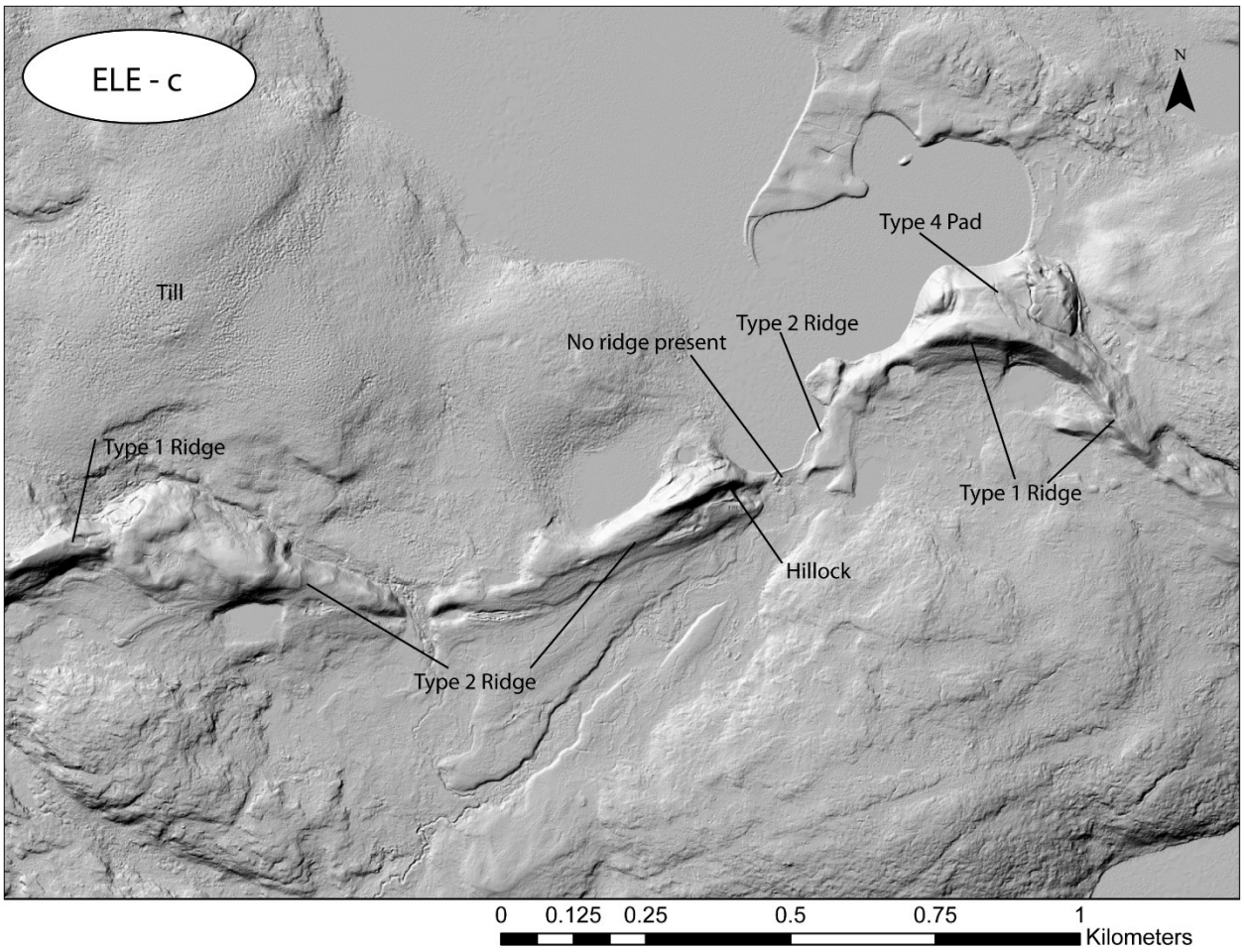

Figure A16: The eastern most portion of the esker in ELE-c is a type 1 ridge that emerges from the Type 2 ridge material at the western edge of the ELE-b area (Figure 2.23). The ridge is flanked by a lower, ice wedged, Type 4 pad, and transitions downhill into a broad, sandy, Type 2 ridge. This ridge is cut by a stream, and re-emerges as a cobbly hillock that rapidly transitions into a Type 2 ridge. This ridge continues, broken once a by a stream until, the western edge of the ELE-c area, where a short Type 1 ridge emerges from a widening of the previous Type 2 component.

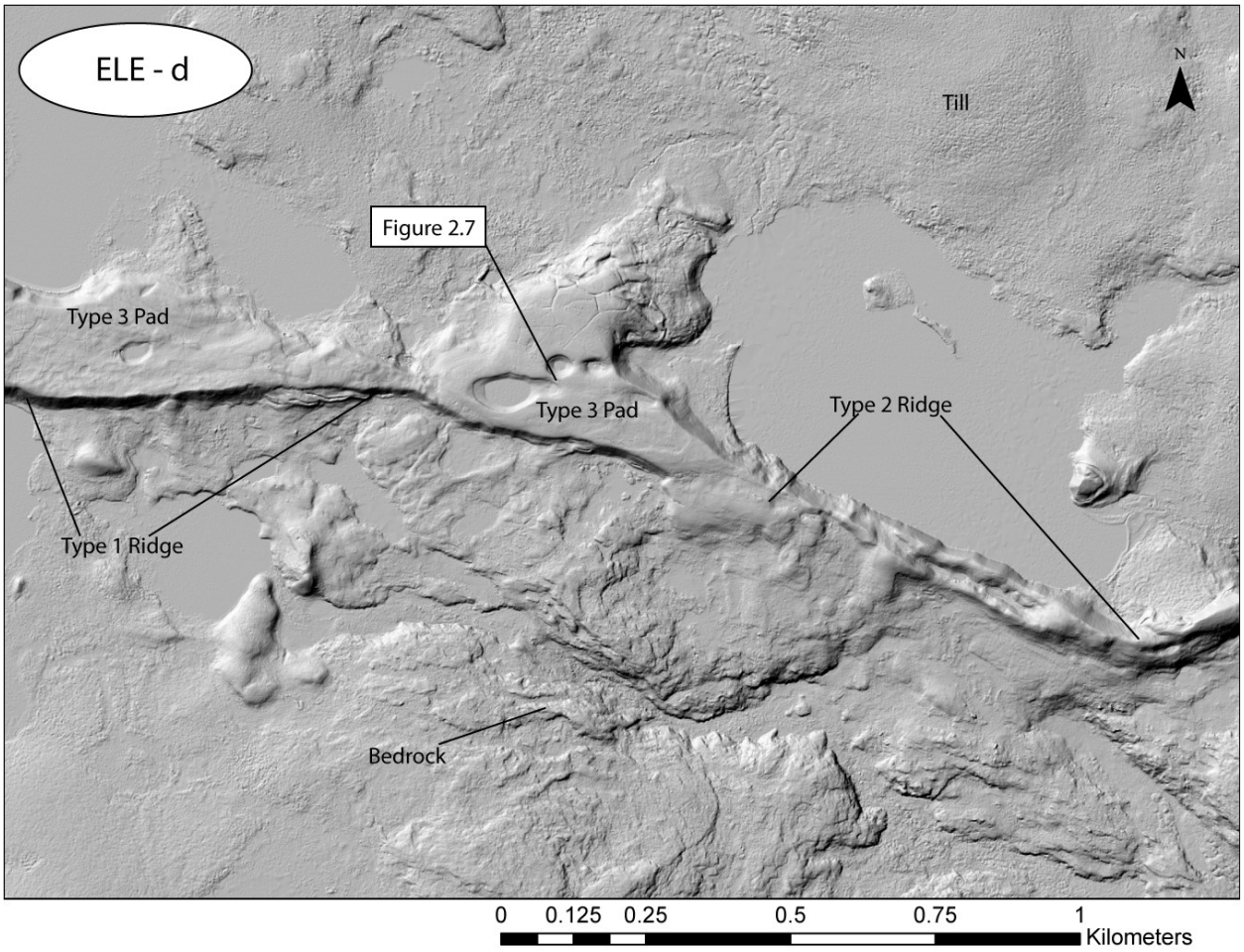

Figure A17: The eastern portion of the ELE-d area is characterized by the presence of a broad crested Type 2 component with a bifurcation of the main ridge. This is similar in appearance to the branching portion of the esker in the ELE-b area (Figure A15), and is interpreted to represent the melt-out of stagnant ice within the meltwater corridor. In the central portion of the ELE-d area, the ridge widens to become a long and wide Type 3 Pad interpreted as such based on the presence of kettle holes on the surface of the landform. On the southern edge of the pad, there is a prominent bouldery Type 1 ridge present, similar in character to the northern flank of the wide, Type 2 ridge in the ELE-a area (Figure 2.22), suggesting that the Type 3 sediment in this figure has been deposited over or directly adjacent to a previously deposited Type 1 ridge.

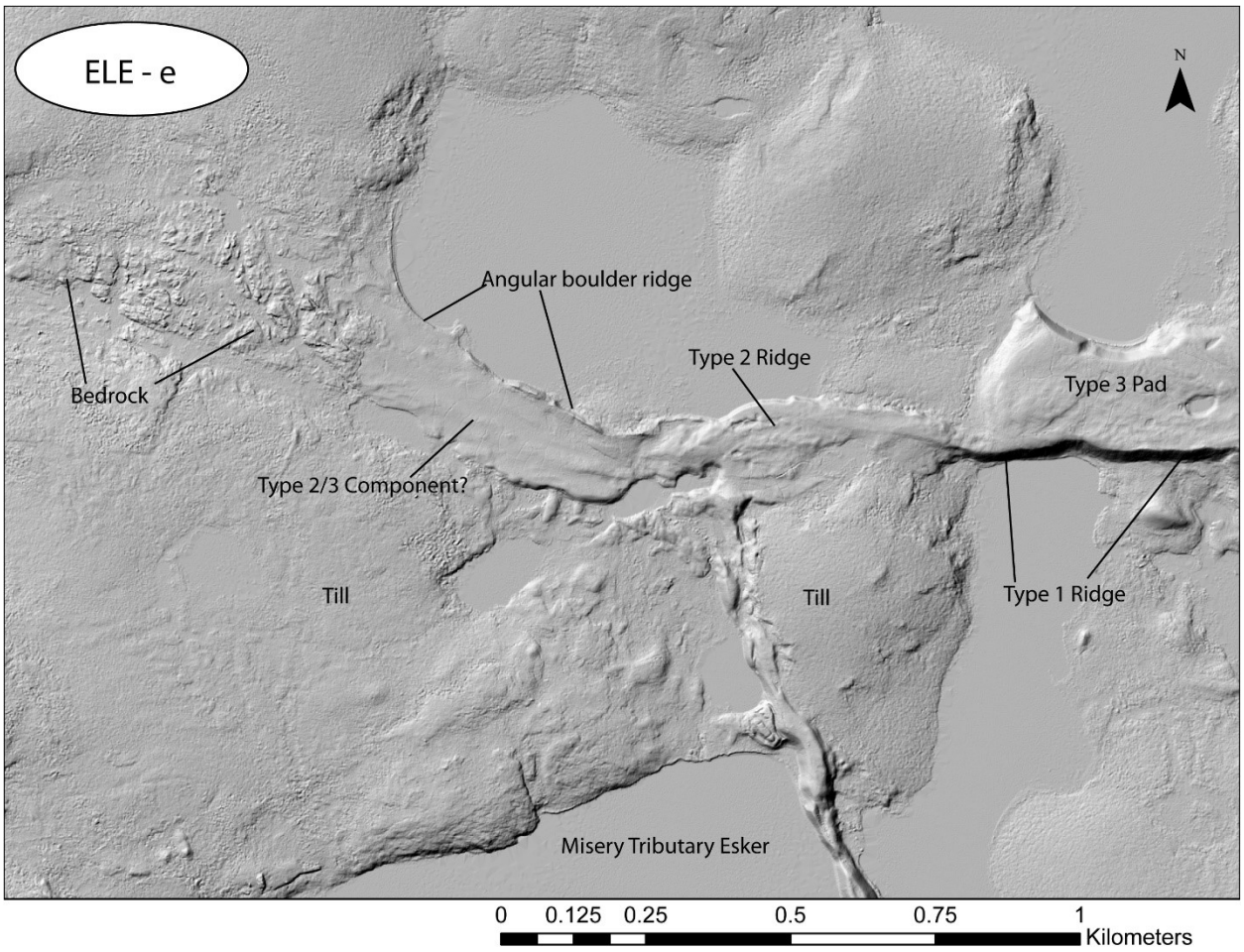

Figure A18: The ELE-e area marks a confluence of the Misery Tributary Esker and the Exeter Lake trunk esker. At the confluence, a coarse, cobbly, flat Type 2 Ridge is interpreted to have been planned by meltwater, perhaps owing to an increase in discharge from the two main esker corridors. To the west, there is no sediment present in the corridor, but rather scoured bedrock, also likely indicating prolonged exposure to meltwater discharge. On the northern margin of the coarse Type 2 Ridge, there is a prominent ridge of large (> 1m) angular boulders that may indicate development of a small moraine developed along the margin of a confining ice block.

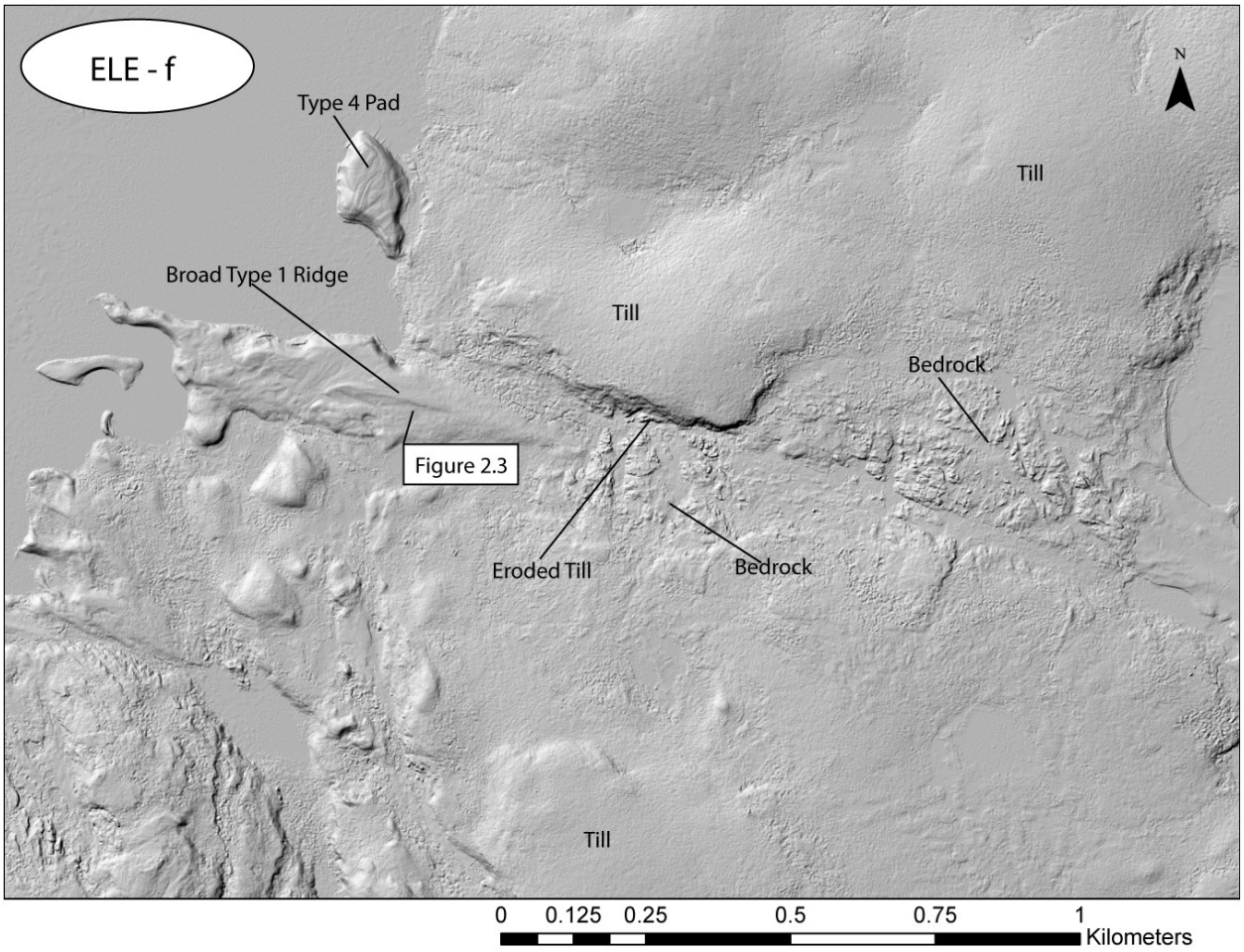

Figure A19: The ELE-f area shows a continuation of the bedrock scour seen in Figure A18, and marks the end of the study area. In the central portion of the figure, the meltwater channel has eroded into a large till hummock, as indicated by the steep, almost vertical, cutbank (see figure 2.9 for photograph) on the southern edge of the hummock. To the west of this, esker material is again present as a broad, low, bouldery Type 1 ridge that gradually fines to cobble sized material at the western most point, where the landform terminates at the lake. This ridge is very similar in character to the low and broad Type 1 ridge in the MTE-i area (Figure A10). This could be interpreted as the very beginnings of esker-ridge deposition or a reworking of a previously deposited, more peaked, Type 1 ridge by the high-energy meltwater responsible for upstream bedrock scour.

Appendix B: Misery Tributary Esker grain-size maps

Appendix B shows detailed surficial grain-size maps of the Misery Tributary Esker starting at the up-esker extent of the MTE-a area (Appendix A, Figure A2) and finishing at the down-esker extent of the MTE-k area (fig. 2.12). Maps are presented at a 1:4000 scale, with data obtained from field notes, on-the-ground photography, and high-resolution orthoimagery. Red dots indicate on-the-ground photograph locations. Dots significantly off esker or over bodies of water indicate photographs taken from a helicopter. Georeferenced photographs are presented as accompanying material included as a DVD with this thesis.

Misery Tributary Esker

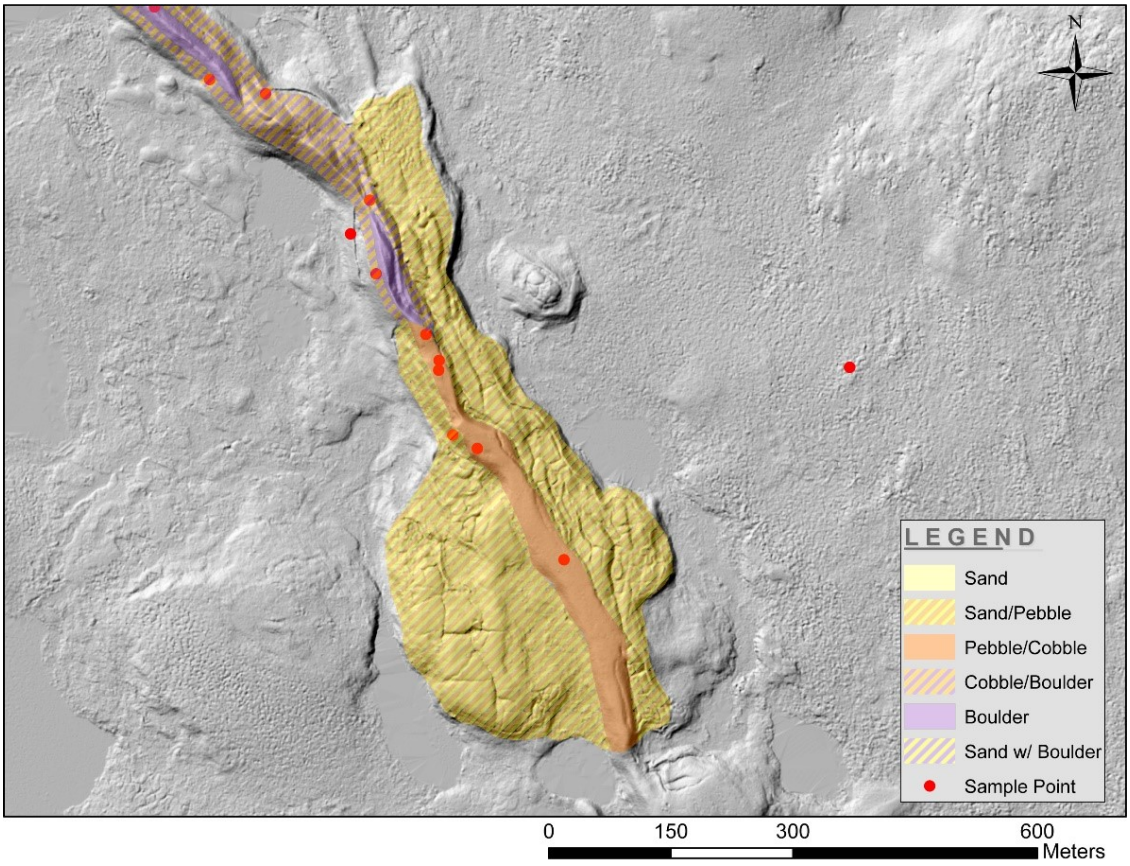

Figure B1: Surficial grain-size map of southernmost (up esker) studied extent of the Misery Tributary Esker.

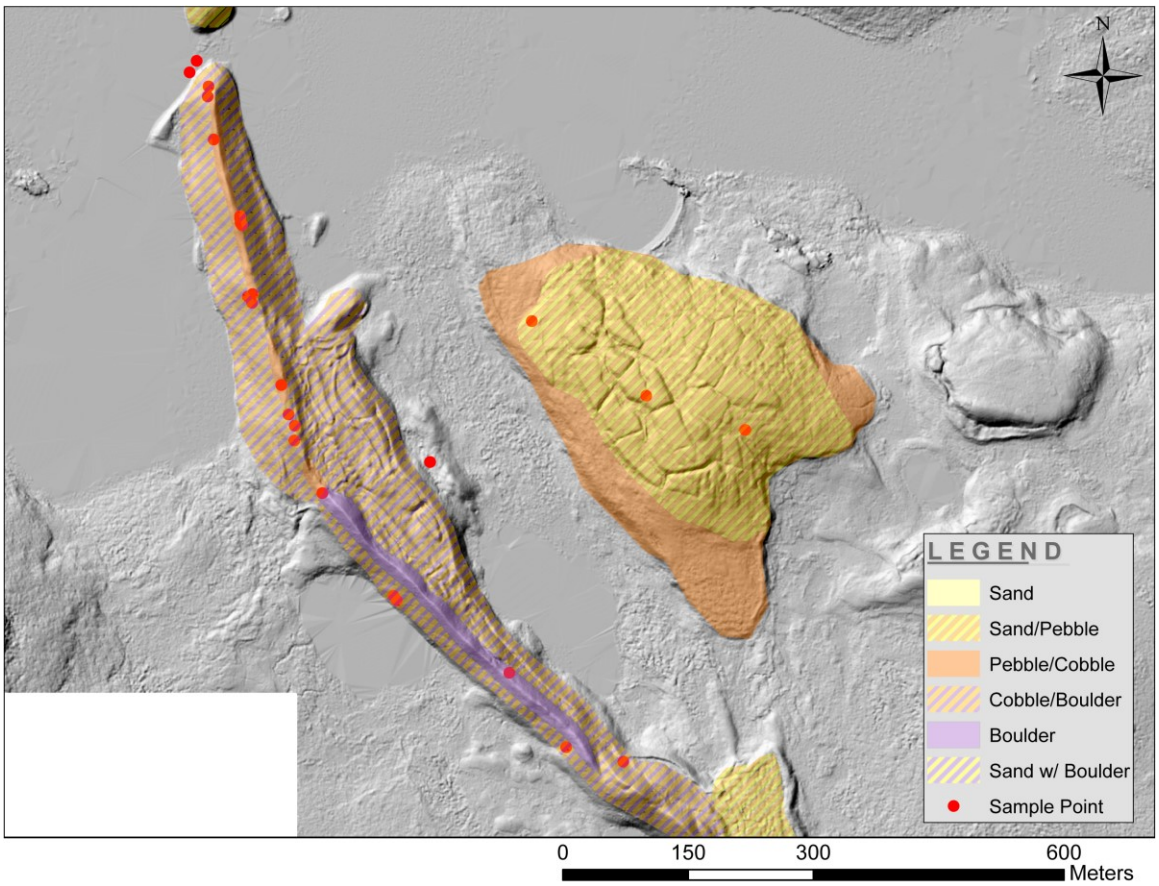

Figure B2: Grain-size map of Misery Tributary Esker, down-esker continuation of figure B1

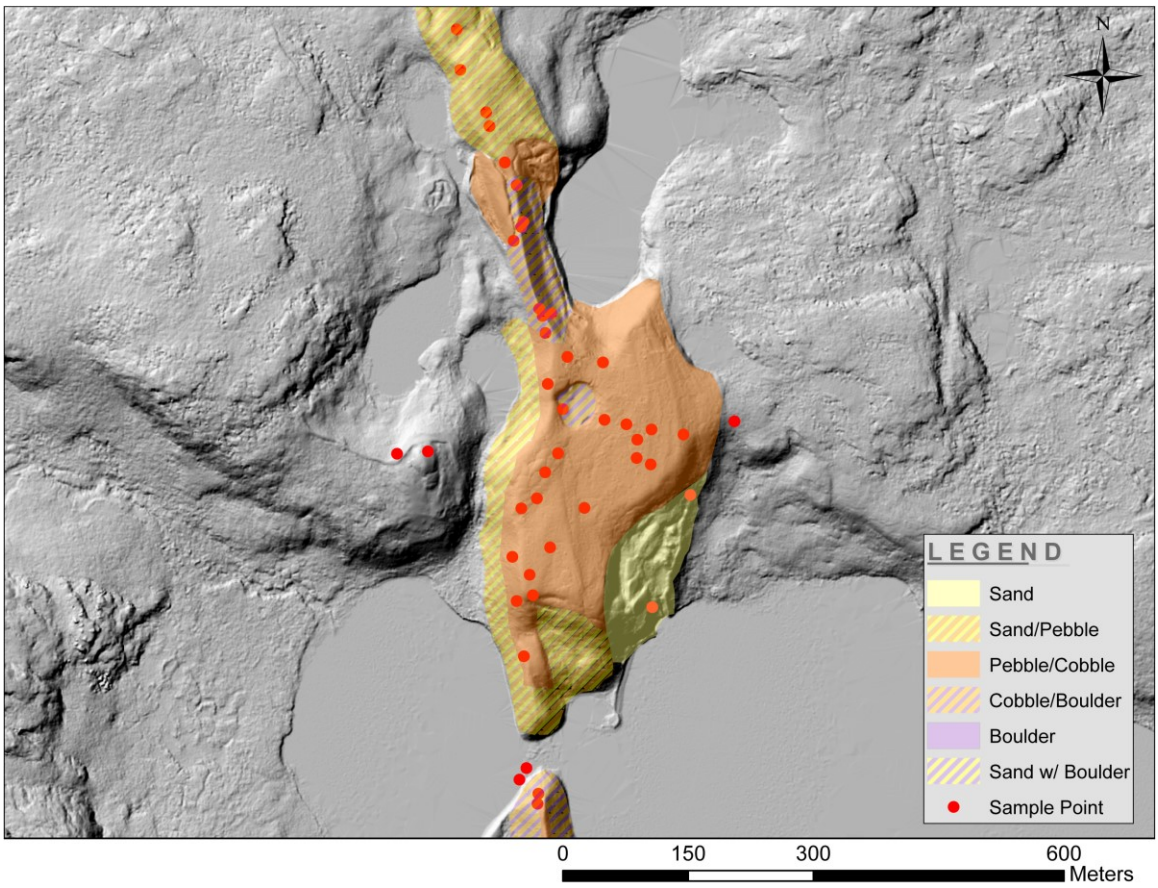

Figure B3: Grain-size map of Misery Tributary Esker, down-esker continuation of figure B2

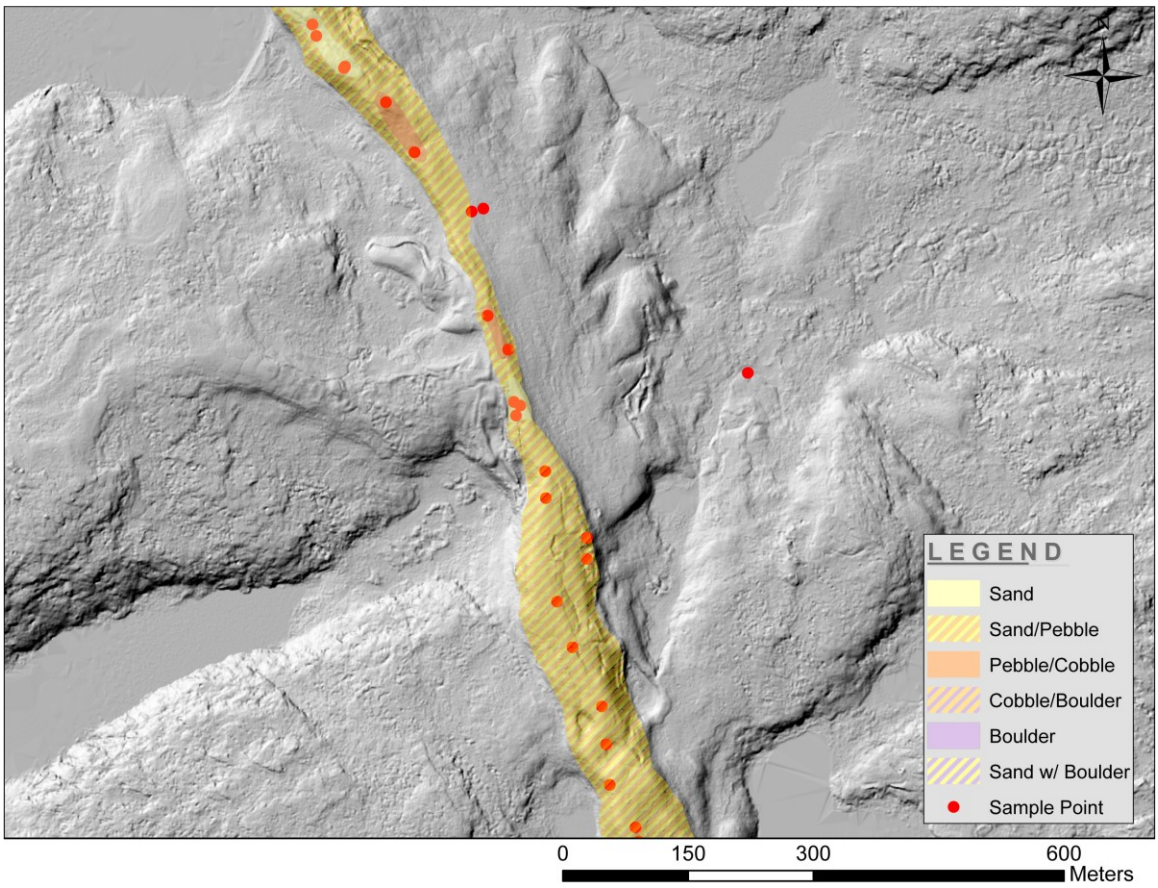

Figure B4: Grain-size map of Misery Tributary Esker, down-esker continuation of figure B3

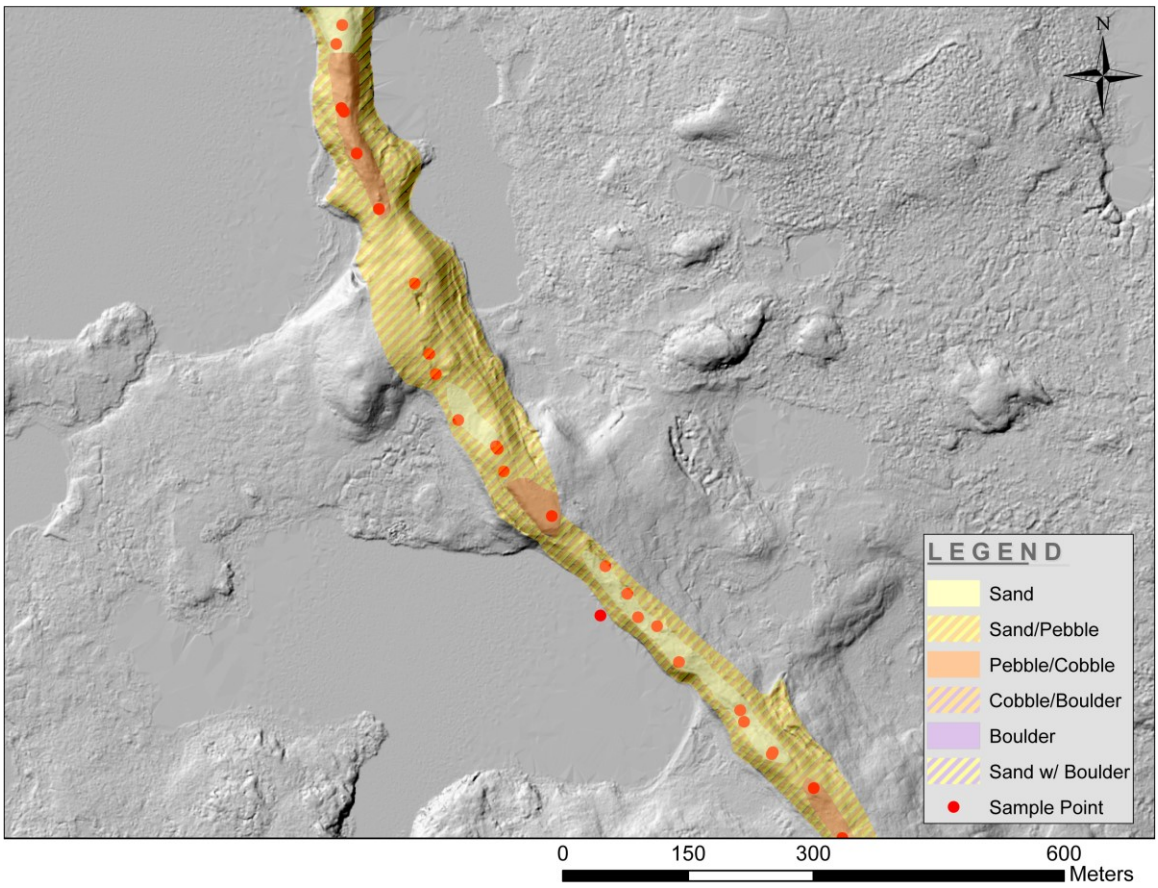

Figure B5: Grain-size map of Misery Tributary Esker, down-esker continuation of figure B4

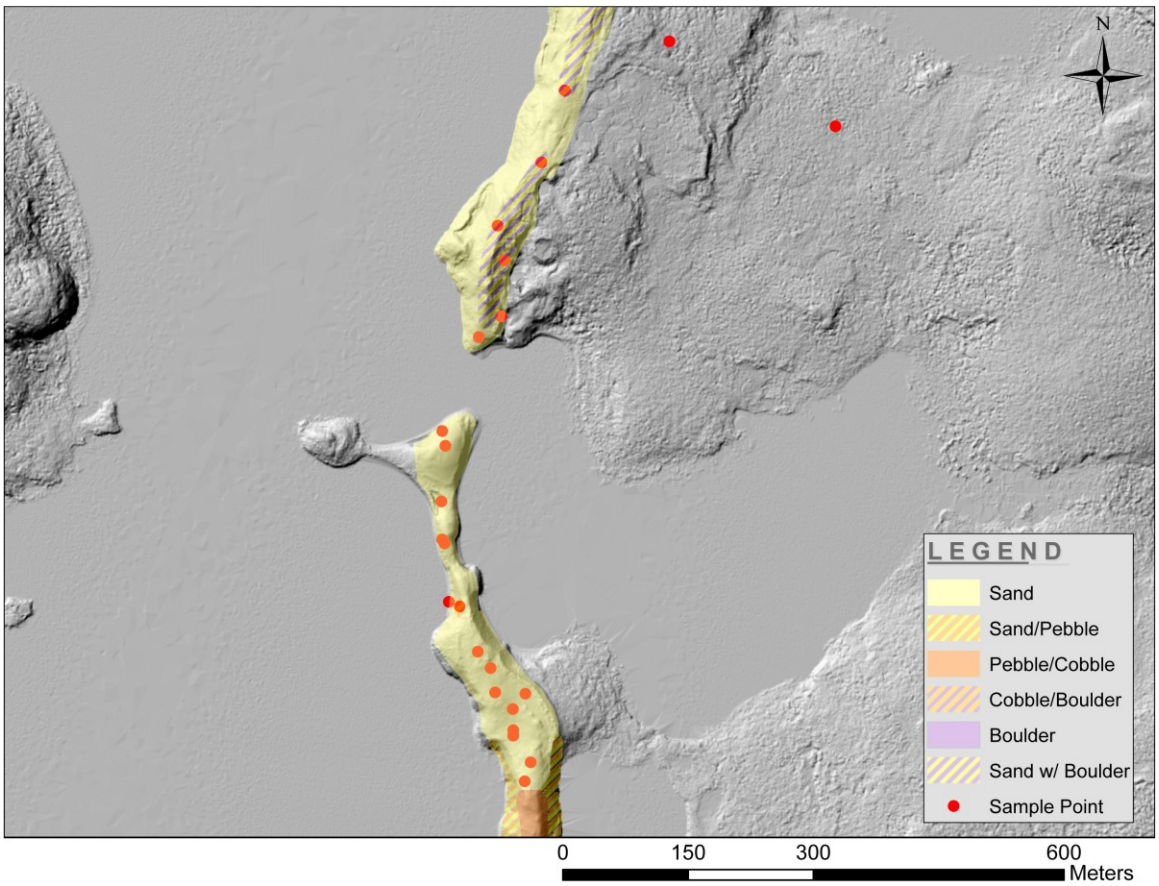

Figure B6: Grain-size map of Misery Tributary Esker, down-esker continuation of figure B5

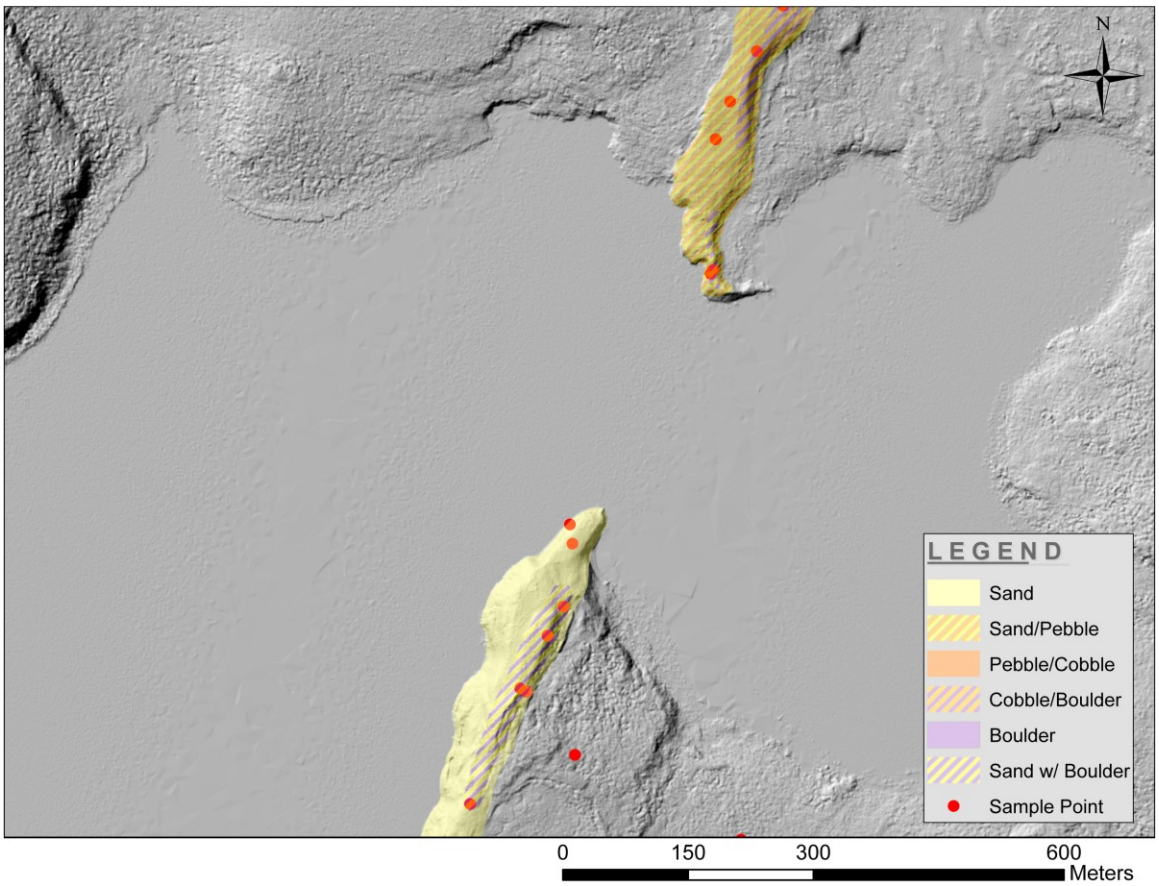

Figure B7: Grain-size map of Misery Tributary Esker, down-esker continuation of figure B6

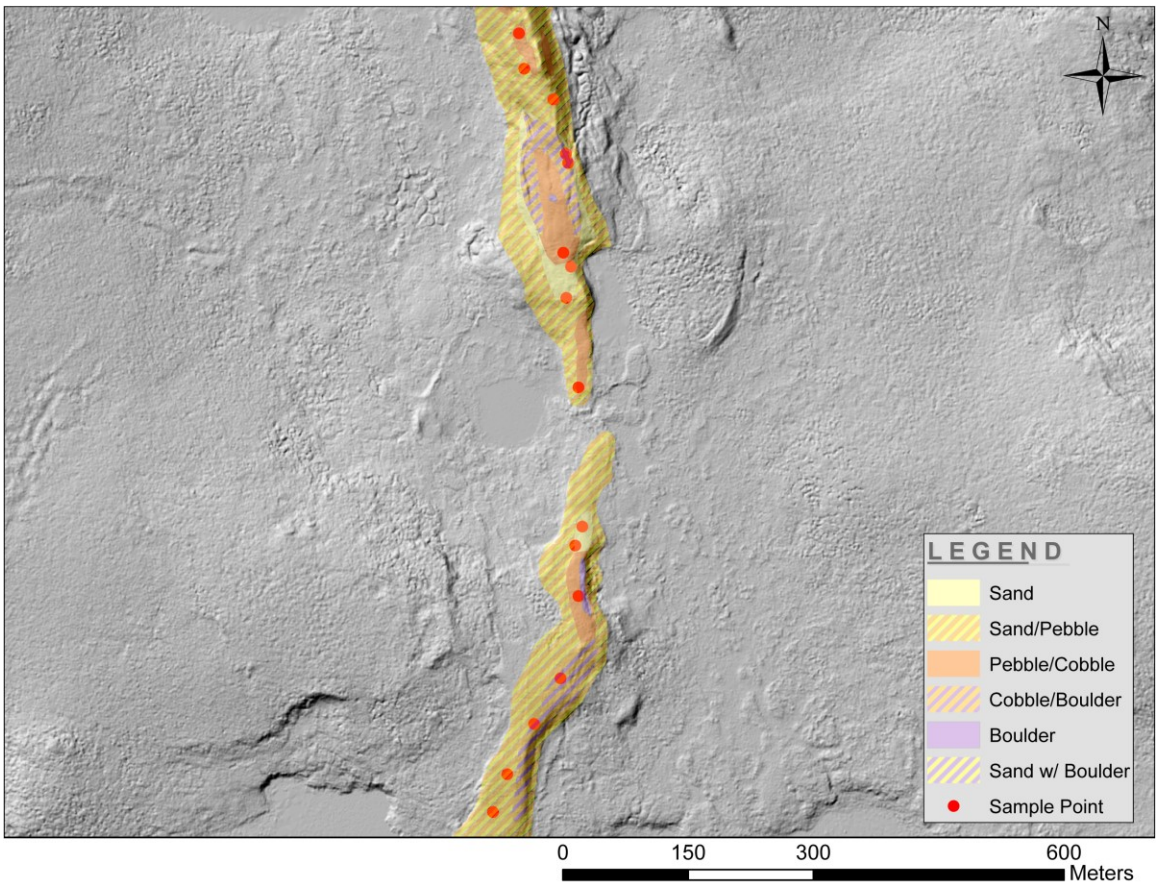

Figure B8: Grain-size map of Misery Tributary Esker, down-esker continuation of figure B7

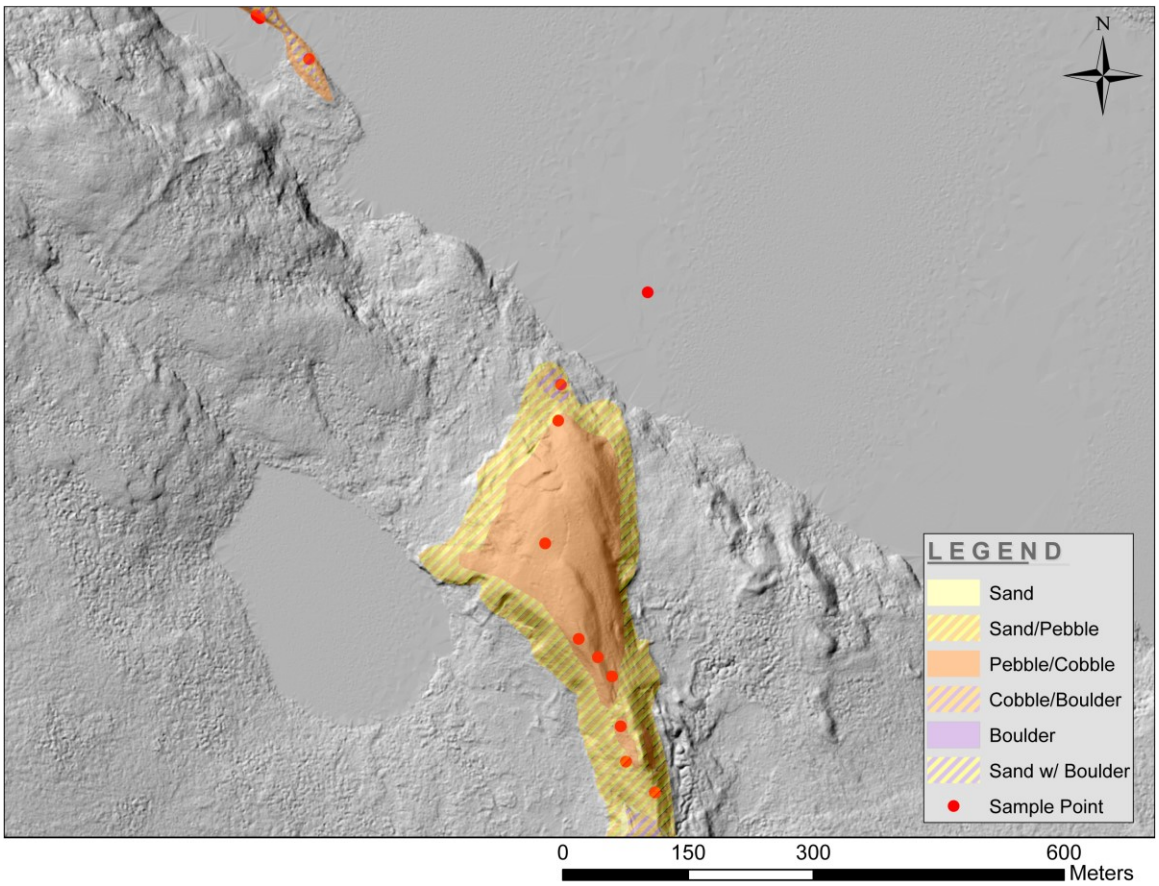

Figure B9: Grain-size map of Misery Tributary Esker, down-esker continuation of figure B8

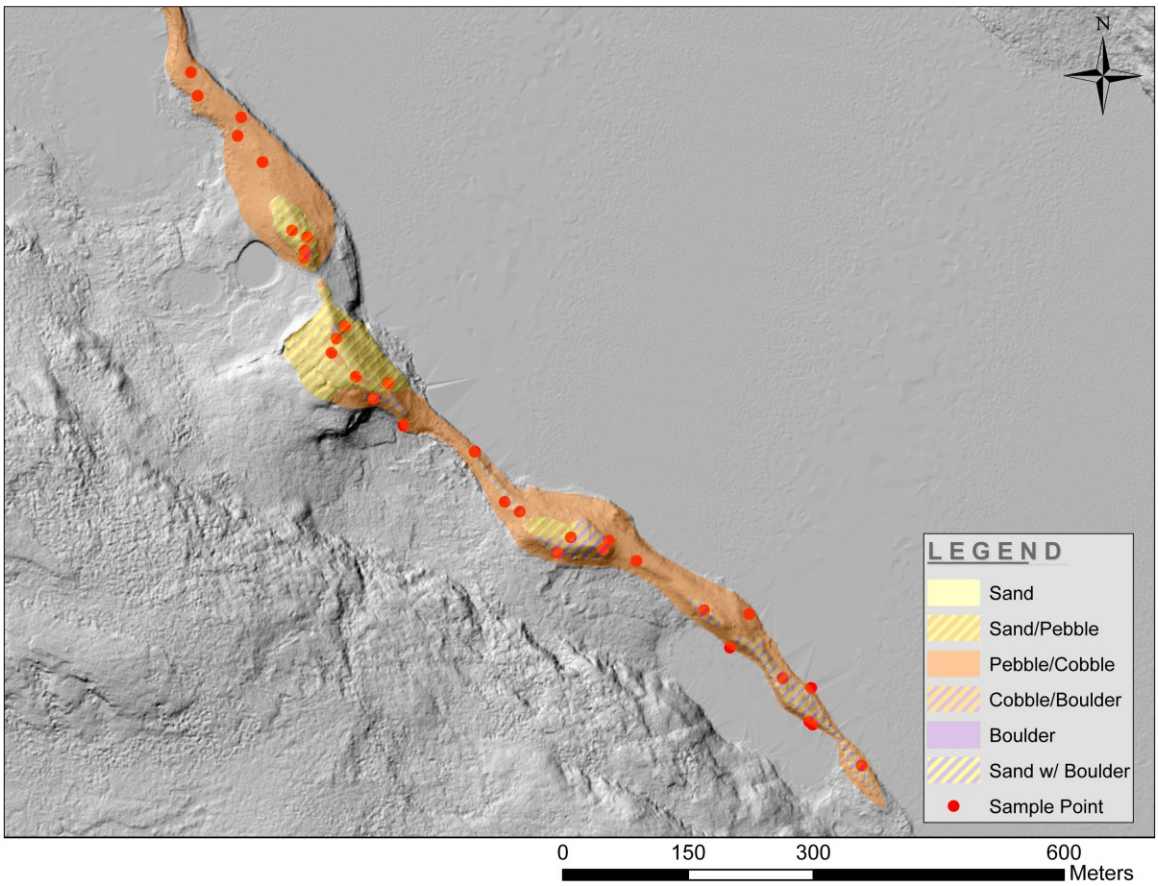

Figure B10: Grain-size map of Misery Tributary Esker, down-esker continuation of figure B9

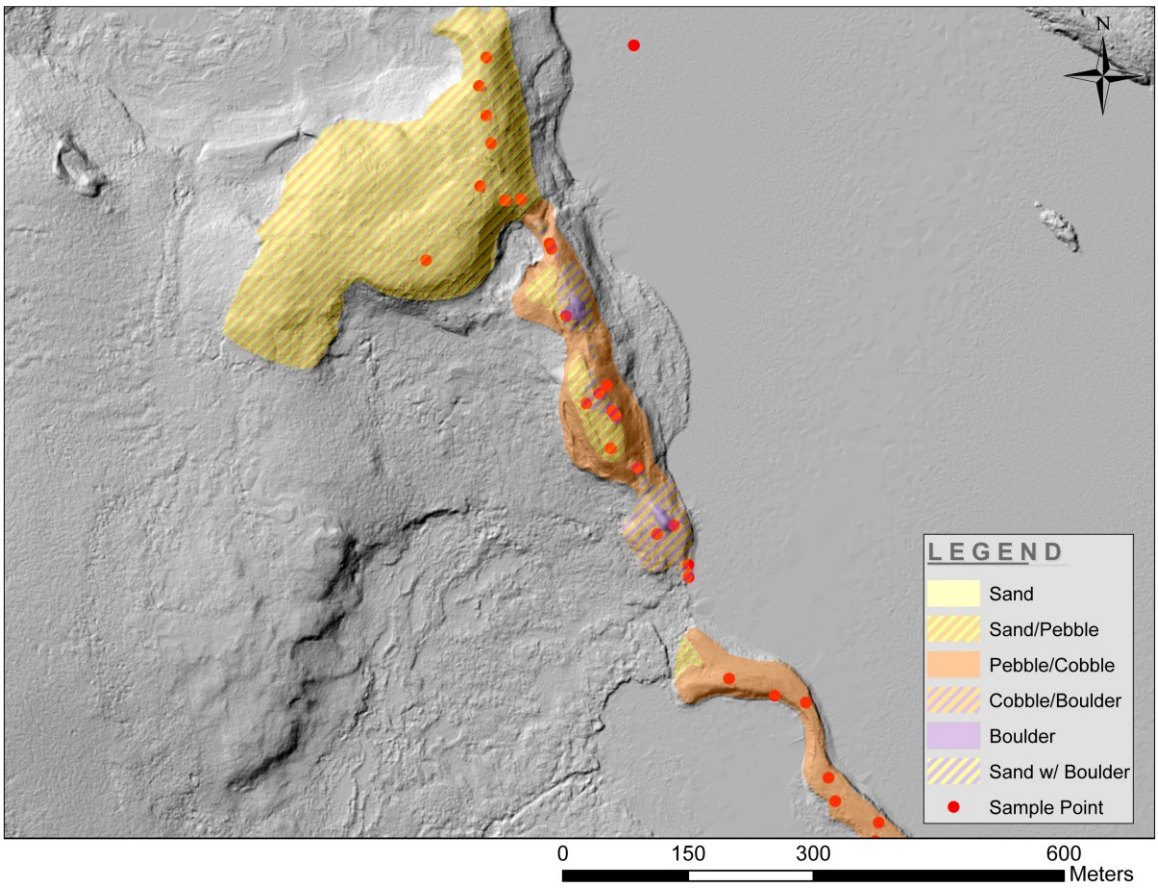

Figure B11: Grain-size map of Misery Tributary Esker, down-esker continuation of figure B10

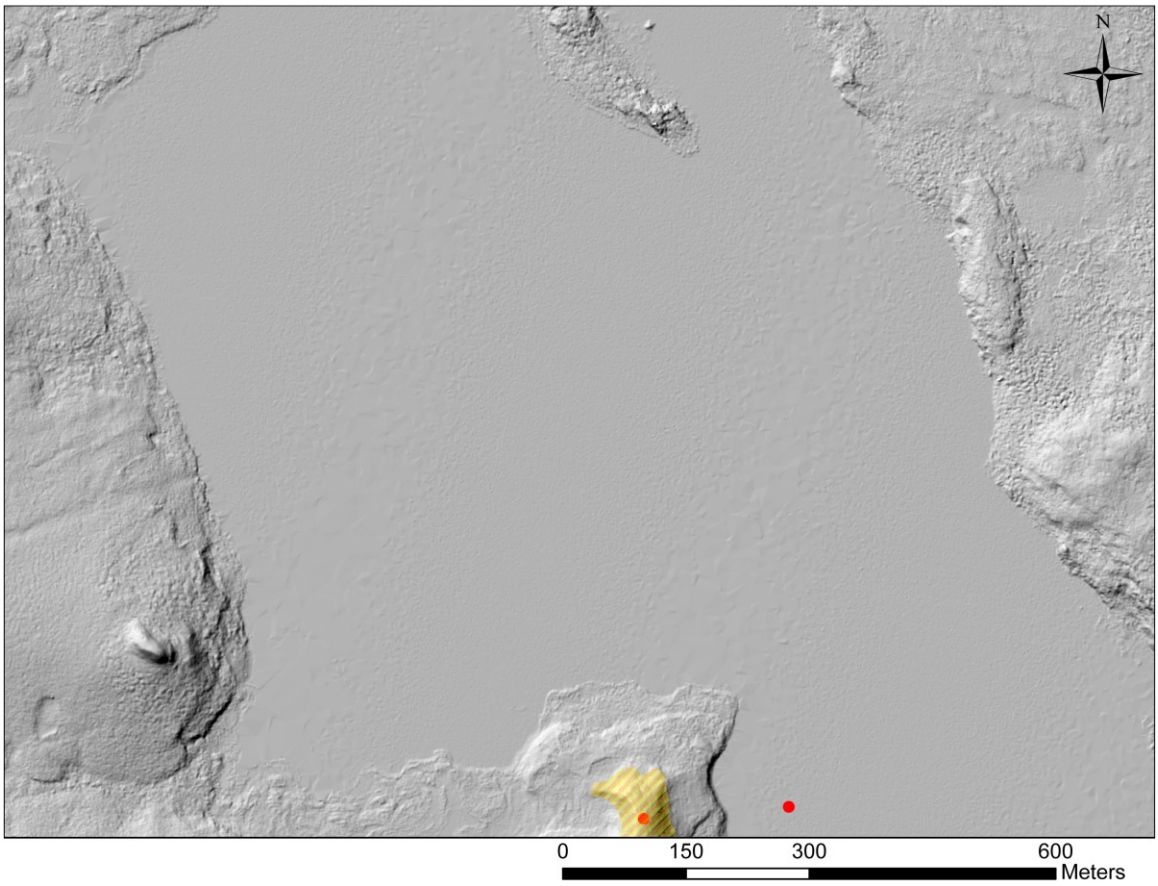

Figure B12: Grain-size map of Misery Tributary Esker, down-esker continuation of figure B11

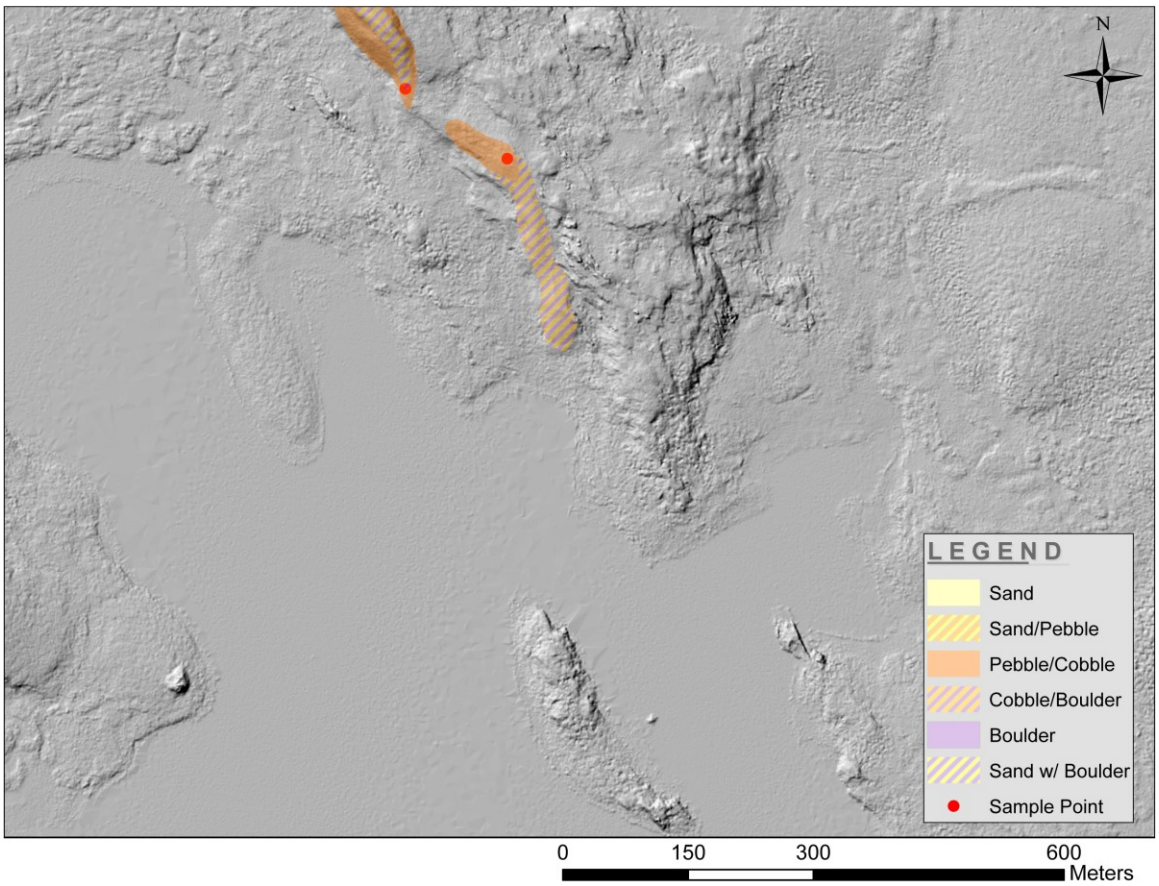

Figure B13: Grain-size map of Misery Tributary Esker, down-esker continuation of figure B12

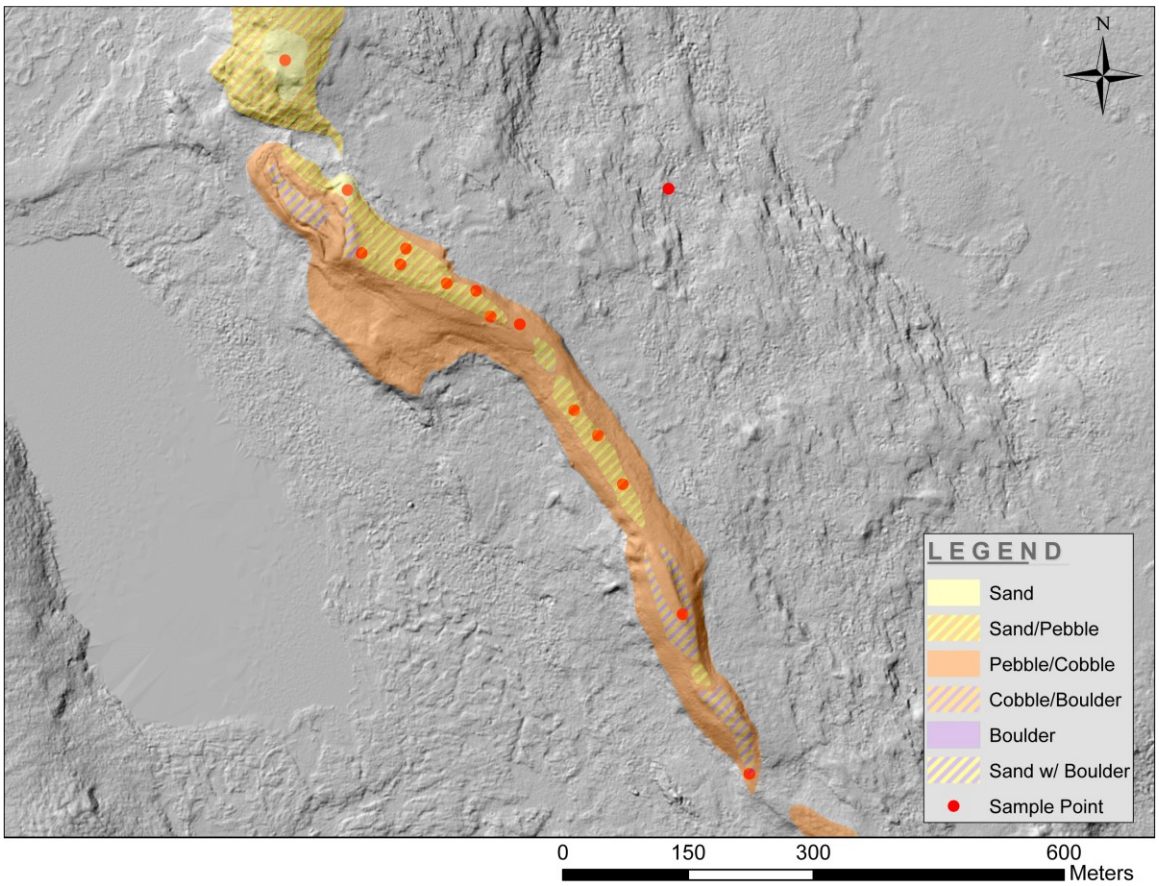

Figure B14: Grain-size map of Misery Tributary Esker, down-esker continuation of figure B13

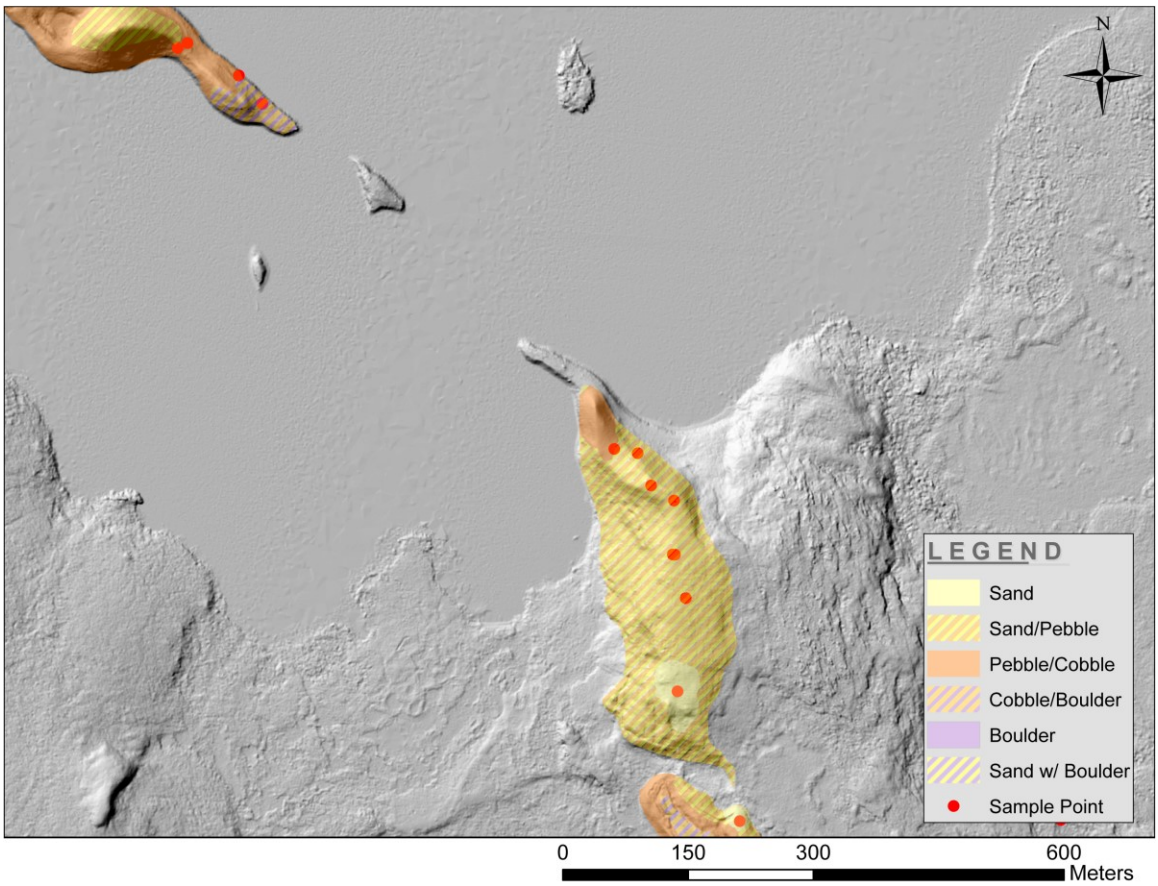

Figure B15: Grain-size map of Misery Tributary Esker, down-esker continuation of figure B14

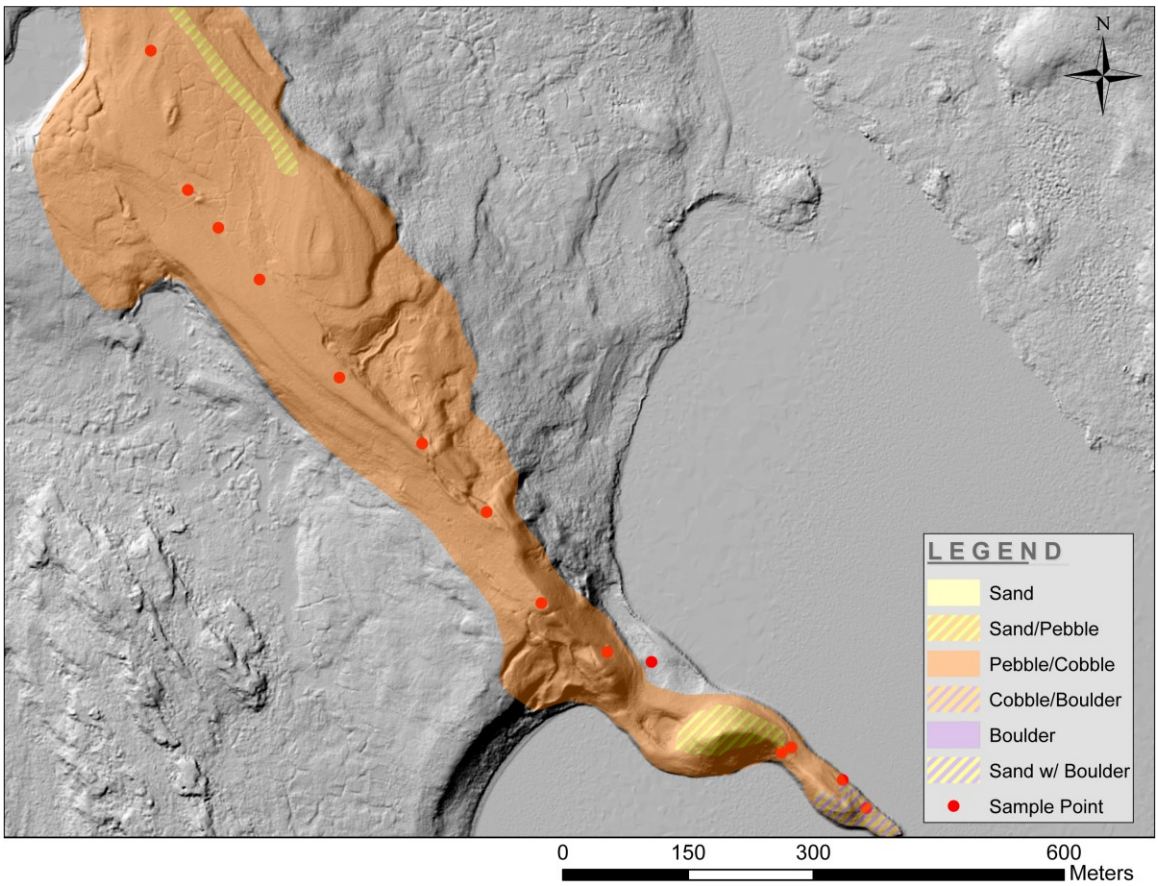

Figure B16: Grain-size map of Misery Tributary Esker, down-esker continuation of figure B15

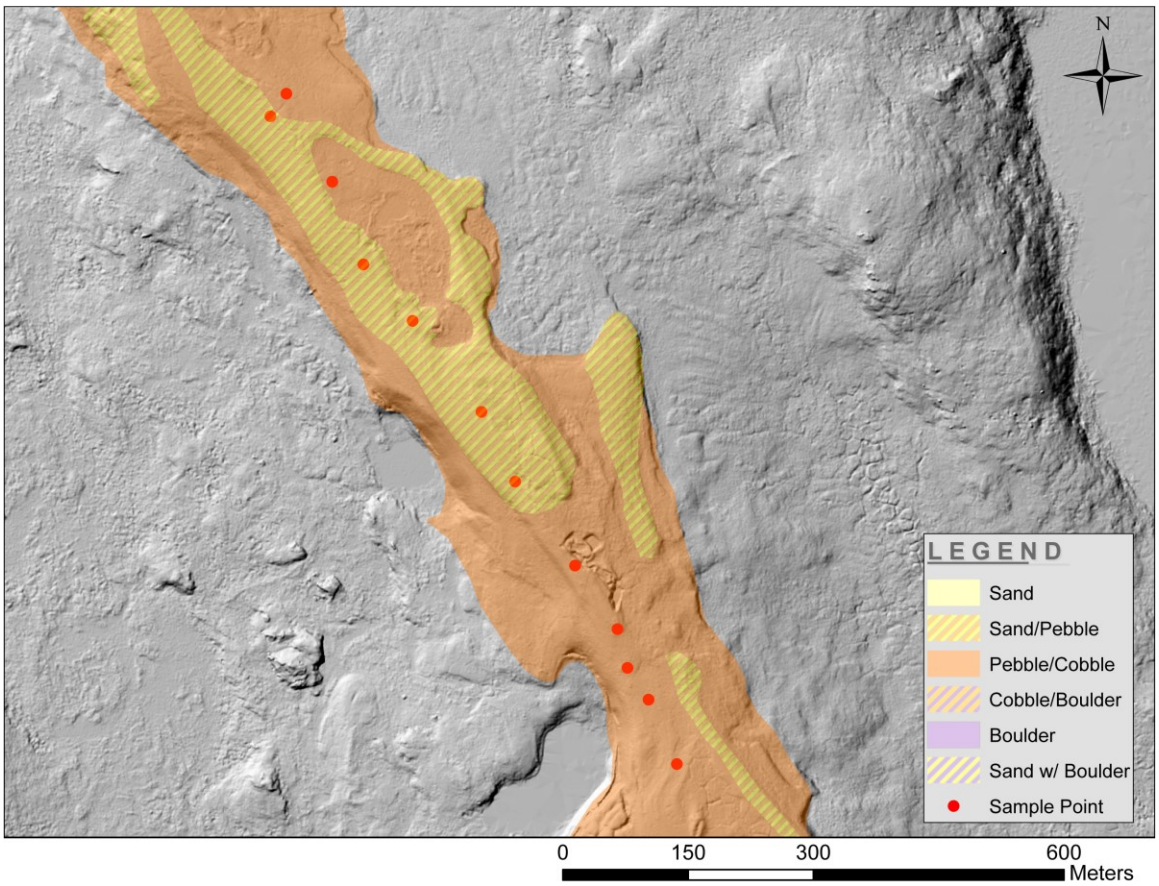

Figure B17: Grain-size map of Misery Tributary Esker, down-esker continuation of figure B16

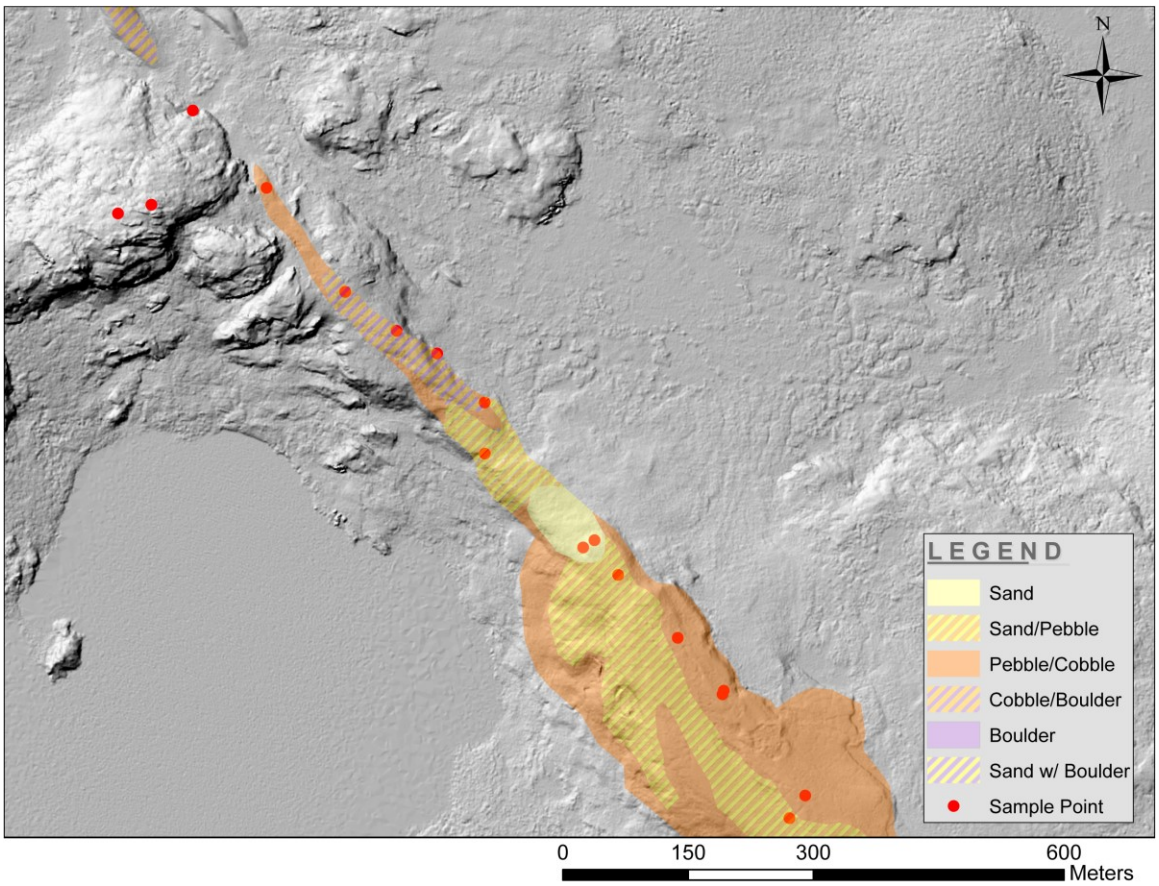

Figure B18: Grain-size map of Misery Tributary Esker, down-esker continuation of figure B17

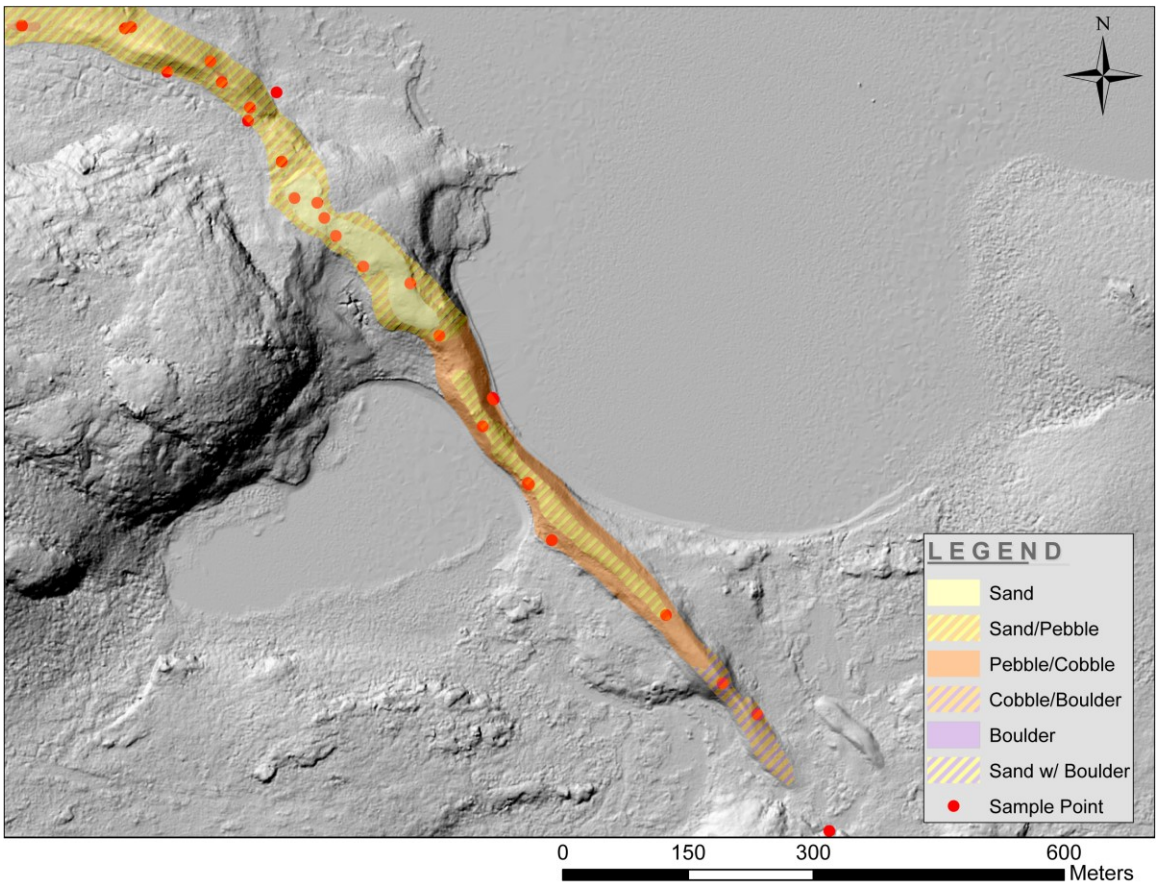

Figure B19: Grain-size map of Misery Tributary Esker, down-esker continuation of figure B18

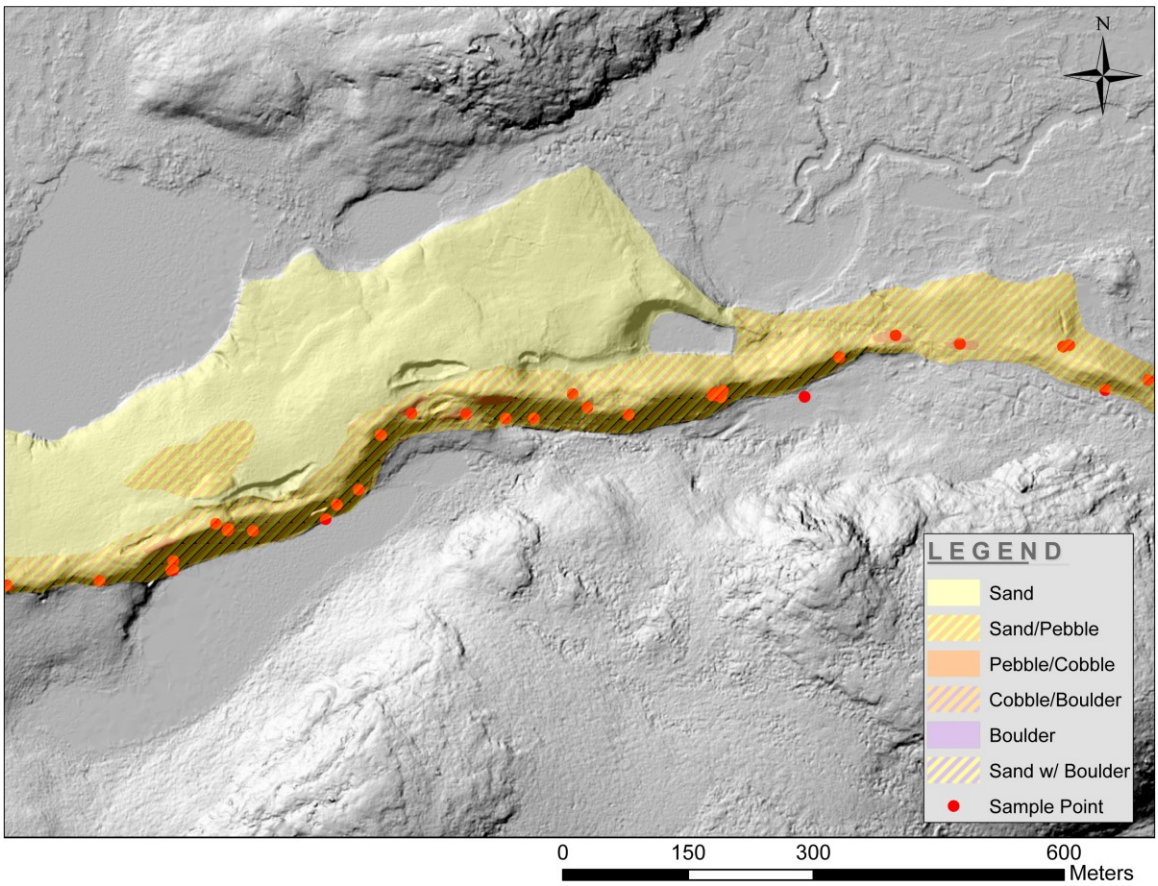

Figure B20: Grain-size map of Misery Tributary Esker, down-esker continuation of figure B19

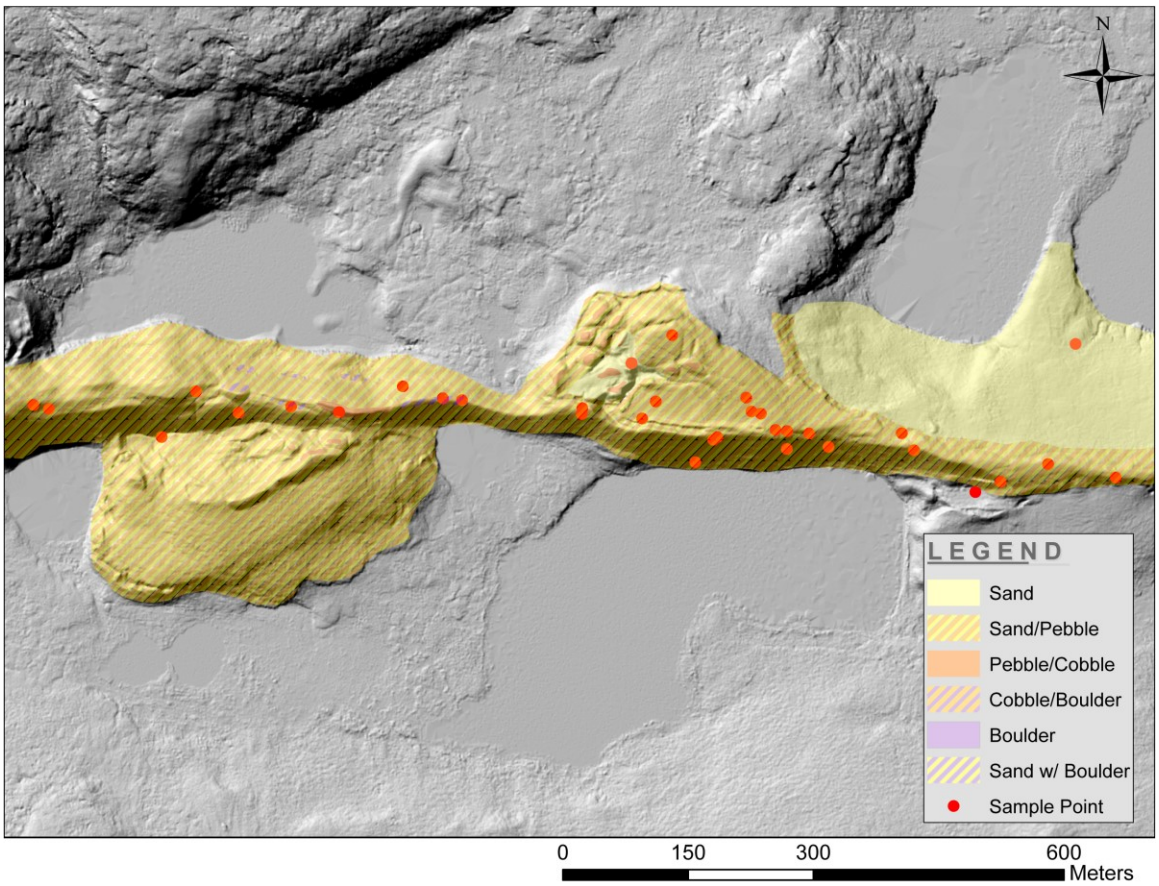

Figure B21: Grain-size map of Misery Tributary Esker, down-esker continuation of figure B20

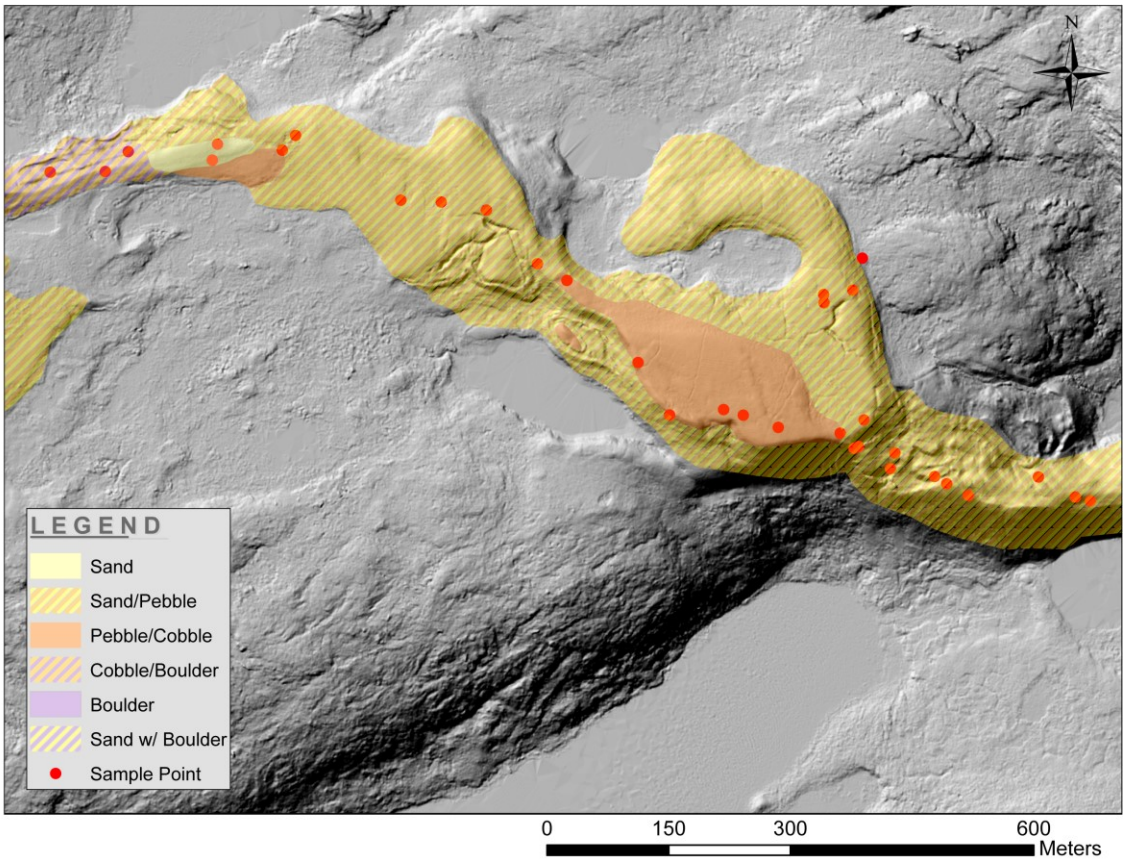

Figure B22: Grain-size map of Misery Tributary Esker, down-esker continuation of figure B21

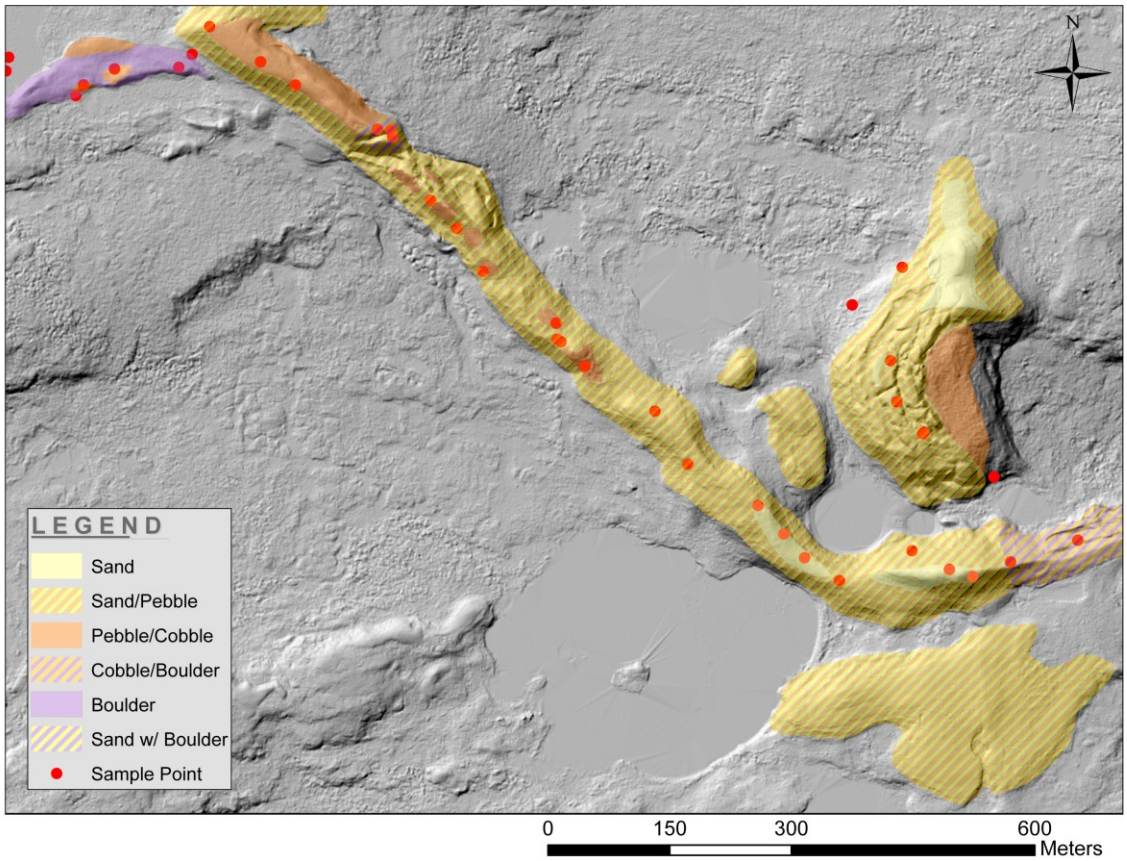

Figure B23: Grain-size map of Misery Tributary Esker, down-esker continuation of figure B22

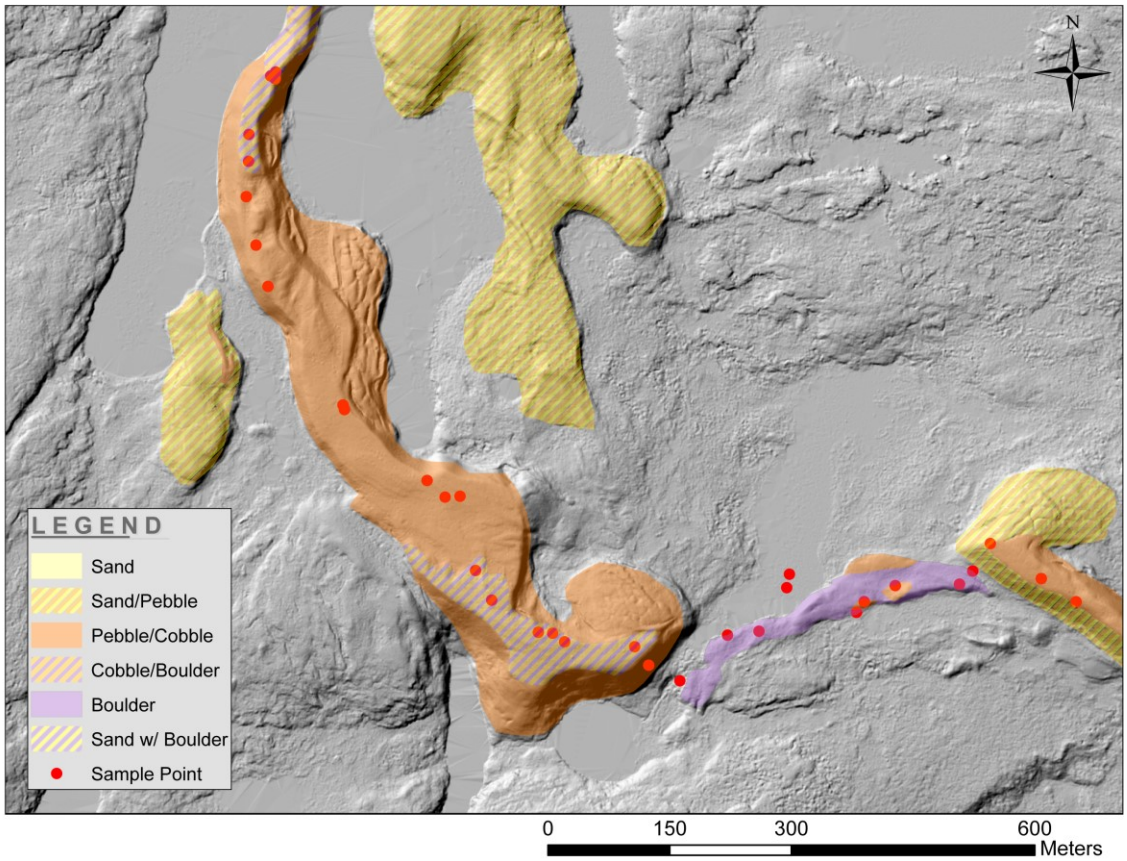

Figure B24: Grain-size map of Misery Tributary Esker, down-esker continuation of figure B23

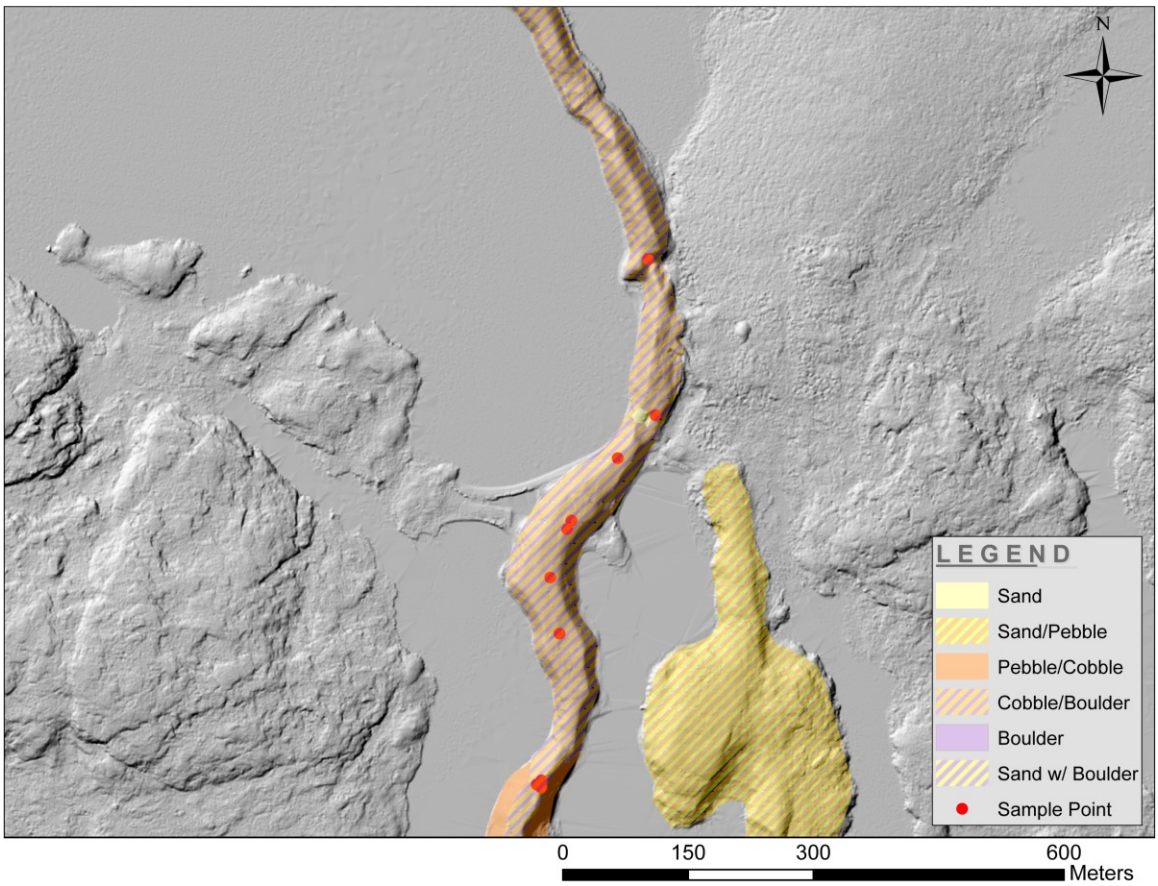

Figure B25: Grain-size map of Misery Tributary Esker, down-esker continuation of figure B24

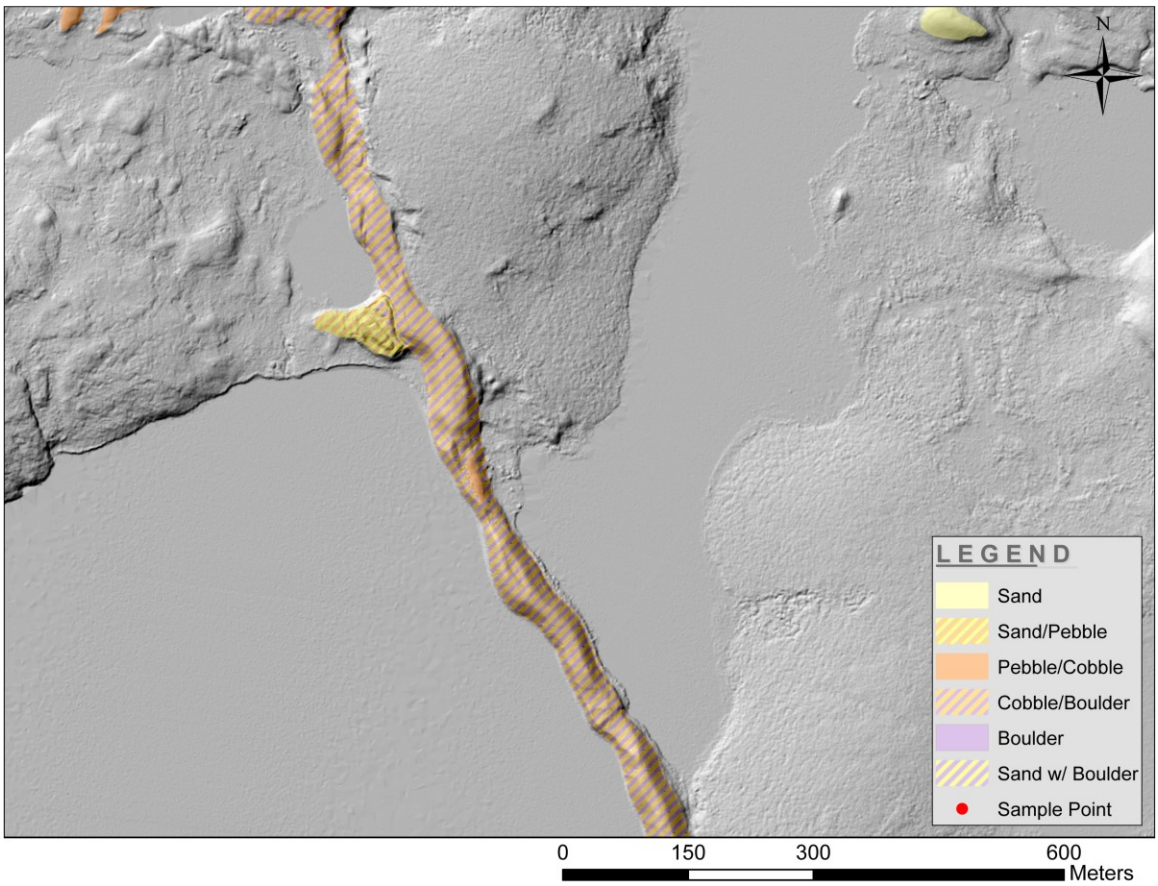

Figure B26: Grain-size map of down-esker terminus of Misery Tributary Esker, down-esker continuation of figure B25

Exeter Lake Esker

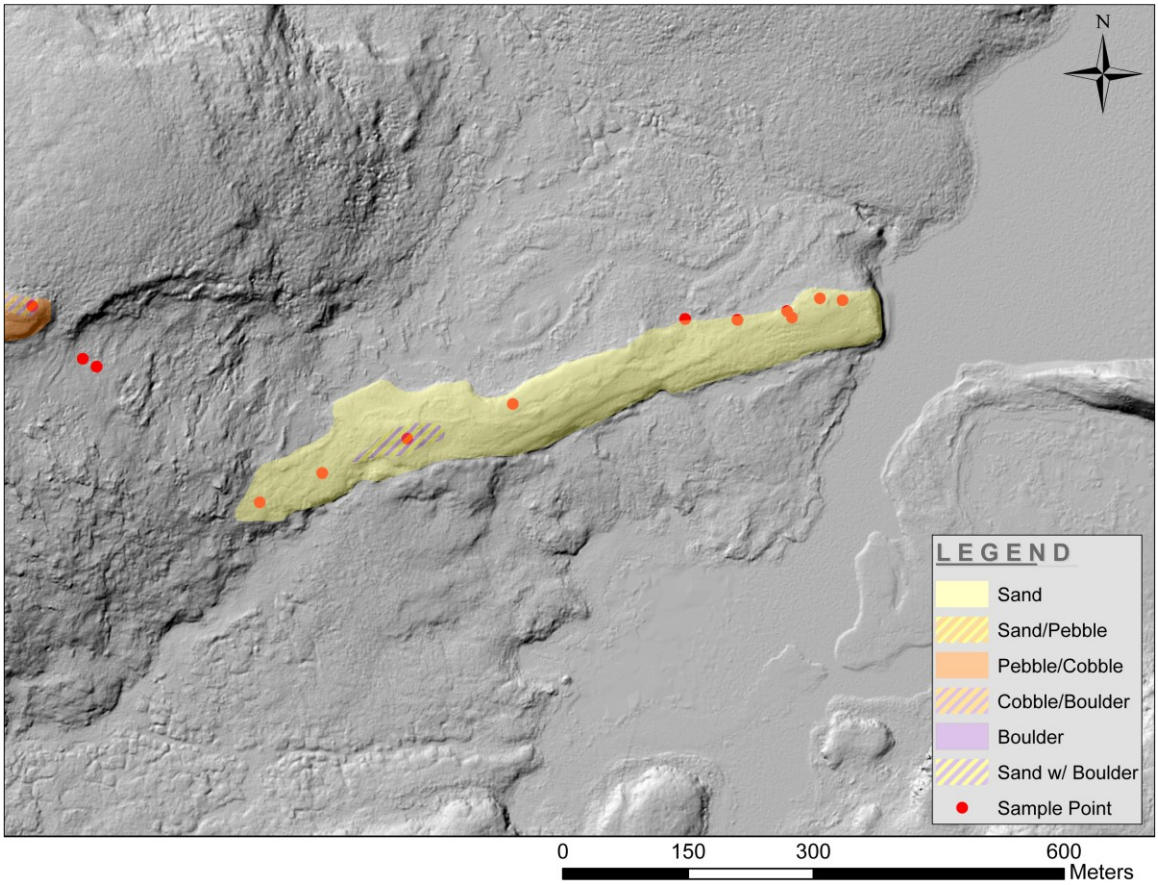

Figure B27: Grain-size map of start of studied portion of Exeter Lake Esker

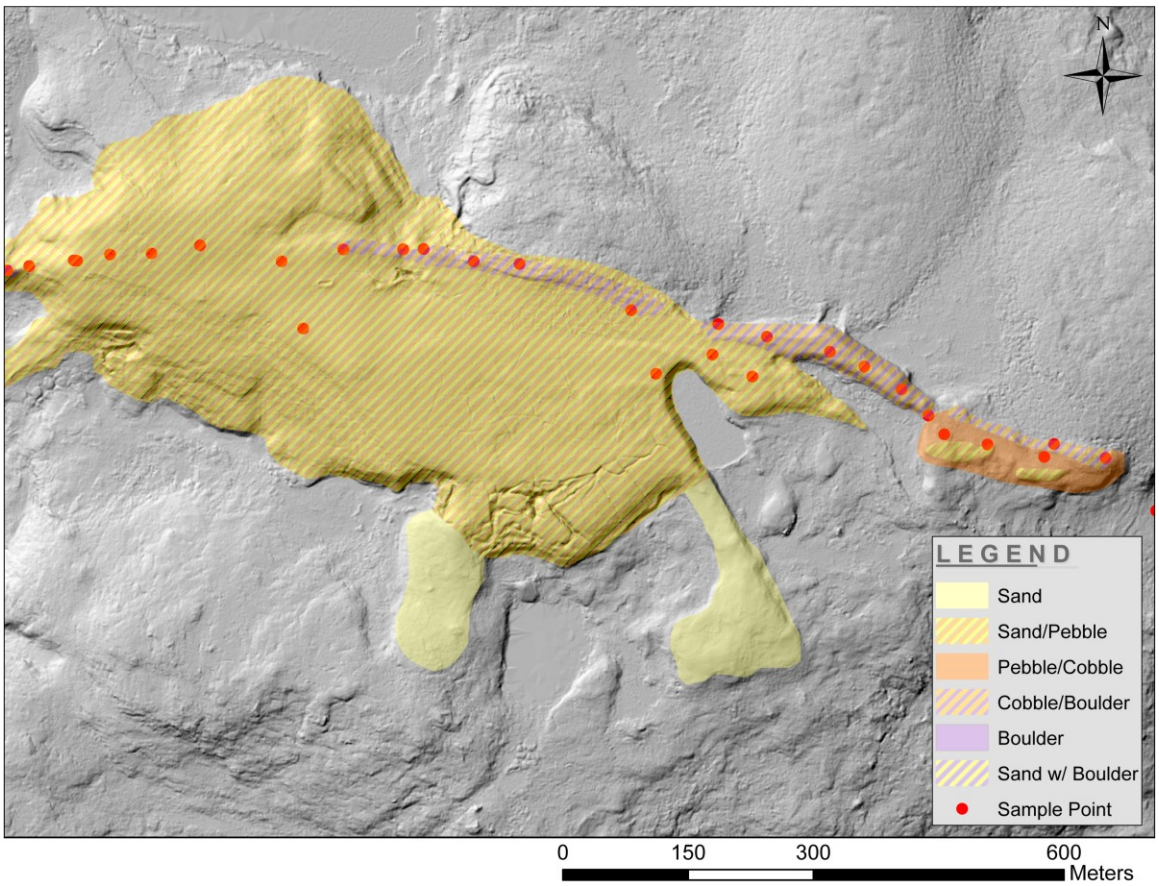

Figure B28: Grain-size map of Exeter Lake Esker, down-esker continuation of figure B27

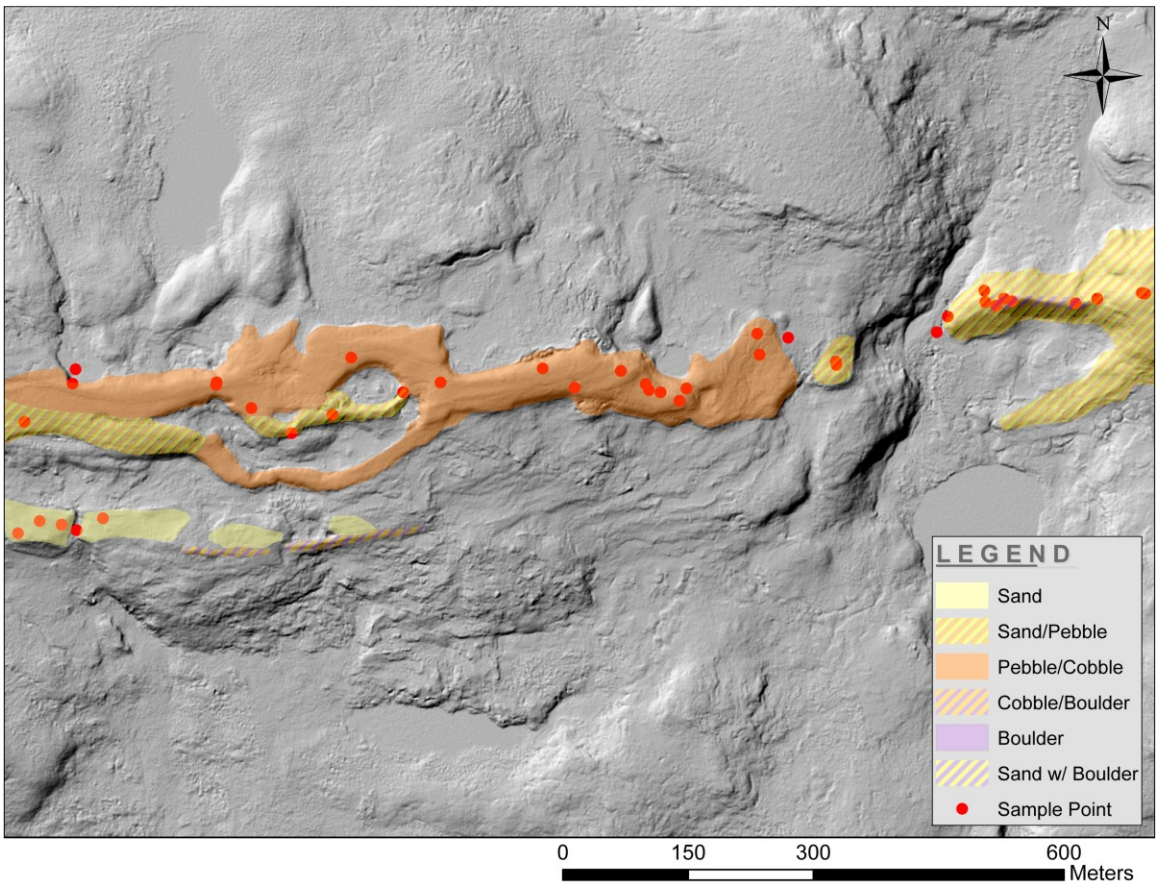

Figure B29: Grain-size map of Exeter Lake Esker, down-esker continuation of figure B28

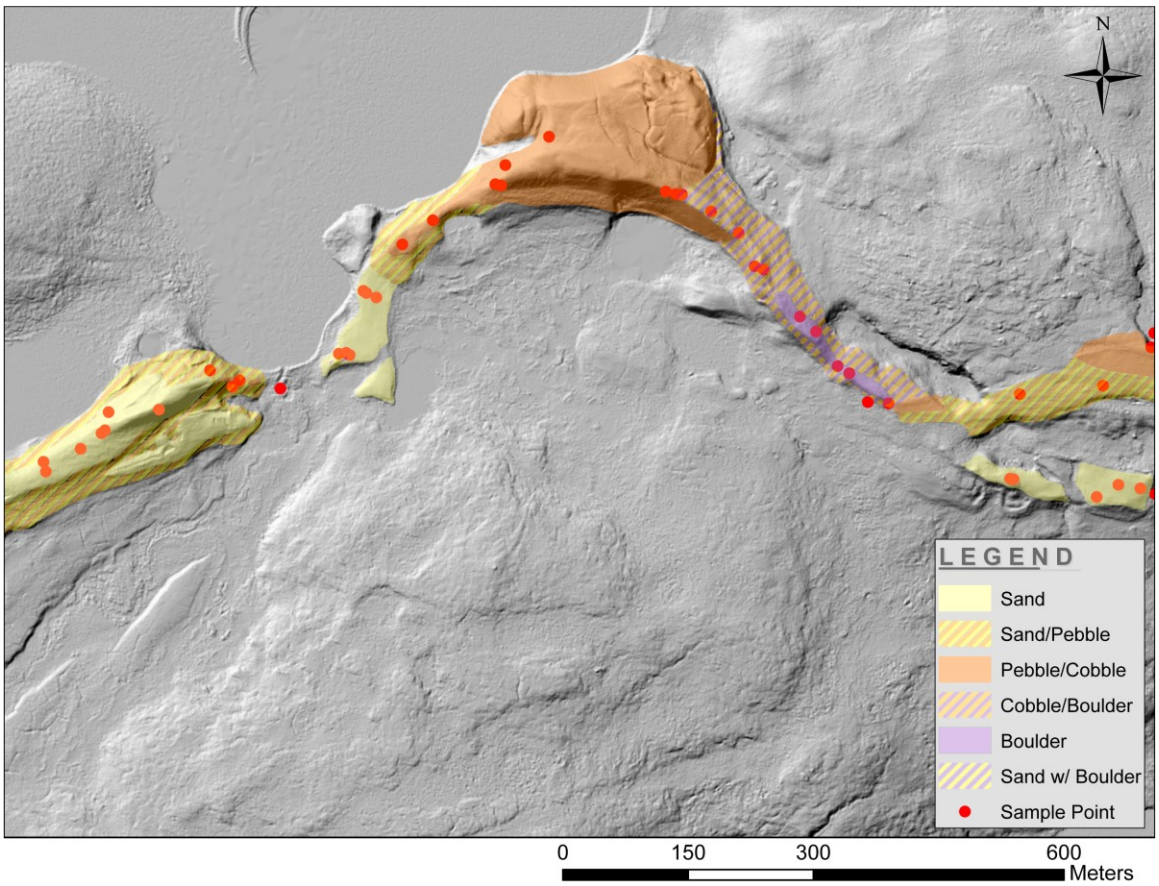

Figure B30: Grain-size map of Exeter Lake Esker, down-esker continuation of figure B29

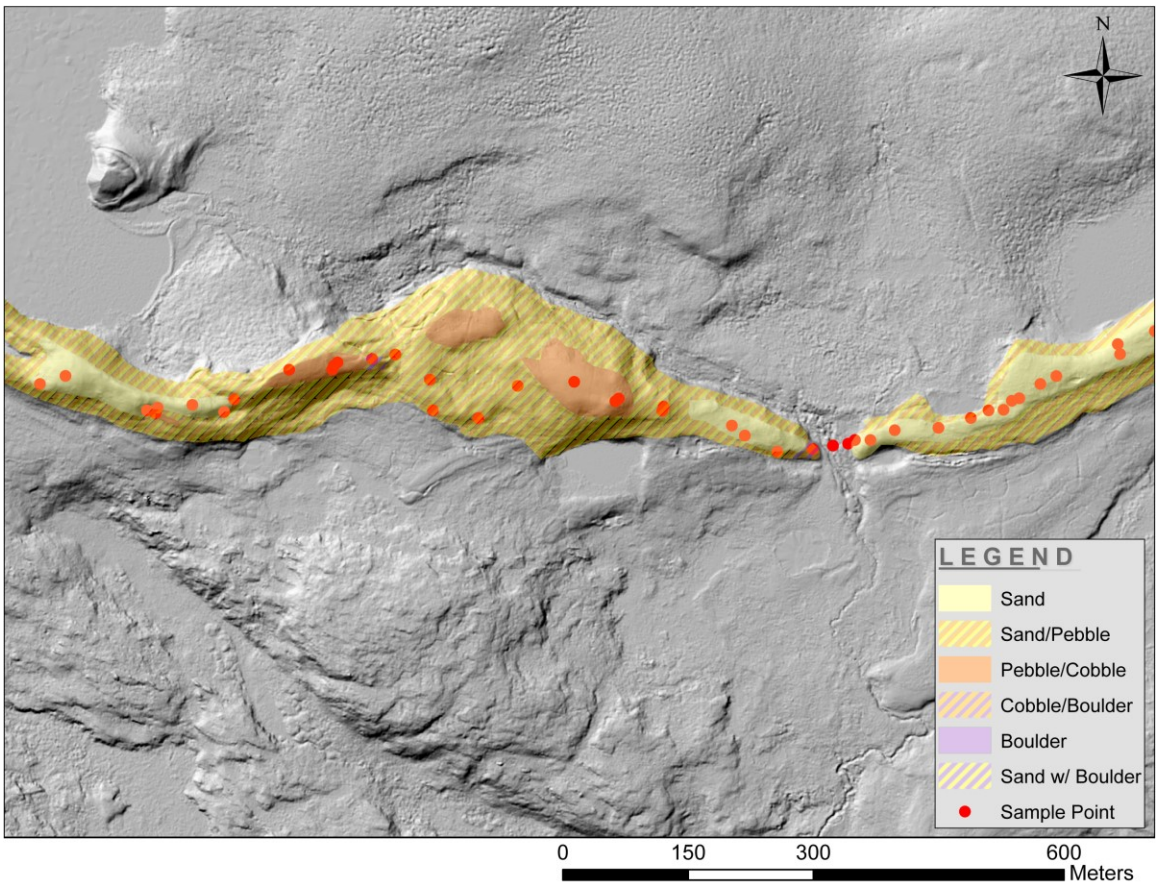

Figure B31: Grain-size map of Exeter Lake Esker, down-esker continuation of figure B30

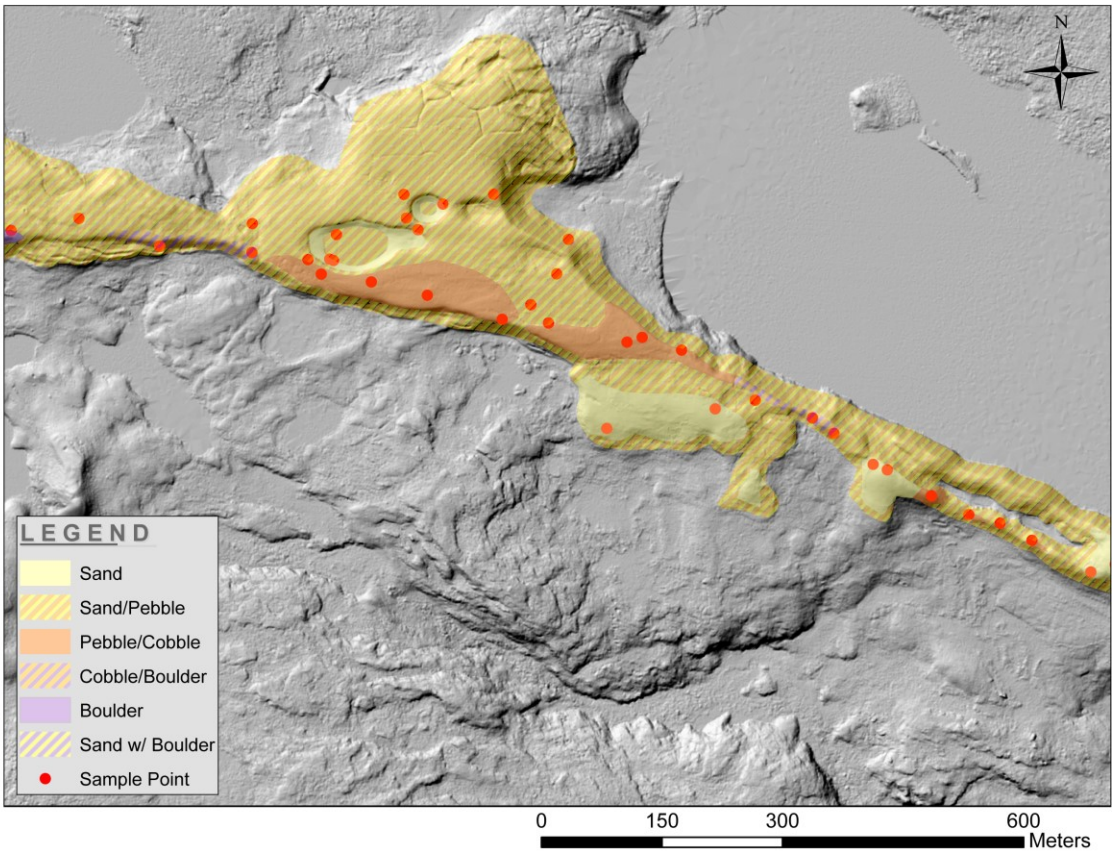

Figure B32: Grain-size map of Exeter Lake Esker, down-esker continuation of figure B31

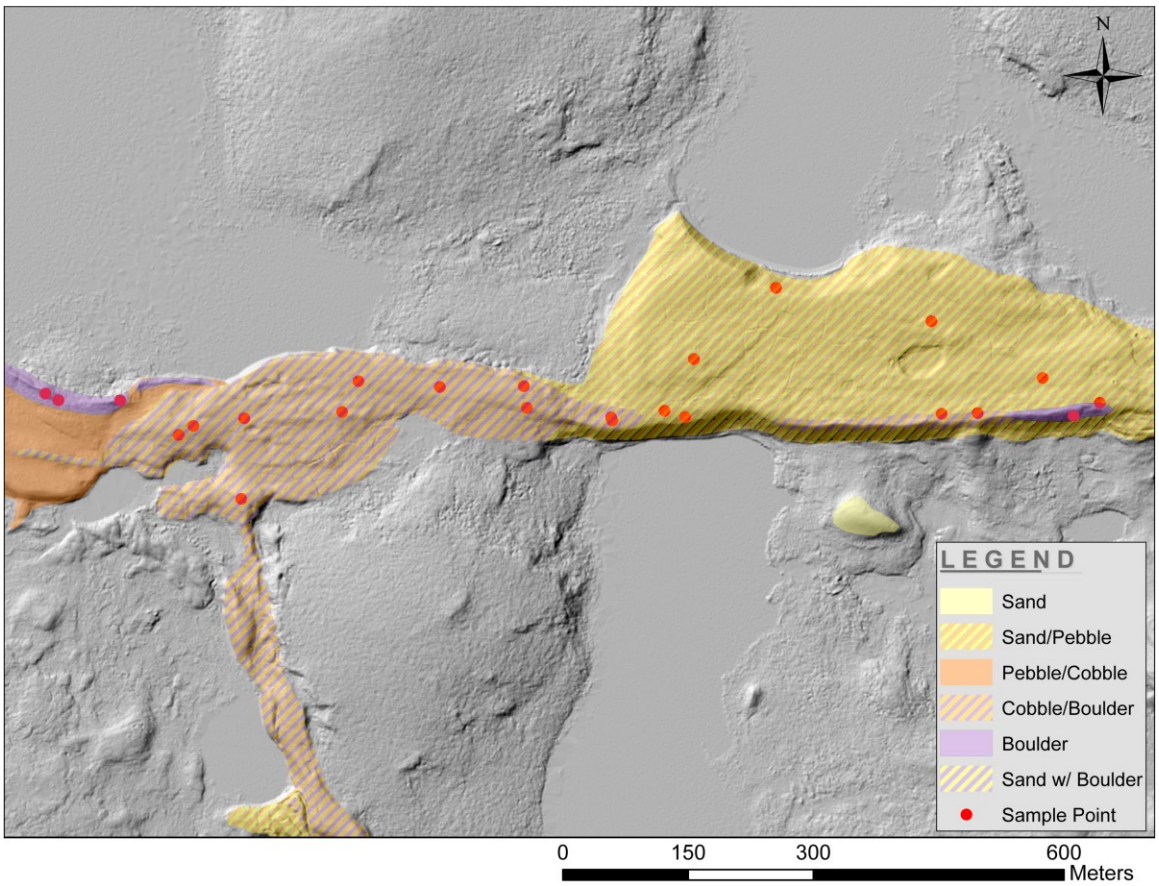

Figure B33: Grain-size map of Exeter Lake Esker, down-esker continuation of figure B32

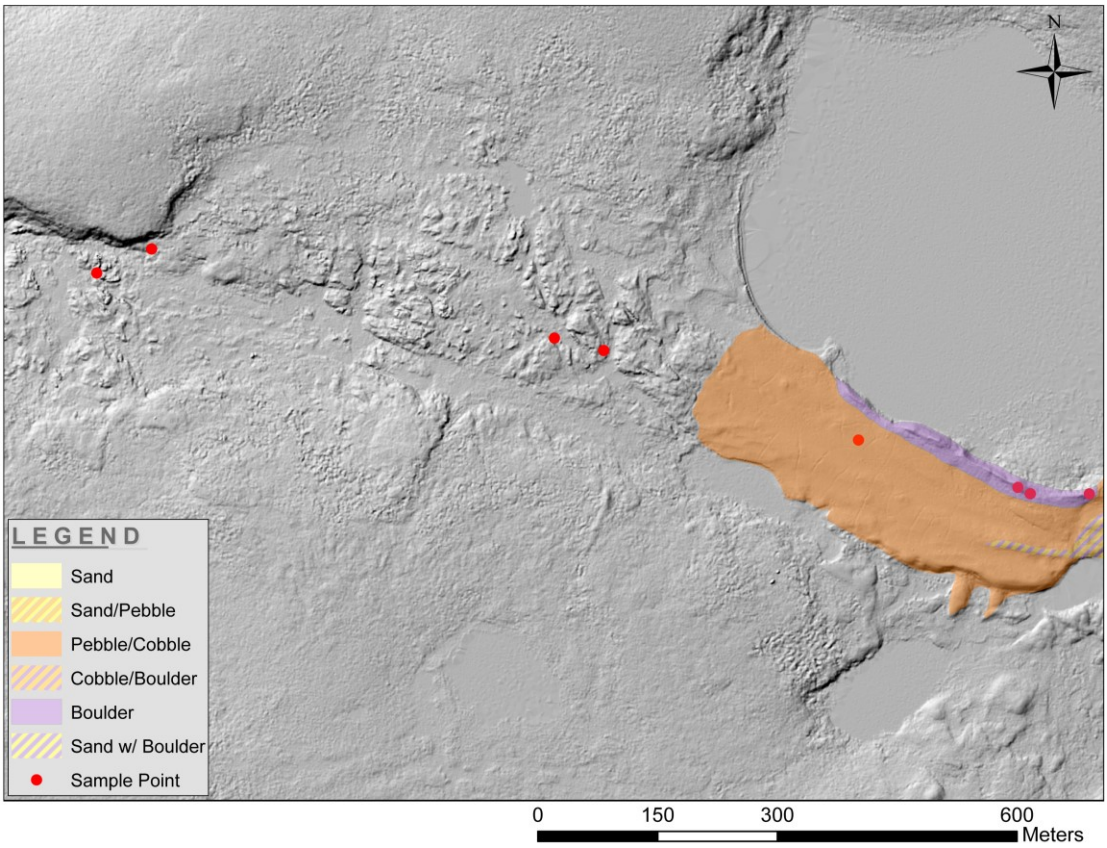

Figure B34: Grain-size map of Exeter Lake Esker, down-esker continuation of figure B33

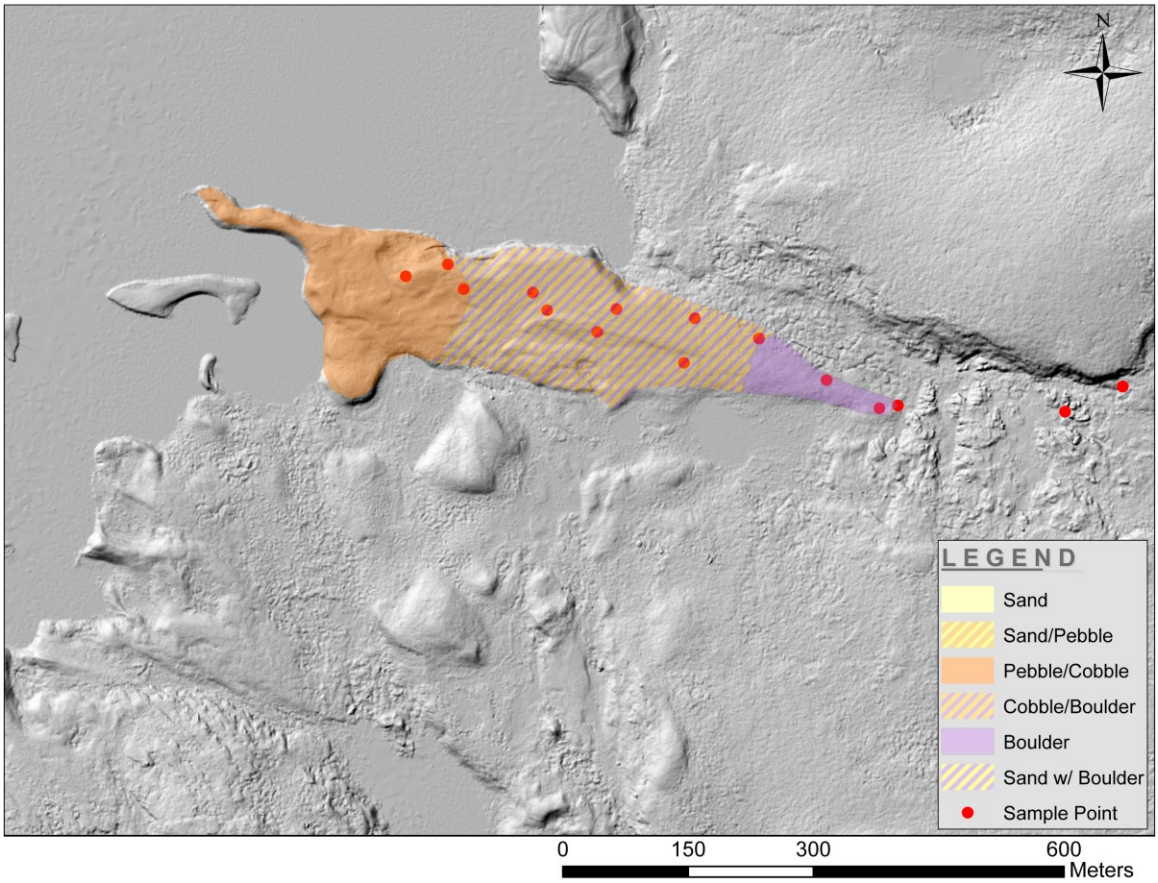

Figure B35: Grain-size map of final studied extent of Exeter Lake Esker, down-esker continuation of figure B34